Insights into molecular and functional mechanisms behind inherited heart and skin disorders

Daniela Nitoiu

Supervisors: Prof David P Kelsell
Dr Dominic Abrams

Submitted in partial fulfilment of the requirements of the Degree of Doctor of Philosophy

Centre for Cutaneous Research, Blizard Institute, Barts and The London School of Medicine and Dentistry, Queen Mary University of London

March 2015

I, Daniela Nitoiu, confirm that the research included within this thesis is my own work or that where it has been carried out in collaboration with, or supported by others, that this is duly acknowledged below and my contribution indicated. Previously published material is also acknowledged below.

I attest that I have exercised reasonable care to ensure that the work is original, and does not to the best of my knowledge break any UK law, infringe any third party's copyright or other Intellectual Property Right, or contain any confidential material.

I accept that the College has the right to use plagiarism detection software to check the electronic version of the thesis.

I confirm that this thesis has not been previously submitted for the award of a degree by this or any other university.

Daniela Nitoiu

Details of collaborations, publications and oral presentations

Publications

Peer reviewed publications:

Blaydon DC, **Nitoiu D**, Eckl KM, Cabral RM, Bland PJ, Hausser I, van Heel DA, Rajpopat S, Fischer J, Oji V, Zvulunov A, Traupe H, Hennies HC, Kelsell DP (2011). Mutations in CSTA, encoding Cystatin A, underlie exfoliative ichthyosis and reveal a role for this protease inhibitor in cell-cell adhesion. American Journal of Human Genetics, 89(4):564-71.

Scott CA, Plagnol V, **Nitoiu D**, Bland PJ, Blaydon DC, Chronnell CM, Poon DS, Bourn D, Gárdos L, Császár A, Tihanyi M, Rustin M, Burrows NP, Bennett C, Harper JI, Conrad B, Verma IC, Taibjee SM, Moss C, O'Toole EA, Kelsell DP (2013). Targeted sequence capture and high-throughput sequencing in the molecular diagnosis of ichthyosis and other skin diseases. Journal of Investigative Dermatology, 133(2):573-6.

Lin Z*, Zhao J*, **Nitoiu D***, Scott CA*, Plagnol V, Smith FJD, Wilson NJ, Cole C, Schwartz ME, McLean WHI, Wang H, Feng C, Duo L, Zhou EY, Ren Y, Dai L, Chen Y, Zhang J, Xu X, O'Toole EA, Kelsell DP and Yang Y (2015). Loss-of-function mutations in *CAST* cause peeling skin, leukonychia, acral punctate keratoses, cheilitis and knuckle pads (PLACK) syndrome. American Journal of Human Genetics (*Joint first authors). American Journal of Human Genetics, 96(3):440-7.

Gupta A, **Nitoiu D**, Brennan-Crispi D, Addya S, Riobo NA, Kelsell DP, Mahoney MG (2015). Cell cycle- and cancer-associated gene networks activated by dsg2: evidence of cystatin a deregulation and a potential role in cell-cell adhesion. PLoS One, 10(3)e0120091.

Invited publications:

Brooke MA*, **Nitoiu D*** and Kelsell DP (2012). Cell-cell connectivity: desmosomes and disease. *Journal of Pathology,* 226(2):158-71 (*Joint first authors).

Nitoiu D, Etheridge SL and Kelsell DP (2014). Insights into desmosome biology from inherited human skin disease and cardiocutaneous syndromes. *Cell Communication and Adhesion*, 21(3):129-40.

Abstracts:

Nitoiu D and Kelsell DP. Genetic and *in vitro* observations support the key role of the protease inhibitor cystatin A in basal epidermal adhesion. Presented at the International Investigative Dermatology Conference, May 8-11, 2013, Edinburgh, UK.

Nitoiu D, Blaydon DC, Cabral R, Bland PJ and Kelsell DP. A key role for the protease inhibitor Cystatin A in keratinocyte adhesion. Presented at the Annual William Harvey Research Day, October 19, 2011, St Bartholomews Hospital, West Smithfield, London, UK.

Nitoiu D, Plagnol V, Barnes M, Kelsell DP. Unravelling desmosome mutations using different high throughput sequencing approaches in ARVC. Presented at the Annual William Harvey Research Day, October 16, 2012, St Bartholomews Hospital, West Smithfield, London, UK.

Oral presentations:

Nitoiu D, Blaydon DC, Cabral R, Bland PJ and Kelsell DP. Genetic and cellular evidence for a key role for a protease inhibitor in desmosomal adhesion. Talk at the British Society for Investigative Dermatology Conference, April 11-13, 2011, Manchester, UK.

Nitoiu D, Blaydon DC, Cabral R, Bland PJ, Zvulunov A, Hennies HC and Kelsell DP. A key role for the protease inhibitor Cystatin A in keratinocyte adhesion. Talk at the European Society of Dermatological Research, September 7-10, 2011, Barcelona, Spain.

Lin Z, **Nitoiu D**, Scott CA, Zhao J, Plagnol V, O'Toole EA, Kelsell DP and Yang Y. Peeling skin, leukonychia, acral punctate keratoses, cheilitis and knuckle pads with milia caused by loss-of-function mutations in calpastatin. Plenary talk at the European Society of Dermatological Research Conference, September 10-13, 2014, Copenhagen, Denmark.

Abstract

Desmosomes are macromolecular, dynamic and adaptable complexes that connect intermediate filaments of neighboring cells in a variety of tissues, generating a large mechanically resilient structure. The importance of maintaining desmosome homeostasis for tissue integrity and optimal organ function has been revealed through the identification of desmosome-associated disorders and mechanistic studies into desmosome regulation. This thesis focuses on inherited skin and heart conditions linked to mutations in desmosomal genes or in genes believed to be implicated in desmosome regulation.

Part of this thesis is focused on the molecular analysis and identification of novel desmosomal mutations in patients clinically diagnosed with Arrhythmogenic Right Ventricular Cardiomyopathy, and the genetic diagnosis of patients with hypotrichosis, hypotrichosis and PPK or acral peeling skin syndrome. Patients were analysed using a number of different genetic techniques including custom capture array, HaloPlex targeted resequencing, exome capture and Sanger sequencing. Both novel and previously reported mutations were identified in *DSP*, *DSC2*, *DSG2*, *PKP2*, *DSG4* or *CSTA* in patients diagnosed with these disorders.

The molecular mechanisms behind mutations in the protease inhibitors cystatin A and calpastatin, leading to the skin disorders exfoliative ichthyosis and PLACK syndrome, were also investigated. *In vitro* analysis, using siRNA-mediated knockdown in the immortalised keratinocyte cell line HaCaT, demonstrated that these mutations, affecting the structure and function of the protease inhibitors, lead to deficient intercellular adhesion, possibly through the indirect regulation of desmosomal complexes through their target proteases.

Table of Contents

List of Figures and Tables

Chapter 1 - Introduction

Chapter 2 - Materials and Methods

Chapter 3 - Genetic strategies for mutation diagnosis in patients with ARVC or genodermatoses

Chapter 4 - Functional analysis of loss-of-function mutations in the protease inhibitor Cystatin A

Chapter 5 - PLACK syndrome due to LOF mutations in the protease inhibitor Calpastatin

Appendices

Abbreviations

3’	3-prime Phosphate
3D	Tridimensional
5’	5-prime Phosphate
µ	Micro
A	Ampere
ADAM	A Disintegrin and Metalloprotease
AML	Acute Myeloid Leukaemia
APC	Adenomatous Polyposis Coli
APSS	Acral PSS
ARVC	Arrhythmogenic Right Ventricular Cardiomyopathy
AT	Annealing Temperature
ATP	Adenosine Triphosphate
Bcl	B-Cell Lymphoma
bp	Base Pair
BSA	Bovine Serum Albumin
^{0}C	Degrees Celsius
Ca^{2+}	Calcium
cAMP	Cyclic Adenosine Monophosphate
CAR	Coxsackievirus and Adenovirus Receptor
CAST	Calpastatin
CCDN1	Cyclin 1 Coding Gene
CCDS	Consensus Coding Sequence
cDNA	Coding DNA
CDSN	Corneodesmosin
cGMP	Cyclic Guanosine Monophosphate
CLM	Cystatin-Like Molecule
CSID	Chromosomal SNP ID
CSTA	Cystatin A
Cx	Connexin
DAPI	4’,6-Diamidino-2-Phenylindole
dbSNP	Database of Single Nucleotide Polymorphisms

DCM	Duchenne Muscular Dystrophy
DEJ	Dermal-Epidermal Junction
dH_2O	Distilled Water
ddH_2O	Double Distilled Water
Der f	Dermatophagoides farina
Der p	Dermatophagoides pteronyssinus
DES	Desmin
DMEM	Dulbecco's Modified Eagle Medium
DMSO	Dimethyl Sulfoxide
DNA	Deoxyribonucleic Acid
dNTP	Deoxyribonucleotide Triphosphate
DSC	Desmocollin
DSG	Desmoglein
DSP	Desmoplakin
dsDNA	Double Stranded DNA
DTD	Desmoglein-Specific Terminal Domain
DTT	Dithiothreitol
EA	Extracellular Anchor Domain
EBS	Epidermolysis Bullosa Simplex
EC	Extracellular Cadherin Repeats
ECD	Extracellular Core Domain
ECD	Enrichment Control DNA
ECL	Enhanced Chemiluminescent
ECM	Extra Cellular Matrix
EDTA	Ethylenediaminetetraacetic Acid
EGFR	Epidermal Growth Factor Receptor
ELISA	Enzyme-Linked Immunosorbent Assay
EM	Electron Microscopy
ET	Exfoliative Toxin
FACS	Fluorescence-Activated Cell Sorting
FAK	Focal Adhesion Kinase
FBS	Foetal Bovine Serum
g	Grams

G	Gravitational Force
GAPDH	Glyceraldehyde 3-Phosphate Dehydrogenase
Gas	Growth Arrest-Specific Protein
GPSS	Generalised PSS
h	Hour
HCl	Clorhidric Acid
H&E	Haematoxilin and Eosin
Hg19	Human Genome 19th Version
HiDi	Highly Deionised Formamide
HNC	Head and Neck Cancer
Hz	Hertz
IA	Intracellular Anchor Domain
ICC	Immunocytochemistry
ICS	Intracellular Cadherin-Binding Site
IDP	Inner Dense Plaque
IF	Intermediate Filament
Ig	Immunoglobulin
IGV	Integrative Genomics Viewer
IHC	Immunohistochemistry
InDel	Insertion/Deletion
IPL	Intracellular Proline-Rich Domain
iRHOM2/RHBDF2	Rhomboid Family Member 2
IVS	InterVening Sequence
JAM	Junction Adhesion Molecule
JUP	Junction Plakoglobin Gene
K	Kilo
Kb	Kilo Bases
KD	Knockdown
KDa	Kilo Daltons
KLK	Kallikrein-Related Peptidase
KO	Knockout
KRT	Keratin
L	Litres

LB Broth	Luria Bertani Broth
LEF	Lymphoid Enhancer-Binding Factor
LEKT	Lympho-Epithelial Kazal-Type-Related Inhibitor
LM-PCR	Ligation-Mediated PCR
LMN	Lamin
LOF	Loss Of Function
m	Mili
M	Molar
MAb	Monoclonal Antibody
MAF	Mutation Annotation Format
Mg^{2+}	Magnesium
$MgCl_2$	Magnesium Cloride
min	Minute
MMP	Matrix Metallo-Proteases
mRNA	Messenger RNA
n	Nano
NAD	Nothing Abnormal Detected
NaOH	Sodium Hidroxide
NCBI	National Center for Biotechnology Information
NGS	Next Generation Sequencing
NHK	Normal Human Keratinocytes
NS	Normal Skin
NTP	Non-Targeting Pool
ODP	Outer Dense Plaque
P53/P63	Tumour Protein P53/P63
PAb	Polyclonal Antibody
PAGE	Polyacrylamide Gel Electrophoresis
PBS	Phosphate Buffer Saline
PCR	Polymerase Chain Reaction
PERP	P53 Apoptosis Effector Related to PMP-22
PF	Pemphigus Foliaceus
PFA	Paraformaldehyde
PG	Plakoglobin

pH	Power of Hydrogen
PID	Primary Immunodeficiency
PKC	Protein Kinase C
PKP	Plakophilin
PLACK	PSS, Leukonychia, Acral punctate keratosis, Cheilitis and Knuckle pads
PLEC	Plectin
PM	Plasma Membrane
PMP	Peripheral Myelin Protein
PNN	Pinin
PPAR	Peroxisome Proliferator-Activated Receptor
PPK	Palmoplantar Keratoderma
PSS	Peeling Skin Syndrome
PV	Pemphigus Vulgaris
RNA	Ribonucleic Acid
ROD	Rod Shaped
rpm	Rotations per minute
RT	Room Temperature
RT-PCR	Reverse Transcription PCR
RUD	Repeating Unit Domain
RYR	Ryanodine Receptor
s	Second
SAM	Severe Dermatitis, Allergies and Metabolic Wasting
SCC	Squamous Cell Carcinoma
SDM	Site-Directed Mutagenesis
SDS	Sodium Dodecyl Sulphate
SERPIN	Serine Protease Inhibitor
SIFT	Sorting Intolerant From Tolerant
siRNA	Small Interfering RNA
SLPI	Secretory Leukocyte Protease Inhibitor
SNP	Single Nucleotide Polymorphism
SP	Serine Proteases
SPINK	Serine Protease Inhibitor Kazal-Type

SPPK	Striate PPK
SPRI	Solid Phase Reversible Immobilisation
SSSS	Staphylococcal Scalded Skin Syndrome
STRN	Striatin
TBE	Tris Borate EDTA
TBS	TRIS Buffered Saline
TBS-T	TBS-Tween 20
TCF	Transcription Factor
TFC	Task Force Criteria
TGF	Tumour Growth Factor
TGM	Transglutaminase
TM	Trans Membranous
TMEM	Transmembrane Protein
TOC	Tylosis with Oesophageal Cancer
TRIS	Tris (hydroxymethyl) aminomethane
TTN	Titin
U	Units
UCSC	The University of California Santa Cruz Database
UPS	Ubiquitin Proteasome System
UV	Ultraviolet Light
v	Volume
V	Volt
WB	Western Blotting
X	Times

Acknowledgements

There are many people both in my professional and my personal life that have contributed immensely to my PhD years and I would like to thank for their unconditional help and support, and for making the last few years more rewarding and enjoyable.

Firstly, I would like to thank both my supervisors Prof David Kelsell and Dr Dominic Abrams, for their endless support, guidance and inspiration throughout my PhD, and especially Prof David Kelsell for his active interest in my work at all times and for receiving his time and attention any time I needed advice and guidance.

I would also like to thank Michael Barnes and Vincent Plagnol for NGS data analysis and help with data interpretation, Charles Mein for SNP array data analysis and the BALM, FACS, Genome Centre and Pathology QMUL Facilities.

Also, thank you to past and present members of the Kelsell group and department members for their friendship, time and advice, and for making the lab an enjoyable place to be, and especially to Benjamin Fell for his help with the calpastatin H&E, Claire Scott for her help with sequencing of CAST and IHC of calpastatin, Diana Blaydon, Anissa Chikh and Sarah Etheridge for carefully reviewing this thesis.

A special thank you to Sarah Etheridge and Tania Garcia for their infinite encouragement, exceptional friendship and invaluable theoretical and technical advice, and all of my other friends for their immense friendship and moral support outside my lab life.

Finally, a very special thank you to my family to whom I cannot be grateful enough for their love, support throughout my life and in all of my decisions, and always having been my inspiration.

-Chapter 1-

Introduction

1.1. The Skin

The skin is key in maintaining the integrity and healthy functioning of the human organism. The skin's most critical function is to form a barrier between the "outer" and "inner" environments, and by this regulating processes such as water loss, thus preventing desiccation, and protecting against chemical (irritants, allergens), mechanical (UV light, temperature variations, mechanical stress) and microbial assaults (fungus, bacteria, viruses) through a permanent rearrangement and regulation of its structural and molecular components (Egberts *et al*., 2004).

The three consisting layers of the skin are the epidermis, the dermis and the hypodermis. The hypodermis is the deepest skin layer, with roles such as body insulation, energy resource and skin protection, and cushion against mechanical stress while serving as a shelter for nerve fibres, blood and lymph vessels. The dermis is the intermediate layer and also the thickest layer of the skin, formed of fibrous, filamentous, diffuse and connective tissue elements which accommodate nerves, glands and vascular components. It serves as a thermal regulator, binds water, protects against mechanical injury and is the main sensorial receptor. The epidermis is the outer layer of the skin and the first barrier against external assaults. Some of the key roles of this layer are UV protection, immune defence and adhesion (Wolff *et al*., 2007).

1.1.1. The epidermis

The epidermis is structured on four layers named after their position or a specific characteristic. These layers stratify from the basal layer, the spinous layer, the granular layer to the stratum corneum which is shed during desquamation (Figure 1.1.). Keratinocytes represent 80% of the cells forming the epidermal layers and intercalate with various other cells such as melanocytes, Langerhans cells, Merkel cells and lymphocytes (Houben *et al*., 2008).

The structure of all keratinocytes is directed by a family of intermediate filaments, named keratins, through a cell-type and tissue-type differentiation stage, developmental stage and disease-dependent co-expression of fifty-four keratins.

The basal layer is where keratinocyte differentiation, a genetically-programmed, carefully regulated and complex morphologic and metabolic process, begins only to end with a terminally differentiated dead keratinocyte which contains keratin and matrix proteins with surface-associated lipids. This layer contains mitotically active keratinocytes which get their columnar shape and attachment to the basement membrane function from keratins 5 (KRT5) and 14 (KRT14). Melanocytes, another epidermal cell type, produce melanin, which is the pigment in these cells, giving the overall skin pigmentation perceived macroscopically. Various studies suggest that the basal layer can exhibit three proliferative potentials, as stem cells, transit amplifying cells and post mitotic cells. It is believed that stem cells are located within the follicular bulge region and that these cells are not only capable of forming the entire pilo-sebaceous unit but also the interfollicular epidermis. The transit amplifying cells arise from stem cells as a consequence of their infrequent division. These daughter cells are the most common cells in the basal layer and represent the stable self-renewed cells which reach their end terminal point in the stratum corneum after a succession of divisions (Wolff *et al*., 2007).

The spinous layer takes its name from the special shape the composing keratinocytes have, which changes as the cells differentiate into the granular layer. These cells retain the stable KRT5 and KRT14 filaments produced in the basal layer, localised around the nucleus and tethered to desmosomes, but do not synthesize any new mRNA, instead they produce KRT1 and KRT10 specific to this epidermal layer. These keratins are specific to differentiated/keratinised cells and their down-regulation together with the up-regulation of KRT6 and KRT16 are a hallmark of hyperproliferative disorders (Wolff *et al*., 2007).

The basophilic keratohyalin granule-containing cells make up the granular layer, which takes its name from this attribute. These granules are composed primarily of profilaggrin, keratin filaments and loricrin. This layer is where many of the characteristics of the epidermal barrier are formed. Release of profilaggrin from the granules results in its calcium-dependent cleavage into filaggrin monomers which aggregate with keratin to form macrofilaments, eventually filaggrin being degraded into UV protective molecules (Wolff *et al*., 2007).

The final stage of keratinocyte differentiation ends with flattened cornified cells that form the stratum corneum. During this differentiation process an apoptotic mechanism results in the destruction of the nucleus together with all intracellular components excepting the keratin filaments and filaggrin matrix. Regulation of permeability, desquamation, antimicrobial peptide activity, toxin exclusion and selective chemical absorption, some of the most important functions of the extracellular lipid matrix, together with mechanical reinforcement, hydration, cytokine-mediated inflammation and protection from UV damage provided by the corneocytes represent the first defence barriers of the human organism against external factors (Egberts *et al*., 2004, Houben *et al*., 2007, Fuchs, 1990, Fuchs, 2007).

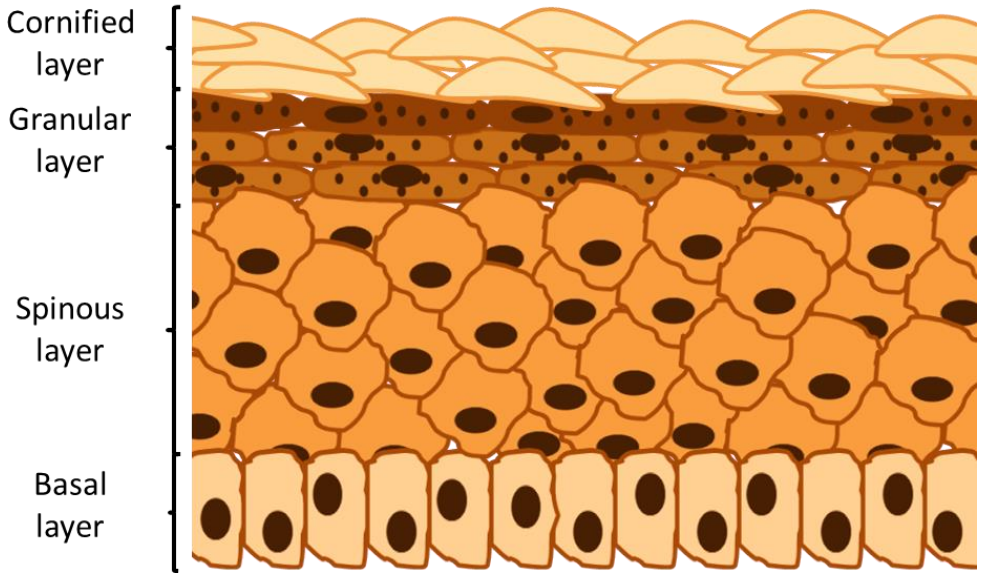

Figure 1.1. Schematic structure of the human epidermis. The different epidermal layers indicative of layer-specific cellular differentiation are shown including the basal, spinous, granular and cornified layers.

1.1.2. The dermal-epidermal junction

The dermal-epidermal junction (DEJ) is a complex form of the basement membrane and it underlies the basal layer of the epidermis, extending into the upper layers of the dermis, and covering the entire length of the epidermis and epidermal appendages such as sweat glands, sebaceous glands and hair follicles. The DEJ consists of three zones which through complex protein-protein interactions provide a strong mechanical stability between the epidermal and dermal structures. The first zone is formed of keratin filaments spanning from the nuclear area of the basal cells of the epidermis into the plasma membrane and associate to hemidesmosomal plaques. External to the plasma membrane of the basal cells, anchoring filaments, seen throughout the lamina lucida, connect to the lamina densa. The second zone, called lamina densa, has been described under higher magnification with a granular-fibrous appearance, mainly formed of collagen IV, nidogen-entactin, perlecan, and laminins, which can polymerize to form networks of variable thickness. The third zone is the subbasal lamina formed of microfibrilar structures such as the anchoring fibrils, mainly collagen VII aggregates, and the elastic fibers. The majority of anchoring fibrils bind to the basal lamina with one end and the fibrous structures of the dermis with the other end. Other fibrils originating from the lamina densa curve in a horse shoe manner and reinsert themselves into the lamina densa or insert into amorphous structures named anchoring plaques. These microfibrils insert into the basal lamina perpendicularly to the basement membrane, and extend into the dermis merging with the elastic fibers to form a plexus parallel to the DEJ (Burgeson and Nimni, 1992, Christiano and Uitto, 1994, Kielty and Shuttleworth, 1997, Tamai *et al*., 2009, Ko and Marinkovich, 2010). The DEJ therefore provides a variety of complex attachments between the reticular dermis and the intermediate filament cytoskeleton of the basal cells of the epidermis.

1.1.3. The dermis

The dermis is the skin layer below the epidermis, usually much thicker than the layer above, it serves as physical support and a source of nutrients for the avascular epidermis, but also as a thermal regulator and a sensorial receptor due to the numerous nervous endings. It is largely composed of a network of collagen and

elastin fibres embedded in the extra-cellular matrix (ECM), a heterogeneous network of complex molecules including proteins and polysaccharides, such as fibronectin, laminins, hyaluronic acid and proteoglycans. Scattered throughout the dermis are cells called fibroblasts which regulate the organisation of the fibrillar dermal matrix and responsible with the synthesis and maintenance of the precursors of the ECM. This complex macromolecular network provides a scaffold through which cells can move, influencing cell behaviour through the constant turnover and remodelling of its components (Halper and Kjaer, 2014).

Structurally, the dermis is divided into the superficial papillary dermis and the deeper reticular dermis. The papillary dermis, presents a looser fibrous texture in comparison to the reticular layer, and is formed of vascular networks, parallel to the skin surface, that communicate between themselves through vertical vessels, together forming the superficial plexus serving different dermal papillae. Similarly to the superficial blood vessels, the collagen bundles follow the structures they surround. The reticular dermis is the thicker layer of the dermis and is formed of larger blood and lymph vessels, thicker collagen and elastic fibres and nerve endings (Halper and Kjaer, 2014).

1.1.4. Keratinocyte adhesion and communication in the epidermis

The skin, as the first defence organ, can successfully accomplish its basic functions with the essential assistance of intercellular junctions which serve to create a tight barrier between keratinocytes. The barrier, formed by adherens junctions, tight junctions and desmosomes together with gap junctions, facilitates both the structural integrity and cell-cell communication homeostasis (Figure 1.2.).

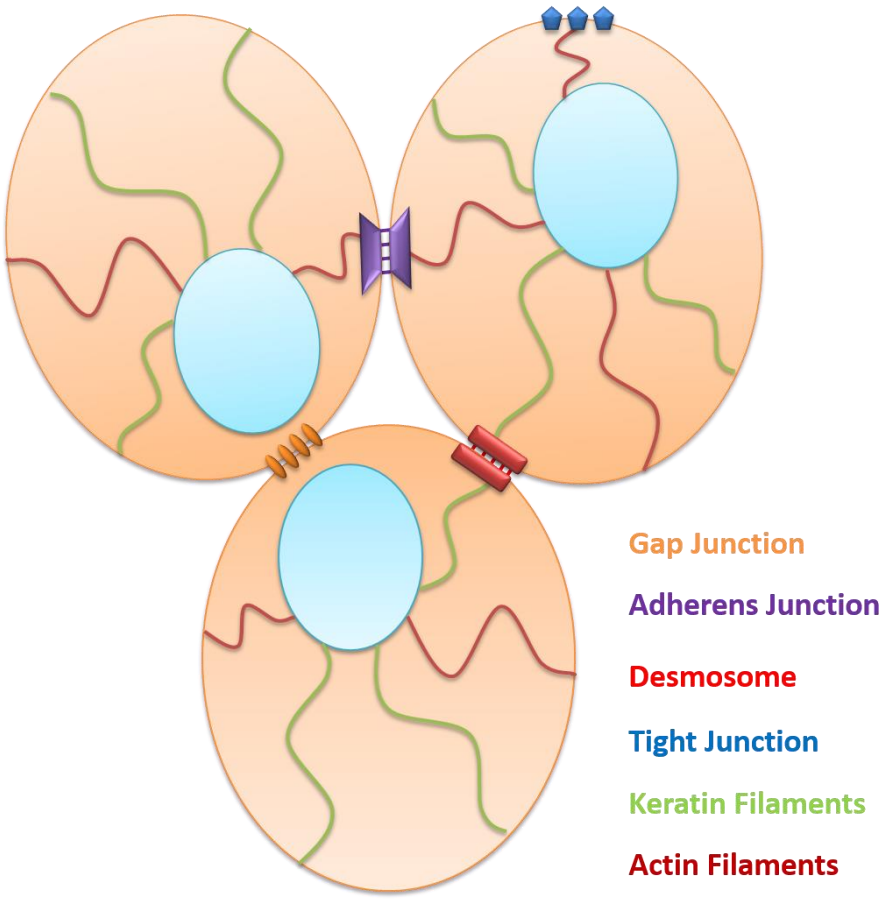

Figure 1.2. Diagram of epidermal intercellular junctions. Intercellular junctions include gap junctions (orange), adherens junctions (purple), desmosomes (red, Sobolik-Delmaire *et al*., 2010) and tight junctions (blue), connecting keratinocytes. Adherens and tight junctions are shown to be connected to actin microfilaments (dark red). Desmosomes are connected to keratin intermediate filaments (green). Adhesion between adherens junctions and desmosomes is mediated by cadherin proteins, which form links between neighbouring keratinocytes.

1.1.4.1. Adherens junctions

The adherens junctions are major cell-cell links that mediate cell recognition, adhesion, morphogenesis and tissue integrity, their importance being highlighted by the maintenance of their structural similarities during evolution (Yonemura, 2011, Oda and Takeichi, 2011). This type of junction is not only found in epithelial tissues but also in non-epithelial cells such as fibroblasts, cardiac muscles and neurons. They are characterised as regions at the interface of two neighbouring cells and enclose a dense undercoat associated with actin filaments at the cytoplasmic surface.

Cadherins, the major components of these junctions, are structurally formed of repeating extracellular cadherin domains and a cytoplasmic region that binds p120-catenin and β-catenin at opposing ends (Oda and Takeichi, 2011). A variety of cadherins are known, with different names depending on their localisation, such as E-cadherin in the epithelium, N-cadherin in the neuronal tissue (Meng and Takeichi, 2009). P120-catenin is known to stabilise cadherins at the intercellular surface, while β-catenin is thought to mediate the interactions of cadherins with the actin filaments through α-catenin, until recently when this theory was dismissed (Yamada *et al*., 2005). Alongside its function in adherens junctions, β-catenin is also a crucial component of the Wnt signalling pathway, which regulates development and homeostasis via gene expression, cell growth, survival and polarity (Moon *et al*., 2002). Under normal conditions Wnt pathway signalling is regulated by phosphorylation and subsequent degradation of β-catenin, meaning that somatic mutations in β-catenin itself, or in those proteins involved in its phosphorylation or degradation (including Dishevelled, Axin, Adenomatous Polyposis Coli [APC], and glycogen synthase kinase-3β) can lead to constitutive β-catenin activation and lead to cancer development (Moon *et al*., 2002).

1.1.4.2. Tight junctions

Tight junctions form the boundary between the apical and basolateral domains of epithelia and serve in preventing the paracellular passage of fluids, electrolytes and macromolecules (Bonazzi and Cossart, 2011). The four main protein groups which constitute the junction are the occludins, the claudins, the junction adhesion

molecules (JAM) and the coxsackievirus and adenovirus receptor proteins (CAR) (Citi and Cordenonsi, 1998). The first two types of proteins, occludins and claudins, have four transmembrane domains and form homodimers via their extracellular loops, while JAMs and CARs have only one transmembrane domain and extracellular IgG-like domain that mediate adhesion. These transmembrane components bind to intracellular components which link them to the actin cytoskeleton. Due to their apical location, tight junctions are easily disrupted by pathogens during host infection and virus spread (Bonazzi and Cossart, 2011).

1.1.4.3. Gap junctions

The main role of gap junctions is to permit intercellular communication, a function vital for controlling homeostasis, and responding to external stimuli, which they accomplish by allowing the transfer of ions (including Ca^{2+} and Mg^{2+}) and small molecules of less than 1 kDa (such as cAMP, cGMP and ATP) between cells (Scott and Kelsell, 2011). Gap junctions consist of plaques of many small channels, each the product of two hexameric hemi-channels on closely apposed cell membranes. Each hemi-channel is a homo- or heteromeric hexamer made up of connexins (Cx) (Storme *et al*.), a protein family of 21 members in humans, named according to their molecular mass (Wei *et al*., 2004). Cx are differentially expressed in the human body, with multiple types expressed in any single tissue type. Microtubules are believed to facilitate the trafficking of hemi-channels to the cell surface where they can be found unopposed to another channel or docked with a hemi-channel on an adjacent cell to form a gap junction connecting the cytoplasms of these two neighbouring cells. Hemi-channels can be either homo- or heterotypic which means that they are composed of identical or different hemi-channels respectively (Caspar *et al*., 1977). Gap junctions composed of different connexins have different properties due to a varied permeability to molecules and ions (Goldberg *et al*., 2004).

1.1.5. The desmosome – a complex intercellular junction

Desmosomes are complex macromolecular structures with a key role in the maintenance of collateral epidermal integrity. These structures were discovered by Italian pathologist Giulio Bizzozero (1846-1901), in a variety of tissue types exposed

to mechanical stress, such as the intestinal mucosa, gallbladder, uterus and oviduct, liver, pancreas, stomach, salivary and thyroid glands, and the epithelial cells of the nephron, but are most abundant in the skin and myocardium (Farquhar and Palade, 1963, Kelly, 1966, Staehelin, 1974, Holthofer *et al*., 2007). A primary function of desmosomes is the anchoring of cytoskeletal keratin intermediate filaments in the epidermis, desmin intermediate filaments in the heart, vimentin intermediate filaments in meningeal cells and the follicular dendritic cells of lymph nodes to the cell membrane (Green and Gaudry, 2000).

1.1.5.1. Ultrastructural organisation of the desmosomal complex

All desmosomes, independent of their localisation, are formed of three main classes of proteins divided into three parallel individual zones, arranged symmetrically on the cytoplasmic faces of the plasma membranes of bordering cells and separated by the extracellular domain. The five known desmosomal components are: the desmosomal cadherins, represented by four desmogleins (DSG1-4) and three desmocollins (DSC1-3), the armadillo family members, plakoglobin (PG)/γ-catenin and the three plakophilins (PKP1-3), and the plakin linker protein desmoplakin (DSP) which anchors the intermediate keratin filaments (Figure 1.3.).

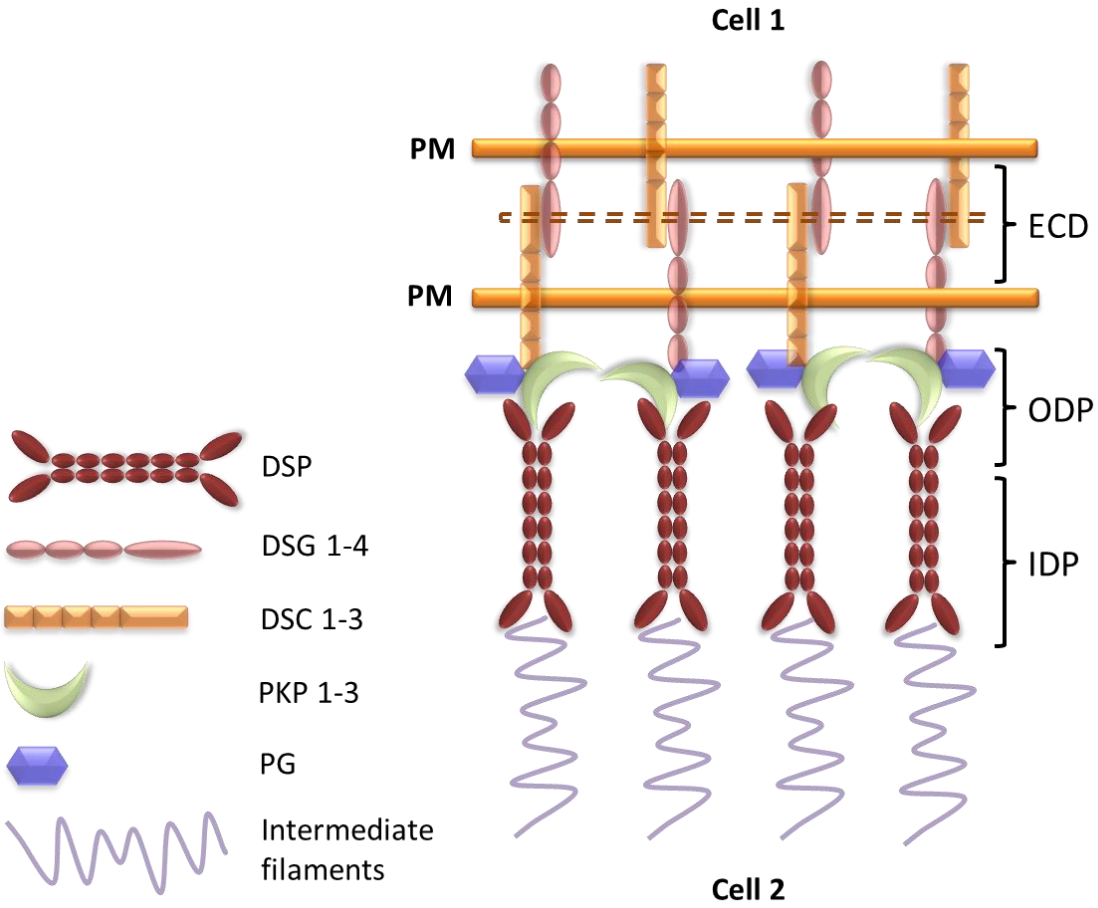

Figure 1.3. Structural organisation of the desmosomal complex. Schematic diagram of the desmosome with the relative localisation of desmosome-associated proteins, the cadherin family (desmogleins, in pink and desmocollins, in orange), the armadillo family (plakoglobin, in purple and plakophillins, in green), the plakin linker (desmoplakin, in dark red) and the intermediate filaments (in light purple) bound to desmoplakin. PM – plasma membrane; ECD – extracellular core domain; ODSP – outer dense plaque; IDSP – inner dense plaque.

1.1.5.2. Molecular composition of desmosome-associated proteins

1.1.5.2.1. The cadherin superfamily of intercellular linkers

The desmosomal cadherins belong to the larger cadherin superfamily which also includes T-cadherin, FAT family cadherins (Angst *et al*., 2001), seven pass transmembrane cadherins, proto-cadherins and classic cadherins, all sharing an approximately 110 amino acid motif involved in adhesion and calcium binding (Takeichi, 1977, Takeichi, 1990).

Desmogleins (DSGs) and desmocollins (DSCs) are the transmembrane components that bridge adjacent cells and are embedded in the cytoplasmic plaques, forming the dense extracellular midline seen in mature desmosomes. They share 30% amino acid identity between each other and with classical cadherins (Garrod *et al*., 2002), with *DSC* genes being more closely related to the classical cadherins than they are to *DSGs* (Kljuic *et al*., 2004).

Structurally, the desmosomal cadherins are formed of five extracellular cadherin repeats (EC1-5) containing Ca^{2+}-binding sites and a cell-adhesion recognition (CAR) site (Tselepis *et al*., 1998, Runswick *et al*., 2001). A unique characteristic of all *DSC* genes is the alternative splicing which generates a complete DSCa form and a shorter DSCb form of the protein by the insertion of a mini-exon containing a stop codon, the shorter C-terminal domain being the only difference between the two isoforms (Collins *et al*., 1991). Desmogleins contain an extended 500 amino acid tail with not yet fully understood functions (Figure 1.4.).

Desmosomal cadherins show complex developmental and differentiation-specific patterns of expression (Holthofer *et al*., 2007), which suggests that desmosomes within different tissues are biochemically and functionally distinct. The precise role for the tissue-specific expression pattern of desmosomal cadherins is not fully understood, however manipulation of desmosomal cadherins expression suggests that tight regulation of their expression pattern is critical to tissue homeostasis (Bannon *et al*., 2001). Within the epidermis these genes are differentially expressed as keratinocytes undergo terminal differentiation (Kottke *et al*., 2006, Holthofer *et al*., 2007) as follows: DSG1 and DSC1 are strongly expressed in the granular and

spinous layers, their levels decreasing in the lower layers of the epidermis (King *et al*., 1995, Shimizu *et al*., 1995, North *et al*., 1996); DSG2 and DSC2 are expressed in all desmosome-bearing tissues, represent the predominant isoforms in simple epithelia (Legan *et al*., 1994, Schafer *et al*., 1996), and are mainly expressed in the basal layers of stratified epidermis (Garrod *et al*., 2002, North *et al*., 1996). DSG4 is primarily expressed in the hair follicle and is restricted to the more differentiated layers in stratified epithelia (Delva *et al*., 2009). DSGs 1, 3, and 4, and DSCs 1 and 3 are predominantly expressed in the epidermis, while DSG2 and DSC2 are highly expressed in the myocardium (Li and Radice, 2010) (Figure 1.5.).

Within the cornified layer of the epidermis (stratum corneum), desmosomes are modified into corneodesmosomes, structures which contain DSG1, DSC1 and corneodesmosin as their major extracellular constituents. The relative thickness of the stratum corneum is achieved by the controlled degradation of corneodesmosomes, any modifications at this level leading to severe barrier defects (Ishida-Yamamoto *et al*., 2011).

1.1.5.2.2. The armadillo family of proteins with multiple complex functions

PG together with the three known plakophilins PKP1-3 (Hatzfeld, 2007, Hatzfeld, 2005), all members of the armadillo family, are adaptor proteins with roles in facilitating the adhesion of DSP to keratin intermediate filaments, in regulating clustering of the desmosomal components, and in mediating important signal transduction pathways. PG is formed of 12 arm repeats that share 65% amino acid identity with β-catenin, the equivalent protein associated with adherens junctions. The central armadillo domain of PG interacts with DSP, which in turn tethers intermediate filaments to the desmosomal plaque (Figure 1.4.). PG can also translocate to adherens junctions and bind E-cadherin in the same manner as β-catenin, but its higher affinity for DSP may explain why PG and not β-catenin locates to desmosomes (Choi *et al*., 2009).

Both PKP1 and 2 exist in two isoforms, a shorter “a” form and a longer “b” form (Mertens *et al*., 1996, Schmidt *et al*., 1997), with the short “a” form more predominant and PKP1b form exclusive to the nucleus. The presence of PKP2 in the nucleus is regulated by the 14-3-3 protein and contributes to the RNA polymerase

III holoenzyme complex (Desai *et al*., 2009). The presence of a previously reported fourth PKP protein, in the desmosome and the adherens junctions, has since been questioned (Hofmann *et al*., 2009).

PKPs 1-3 share 50-55% sequence similarity with the arm domain of p120-catenin (Hatzfeld, 2007), another armadillo family protein. Based on structural analysis studies, PKPs contain 9 arm repeat domains (Choi and Weis, 2005), with 21 additional amino acids added to PKP1 and 44 amino acids added to PKP2. PKPs show tissue and differentiation specific patterns of expression similar to the desmosomal cadherins. It has been observed that while PKP3 shows expression throughout simple epithelia and all layers of stratified epithelia, apart from hepatocytes, PKP1 is mostly expressed in the suprabasal layers of stratified epithelia, and PKP2 expression extends to simple epithelia, lower layers of stratified epithelia and non-epithelial tissues such as lymph nodes and the cardiac muscle, where it is the only isoform (Heid *et al*., 1994, Mertens *et al*., 1996, Schmidt *et al*., 1997, Mertens *et al*., 1999, Bonne *et al*., 1999, Franke *et al*., 2007) (Figure 1.5.).

PKPs appear to play a role in the clustering of desmosomal proteins during the formation of desmosomes. The N-terminal head domain of PKP1 can associate with DSG1, PG, keratin and actin filaments, and ultimately with DSP through what appears to be a robust association which drives DSP recruitment to cell-cell junctions (Kowalczyk *et al*., 1999, Hatzfeld *et al*., 2000, Wahl, 2005, Hofmann *et al*., 2000). PKP3 interacts with the largest number of desmosomal proteins, including DSP, PG, DSG1-3, DSC3a and DSC3b, and DSC1a and DSC2a (Hatzfeld, 2007). PKP2 plays an important role in transport of DSP to the plasma membrane during desmosome assembly, but does so less efficiently than PKP1 (Green *et al*., 2010, Chen *et al*., 2002). The mechanism behind PKP1 and PKP3 mediated-desmosomal assembly is not yet fully determined, although it appears that PKP2 functions as a scaffold for PKC-α and regulates DSP association to the intermediate filaments (Godsel *et al*., 2010, Godsel *et al*., 2005, Bass-Zubek *et al*., 2008).

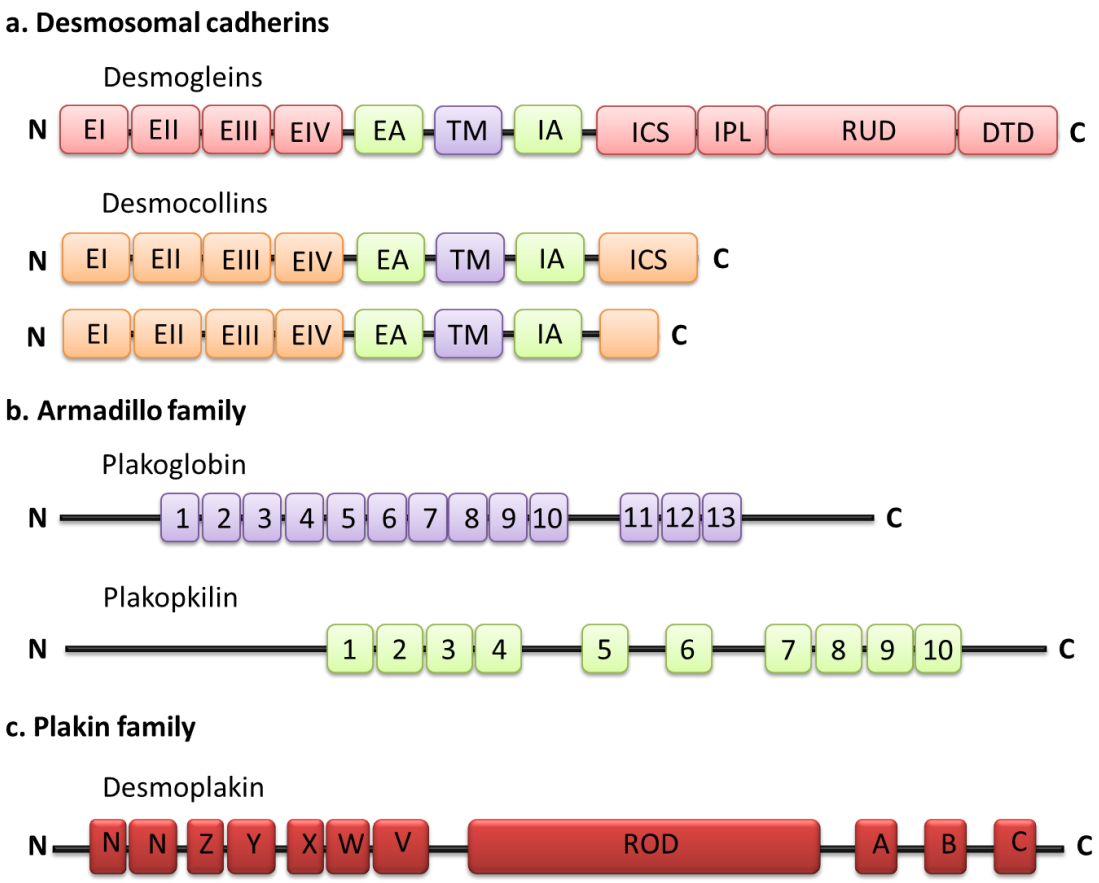

Figure 1.4. Structure of desmosome-associated proteins. (a) Similar to the classic cadherins, desmosomal cadherins are type I membrane molecules with extracellular calcium binding sites. The four members of the desmoglein subfamily (~160 kDa) are unique in having extended tails beyond the intracellular catenin-binding site (Coonrod *et al*., 2014). The three members of the desmocollin subfamilly (110–115 kDa) each have two splicing isoforms. The 'b' isoform lacks the ICS making it unable to bind plakoglobin. **(b)** The desmosomal armadillo family includes plakoglobin, and the plakophilins. Plakoglobin, functionally related to β-catenin, links the desmosomal cadherin tails to desmoplakin through binding sites, but is believed to engage in lateral interactions as well. Plakophilins, more related to p120, appear to have more restrictive binding sites than plakoglobin. **(c)** Desmoplakin is formed of three domains, a central α-helical coiled-coil ROD, flanked by globular C- and N-terminal domains, which interact with intermediate filaments and armadillo/cadherin family members. The N-terminus contains a series of predicted α-helical bundles designated NN, Z, Y, X, W and V, whereas the C-terminus contains the intermediate-filament-binding domain formed of homology units A, B and C (Adapted from Green and Gaudry, 2000).

1.1.5.2.3. The plakin linkers – tethers of intermediate filaments

DSP, the most abundant desmosomal protein, plays a key role as the linker between the plasma membrane and the intermediate filament complex (Delva *et al*., 2009). The protein is predicted to form homodimers through an α-helical coiled-coil rod domain which also interconnects a globular N-terminus domain, responsible for binding the arm proteins PG and PKPs, and a C-terminus domain, responsible for the attachment of intermediate filaments (Holthofer *et al*., 2007, Kowalczyk *et al*., 1994, Bornslaeger *et al*., 2001, Choi *et al*., 2002, Yin and Green, 2004) (Figure 1.4.). Until recently only two isoforms of DSP (DSP I and DSP II) have been known. As with the "a" and "b" forms of desmocollins, DSP I and II isoforms are produced as a result of alternative mRNA splicing, with DSP II the shorter isoform of the two. Both are widely expressed in numerous tissues, although DSP II is absent from the heart and from simple epithelia (Angst *et al*., 1990). A minor DSP isoform derived from DSP I, named DSP Iα, produced by the alternative splicing of DSP I mRNA has also been described, detectable in lower levels than the dominant isoforms, and presenting a similar tissue distribution (Cabral *et al*., 2010b).

By immunogold labelling of DSP, Franke *et al*. have observed that in normal heart muscle DSP is located in all plaques of the desmosome-like and fascia adherens-type junctions, with a very intense signal within the desmosome-like junctions (Franke *et al*., 2006). Several *in vivo* and *in vitro* studies support the importance of DSP in desmosome assembly and function, and show its pivotal role in the development of epidermis, neuro-epithelium, heart and blood vessels (Gallicano *et al*., 2001, Vasioukhin *et al*., 2001). In keratinocytes, DSP II appears to play a more significant role than DSP I, in maintaining robust adhesion, suggesting cell-type specific functions for the DSP isoforms (Cabral *et al*., 2012b) (Figure 1.5.).

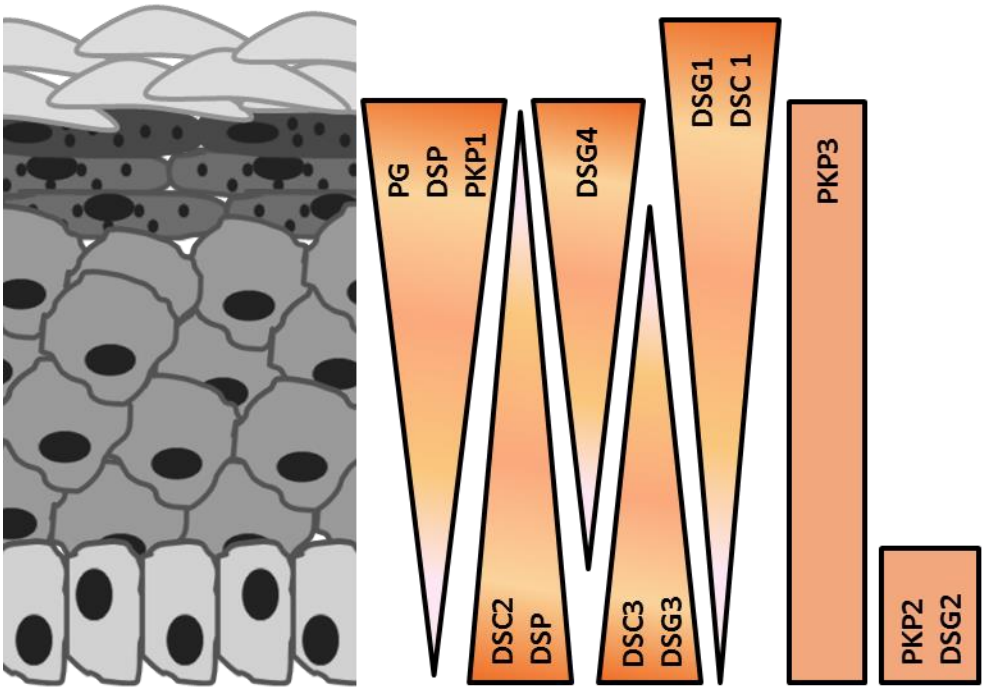

Figure 1.5. Desmosome-associated proteins in the epidermis. The figure illustrates the differential distribution and approximate expression levels of the desmosome-associated proteins in the human epidermis.

1.2. Modulation of desmosomal adhesion

Desmosomes are not just static structures that glue cells together; instead, they are very dynamic and adaptable complexes as shown by their ability to adopt different conformations with different adhesive affinities, suppressing pathways important for establishing cell polarity and determining the balance between proliferation and differentiation, all done through interactions with signalling cascades. Modulation of these structures is highlighted in pre-programmed processes such as apoptosis but also in malignant processes such as tumour invasion and metastasis. Desmosome regulation is ultimately the indirect regulator of downstream nuclear and signalling processes through regulation of subcellular distribution of desmosomal components.

The hyper-adhesiveness of desmosomes is regulated by the presence or absence of Ca^{2+}, PKC, proteolytic processing through ADAM proteins, EGFR expression levels, raft regulation and the yet unclear mechanism of the ubiquitin-proteasome system (UPS), all with a role in mediating desmosome assembly and function (Nekrasova and Green, 2013, Yin and Green, 2004, Stahley *et al*., 2014, Loffek *et al*., 2012, Blaydon *et al*., 2011a, Blaydon *et al*., 2011b).

1.2.1. Calcium-dependent modulation

During Ca^{2+} regulation the key players are DSGs and DSCs, required for strong cell-cell adhesion (Getsios *et al*., 2004), via their interaction with each other, across the intercellular space, in a homophilic and/or heterophilic manner. Via several binding motifs within their structure, DSGs and DSCs bind Ca^{2+} and assume a rigidified functional conformation (Pokutta and Weis, 2007), thereby increasing the level of adhesion between neighbouring cells and creating what has been described as the dense midline of desmosomes. In low-Ca^{2+} conditions (less than 0.5 mM) the desmosomal plaque components and membrane proteins are transported to the plasma membrane, together or in separate compartments, but when desmosomal assembly is triggered, cadherins and DSP complexes do not associate as in normal Ca^{2+} conditions and remain separated (Cirillo *et al*., 2010). It has been observed that during the early stages of desmosome formation the assembly can reverse between

the mature and young phases but ultimately desmosomes mature and can no longer be dissociated by calcium depletion (Watt *et al*., 1984), especially in stratified epithelia. Adhesion strength in cultured keratinocytes increases after 6 days in culture due to this phenomenon (Cirillo *et al*., 2010), in a similar way to intact epithelia *in vivo* (Garrod *et al*., 2005, Wallis *et al*., 2000). This is referred to as hyper-adhesion, and represents the result of high-affinity and stable adhesive binding of desmosomal components into mature structures. It has not been observed in adherens or tight junctions, making it specific to desmosomes and explaining the hyper-adhesive state of keratinocytes (Kimura *et al*., 2007).

There are various situations in which desmosomes switch from a Ca^{2+}-independent to a Ca^{2+}-dependent state. It has been observed that upon "wounding" of keratinocyte cell monolayers the desmosomes of cells situated at the edge of the "wound" lose their hyper-adhesiveness and become Ca^{2+}-dependent, permitting the cell motility required for wound re-epithelialisation (Wallis *et al*., 2000). In this case, protein kinase C-alpha (PKCα), a conventional PKC isoenzyme and serine-threonine kinase, localises to the dense plaque of wound-edge epidermal desmosomes, normally absent from hyperadhesive desmosomes.

Desmosomal proteins undergo both serine-threonine and tyrosine phosphorylation that regulate their fate and interactions with other proteins, and this is where PKC can play both positive and negative roles in desmosome assembly with protein phosphatase activity being a requirement for the final stages of desmosomal plaque formation (Yin and Green, 2004). The main focus of these studies has been PG as this desmosomal protein is regulated by all of the above processes. It appears that PG is more highly phosphorylated in the soluble non-junction pool therefore it is believed that phosphorylation regulates its fate during desmosome assembly (Pasdar *et al*., 1995).

While the passage of desmosomes from a less adhesive to a hyper-adhesive state is Ca^{2+}-dependent, O-glycosylation of the desmosomal plaque component PG has also been shown to augment desmosomal adhesion in keratinocytes (Hu *et al*., 2006).

Activation of PKCα has been reported to stimulate desmosome formation under low-Ca^{2+} conditions and in the absence of adherens junctions (Green *et al*., 2010),

by regulating the availability of DSP for desmosome assembly (Bass-Zubek *et al*., 2008). A recent report by Kroger *et al.*, showed that cells lacking all keratin intermediate filaments exhibited higher PKC-dependent DSP phosphorylation levels, resulting in an increase in desmosome dynamics and internalisation (Kroger *et al*., 2013).

With regards to desmosomal cadherins, the levels of DSG1 were found to be regulated by two Ca^{2+}-independent 'novel' PKC isoforms, increased by the differentiation-promoting PKCδ and decreased by the growth-promoting PKCε. The expression of DSG3 is also regulated by these isoenzymes, but also inhibited by PKCα (Szegedi *et al*., 2009). Kimura *et al*. have shown that there are other situations, such as mitotically active basal cells and during tumour invasion, when the transition from a Ca^{2+}-dependent to a Ca^{2+}-independent state happens with the induction of hyper-adhesion via modulation of PKCα signalling (Kimura *et al*., 2007).

More recent research studies indicate that intact membrane rafts and therefore cholesterol could be another mechanism of desmosome regulation. Membrane rafts are cholesterol-enriched membrane domains which have been shown to associate desmosomal proteins and release them during desmosomal assembly. Resnik *et al*. have shown that a reduction in cholesterol is equivalent to DSC2 release from the rafts and decrease in cell-cell adhesion (Resnik *et al*., 2011). These findings are supported by a more recent study by Stahley *et al*., which has added DSG3 to the other desmosomal proteins, DSC2, DSG2, PG and DSP, previously observed to be raft associated, and therefore suggest that their integration and assembly into desmosomes is cholesterol regulated (Stahley *et al*., 2014, Resnik *et al*., 2011, Nava *et al*., 2007, Brennan *et al*., 2012).

1.2.2. Apoptotic modulation

During apoptosis, between the substrates targeted by effector caspases, a number of proteins involved in the regulation of cell contacts and of the cytoskeleton such as focal adhesion kinase (Crouch *et al*., 1996), E-cadherin (Schmeiser and Grand, 1999), PG (Brancolini *et al*., 1998), fodrin (Janicke *et al*., 1998), Gas2 (Brancolini *et al*., 1995) and β-catenin (Brancolini *et al*., 1998) were identified. In addition to

previously published research showing that PG is cleaved by caspase3 during apoptosis, recent biochemical and cell biological studies have shown that DSGs and DSCs are also specifically cleaved. These studies suggest that the cytoplasmic tail of human DSG3 is cleaved by caspases at two distinct sites and that the extracellular domain is released from the cell surface by metalloproteinases. Inhibition studies have shown that the DSG3 release during apoptosis is different to the release of the extracellular domain of E-cadherin. Weiske *et al*., have also shown that PKP1 and both isoforms of DSP are being cleaved by caspases during apoptosis, this process leading to the disruption of the desmosomal structure and thus facilitating apoptotic cell-specific changes (Weiske *et al*., 2001).

1.2.3. Desmosomal dysregulation promotes cancer

Desmosome regulation was observed to play a role in cancer progression, with various desmosome-associated proteins dysregulated in a variety of tumours. Numerous models have been used to provide a clarification for how desmosome regulation promotes tumour metastasis and invasion, with little success as these studies produced contradictory and confusing results. Some cancers, such as head and neck, prostate, lung and some skin cancers present with an overexpression of desmosomal proteins DSG2, DSG3 and PKP3, in comparison to normal tissue (Brennan and Mahoney, 2009, Chen *et al*., 2007, Furukawa *et al*., 2005, Kurzen *et al*., 2003, Breuninger *et al*., 2010). In contrast, the down-regulation of other desmosomal components, DSG1-3, DSC2, DSC3, PG, PKP1-3 and DSP was observed in the metastatic progression and development of other human cancers such as breast, bladder, prostate, cervical and endometrial, head and neck, gastric, colorectal and some skin cancers (Dusek and Attardi, 2011), and in some instances no changes in expression of desmosome-associated proteins was noted (Kurzen *et al*., 2003).

The most studied model is based on the release of specific desmosomal components, such as PG which can display oncogenic activity through its β-catenin-like signalling activity. It is believed that PG replaces β-catenin in adherens junctions thus freeing β-catenin which can stimulate the transcription of Wnt target genes, including oncogenic targets such as CCDN1 (cyclin D1) (Conacci-Sorrell *et al*., 2002). In

addition to this, PG can transit to the nucleus and directly activate the oncogenic β-catenin-LEF/TCF target genes or potentially stimulating the expression of uncharacterised targets which promote proliferation or transformation (Zhurinsky *et al*., 2000), while concomitantly inhibiting apoptosis by induction of Bcl-2, an anti-apoptotic protein (Hakimelahi *et al*., 2000). Recently, Chen *et al*. have shown in their *in vitro* studies that a PG-dependent mechanism can be activated by knockdown of *DSG3*, which led to translocation of PG to the nucleus and suppression of TCF/LEF transcriptional activity, thus leading to the inhibition of expression of c-myc, CCDN1 and MMP-7 target genes (Chen *et al*., 2013).

The nuclear localisation of PKPs in specific conditions suggests that these proteins could modulate gene expression and it has been shown that PKP2 can interact with β-catenin leading to increased β-catenin-TCF transcriptional activity; whether this process is direct or takes place through mediators it remains unknown (Sobolik-Delmaire *et al*., 2010). In addition PKP1 and PKP3 localise to certain cytoplasmic compartments where they can interact with translation-initiation factors and stimulate translation, the implication of PKPs in tumourigenesis being supported by the observed redistribution of these proteins from the plasma membrane to the cytoplasm (Wolf and Hatzfeld, 2010). It is believed that the simple loss of the hyper-adhesive strength that is unique to desmosomes may contribute to cancer progression by releasing a barrier to invasion and metastasis (Dusek and Attardi, 2011). Similarly to *in vivo* observations, several *in vitro* studies have reported conflicting results with regards to a clear mechanism behind metastatic proliferation, apoptosis and invasion, and whether this mechanism is dependent on the up-regulation or down-regulation of desmosomal proteins (Dusek and Attardi, 2011).

Another desmosome-related protein associated with cancer is PERP (p53 apoptosis effector related to PMP-22), a p53/p63 regulated membrane protein, required for desmosome assembly. Initially identified as a transcriptional target of the p53 tumour suppressor, upregulated during apoptosis, and subsequently seen as a target of p63, promoting intercellular adhesion and preserving epithelial integrity (Attardi *et al*., 2000, Ihrie *et al*., 2005). Mouse studies have shown that mice with *Perp* knockout or LOF mutations, exposed to UVB light have an increased tendency

to develop squamous cell carcinomas (SCCs), *Perp*-ablation leading to both tumour initiation and progression in various types of tumours (Beaudry *et al*., 2010b, Beaudry *et al*., 2010a). Moreover, *Perp*-deficient tumours show a significant down-regulation of desmosomal components, while adherens junctions remain intact, suggesting a specific role for desmosomes in tumourigenesis. These observations were confirmed in human SCCs, and suggest a clear implication of *Perp,* as a critical mediator of p53 tumour suppressor, in SCC development (Beaudry *et al*., 2010b).

1.2.4. Regulation of desmosomal adhesion through proteases and their inhibitors

Proteases are key factors in orderly processes such as desquamation and regulation of the skin's barrier function. On the basis of their catalytic domain, proteases were classified into aspartate-, cysteine-, glutamate-, metallo-, serine-, and threonine proteases. Particularly, serine proteases (SPs) contribute to epidermal permeability barrier homeostasis, as acute barrier disruption increases SP activity in skin and inhibition by topical SP inhibitors accelerated recovery of barrier function (Meyer-Hoffert and Schroder, 2011).

Endogenous and exogenous proteases such as kallikreins, matriptase, caspases, cathepsins, and proteases derived from microorganisms are important in the desquamation of the stratum corneum and are able to regulate the activity of defence molecules in the human epidermis. Protease inhibitors such as LEKTI, elafin, SLPI, SERPINs and cystatins regulate their proteolytic activity and contribute to the integrity and protective barrier function of the skin. Changes in the proteolytic balance of the skin can result in inflammation, which leads to the typical clinical signs of redness, scaling, and itching (Meyer-Hoffert, 2009).

As two of the results chapters of this thesis are focused on exfoliative ichthyosis, an inherited skin disorder linked to mutations in *CSTA* encoding for cystatin A (Blaydon *et al*., 2011b), and on a novel clinical entity which we have named PLACK syndrome, linked to mutations in *CAST*, the gene encoding for calpastatin (Lin *et al*., 2015), the following introductory subsections will expand on these specific protease inhibitors and their target proteases.

1.2.4.1. Cysteine protease inhibitors of papain-like proteases

Cystatins are part of a large superfamily of cysteine protease inhibitors, also named class I cystatins, initially described as inhibitors of lysosomal cysteine proteases, and in recent years also reported to have a variety of other roles. Cystatins have been divided into four protein families, three families of inhibitory proteases and one family of enzymes with non-inhibitory function (Rawlings and Barrett, 1990). The three families with inhibitory functions are: family I, comprised of the mainly endogenous stefins A and B with one inhibitory domain, expressed in a variety of organisms and tissue types, stefin C discovered in bovine thymus (Turk *et al*., 1993) and stefin D identified in pigs (Lenarcic *et al*., 1996); family II, comprised of exogenous cystatins C, D, E/M, F, G, S, SN and SA (Abrahamson *et al*., 2003), the male reproductive tract cystatins 8 (CRES, cystatin-related epididymal spermatogenic protein), 9 (testatin), 11 and 12 (cystatin T), the bone marrow-derived cystatin-like molecule CLM (cystatin 13) and the secreted phosphoprotein ssp24 (cystatin 14) with one inhibitory domain (Keppler and Sierra, 2005), where cystatin C is expressed in a variety of tissues while the other cystatins are more tissue-specific (Magister and Kos, 2013), and family III, comprised of the so called L- and H-kininogens in a variety of species and T-kininogen only in rats (DeLa Cadena and Colman, 1991), intravascular inhibitors, with three inhibitory domains. The fourth non-inhibitory family consists of homologues of two cystatin-like domains, the human α-$_2$SH-glycoprotein (fetuin) and histidine-rich glycoprotein (Brown and Dziegielewska, 1997).

1.2.4.1.1. Cystatin A protease inhibitor – structure and function

Cystatin A (also known as stefin A, acid cysteine protease inhibitor, epidermal SH-protease inhibitor), a member of family I of cysteine protease inhibitors, isolated initially from rat skin, is the first cysteine inhibitor described in mammals (Jarvinen and Hopsu-Havu, 1975). With a selective expression pattern, CSTA is abundantly expressed in the cytoplasm of epithelial cells (Rinne *et al*., 1978, Rasanen *et al*., 1978, Rinne *et al*., 1980), dendritic reticulum cells of lymphoid tissue (Soderstrom *et al*., 1995), Hassall's corpuscles (Soderstrom *et al*., 1994), liver neutrophils (Davies and Barrett, 1984) and in thymic medullary cells (Soderstrom *et al*., 1994), suggesting a

key role in the first line defence mechanism against pathogens in various organs. CSTA is thought to play an important role in a variety of mechanisms, from skin protection against allergens such as dust mites (Kato *et al*., 2005) and cellular proliferation to regulating the activity of several target proteases in different types of cancers, including tumours of the breast (Kuopio *et al*., 1998), lung (Butler *et al*., 2011), prostate (Sinha *et al*., 1999), and SCCs of the head and neck (Strojan *et al*., 2000).

Structurally, CSTA is a 98-amino acid protein, with a molecular mass of approximately 11 kDa, sharing 58% identity with stefin B. The 3D structure of CSTA was studied for the first time in solution and through its interaction with cathepsin H, one of the target proteases of CSTA (Machleidt *et al*., 1983). Although it is believed that CSTA is less selective in its inhibitory function than the exogenous cystatins, some of the more studied target proteases of CSTA are cathepsins B, H, L, V and S, with the first three frequently dysregulated in a variety of cancers, appearing to facilitate tumour invasion and metastasis through cleavage of cell-to-cell junctions (Strojan *et al*., 2000).

The conformation of this inhibitor, initially suggested following a study on chicken CSTA, is formed of five stranded antiparallel β-sheets wrapped around a five turn α-helix with an additional C-terminal strand running along the convex side of the sheet (Bode *et al*., 1988). The N-terminal end and two β-hairpins form the edge of a wedge-shaped surface which binds into the active site cleft of the target proteases in what was called the "elephant trunk" model. Jenko *et al.* have looked at the crystal structure of CSTA in relation to cathepsin H and have confirmed the mode of interaction previously described. It appears that on binding, the N-terminal end of CSTA becomes like a hook which pushes away the mini-chain residues of cathepsin H, leading to structural changes on the surface of both proteins involved in the complex (Jenko *et al*., 2003), a mechanism confirmed for the interaction between CSTA with cathepsin B (Renko *et al*., 2010).

Some of the pathologic processes that CSTA has been linked with cover both disorders arisen due to a defective inhibitory function, the inhibition of the major dust mite allergens Der f 1 and Der p 1 (Kato *et al*., 2005), and its dysregulation in a

variety of cancers (Rivenbark and Coleman, 2009, Rinne, 2010), and also disorders arisen due to sequence variations in the *CSTA* gene, such as a polymorphism leading to the inflammatory condition atopic dermatitis (Vasilopoulos *et al*., 2007), the association with psoriasis (Vasilopoulos *et al*., 2008), loss-of-function mutations linked to exfoliative ichthyosis (Blaydon *et al*., 2011b, Moosbrugger-Martinz *et al*., 2014) and acral peeling skin syndrome (APSS) (Krunic *et al*., 2013).

Up to date the target proteases inhibited by CSTA, cathepsins B, H and L have only been described in relation to a variety of cancers through their role in the degradation of the ECM, facilitating the growth, invasion and metastasis of tumour cells, and also in tumour angiogenesis (Rivenbark and Coleman, 2009). Increased activity of cathepsins B, L and H is associated with a lower CSTA inhibitory activity in the majority of examined patients with breast neoplasms (Lah *et al*., 1992, Gabrijelcic *et al*., 1992) and in non-small-cell lung cancer patients (Leinonen *et al*., 2007). In contrast, Kuopio *et al*. have demonstrated that positive expression of CSTA in breast tumours is associated with a poor outcome, and that co-expression of CSTA with p53 in this type of cancers is associated with a high risk of death (Kuopio *et al*., 1998). An independent study has revealed that inhibition of cathepsin B *in vitro* reduced bone metastasis in breast cancer patients (Withana *et al*., 2012). Similarly, in the cytosol of patients suffering from head and neck carcinoma, the activities of cathepsins B and L correlated significantly with those of CSTA (Kos *et al*., 1995). Strojan *et al*. have observed that, in patients with SCC of the head and neck, the CSTA activity could predict both the tumour aggressiveness as well as the likelihood of disease recurrence (Strojan *et al*., 2011), with patients that present with low CSTA expression having a significantly higher recurrence rate than patients with high CSTA expression (Strojan *et al*., 2000). Two other studies looking at patients with SCCs have revealed that the immunohistochemical analysis of cathepsin L and CSTA is a very good indicator for an aspect of malignancy in human epidermal keratinocytes (Palungwachira *et al*., 2002) and overexpression of CSTA delayed the *in vivo* and *in vitro* cell growth and metastasis of oesophageal SCC (Li *et al*., 2005). The direct role of CSTA in various human neoplasms requires further study, as up to date studies have shown its implication in cell mobility, invasion and tumorigenic potential.

1.2.4.2. Calpastatin protease inhibitor and the target proteases

Calpastatin (CAST) is a ubiquitously expressed, specific endogenous protease inhibitor of the cysteine proteases calpains 1 and 2, existing in two types: tissue type and erythrocyte type, resulted from alternative splicing and proteolytic processing (Takano *et al*., 1991, Takano *et al*., 1993). Biochemical analysis of CAST has revealed that the 126 kDa structure is formed of a unique leader domain (L-domain) in the N-terminal end, with no inhibitory properties, and four homologous repetitive domains (domains 1-4) with the capacity to bind and inhibit several calpain molecules (Minobe *et al*., 2011). Each of the four inhibitory domains of CAST are structured into three subdomains A, B and C, with A and C responsible for binding to different domains of calpain and having inhibitory function only due to the presence of subdomain B, however increasing the inhibitory capacity of this subdomain. It has also been observed that the peptides of subdomain B have no inhibitory activity unless they are 13 amino acids or over, the increase in the number of amino acids of this subdomain being directly proportional with the inhibitory strength, suggesting the need of a large calpain interaction area. Also, as this subdomain has not been seen to interact with the active site of calpains, it is believed that it may bind to a domain of calpain only after calpain activation by Ca^{2+} (Wendt *et al*., 2004, Hanna *et al*., 2008, Moldoveanu *et al*., 2008).

A study by Kawasaki *et al*. has revealed two roles for CAST: a role in inhibiting the proteolytic activity of calpains through the interaction between the catalytic site of calpain and the inhibitory sequence of CAST, and a role in inhibiting the binding of calpains to the cell membrane through the interaction between the regulatory site of calpain and the regulatory inhibition site of CAST. Moreover, it appears that the modes of action of the two CAST sites do not overlap. Kawasaki *et al*. concluded that the regulation of calpain binding to the cell membrane is essential for the regulation of calpain activity (Kawasaki *et al*., 1993).

The target cysteine proteases of CAST, "conventional" calpains 1 and 2, initially named μ-calpain and m-calpain, based on the concentration of calcium required for their activation (Ando *et al*., 1988, Goll *et al*., 2003), are non-lysosomal, Ca^{2+}-activated neutral cysteine proteases with an intracellular localisation, expressed

ubiquitously. Crystal analysis of the calpain structure showed that both enzymes are heterodimers, sharing one 29 kDa light subunit to which another 83 kDa or 80 kDa heavy subunit is added for calpain 1 and 2 respectively, both proteases initially seen to cleave keratin filaments into small fragments (Ando *et al*., 1988).

CAST together with its target proteases have been named the calpain system, which controls a variety of cellular functions such as cytoskeletal remodelling, cell cycle progression, gene expression, apoptotic and necrotic cell death, ischemia formation and exocytosis (Hanna *et al*., 2008, Salehin *et al*., 2011).

Up to date the calpain system has been linked to numerous disorders, from its influence in the tumour formation and progression of various cancers such as skin, breast, renal cell, ovarian and prostate (Moretti *et al*., 2014), to CAST depletion and calpain 2 activation in Alzheimer's Disease (Rao *et al*., 2008), calpains 1 and 2 overexpression in Duchenne muscular dystrophy (Ueyama *et al*., 1998), autoantibodies targeting CAST in rheumatoid arthritis (Goldbach-Mansky *et al*., 2000), calpain regulation in Huntington's disease (Menzies *et al*., 2014) and a requirement for a balanced expression of calpain 1 and CAST in acute renal allograft rejection (Letavernier *et al*., 2011), to name a few. Also, calpains play a key role in myogenesis, especially in the early stages of this process, myoblast migration and fusion. It was observed that calpain activity increases significantly during fusion and that CAST inhibits myoblast migration and fusion (Barnoy *et al*., 1996, Barnoy *et al*., 2005, Cottin *et al*., 1994, Dedieu *et al*., 2004, Temm-Grove *et al*., 1999, Leloup *et al*., 2006). With regards to the skin, the calpain system has previously been linked with psoriasis due to autoantibodies targeted against CAST but also other autoimmune skin disorders, suggesting that CAST may play a role in the inflammation process associated with these disorders (Matsushita *et al*., 2005).

1.3. Acquired desmosome-linked disorders

The crucial role played by accurate desmosomal assembly and function in skin homeostasis, is also highlighted by autoimmune and infectious disorders and also through desmosome-linked cancers.

1.3.1. Autoimmune disorders

Pemphigus foliaceus (PF) and Pemphigus vulgaris (PV), a pair of potentially fatal autoimmune disorders, characterised by the loss of intercellular adhesion in keratinocytes (a process named acantholysis) together with blister formation, appear as a consequence of autoantibodies targeting a pair of desmosomal cadherins, DSG1 (in PF; (Ishii *et al*., 1997)) and DSG3 with or without DSG1 (in PV; (Amagai *et al*., 1991)). Independent studies have reported that in early-PV patients, presenting with mucosal lesions only, the autoantibodies are targeted only against DSG3, and that patients in the later disease stages, presenting with both skin and mucosal lesions, autoantibodies target both DSG1 and DSG3 (Ding *et al*., 1997), giving a more severe phenotype, reflective of the desmosomal cadherin expression patterns between skin and mucosal tissues (Shirakata *et al*., 1998).

These clinical differences between PF and PV patients were explained by the compensatory theory, which takes into consideration the difference in expression of DSG1 and DSG3 in the epidermis and mucosal tissues. While DSG1 is expressed in the upper layers of the epidermis with very low, if any, expression in mucosal tissues, DSG3 is expressed in the basal layers of the epidermis and is the main cadherin expressed in mucosal tissues. It has been suggested that in PF patients, autoantibodies targeting DSG1 disturb the cell-cell adhesion in the more superficial layers of the epidermis, generating the PF-characteristic superficial acantholysis and blistering, the more subtle phenotype being a result of DSG3 compensation for DSG1 in the basal layers of the skin and in mucosal tissues. On the contrary, in PV patients (mucous type), whose sera contains DSG3 autoantibodies, the blistering occurs mainly in the mucosal tissues, where DSG1 is expressed in very low levels and therefore cannot compensate for the lack of DSG3, and rarely causing blisters in the skin where DSG1 is expressed and can therefore compensate. This theory becomes evident in PV patients (muco-cutaneous type) whose sera contains autoantibodies for both DSG1 and DSG3, leading to severe epidermal and mucosal blistering due to severe dysregulation of intercellular adhesion in all layers of the epidermis, linked to loss of DSG1 and DSG3 (Mahoney *et al*., 1999, Amagai *et al*., 2006). Two independent theories were suggested in an attempt to explain the mechanism of autoimmune DSG3 antibodies in PV.

Initial studies have shown half-formed desmosomes covered with IgG-labelled particles (Iwatsuki *et al*., 1989, Shimizu *et al*., 2004), suggesting that PV autoantibodies targeting the N-terminal domain of DSG3 could interfere with the adhesive function of DSG3, directly leading to breakage of desmosomal connections (Mahoney *et al*., 1999, Sekiguchi *et al*., 2001, Futei *et al*., 2003, Stanley and Amagai, 2006). An *in vitro* study by Aoyama *et al*. has revealed that the use of IgG-labelled particles, in low calcium conditions, leads to attachment of these particles to half-desmosomes, and that upon switching to high-Ca^{2+} these desmosomes couple to form complete-desmosomes (Aoyama *et al*., 2010). These results suggest that binding of the PV-specific anti-DSG3 autoantibodies could not split the desmosome as the forces are not strong enough to cause the splitting, also supported by a *Dsg3*-deficient knockout mouse that formed nearly structurally-intact desmosomes, as observed in independent studies (Koch *et al*., 1997, Chernyavsky *et al*., 2007).

The second theory suggests that anti-DSG3 autoantibodies bind to DSG3 prior to the assembly of DSG3 into desmosomes, and thus triggering a mechanism of endocytosis of the autoimmune complexes (Calkins *et al*., 2006, Delva *et al*., 2008, Sato *et al*., 2000, Mao *et al*., 2009). Oktarina *et al*. have used double staining to show that in skin biopsies from PV patients only DSG3 co-localised with IgG antibodies and not DSG1, suggesting that DSG3 becomes sequestered from desmosomes leaving only DSG1, thus leading to disturbed desmosome assembly and DSG3-depleted desmosomes (Oktarina *et al*., 2011). All these observations support the non-assembly and depletion hypothesis, by which the compromised function of PV-affected desmosomes, with an insufficient amount of DSG3, are being split by external factors, such as mechanical stress (Aoyama *et al*., 2010, Amagai, 2010, Kitajima, 2013).

1.3.2. Infectious diseases

Bullous impetigo, and its generalised form Staphylococcal Scalded Skin Syndrome (SSSS), are two infectious disorders mostly affecting children under the age of 6 and immuno-compromised adults (Amagai, 2010), characterized by severe blistering as a result of keratinocyte acantholysis. This condition is a result of exfoliative toxins (ETs), unique serine proteases that show lock and key specificity to the desmosomal

cadherin DSG1, and not the closely related DSG3. These peptide toxins are produced by some strains of pathogenic *Staphylococcus aureus* bacteria (Amagai *et al*., 2000, Amagai *et al*., 2002). The three known ETs affecting humans, ETA, ETB and ETD, use Ca^{2+} to cleave a single peptide bond at a Ca^{2+}-binding site within the extracellular domain of DSG1, thus removing residues 1-381 of the DSG1 ectodomain, producing a truncated protein which in turn disrupts keratinocyte adhesion leading to formation of blisters (Hanakawa *et al*., 2003). The severity of the phenotype is reflected by the location and depth of the blisters, and resembles characteristics seen in PF (see section 1.3.1.), most likely as a result of the same compensatory theory, by which DSG3 can only compensate if expressed in the areas where DSG1 is affected. Amagai *et al*. have shown that by injecting neonatal mice with PF IgGs or ET, the mice developed blisters with essentially the same histology, suggesting that the two disorders may share a similar mechanism of action targeting DSG1, thus supporting the compensatory theory. In the same study Amagai *et al*. have demonstrated that DSG1 expression was significantly affected in the suprabasal layers of neonatal mice after incubation with ETA toxin for an hour. Furthermore, the direct proteolysis of DSG1 by ETA toxin was demonstrated by incubating mouse and human soluble recombinant forms of the extracellular domains of DSG1 and DSG3 with ETA toxin, which cleaved both the human and mouse recombinant forms of DSG1 in a dose-dependent manner (Amagai, 2010). These studies taken together suggest that cleavage of the N-terminal domain of DSG1 is enough to induce epidermal blister formation (Nishifuji *et al*., 2010).

1.4. Inherited cardio-cutaneous disorders in humans and mouse models

The complexity and incomplete understanding of how desmosomal components interact with each other and with other compartments in a cell-type and differentiation-dependent manner is reflected by the wide range of genetic disorders arising from mutations in desmosomal genes (Table 1.1.). The large number of publications reporting various mutations affecting all desmosomal genes highlight the phenotypic heterogeneity behind these conditions, different mutations resulting in similar cutaneous disorders with or without cardiac and hair

implications, named generically cardio-cutaneous disorders (Bolling and Jonkman, 2009). *In vivo* mouse models are also being used to decipher the disease mechanisms behind these inherited disorders.

A large number of mutations in genes encoding for desmosome-associated proteins and interacting partners were reported to date (Al-Jassar *et al*., 2013), leading to disorders such as woolly hair with/without cardiac implications (Norgett *et al*., 2000, Simpson *et al*., 2009b), striate palmoplantar keratoderma (SPPK) (Simpson *et al*., 2009b) and hypotrichosis (Kljuic *et al*., 2003a).

1.4.1. Human disorders associated to mutations in Armadillo proteins

Twelve mutations in *PKP1* reported to date, arising from missense and nonsense mutations to splice-site and compound heterozygous changes, appear to result in phenotypes ranging from skin fragility to severe autosomal recessive ectodermal dysplasia, including peri-oral cracking and inflammation, scant hair, reduced sweating and astigmatism (McGrath *et al*., 1997, Boyce *et al*., 2012, Hernandez-Martin *et al*., 2013, Pieperhoff *et al*., 2010, Tanaka *et al*., 2009, Zheng *et al*., 2005, Ersoy-Evans *et al*., 2006). *PKP2* mutations are a major genetic cause of non-syndromic autosomal dominant ARVC (Gerull *et al*., 2004).

With regards to the armadillo family member PG, the first human genetic studies in individuals from the Greek Island of Naxos, affected with an autosomal recessive condition known today as "Naxos Disease", clinically characterised by ARVC, woolly hair and mild epidermolytic PPK, have revealed homozygous truncating mutations in *JUP*, the gene encoding for PG, as responsible for this disorder (McKoy *et al*., 2000, Protonotarios and Tsatsopoulou, 2004, Delmar and McKenna, 2010). In two other independent studies, Erken *et al*. have described a recessive missense mutation in *JUP* in a patient presenting with PPK and total alopecia with a cardiac phenotype (Erken *et al*., 2011), while Pigors *et al*. reported a lethal phenotype caused by a homozygous nonsense mutation in JUP leading to severe congenital skin fragility, generalized epidermolysis, massive transcutaneous fluid loss and no apparent cardiac dysfunction, due to a complete loss of PG in patient skin, leading to fewer desmosomes and no adhesion structures between keratinocytes (Pigors *et al*.,

2011). The complexity of the disease mechanisms behind these disorders is highlighted by yet another report of loss-of-function *JUP* mutations linked to a recessive syndrome of skin fragility, diffuse PPK and woolly hair with no signs of ARVC (Cabral *et al*., 2010a), leading to little or no expression of PG.

1.4.1.1. Armadillo mouse models

Pkp2-null mice studies have shown mid-gestational embryonic lethality caused by cardiac patterning defects and fragility of the myocardium (Grossmann *et al*., 2004), alongside retraction of intermediate filaments from the plasma membrane, thus demonstrating the importance of PKPs in DSP recruitment and intermediate filament tethering to desmosomes (Delva *et al*., 2009). Despite no disease-causing mutations reported, to our knowledge, in humans for *PKP3*, ablation of this isoform in mice results in defective hair follicle morphogenesis, increased keratinocyte proliferation and DSP mislocalisation, leading to susceptibility to dermatitis and secondary alopecia (Sklyarova *et al*., 2008).

The key role for PG in desmosome assembly has been demonstrated by knockout studies in mice, which show acantholysis, indicative of compromised desmosome function, and are lethal due to fragility of myocardium (Bierkamp *et al*., 1996, Acehan *et al*., 2008). In some cases mouse pups were born but presented epidermal fragility, heart defects and died shortly after birth (Bierkamp *et al*., 1996, Ruiz *et al*., 1996). Recently, Li *et al*. created an epidermal conditional *Jup*-knockout mouse with a skin phenotype characterised by perturbed cell proliferation, apoptosis, differentiation and compromised immune defence (Li *et al*., 2012).

1.4.2. Desmoplakin mutations in cardio-cutaneous disorders

DSP is the most abundant component of the desmosomal complex and a variety of genetic disorders are associated with mutations in this gene, resulting in conditions with varying degrees of severity (Lai Cheong *et al*., 2005). The first reported link between *DSP* mutations and human skin disease was in association with autosomal dominant SPPK, characterised by a longitudinal pattern of hyperkeratosis, the loss-of-function mutations suggesting that the disease mechanism was haploinsufficiency and that dosage of DSP was critical in the stressed areas of the

skin such as the palm and sole (Armstrong *et al*., 1999). In addition, the first recessive *DSP* mutation was identified in Ecuadorian families with Carvajal syndrome, an ARVC variant which presents with dilated cardiomyopathy, accompanied by woolly hair and SPPK, but also with hyperkeratosis at other stress sites in the skin including the flexure. The homozygous mutation truncates the DSP protein leading to the loss of a portion of the IF-binding site, again leading to loss of cell adhesion and a collapsed IF network (Norgett *et al*., 2000, Huen *et al*., 2002).

Moreover, a significant number of genetic *DSP*-associated conditions known as cardio-cutaneous disorders have been reported, presenting with varied degrees of severity. A homozygous mutation, identified by Uzumcu *et al*., leads to complete absence of DSP I, but normal levels of DSP II, the loss of DSP I being associated with autosomal recessive mild epidermolytic PPK, woolly hair and aggressive ARVC, leading to severe ventricular dysfunction and associated arrhythmia (Uzumcu *et al*., 2006). An example of DSP-compound heterozygosity is the identification of an N-terminal missense mutation and a C-terminal nonsense mutation leading to severe keratoderma, skin fragility and woolly hair, or alopecia with or without cardiac involvement (Asimaki *et al*., 2007, Whittock *et al*., 2002). Another variation of the cardio-cutaneous disorders in association with woolly hair and tooth agenesis, was reported by Norgett *et al*. in a patient with a 30 bp insertion in the *DSP* gene (Norgett *et al*., 2006, Chalabreysse *et al*., 2011, Boule *et al*., 2012).

Alongside *DSP* mutations linked to cardio-cutaneous disorders, a number of cutaneous conditions with and without hair implications have also been reported. A heterozygous mutation which truncated the C-terminus of DSP leads to severe acantholytic epidermolysis bullosa, a lethal disorder characterised by complete alopecia, neonatal teeth, nail loss and death due to transcutaneous fluid loss as a result of extensive skin erosion (Jonkman *et al*., 2005). Furthermore, dominant *DSP* mutations have also been reported linked to non-syndromic ARVC but no obvious cutaneous phenotype (Rampazzo *et al*., 2002, Norman *et al*., 2005).

1.4.2.1. Desmoplakin mouse models

All previous studies on *Dsp* knockout mice confirm the lethality of this model in early embryonic stages, presumably due to loss of integrity of the embryonic ectoderm,

as a result of a significant reduction in the number of desmosomes coupled with a disrupted IF network and lack of keratin IF attachment in the remaining desmosomes (Gallicano *et al*., 1998, Vasioukhin *et al*., 2001).

1.4.3. Inherited cadherin-linked disorders

The first linkage of human disease to mutations in desmosomal cadherins came from the autosomal dominant skin disorder SPPK, linked to *DSG1* haploinsufficiency mutations (Rickman *et al*., 1999, Kljuic *et al*., 2003b, Amagai and Stanley, 2012). Recently, two homozygous variations for these loss-of-function *DSG1* mutations underlie a syndrome characterised by severe dermatitis, allergies and metabolic wasting (SAM) (Samuelov *et al*., 2013). A number of monogenic human disorders have also been linked to mutations in desmosomal cadherins (Brooke *et al*., 2012), such as dominant *DSC2* and *DSG2* associated with non-syndromic ARVC (Syrris *et al*., 2006, Pilichou *et al*., 2006). Moreover, a variety of *DSG4* mutations ranging from frameshift, splice-site, missense and nonsense are responsible for the autosomal recessive condition Monilethrix and for the hair-follicle differentiation-deficient phenotype known as hypotrichosis (Zlotogorski *et al*., 2006, Schaffer *et al*., 2006, Shimomura *et al*., 2006). DSC3 is another desmosomal gene associated with hypotrichosis, where homozygous nonsense mutations resulted in large skin vesicles filled with watery fluid with sparse and fragile hair on the scalp and absent eyebrows and eyelashes (Ayub *et al*., 2009). It has been observed that the impact level of *DSG1* and *DSG4* mutations in the skin is proportional to their expression profiles.

1.4.3.1. Cadherin mouse models

Knockout mouse models have shown that the lack of Dsg2 and Dsc3 result in early embryonic lethality, while Dsg2 deficiency leads to defects in embryonic stem-cell viability and proliferation (Desai *et al*., 2009) Dsc3-deficient mice are lethal in the very early embryonic stage, highlighting its importance in desmosomal assembly. Despite of the lack of disease-causing mutations being identified in *DSG3* and *DSC1* in humans, a *Dsg3*-knockout mouse presented with hair loss and loss of epithelial integrity (Koch *et al*., 1997), while the Dsc1 deficient mice causes defects of the skin

which become more apparent 2 days after birth, and later on develop into localised lesions and epidermal fragility with localised hair loss (Chidgey *et al*., 2001). Mutations leading to Dsg4 deficiency present with a lanceolate hair phenotype, characterised by sparse, fragile, broken hair shafts, follicular dystrophy and ichthyosiform dermatitis (Jahoda *et al*., 2004, Bazzi *et al*., 2005).

Gene	Inheritance	Disorder
DSP	Dominant	ARVC alone (Rampazzo *et al*., 2002, Norman *et al*., 2005)
		SPPK (Armstrong *et al*., 1999)
		PPK, woolly hair & ARVC (Norgett *et al*., 2006)
	Recessive	SPPK, woolly hair & ARVC (Carvajal syndrome) (Norgett *et al*., 2000, Alcalai *et al*., 2003)
		Skin fragility & woolly hair (SFWHS) (Whittock *et al*., 2002)
		Lethal acantholytic epidermolysis bullosa (Jonkman *et al*., 2005)
		Naxos-like disease affecting DSP I only (Uzumcu *et al*., 2006)
JUP	Dominant	ARVC alone (Asimaki *et al*., 2007)
	Recessive	Focal and diffuse PPK & woolly hair (Cabral *et al*., 2010a)
		ARVC, PPK & total alopecia (Erken *et al*., 2011)
		Lethal acantholytic epidermolysis bullosa (Pigors *et al*., 2011)
		PPK, woolly hair & ARVC (Naxos disease) (McKoy *et al*., 2000)
PKP1	Recessive	Ectodermal dysplasia/Skin fragility syndrome & ARVC (McGrath *et al*., 1997)
PKP2	Dominant	ARVC alone (Gerull *et al*., 2004)
	Recessive	ARVC alone (Awad *et al*., 2006)
PKP3	No mutations in humans to date	
DSG1	Recessive	SPPK (Rickman *et al*., 1999)

Gene	Inheritance	Disorder
		PPK, Hypotrychosis & hyper-IgE (EPKHE) (Samuelov *et al*., 2013)
DSG2	Dominant	ARVC alone (Pilichou *et al*., 2006)
	Recessive	ARVC alone (Syrris *et al*., 2007)
DSG3	No mutations in humans to date	
DSG4	Recessive	Hypotrichosis (Kljuic *et al*., 2003a)
		Monilethrix-like Hypotrichosis (Shimomura *et al*., 2006)
DSC1	No mutations in humans to date	
DSC2	Recessive	ARVC alone (Syrris *et al*., 2006, Heuser *et al*., 2006)
		ARVC, PPK & woolly hair (Simpson *et al*., 2009b)
DSC3	Recessive	Hypotrichosis with skin vesicles (Ayub *et al*., 2009)

Table 1.1. Inherited cardio-cutaneous disorders with/without hair association, linked to mutations in genes encoding for desmosome-associated proteins (adapted from Nitoiu *et al*., 2014).

1.5. Hypotheses of this study

Two major hypotheses constitute the basis of this project and together they look at the role desmosome homeostasis plays in epidermal integrity, directly though mutations in desmosome-associated proteins and indirectly through mutations in protease inhibitors, ultimately targeting desmosome regulation.

The first investigations were based on a cohort of patients with non-syndromic ARVC, seen both in the UK and New Zealand. Based on the large number of publications reporting mutations in genes encoding for proteins specific to the cardiac desmosome linked to heart disorders, we suspected that our patients would also present mutations in genes encoding for the desmosome-associated proteins, DSP, PG, PKP2, DSC2 and DSG2 (Brooke *et al*., 2012, Nitoiu *et al*., 2014). Additionally, patients with acral peeling skin syndrome, hypotrichosis and hypotrichosis with PPK were also studied. As it has previously been shown that different desmosome-associated protein isoforms may have different functions within the desmosome, it is expected that the identified mutations will affect different aspects of keratinocyte and cardiomyocyte adhesion, differentiation and/or signalling (Cabral *et al*., 2012b). A number of molecular techniques were used in the identification of mutations including the application of two high throughput sequencing platforms.

The second hypothesis is based on the identification of loss-of-function mutations in *CSTA* (Blaydon *et al*., 2011b) and *CAST* (Lin *et al*., 2015) genes encoding for the protease inhibitors cystatin A and calpastatin. *CSTA* LOF mutations are linked to exfoliative ichthyosis, a skin disorder characterised by dry, scaly skin over most of their body with nonerythematous peeling of skin on their palms and feet, exacerbated by moisture and minor trauma (Hatsell *et al*., 2003). Cystatin A is a cysteine protease inhibitor of cathepsins B, H and L, frequently dysregulated in a variety of cancers, facilitating tumour invasion and metastasis through cleavage of cell-to-cell junctions (Strojan *et al*., 2000). *CAST* LOF mutations lead to a new clinical entity, named PLACK syndrome characterised by peeling skin, leukonychia, acral punctate keratoses, cheilitis and knuckle pads with milia. Calpastatin is a specific protease inhibitor of calpains, intracellular cysteine proteases that require calcium or epidermal growth factor for their catalytic activity, and have been related to a

variety of processes such as the growth, migration and death of keratinocytes (Carragher and Frame, 2004).

Based on previous observations on the mechanisms of action of these protease inhibitors and their target proteases in other disorders, it is expected that the disease phenotypes observed are the result of the indirect regulation of epidermal homeostasis through the target proteases and perhaps through desmosome assembly and function.

The four sub-hypotheses addressed in this thesis are: (1) unrelated non-syndromic ARVC patients harbour disease-associated mutations in genes encoding for desmosome-associated proteins essential for cardiomyocyte adhesion and function; (2) independent patients with hypotrichosis and hypotrichosis with PPK, presenting with a similar clinical phenotype, harbour mutations in genes encoding for desmosome-associated proteins important in keratinocyte intercellular adhesion; (3) and (4) LOF mutations in *CSTA* and *CAST* lead to dysregulation of activity of their target proteases leading to disruption of epidermal homeostasis through dysregulation of desmosome assembly and/or activity.

1.6. Aims of this study

In order to test the first hypothesis, genetic analyses were undertaken:

1. Identification of desmosomal gene variants by custom capture array and HaloPlex targeted resequencing in patients with non-syndromic ARVC;
2. SNP array and exome capture analysis in patients with hypotrichosis and PPK;
3. Validation of variants and assignment to corresponding patients by PCR and conventional sequencing techniques;
4. Sanger sequencing analysis of *DSG4* and *CSTA* genes in patients with hypotrichosis and acral peeling skin syndrome.

In order to test the second hypothesis the following approaches were carried out:

1. Analysis of expression of CSTA, CSTA target proteases and CAST in skin (control and/or patient) and immortalised keratinocytes by immuno-microscopy and western blotting;
2. siRNA technology was used to mimic the LOF mutations in *CSTA* and *CAST*;
3. Observations on the effects of *CSTA* and *CAST* knockdown on intercellular adhesion and migration in keratinocyte monolayers by mechanical stretch, dispase-based dissociation assay and scratch assay;
4. Examination of cell death in *CAST* knockdown monolayers;
5. Analysis of desmosomal proteins following *CSTA* and *CAST* knockdown by immunocytochemistry and/or western blotting;
6. Examination of cathepsin expression in *CSTA* knockdown cell monolayers following mechanical stretch.

-Chapter 2-

Materials and Methods

2.1. Chemicals and tissue culture consumables

All chemicals were purchased form Sigma-Aldrich (St. Louis, MO) and all laboratory consumables were purchased from Fisher (Leicestershire, UK), unless otherwise stated.

2.2. Molecular Biology I – DNA and RNA methods

2.2.1. Patient samples

All patient samples, processed as described in the following chapters were received as blood or genomic DNA, are enumerated in Appendix Table A1., together with the country of origin and screening method. The projects presented in this thesis were approved by the Clinical Research Ethics Committee of the Peking University First Hospital, East London and City Health Authority Research Ethics Committee, Western Institutional Review Board, Health Research Council of New Zealand and the Institutional Review Board of the University Hospital of Munster, which all comply with all principles of the Helsinki Accord, and all patients enrolled gave their informed consent.

2.2.2. Extraction of DNA from blood

DNA was extracted from whole blood samples using the QIAamp DNA blood midi/maxi kit (QIAGEN) following the manufacturer's specifications. Briefly, 200 µl proteinase K was mixed with 1-2 ml blood. 2.4 ml buffer AL were added and mixed by inversion of the tube, followed by incubation for 2 min. The tubes were incubated at 70^0C for 10 min, and mixed by inversion 10 times with 2 ml 96-100% ethanol. The above mixture was added onto the QIAamp Midi column placed in a 15 ml centrifuge tube and spun at 3000 rpm for 3 min. The column was firstly washed with 2 ml of buffer AW1 followed by 2 ml buffer AW2 and spun between washes at 5000 rpm for 1 min after the AW1 buffer and 15 min after the AW2 buffer. 300 µl buffer AE were added onto the membrane of the Midi column and incubated at room temperature for 5 min followed by centrifugation at 5000 rpm for 2 min. DNA was resuspended in 200-300 µl distilled water by centrifugation at 5000 rpm for 3 min.

2.2.3. RNA isolation from cells

Total RNA was isolated from cultured cells at 80-90% confluency, using the RNeasy mini kit (Qiagen) according to the manufacturer's specifications. Briefly, cells were washed in phosphate buffered saline (PBS), and subsequently pelleted and lysed directly by the addition of disruption buffer. The lysates were transferred to mini columns and washed several times with several ethanol supplemented buffers in order to remove any residues. RNA was resuspended in 30 µl RNase-free water.

2.2.4. Nucleic acid quantification

Nucleic acid concentration was measured by NanoDrop ND-1000 Spectrophotometer (Thermo Fisher Scientific, Waltham, MA), according to the manufacturer's specifications. An assessment of nucleic acid purity was achieved by determining the ratios of spectrophotometric absorbance of the sample at 260/230nm and 260/280nm. Pure preparations of DNA and RNA have an A260/A280 ratio of approximately 1.8 and 2.0, respectively, and an A260/A230 ratio of approximately 2.2.

2.2.5. Polymerase Chain Reaction (PCR)

2.2.5.1. Primer design

All primers were purchased from Sigma-Aldrich (Appendix B). Specific primer pairs were designed either to PCR amplify or sequence the regions of interest, using Primer3 software (v.0.4.0). The oligonucleotide length varied from 18 to 24 bp depending on the GC content, which ranged from 45-65%. The annealing temperature (AT) for each primer pair was initially optimised using a gradient PCR with temperatures varying between 55^0-65^0C and the optimum AT was then used for further screening.

2.2.5.2. Genomic PCR for mutation screening

PCRs for the screening of all mutations described in this report were performed using either the GoTaq DNA Polimerase (Promega, UK) or the BioTaq PCR Kit (Bioline, UK). Briefly 25 µl PCR reaction comprised: 5 µl of 5x (2.5 µl of 10x) reaction

buffer, 1.5 µl of 25 mM (0.75 µl of 50 mM) $MgCl_2$, 0.25 µl of 5 U/µl of Taq enzyme; 200 µM of each nucleotide (Bioline, UK); 1 µM of each primer and 20-30 ng of template DNA. Reactions were incubated on a DNA engine Tetrad 2 Peltier Thermocycler (MJ Research) and the cycling conditions consisted of 95^0C for 5 min, followed by 35 cycles of 95^0C for 30 s, optimised primer annealing temperature for 30 s and 72^0C for 30 s, with a final extension step at 72^0C for 10 min and incubation at 4^0C for 10 min. In addition to patient DNA, control DNA was used to amplify desired sequences. Resulting PCR products were resolved on DNA agarose gel electrophoresis (as described in section 2.2.6.) or digested using restriction digest enzymes (as described in section 2.2.12.).

2.2.5.3. Reverse Transcription-PCR (RT-PCR)

RNA extracted as previously described in section 2.2.3. was used to make cDNA by RT-PCR. Briefly, 50 ng of RNA were added to 0.64 µl random hexamers (200 µM), 1 µl dNTPs (10 mM) made up to 12 µl final volume with dH_2O. The reactions were incubated at 65^0C for 5 min, chilled on ice and 4 µl of 5x first strand buffer, 2 µl of 0.1 M DTT and 1 µl RNase OUT (all Invitrogen, California, USA) were added to the reaction. The mixtures were then incubated at 25^0C for 2 min before 1 µl (200 units) of superscript II reverse transcriptase (RT) (Invitrogen) was added. A negative control was simultaneously prepared using RNase free water instead of the enzyme. Samples were incubated at 42^0C for 50 min, followed by heat inactivation at 70^0C for 15 min. One µl of cDNA was added to a standard PCR. The primer binding sites for RT-PCR primers are located in the exons and apart from cDNA amplification they would also amplify genomic DNA with short intronic sequences.

2.2.6. Agarose Gel Electrophoresis

Agarose gels were used to identify and separate PCR products and restriction digest fragments. For separation of fragments shorter than 800 bp, 1.5% (w/v) agarose (Bioline, London, UK) gels were prepared. Briefly, the agarose was melted in the appropriate volume of Tris-Borate-EDTA buffer and 0.5 µg/ml of ethidium bromide or 10 µl of 10,000x PAGE GelGreen (Biotium) were added to the solution. The clear mixture was poured into a gel tray with a suitable comb to form the sample wells,

and left to solidify. The gel was flooded with TBE in an electrophoresis tank. For detection of fragments longer than 800 bp, 1% (w/v) agarose gels were prepared in a similar way. DNA samples were mixed with 6 x Orange G DNA loading buffer and loaded on the gel alongside a 1 Kb Plus DNA ladder (10% (v/v) (Invitrogen), 16% (v/v) loading buffer). Samples were electrophoresed at a constant voltage of 80-120 V. DNA was visualised and photographed under UV transillumination (MultiImage Light Cabinet, Alpha Innotech Corporation; pictures printed on Sony P-D890).

2.2.7. Sanger Sequencing

Sequencing was performed using the BigDye Terminator v3.1 Cycle Sequencing Kit (Applied Biosystems, Foster City, CA). The optimal amount of PCR product (0.5-3 µl) was incubated with 6 µl ExoSAP-IT (Affymetrix) at 37^0C for 45 min followed by 80^0C for 15 min and 4^0C for 5 min; this enzymatic reaction eliminated any unincorporated primers and dNTPs. Clean sequences were then added to a reaction containing 1 µl of BigDye® Terminator Master mix v3.1, 3 µl of better buffer (Microzone, Ottawa, Canada), 1 µl of 10 µM specific forward or reverse primer and ddH_2O up to a final volume of 11.5 µl. Cycling conditions consisted of 25 cycles at 96^0C for 30 s, 58^0C for 15 s, 60^0C for 1 min, followed by a final incubation at 4^0C for 10 min.

The reaction products were precipitated with ethanol and EDTA. Briefly, 2.5 µl of 125 mM EDTA and 30 µl of ice cold absolute ethanol were added to the sequencing reaction and incubated on ice for 10 min. The mixture was centrifuged at 4000 rpm at 4^0C for 20 min; the pellet was washed with 125 µl 70% ethanol and incubated on ice for another 2 min, then centrifuged for 5 min at 4000 rpm. Precipitated DNA was air dried at room temperature (RT) or on the hot block at 62^0C for 10 s. Precipitated products were resuspended in 10 µl HiDi formamide (Sigma-Aldrich, UK), incubated at 95^0C for 3 min and on ice for 3 min, centrifuged for 2 min to remove any air bubbles and loaded on the ABI Prism 3130*xl* Genetic Analyser (Applied Biosystems, Life Technologies, USA). Traces were visualised using the Chromas LITE v 2.01 software (Free software from Technelysium Pty Ltd). The DSP plasmids obtained following site-directed mutagenesis were sequenced using the Sanger sequencing service offered by Source BioScience (Source BioScience LifeSciences, UK).

2.2.8. Capture array

For this experiment a customised 385K Sequence Capture Array (NimbleGen, Roche) was designed. All enzymes and reagents used for this procedure were purchased from New England Biolabs (NEB, UK) unless otherwise stated. Adapters and Primers used in the final reaction were custom made by Sigma-Aldrich. The manufacturer's protocol was used with a few modifications described below.

2.2.8.1. Quant-iT PicoGreen DNA quantification

DNA was quantified using the Quant-iT PicoGreen dsDNA kit (Invitrogen) following the manufacturer's instructions, and was run on the FLUOstar OPTIMA fluorescence plate reader (BMG Labtech).

2.2.8.2. Preparing the DNA pool

Equal amounts of genomic DNA from all patients were pooled to a final DNA concentration of 20 µg which was split into 4 lo-bind tubes. ddH2O was added up to a final volume of 100 µl. DNA was fragmented using the Bioruptor UCD-200 (Life Technologies) at 4^0C for 10 min on high, this step was repeated 3 times, replacing the ice and spinning tubes after each 10 min burst. Size was confirmed by running 1 µl of each DNA pool on a Bioanalyzer 7500 chip (Agilent Technologies), using the Agilent 2100 Bioanalyzer (Agilent Technologies), following the manufacturer's specifications. The 4 samples were then cleaned using the QIAquick PCR purification kit (Qiagen, UK), and each sample was eluted in 30 µl of buffer EB into new lo-bind tubes.

The end repair, adenylation of 3' ends, ligation of adapters and SPRI bead (Invitrogen) purification were performed as per manufacturer's specifications. After the end repair and adenylation of 3' ends reactions the samples were purified using the QIAquick PCR purification kit; 1.2 µl of each sample were kept before each purification and run on the Bioanalyzer 7500 chip. After the final purification using AMPure XP beads (Beckman Coulter), sample concentration was read on the NanoDrop. Only 5 µg of DNA pool were needed to hybridise to the capture array. At this point DNA samples were stored at -20^0C.

2.2.8.3. Hybridisation to array

All volumes prepared in this step are given for the 385K array. 100 µl of 1 mg/ml Cot-1 DNA (Invitrogen) were added to the sample to be hybridised, then the mixture was fully dried in a DNA concentrator (Divac 2.4 l DNA Concentrator) at 60^0C. DNA was rehydrated with 4.8 µl of ddH_2O. Samples were then incubated on the heat block at 70^0C for 10 min to fully solubilise the DNA. 8 µl of 2x SC Hybridisation buffer and 3.2 µl of SC Hybridisation Component A were added to the mixture and incubated on the hot block at 95^0C for 10 min to denature the DNA. The sample was centrifuged at maximum speed for 30 s and hybridised to array within 15 min of denaturation. The capture array slide was prepared and loaded as per manufacturer's specifications. The reaction was incubated at 42^0C for 64-72 h.

2.2.8.4. Washing and eluting hybridised DNA

Wash and elution buffers were prepared 2 days in advance as per manufacturer's specifications and the buffers which needed a specific temperature were incubated at 47.5^0C until temperature was equilibrated. DNA was eluted at RT immediately after the washing steps, by pipetting 425 µl of 125 mM fresh NaOH through the top of the elution chamber. Eluted DNA was collected into a new lo-bind 1.5 ml tube and any remaining 125 mM NaOH which did not fit into the elution chamber was added to the eluted DNA. 16 µl of 20% acetic acid was mixed with 500 µl Qiagen buffer PBI and the mixture was added to the eluted DNA. The solution was pipetted to a single QIAquick column and centrifuged for 1 min at 13000 rpm. 750 µl of buffer PE was used to wash the column before replacing the collection tube with a fresh 1.5 ml tube and resuspending the DNA in 50 µl of buffer EB.

2.2.8.5. Post capture LM-PCR

The LM-PCR reaction mix was prepared for 13 reactions, 2 reactions with DNA and SYBR green I dye (Invitrogen) at 1x concentration, 2 reactions with SYBR green I dye at 1x concentration and no DNA and 10 reactions with DNA and no SYBR green. A 1x reaction contained 10 µl of 5x Phusion Buffer, 1 µl of 10 mM dNTPs, 1 µl of each homemade Primer PE 1.0 and 2.0 (25 µM) (Sigma-Aldrich), 1 µl of 1x SYBR green, 0.5 µl Phusion polymerase, 4 µl eluted DNA and ddH_2O up to 50 µl reaction.

Reactions were run on the Rotor Gene-3000 (Corbett Research, Australia) using the following cycling programme: 98^0C for 30 s, 98^0C for 10 s, 65^0C for 30 s and 72^0C for 30 s (results were collected at this step). The reactions were terminated before amplification reached plateau curve.

Two pools were made from the 10 reactions without SYBR green and diluted with 1250 µl Qiagen PBI buffer. The mixtures were then purified using the QIAquick PCR purification kit (Qiagen, UK) and eluted with 50 µl buffer EB. The two resulting pools were mixed together and DNA concentration was quantified on the NanoDrop before being sent for Next Generation Sequencing performed by the Genome Centre on the Illumina Genome Analyser IIx (Illumina, San Diego, USA).

2.2.9. Exome capture

Paired end PCR primers and adapters were purchased from Sigma, library preparation kit components for exome sequence capture and subsequent Illumina GAllx paired end sequencing were purchased from NEB.

2.2.9.1. Preparing the DNA pool

DNA was quantified and fragmented as described above (2.1.8.1. and 2.1.8.2.) with some changes. The samples were pooled to a final concentration of 5 µg and ddH_2O was added up to 80 µl. End repair, adenylation to the 3' end and ligation of adaptors reactions were performed as previously described, and reactions were cleaned using a QIAquick PCR purification kit (Qiagen). Final purification, before hybridisation, was performed using AMPure XP beads (Beckman Coulter). DNA was resuspended in 100 µl molecular biology water. 1.2 µl of each reaction before purification steps was run on the Agilent Bioanalyzer 7500 chip (Agilent) as per manufacturer's specifications. Samples were quantified on the NanoDrop (NanoDrop Spectrophotometer ND-1000, Software NanoDrop 1000 version 3.7.1.) and stored at -20^0C until hybridisation.

2.2.9.2. Hybridisation to beads

1 µg pooled DNA was mixed with 100 µl of 1 mg/ml Cot-1 DNA and 1 µl of each 1000 µM PE-HE1 and PE-HE2 oligos. The mixture was dried in a SpeedVac DNA

concentrator at 60^{0}C. To each dried library, 7.5 µl of 2x SC Hybridisation buffer and 3 µl of SC Hybridisation component A were added. Samples were vortexed and centrifuged at maximum speed for 10 s then incubated in a 95^{0}C hot block for 10 min to denature DNA. The sample was then centrifuged and transferred to a 0.2 ml PCR tube and incubated on a thermal cycler at 47^{0}C for 64-72 h.

2.2.9.3. Washing and eluting hybridised DNA

Wash buffers and Streptavidin Dynabead elution buffer were prepared in advance and equilibrated at the required temperature. Streptavidin Dynabeads M-270 (Invitrogen) were prepared as per manufacturer's indications and used immediately. DNA was washed and eluted onto the Streptavidin Dynabeads following the manufacturer's instructions and resuspended in 50 µl PCR-grade water (Sigma). Hybridised DNA was stored at -20^{0}C post-bead clean-up.

2.2.9.4. Amplification of hybridised DNA sequences

Amplification protocol, cycling conditions and post LM-PCR clean-up steps were identical to the ones described in section 2.1.8.5. Next Generation Sequencing was performed by the Genome Centre on the Illumina Genome Analyser IIx (Illumina, San Diego, USA).

2.2.10. HaloPlex Target Enrichment System

For this experiment all target sequences were specifically prepared to cover required regions of interest (Table 2.1.). All restriction enzymes and reagents used for this procedure were purchased from Agilent Technologies unless otherwise stated. The manufacturer's protocol was used with a few modifications described below.

Gene	Coverage	Source
ADAM17	99.7 %	CCDS1665.1, User modified
DES	93.5 %	CCDS33383.1, User modified
DSC2	98.7 %	NM_024422, NM_004949, User modified
DSG2	97.7 %	CCDS42423.1, User modified
DSP	99.1 %	CCDS47368.1, CCDS4501.1, User modified
JUP	99.8 %	NM_002230, NM_021991, User modified
PKP2	97.5 %	CCDS31771.1, CCDS8731.1, User modified
TMEM43	99.4 %	CCDS2618.1,User modified

Table 2.1. Sequence coverage of selected genes and source information.

2.2.10.1. Restriction enzyme digestion

Initially all DNA samples were diluted to 20 ng/µl in a final volume of 45 µl (900 ng). Enrichment Control DNA (ECD) was also included in this step. A restriction enzyme mix was prepared by mixing 8 different sets of restriction enzymes. 5 µl of DNA from each patient were mixed with 5 µl from each of the 8 restriction enzyme mixtures, mixed gently and incubated at 37^0C for 4 h followed by an inactivation incubation at 80^0C for 20 min. Each restriction digest reaction was verified on a 2% agarose gel prepared as previously described. The 8 restriction digests from the same sample were pooled together.

2.2.10.2. Hybridisation to HaloPlex probes

Each digested sample pool was mixed with 65 µl hybridisation buffer, 14 µl HaloPlex Probes and 1 µl primer cassette, then incubated overnight on a thermal cycler on the following program: 95^0C for 10 min, 75^0C for 30 min, 68^0C for 30 min, 62^0C for 30 min, 55^0C for 30 min, 46^0C for 10 min and 8^0C forever.

2.2.10.3. Solid phase capture and DNA ligation

Using a magnetic plate (Life Technologies), the storage buffer of 20 µl of magnetic beads was removed and 40 µl of capture solution was added over the remaining beads and incubated at RT for 15 min. The supernatant was removed and 100 µl wash solution was added to each reaction and incubated in a thermal cycler at 46^0C

for 10 min. The supernatant was removed and the beads were resuspended in 47.5 µl ligation solution and 2.5 µl DNA ligase and incubated at 55^{0}C for 10 min. Finally the supernatant was removed.

2.2.10.4. Enrichment by PCR

To each sample 22.5 µl Haloase A Buffer, 0.5 µl Haloase A1 and 2 µl Haloase A2 were added and the mix was incubated in a thermal cycler at 37^{0}C for 30 min. The supernatant was then removed and 21.5 µl Haloase B Buffer were added and the mix was incubated in a thermal cycler at 80^{0}C for 20 min. The reactions were then cooled down to RT and 3.5 µl Haloase B enzyme were added; the mix was incubated in a thermal cycler at 37^{0}C for 30 min. The PCR mix was prepared as detailed in Table 2.2. 20 µl of PCR master mix were distributed to 0.2 µl tubes and 10 µl of the appropriate barcode primer from the 96-barcode plate were added. Using the magnetic plate 20 µl of the supernatant from the Haloase B reaction were added to the corresponding PCR reaction and incubated on a thermal cycler as follows: 98^{0}C for 30 s, 17 cycles at 98^{0}C for 10 s, 65^{0}C for 30 s, 72^{0}C for 30 s, followed by 72^{0}C for 5 min and 8^{0}C forever.

Reagent	Concentration	1x
Phusion HF Buffer (Thermo Scientific)	5x	6 µl
dNTP	25 mM	0.4 µl
PCR Primer 1.0	25 µM	1 µl
Phusion HotStart II (Thermo Scientific)	2 U/µl	0.5 µl
ddH_2O	---------	12.1 µl
Total volume:		20 µl

Table 2.2. HaloPlex Enrichment PCR Mix.

2.2.10.5. HaloPlex Cleanup

Following the PCR reaction, 40 µl of each reaction were mixed with 60 µl of 1.5x (v/v) Agencourt Ampure XP beads (Beckman Coulter) and incubated at RT for 10 min. The supernatant was removed after separation on a 96-well magnetic plate and 200 µl freshly prepared ethanol were added to each reaction without removing the reactions from the magnetic plate. The mix was incubated at RT for 1 min and the step was repeated one more time. Following the ethanol wash the samples were air dried and 40 µl Tris-HCl buffer (10mM pH 8.0) were added to each reaction and incubated at RT for 10 min to elute DNA. Reactions were placed on the magnetic plate and when the liquid was clear the supernatants were transferred to new tubes. Quality was assessed using a High Sensitivity DNA Bioanalyzer chip (Agilent Technologies), as per the manufacturer's specifications. Following quality control peak analysis was performed by the Genome Centre prior to Next Generation Sequencing of samples, also by the Genome Centre on the Illumina Genome Analyser IIx (Illumina, San Diego, USA).

2.2.11. Analysis of next generation sequencing data

Raw paired end FASTQ reads were aligned against the reference genome sequence (Hg19). Unique homozygous changes were identified by filtering the resultant data set against variations reported on dbSNP (*www.ncbi.nlm.nih.gov/snp/*) and the 1000 genome project (*www.1000genomes.org/*). Initial sequence analysis, including soft clipping, adapter trimming, and quality calibration options were performed by Dr Vincent Plagnol (University College London, UK) or Dr Michael Barnes (William Harvey Research Institute) and subsequently examined using the Integrative Genomics Viewer (IGV, Broad Institute).

2.2.12. Restriction enzyme digest

Restriction enzyme digests were used to confirm the presence of mutations in patient against control genomic DNA samples and to specifically linearise plasmid vectors to confirm the presence of the required DNA constructs in the desired orientation prior to site-directed mutagenesis experiments. Digests were performed according to the manufacturer's specifications. Generally, the required

quantity of DNA (between 1-2 µg of plasmid DNA or 5 µl of PCR amplified DNA) was incubated with 1 µl of the suitable restriction endonuclease (New England Biolabs, Ipswich, MA) and 1 µl of the appropriate 10x reaction buffer in a final volume of 10 µl. Where necessary, the reaction was scaled up to a larger final volume and when more than one enzyme was used in the same reaction the total volume of enzyme did not exceed 1/10 of the final reaction volume. The reactions were incubated on the DNA engine Tetrad 2 Peltier Thermocycler (MJ Research) on the following program: 4 h at 37^0C, 20 min at 65^0C and a final incubation at 4^0C. The restrictions digests were verified on a 1% agarose gel as previously described in section 2.2.6.

2.3. Molecular Biology II – DSP cloning strategies

2.3.1. DSP clone amplification on agar plates

DSP I Piece number	Clone number
1 + 2 + 3a	C2
1 + 2	C5
1 + 2 + 3a + 3 (complete seq)	C2
1	C7
2	C8
1 + 2 + 3a + 3 (complete seq)	C1
1 + 2 + 3a + 3 (complete seq)	C8
2 + 3a	C12
3	C8
1	C8
1 + 2 + 3a + 3 (complete seq)	C3
2 + 3a	C5
2	C5

Table 2.3. Summary of the DSP I clones used for site-directed mutagenesis and have been cloned by Dr Rita Cabral.

2.3.2. Small scale plasmid preparation

Small scale plasmid DNA preparations were obtained using the QIAprep Miniprep kit (Qiagen) according to the manufacturer's specifications, with some modifications. Briefly, a single colony was picked from a freshly streaked selective plate and grown in 5 ml LB broth (Invitrogen) containing 50 µg/ml of ampicillin for 16-18 h at 37^0C. Cell cultures were transferred to 1.5 ml tubes and pelleted by centrifugation for 5 min at 13,000 rpm and the pellet was re-suspended in cell re-suspension solution. Cells were lysed and then the lysis buffer was neutralised. The lysate was centrifuged at 13,000 rpm for 10 min and the supernatant was applied to a mini column. The column was firstly centrifuged at 13,000 rpm for 1 min, then washed twice with column wash solution and centrifuged for 1 min at 13,000 rpm after each wash. The plasmid DNA was eluted from the column with 50 µl of nuclease-free ddH_2O by centrifugation at 13,000 rpm and stored at -20^0C.

2.3.3. Site-directed mutagenesis

Site-directed mutagenesis (SDM) was performed using the QuikChange II XL site-directed mutagenesis kit (Agilent Technologies), as per the manufacturer's specifications. Briefly for the control reaction, 10 ng of pWhitescript 4.5 kb control plasmid were incubated with 5 µl of 10x reaction buffer, 125 ng of each control primers, 1 µl of dNTP mix, 3 µl of QuikSolution reagent and 1 µl of PfuUltra HF DNA polymerase (2.5 U/µl) and ddH_2O water up to 50 µl final volume. For the test reactions, 10 ng of plasmid DNA were used for each reaction together with specific primers (Table 2.4.). The reactions were incubated for 1 cycle at 95^0C for 1 min, for 18 cycles at 95^0C for 50 s, 60^0C for 50 s, 68^0C for 14 min (varies according to plasmid size, 1 min per kb of plasmid), for 1 cycle at 68^0C for 7 min and for 1 cycle at 37^0C for 2 min. SDM products were incubated with 1 µl *DpnI* (10 U/µl) restriction digest enzyme for 1 h at 37^0C in order to linearise plasmid and verify, by Sanger sequencing, whether SDM was successful.

Genetic variation	Primer name	Primer sequence
DSP 11G>C (ARVC)	G63C	AGGTGCAGAACTTGGTAAACAACTCTAAGAAGA TTGTACAG
DSP 11G>C (ARVC)	G63C - antisense	CTGTACAATCTTCTTAGAGTTGTTTACCAAGTT CTGCACCT
DSP 12C>T (hypotrichosis and PPK)	C113T	CGTGACGGGCCTGGGAGGCGTTG
DSP 12C>T (hypotrichosis and PPK)	C113T - antisense	CAACGCCTCCCAGGCCCGTCACG

Table 2.4. Primers used for site-directed mutagenesis of novel gene variations in *DSP* identified in patients with ARVC and hypotrichosis and PPK.

2.3.4. Transformation of chemically competent bacterial cells

Following restriction digest with *DpnI*, as described in section 2.3.3., the confirmed required constructs were used to transform chemically competent *E. coli* cells. The chemical transformation protocol was performed using XL10-Gold ultracompetent *E. coli* cells (Agilent Technologies), according to the manufacturer's instructions. Briefly, 2 µl of each construct generated by SDM were mixed with XL10-Gold ultracompetent *E. coli* cells and β-mercaptoethanol. Following an incubation of 30 min on ice, cells were heat-shocked for 30 s at 42^0C and then immediately transferred to ice for another 2 min. After addition of 1 ml of RT LB-broth, cells were incubated with shaking at 225-250 rpm at 37^0C for 1 h to allow expression of the antibiotic resistance genes. After the 1 h incubation cells were centrifuged for 5 min at 13,000 rpm and resuspended in 100 µl LB-broth. Cells were then plated on a pre-warmed LB agar plate containing 50 µg/ml ampicillin. Inoculated agar plates were incubated at 37^0C overnight (minimum 16 h).

2.4. Molecular Biology III – Protein Methods

2.4.1. Antibodies

Primary antibodies used for western blotting and microscopy and associated information and working dilutions are listed in Appendix C, Table C1.

2.4.2. Immunocytochemistry

Immunocytochemistry was performed both on cells plated on coverslips as well as on cells plated on Flexcell membranes following mechanical stretch. Cells were plated on coverslips at approximately 80% confluency in 12-well plates and grown overnight at 37°C. Cells were washed twice in PBS and fixed either in ice-cold methanol : acetone (1:1) or in 4% paraformaldehyde (PFA). Following fixation, cells were washed three times in PBS, then permeabilised in 0.1% Triton X-100 in PBS (PBST) for 5 min at RT (PFA fixed cells only), and finally blocked with 3% BSA in PBS (blocking buffer) for 30 min at RT. The cell-containing coverslips/membranes were then inverted onto a 50 µl drop of primary antibody-containing blocking buffer at the appropriate dilution and incubated for 2 h at RT or 4^0C overnight. Cells were washed three times in PBS and then incubated with the appropriate Alexa Fluor 488- (green) conjugated goat anti-rabbit, mouse or guinea pig IgG secondary antibody (Invitrogen), at a 1:800 dilution in PBS, for 1 h at RT. Cells were washed twice in PBS, incubated in DAPI (nuclear stain at 100 ng/ml) for 2 min at RT and washed three times in PBS. Cells were mounted with Immu-mount (Thermo Fisher Scientific).

Immunofluorescence images were acquired with a Zeiss LSM 510 and Zeiss LSM 710 laser scanning confocal microscopes (Carl Zeiss Ltd, Hertfordshire, UK) and processed using the LSM image browser (Zeiss).

2.4.2.1. Methanol-Acetone fixation

Cells were washed twice with PBS and fixed in ice cold methanol:acetone (50:50) for 5 min at -20°C. This fixation method was used for staining with all primary antibodies targeting membranous proteins. If cells were not used immediately they were left to air dry following fixation and stored at -20^{0}C until use.

2.4.2.2. Paraformaldehyde fixation

A fresh solution of 4% PFA in PBS was prepared (described below), aliquoted and stored at -20^{0}C and defrosted prior to each use. To this end, 2 g of PFA were dissolved in approximately 40 ml of boiling ddH_2O containing 20 µl of 2 M NaOH. The solution was cooled to RT and 5 ml of 10 x PBS were added. Water was added to a final volume of 50 ml. Cells were washed twice with PBS and fixed in 4% PFA for 20 min. This fixation method was used for staining with the primary antibodies targeting non-membranous proteins.

2.4.3. Immunohistochemistry

Immunohistochemistry was performed on frozen sections of normal and palm skin. Briefly, frozen skin sections were air-dried at RT for 1 h, then fixed with 4% PFA in PBS for 20 min or briefly in methanol:acetone (50:50) at RT and permeabilised in 0.1% Triton X-100 in PBS (PBST) for 5 min at RT, and finally blocked with 3% BSA in PBS (blocking buffer) for 30 min at RT. Sections were then incubated with 100-150 µl of primary antibody for 2 h at RT or at 4^{0}C overnight. Sections were then washed three times in PBS and then incubated with the appropriate Alexa Fluor 488- (green) conjugated goat anti-rabbit, mouse or guinea pig IgG secondary antibody (Invitrogen), at a 1:800 dilution in PBS, for 1 h at RT. Cells were washed twice in PBS and incubated with DAPI (nuclear stain at 100 ng/ml) for 2 min at RT prior to washing three times in PBS. Stained skin sections were mounted with Immu-mount (Thermo Fisher Scientific). Immunofluorescence images were acquired with the same apparatus as described for immunocytochemistry visualization.

2.4.4. Western Blotting

2.4.4.1. Protein preparation from cell extracts

Whole-cell protein extracts were prepared from HaCaT keratinocytes when approximately 90% confluent. The cells were washed in ice-cold PBS before lysis and then detached with boiling SDS sample buffer. Cells were scraped and the cell lysates were transferred to microcentrifuge tubes and heated to 95°C for 5 min before being spun briefly and stored at -20^{0}C.

2.4.4.2. SDS-polyacrylamide gel electrophoresis (PAGE) and transfer

Briefly, a separating polyacrylamide gel mixture (10-12% depending on protein size) was prepared and poured between two glass plates and 0.75 mm spacers in a gel electrophoresis apparatus (BioRad, Hemel Hempsted, UK). The gel mixture was overlaid with 1 ml of isopropanol, and left to polymerise at RT for approximately 20 min. When the gel was polymerised, the isopropanol was removed. A 5% stacking gel mixture was prepared and cast with sample combs over the resolving gel, and left to polymerise at RT for approximately 30 min. Between 10-20 µl of protein sample as well as 6-10 µl of full-range Rainbow molecular weight marker (GE Healthcare) were loaded on the SDS-polyacrylamide gel. The gel was run at 12 mA/gel in running buffer until the desired separation was obtained.

Proteins were transferred onto a Hybond–C Extra nitrocellulose membrane (GE Healthcare) in a wet transfer electrophoretic cell (BioRad) with transfer buffer, usually at 300 mA/tank for 1.5 h (or 100 mA/tank overnight). Quality of loading for each transfer was assessed by staining of the membrane with Ponceau Red stain solution for 5 min, followed by de-stain in ddH_2O and a final wash in Tris-Buffered Saline–Tween 20 (TBS-T).

2.4.4.3. Pre-cast gradient SDS-polyacrylamide gels and transfer

Whole cell lysates were resolved on NuPAGE Novex 4-12% Bis-Tris Mini Gels for NuPAGE Novex 3-8% Tris-acetate Mini Gels (Invitrogen), when western blotting for DSP according to the manufacturer's specifications. Approximately 10-20 µl of protein sample and 10-12 µl of High Mark Pre-stained Molecular Weight Marker

(Invitrogen) were loaded on the pre-cast SDS-polyacrylamide gels. The gel was run at 24 mA/gel until the desired separation was obtained. Proteins were subsequently transferred onto a Hybond – C Extra nitrocellulose membrane (GE Healthcare, Buckinghamshire, UK) in a wet transfer electrophoretic cell (Invitrogen) with transfer buffer, usually at 300 mA/tank for 1.5 h (or 100 mA/tank overnight). Quality of loading/transfer was assessed by staining of the membrane with Ponceau Red stain solution for 5 min, followed by de-stain in ddH_2O and a final wash in TBS-T.

2.4.4.4. Immunoblotting and visualisation

Non-specific antibody binding to the membrane was prevented by incubating the membrane in 10% (w/v) non-fat milk diluted in TBS-T or 5% (w/v) BSA diluted in TBS-T for 30 min at RT. Blocked membranes were incubated at RT for 2 h or at 4^0C overnight in 5% (w/v) non-fat milk TBS-T or 5% (w/v) BSA TBS-T containing the appropriate primary antibody at the suitable dilution. Following three 5 min washes in TBS-T, membranes were incubated in TBS-T containing the appropriate peroxidase-conjugated anti-mouse or anti-rabbit immunoglobulins (Dako, Ely, Cambridgeshire, UK), for 1 h at RT. Membranes were subsequently washed again as described above, incubated in ECL, ECL Plus solution (Amersham, GE Healthcare, Buckinghamshire, UK) or ECL Immobilon (Merck Millipore, UK) for 3 min, sealed in a plastic sheet, and exposed to chemiluminescence sensitive film (GE Healthcare).

2.4.4.5. Stripping membranes for antibody re-probing

Western blotting membranes were incubated in stripping buffer, prepared in house, at 50^0C-55^0C for 30 min. Membranes were then washed 3 times in TBS-T and developed as described above to check efficiency of stripping. For use the membrane was firstly blocked in the appropriate blocking buffer, 10% milk in TBS-T or 5% BSA in TBS-T, before proceeding with incubation with primary antibody and the steps described above.

2.5. Cell Methods

2.5.1. Cell culture conditions

The HaCaT spontaneously immortalised human keratinocyte cell line was cultured in DMEM : Ham's F12 or DMEM (Sigma-Aldrich, UK) supplemented with 10% (v/v) FBS (Biosera), 2 mM L-glutamine (Biosera), 100 U/ml penicillin, 100 µg/ml streptomycin and 1% RM^+ or no RM^+ when DMEM was used. Cells were maintained at 37^0C in a 5% CO_2 humidified incubator. When 80-90% confluent cells were washed in PBS and incubated in a mixture of one part 10% trypsin-EDTA and two parts PBS at 37^0C until detached. The reaction was stopped using complete medium, cells were pelleted by centrifugation at 1200 rpm for 5 min and re-suspended in complete medium. Approximately 2 million cells were then transferred to a new flask. Growth medium was changed every 3 days. All *in vitro* studies presented in this thesis used cells passaged for no more than 30 passages.

2.5.2. Cryopreservation of cells

For cryopreservation, 80-90% confluent cells were detached from the culture dish with trypsin-EDTA as described (section 2.3.1), pelleted by centrifugation and resuspended in 90% FBS:10% DMSO. Vials were frozen slowly at -80°C for at least 24 h and then transferred into vapour-phase nitrogen for long term storage. When a new cell culture was started, vials were defrosted quickly, in order to minimise cell death, and mixed with complete medium. The resuspended cells were pelleted at 1200 rpm for 5 min and reseeded into a flask with complete medium.

2.5.3. Mycoplasma testing

All cell cultures were tested using the MycoAlert™ Mycoplasma Detection Kits LT07-418 and MycoAlert Assay Control Set LT07-518 (Cambrex) as per manufacturer's specifications. Briefly, the reagent and substrate buffers and the positive and negative controls were thawed to RT. 1.5 ml of cell culture medium, kept on cells for 72 h, was cleared by centrifuging at 1500 rpm for 5 min. 100 µl of cleared supernatant from each sample was transferred to a well of a 96-well plate and incubated for 5 min with 100 µl of MycoAlert reagent. The plate was read in the plate

reader on the luminescence program (Bio-Tek Synergy HT Multi-Detection Microplate Reader, KC4 version 3.4 REV. 18). 100 µl of MycoAlert substrate was added to each sample and incubated for 10 min. After the 10 min incubation the plate was read on the luminescence program and the ratio between the second reading and the first reading was calculated. A ratio less than 1 was indicative of uninfected cells.

2.5.4. Transient siRNA mediated knockdown

Transfection conditions were optimised using siGLO Cyclophilin B Control siRNA (Thermo Fisher Scientific). For transient down-regulation siRNA OnTarget plus SmartPool (Dharmacon) was used to target all possible splice variants. Table 2.5. summarises the characteristics of these siRNAs.

Transfections were performed in RNase-free conditions according to the DharmaFECT general transfection protocol (Dharmacon) and optimised for a 6-well plate format. HaCaT cells were plated at a density of $2x10^5$ cells per well of a 6-well plate and incubated in complete medium at 37°C, 24 h prior to siRNA transfection. In separate polystyrene tubes, 10 µl of CSTA siRNA (200 nM final concentration)/10-20 µl of CAST siRNA (200-400 nM final concentration)/10 µl of DSP I/II (200 nM final concentration) and 6 µl of DharmaFECT were mixed in serum- and antibiotic-free media, up to 200 µl per reaction and incubated at RT for 5 min. The siRNA-containing medium was added to the tube containing the DharmaFECT, mixed and incubated for 20 min at RT. Complete antibiotic-free media was added to the mix (transfection media). The culture media was then removed from the cells in the 6-well plate and 2 ml of transfection media were added to each well. Cells were incubated in transfection media for approximately 24 h at 37°C and then this media was replaced by complete medium. Cells were maintained in this media for 2-10 days and subsequently harvested for experiments. Cells transfected with a pool of non-targeting (NT) siRNAs (OnTarget plus siControl non-targeting pool; Thermo Fisher Scientific) were used as a negative control.

	siRNA	siRNA sequence	Target mRNA	Position in target mRNA#
CSTA siRNA pool	si1	GGAGAUUGUUGAUAAGGUU	CSTA	180 - 198
	si2	ACAAAUGAGACUUACGGAA		220 - 238
	si3	GUACGAGCAGGUGAUAAUA		298 - 316
	si4	AAUGAGGACUUGGUACUUA		358 - 376
CAST siRNA pool	si1	UGACAAAGACCUCGAUGAU	CAST	1623 - 1641
	si2	UAAACUCUCUGACAGUCUA		1650 - 1668
	si3	GACACUAUCCCACCUGAAU		1768 - 1786
	si4	GCGAAGGAUUCAGCAAAGA		2008 - 2026
DSP I/II siRNA	siI/ II	AACCCAGACTACAGAAGCAAT	DSPI/II	1633-1653

Table 2.5. Characteristics of the siRNAs used. #Position of siRNAs according to NCBI reference sequences NM_005213.3 for *CSTA*, NM_173060 for *CAST* and NM_004415.2 for *DSPI*.

2.6. Adhesion assays

2.6.1. Dispase-based assay

Cells were grown to a high density and treated in cell culture flasks, then detached using 10% trypsin-EDTA (diluted 1:3 with PBS) and reseeded at a density of 3 x 10^6 cells/ml in 60 mm dishes. After 24 h cells were washed once in Ca^{2+} and Mg^{2+} enriched PBS before being incubated with 5 mg/ml dispase. Ca^{2+} and Mg^{2+} enriched PBS was used in order to preserve intercellular connections intact upon exposure

to dispase. After 20 min incubation, pellets were gently transferred to 15 ml tubes containing 5 ml PBS with Ca^{2+} and Mg^{2+}. Tubes were inverted rapidly 10-20 times (until breakage was observed) then the fragments were transferred back into the corresponding dishes and counted under a dissecting microscope.

2.6.2. Flexcell adhesion assay

The Flexcell FX-4000 Tension System (Flexcell, Hillsborough, NC) is a computer-regulated bioreactor that uses vacuum pressure to apply cyclic or static strain to cells cultured on flexible-bottomed culture plates. This system was used to subject cell monolayers to mechanical stress. HaCaT cells were grown to approximately 90% confluency on BioFlex 6-well plates (Flexcell) which contain a rubber membrane coated with pronectin in each 35 mm well. Each plate was placed over the loading station containing 6 planar faced cylinders or posts. Each post (25 mm) is centred beneath the rubber membrane of each 35 mm well. Cells were subjected to cyclic mechanical stretch with a frequency of 5 Hz (i.e. five cycles of stretch and relaxation per second) and an elongation of amplitude ranging from 11 to 14% (i.e. increase in diameter across the silicone membrane from 11 to 14%). Cells were stretched for different periods of time, between 0 h (non-stretched) and 4 h, and then prepared for immunocytochemistry as described. In order to stain the cells contained in each well of the 6-well dish with more than one antibody, the flexible rubber membrane was cut into 8 triangular segments with a scalpel. Each of these cell-containing segments was stained with a different antibody.

2.7. Wound-healing assay

Cells were plated and treated in 6-well plates and left to reach confluency (time-course permitting). The medium was removed and cells were incubated at 37^0C, 5% CO_2 for 2 h in Mitomycin C (10 μg/ml) diluted in complete medium to inhibit cellular proliferation. After 2 h the medium with Mitomycin C was removed and cells were washed 3 times in PBS. Using the top of the plate as a ruler and a P1000 tip the cell monolayers were scratched in the shape of a cross connecting the well edges. The cells were washed 3 times in PBS to remove any debris and complete medium was added. Pictures were taken at various time points using either a simple microscope

(Nikon Eclipse TE 2000-S and Nikon Digital Sight) or by Timelapse (Timelapse Epi inverted – TES, Zeiss), as per manufacturer's specifications.

2.8. Enzyme-Linked Immunosorbent Assay (ELISA)

All reagents were purchased from R&D Systems except for PBS, wash buffer, reagent diluent and stop solution which were made in house. The assay was performed as per manufacturer's instructions. Briefly, complete medium was removed from cells after 72-96 h and spun at 1200 rpm for 5 min. The supernatant was moved to fresh tubes and kept at -80^{0}C until use. Capture antibody was diluted to a suggested concentration (as per manufacturer's specifications) in PBS and each well of a 96-well plate was coated with 100 µl and incubated overnight. The next day the capture antibody was removed and the plate was washed 3 times in wash buffer and blotted against clean paper towels to remove all liquid. 300 µl of reagent diluent were added to each well and the plate was incubated at RT for 1 h. The wash step described above was repeated 3 times. 100 µl of sample or standard diluted in reagent diluent were added to the corresponding well and the plate was incubated at RT for 2 h. This step was repeated 3 times. 100 µl detection antibody, diluted in reagent diluent were added to each well and the plate was incubated at RT for 2 h. The wash step was repeated 3 times. 100 µl of the working dilution (suggested by the manufacturer) of streptavidin-HRP were added to each well and the plate was incubated in the dark at RT for 20 min. Wash step was repeated 3 times. 100 µl of substrate solution were added to each well and the plate was incubated in the dark at RT for 20 min. 50 µl stop solution were added to each well and mixed by gentle tapping. The optical density of the reactions was read using a plate reader (Bio-Tek Synergy HT Multi-Detection Microplate Reader, KC4 version 3.4 Rev. 18) set to 450 nm with a wavelength correction set to 540 nm.

2.9. Fluorescence-Activated Cell Sorting (FACS)

All media, wash buffers and cells have been kept for apoptosis analysis by FACS. Cells plated in 6-well plates were detached using trypsin-EDTA as previously described and all buffers used for each well were mixed in separate tubes. Tubes were pelleted by centrifugation at 1500 rpm for 5 min and the supernatants were

discarded. The pellet was resuspended in 400 µl Annexin V binding buffer and moved into FACS tubes. 1.7 µl Annexin V–FITC were added to the cell – buffer mix and incubated at RT for 15 min. 16 µl DAPI (200 ng/ml) were added to each tube. 30,000 events were analysed for each tube. Cells were counted and the percentage of early and late apoptotic death in each cell group was analysed using (BD FACSCanto II Flow Cytometer, BD Biosciences and FlowJo software, Tree Star Inc.).

2.10. Statistical analysis

The tools used were the two-tailed, paired t-test on Microsoft Excel. $p<0.05$ was significant (*); $p<0.01$ was highly significant (**); $p<0.001$ was very highly significant (***).

-Chapter 3-

Genetic strategies for mutation diagnosis in patients with ARVC or genodermatoses

3.1. Introduction

A variety of mutations have been identified in genes encoding desmosomal proteins as the underlying cause of an array of cardio-cutaneous syndromes (Brooke *et al*., 2012). Studies have been performed to try and elucidate the disease mechanisms behind these mutations using both *in vivo* and *in vitro* methods. However, it is still unclear why distinct mutations in the same desmosomal gene lead to different phenotypes and how mutations in different genes lead to similar phenotypes.

The focus of this chapter is the molecular analysis and identification of novel desmosomal mutations in patients clinically diagnosed with Arrhythmogenic Right Ventricular Cardiomyopathy/Dysplasia (ARVC/D), and secondly the genetic diagnosis of patients with hypotrichosis, hypotrichosis and PPK or acral peeling skin syndrome (APSS). In the latter patient cohort, mutations in protease-inhibitors were identified and shown to regulate aspects of desmosomal cell adhesion. Patient DNA was analysed using a number of different genetic techniques including custom capture array, HaloPlex targeted resequencing, exome capture and conventional Sanger sequencing. The following sections describe these different sequencing approaches and the novel mutations identified.

3.2. Results

3.2.1. Capture array and HaloPlex targeted resequencing in patients with ARVC

Forty-nine patients were recruited from Barts and The London NHS Trust and from two collaborating centres, Bristol Heart Institute and the Cardiac Inherited Disease Group based in Auckland, New Zealand (Dr Dominic Abrams). Specific information on patient demographics is presented in Appendix A. Clinicopathological data was not available for patients seen in New Zealand. The vast majority of patients recruited fulfilled diagnostic criteria for the condition, either using standard or modified ARVC criteria, or presented with an increasingly recognised variant of ARVC, namely predominant left ventricular involvement. The family pedigree below is representative for patient ARVC 2010 0009 (Figure 3.1.).

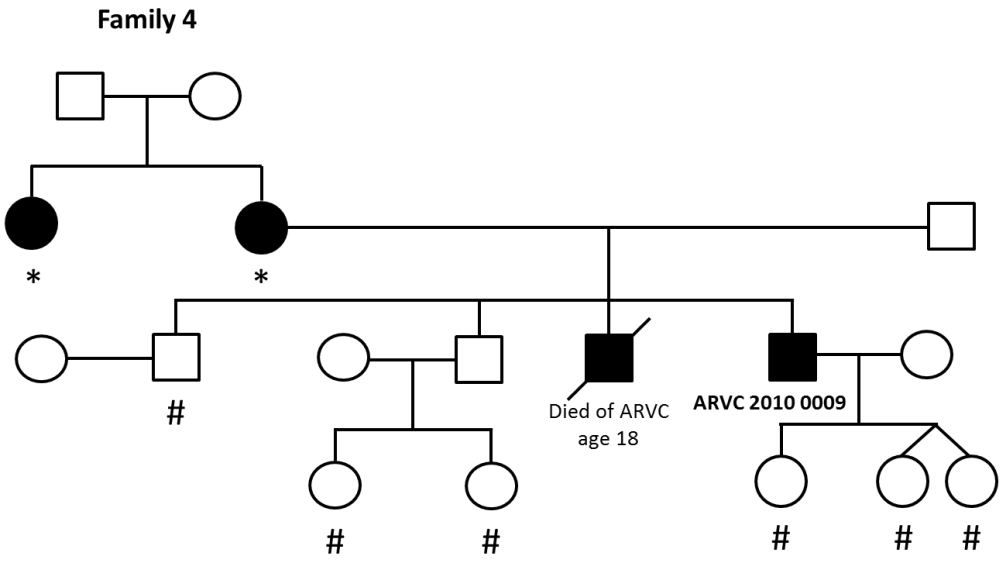

Figure 3.1. Pedigree structure of a family investigated in the ARVC study, where other family members have been diagnosed with ARVC. Filled symbols represent affected family members (diagnosed in this study ARVC 2010 0009). Squares represent male and circles represent female individuals. (*) represent patients treated at another hospital and (#) represent patients screened with nothing abnormal detected (NAD). No other members from this family have been screened in this study.

3.2.1.1. Illumina custom capture array

Twelve patient DNA samples were analysed on the 385K sequence capture array containing genomic DNA sequences from five different desmosomal genes that are known to be involved in ARVC namely: *DSP, PKP2, JUP, DSC2 and DSG2*. Following PCR enrichment, samples were run on the Illumina Genome Analyser IIx (GAIIx) at the QMUL Genome Centre, London. Raw 76 bp paired-end FASTQ reads were aligned against the reference genome sequence (Hg19). Unique sequence variants were identified by filtering the resultant data set against variations reported on dbSNP (*www.ncbi.nlm.nih.gov/snp/*) and the 1000 genome project database (*www.1000genomes.org/*). Initial sequence analysis, including soft clipping, adapter trimming, and quality calibration options were performed by Dr Vincent Plagnol at University College London.

Following initial analysis, the BAM files corresponding to the unique homozygous changes were aligned in the Integrative Genomics Viewer (IGV) against the genomic reference sequence (bottom of each IGV window); the IGV layout for six of the confirmed likely ARVC-associated DNA variants are shown in Figure 3.2. A-F. The centre of each alignment shows a variant present in the heterozygous state. Due to the DNA pooling strategy, it was unknown at this stage which patients harboured these specific sequence variants. The percentage of reads for each variation was analysed. A percentage of variation reads of approximately 4% was representative for a heterozygous variation and a multiple of 4%, such as 8%, 16%, was representative for a homozygous variation or a heterozygous variation present in more than one patient. This was indicative of a real or false call prior to Sanger sequencing analysis.

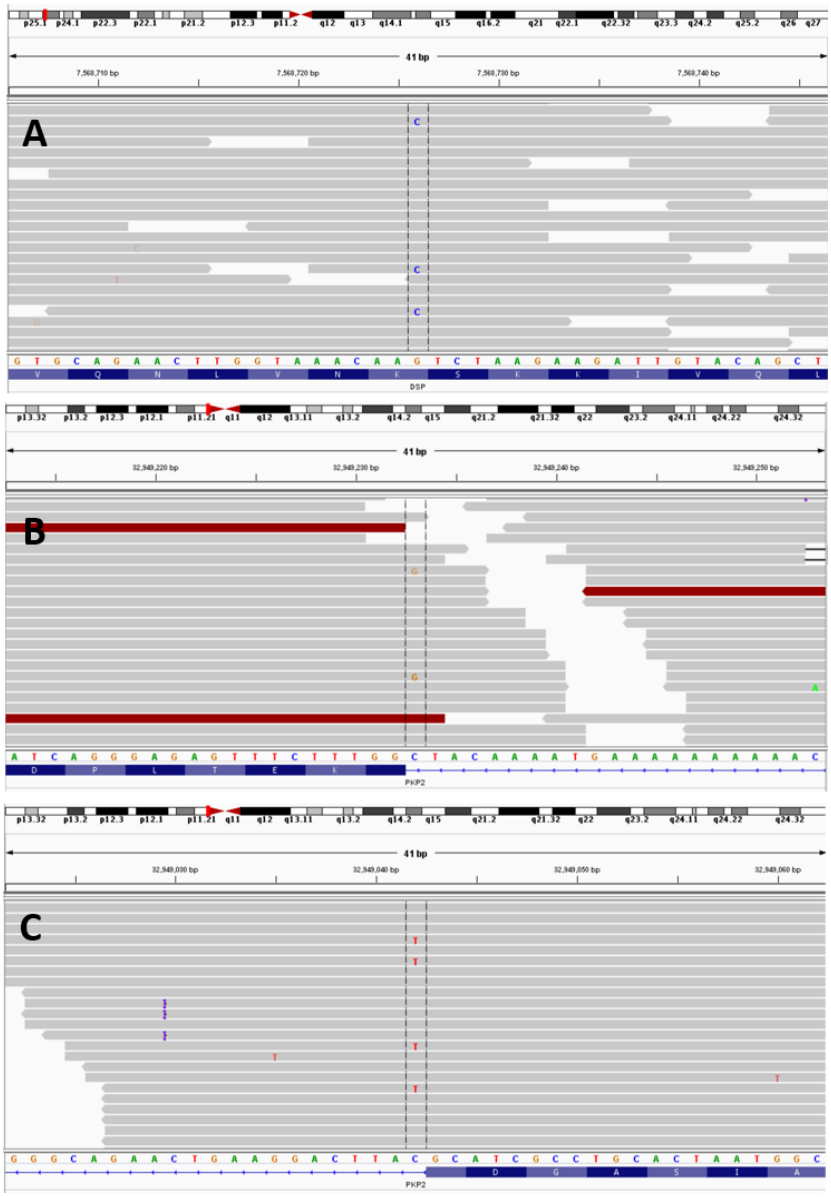

Figure 3.2. IGV layout of NGS results following a targeted-capture array of ARVC patients. Data was analysed for a high number of variation reads and aligned against the Human Reference Genome version 19 (GRCh37/Hg19). A percentage of reads of approximately 4% was indicative of a variation affecting one allele only whilst a multiple of 4% (such as 8%, 16%) was indicative of a number of alleles being affected. **(A)** to **(F)** are the representations (as seen in IGV) of NGS data corresponding to affected ARVC patients: **(A)** NM_001008844:c.G1323C:p.K441N in *DSP*, **(B)** IVS11-1G>C in *PKP2* and **(C)** IVS12+1G>A in *PKP2*.

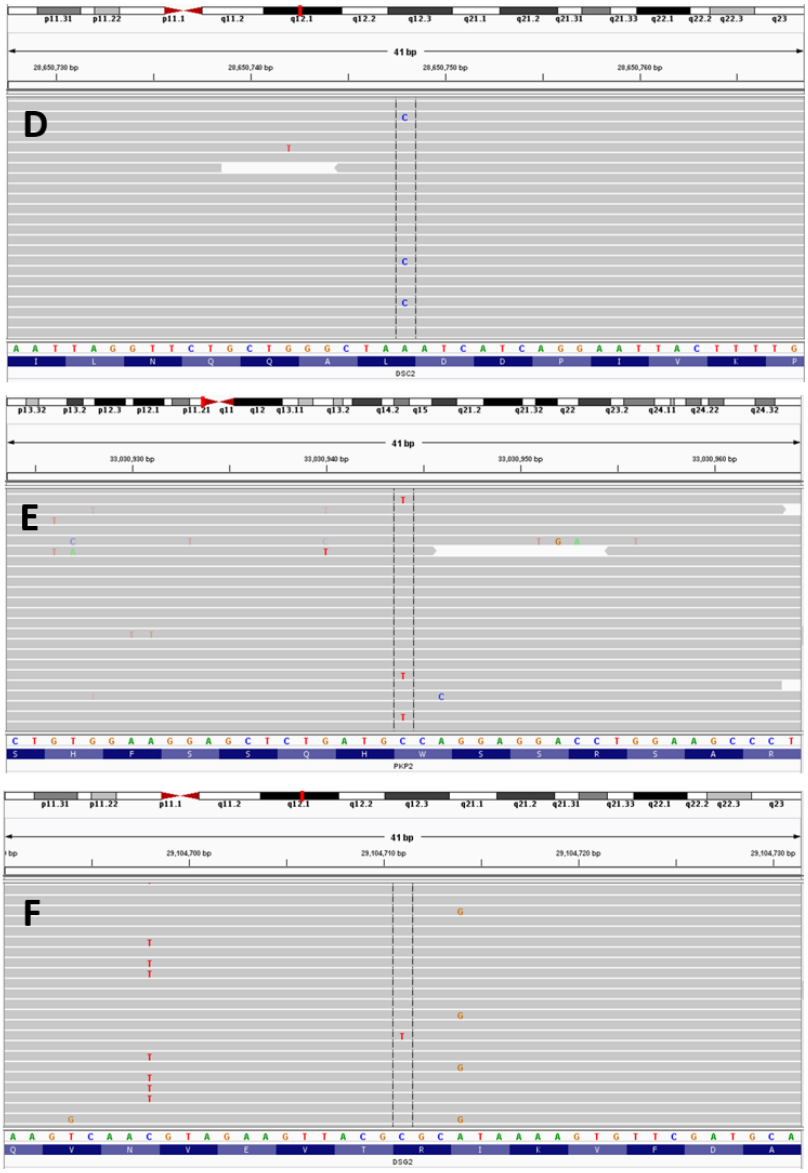

Figure 3.2. IGV layout of NGS results following a targeted-capture array of ARVC patients (continued). Data was analysed for a high number of variation reads and aligned against the Human Reference Genome version 19 (GRCh37/Hg19). A percentage of reads of approximately 4% was indicative of a variation affecting one allele only whilst a multiple of 4% (such as 8%, 16%) was indicative of a number of alleles being affected. **(A)** to **(F)** are the representations (as seen in IGV) of NGS data corresponding to affected ARVC patients: **(D)** NM_001005242:c.G870A:p.W290X in *PKP2*, **(E)** NM_024422:c.T2194G:p.L732V in *DSC2*, **(F)** NM_001943:c.C874T:p.R292C in *DSG2*.

3.2.1.2. Genetic screening of DSP, PKP2, JUP, DSC2 and DSG2 genes in patients clinically diagnosed with ARVC following custom capture array

Preliminary data analysis, selecting against read depth, gene of interest and percentage of reads, revealed nine likely disease-causing mutations in the twelve sequenced patients (Table 3.1.).

Sanger sequencing was performed to confirm each of the sequence variants and to identify the specific patients harbouring these variants. Three were identified as false positive variants and six were confirmed in five patients as follows (Figure 3.3.):

i) a heterozygous transversion from guanine to cytosine at coding position 1323 of *DSP*, which changes a lysine amino acid codon to an asparagine amino acid (c.G1323C:p.K441N) in patient ARVC 2010 0006;

ii) two heterozygous transversions from a guanine to cytosine and guanine to adenine, respectively, predicted to affect the splice sites of exons 11 (IVS11-1G>C) and 12 (IVS12+1G>A, rs111517471 – Minor Allele Frequency (MAF): < 0.01) of *PKP2* in patients ARVC 2010 0006 and ARVC 2010 0009;

iii) a heterozygous transversion from guanine to adenine at coding position 870 of *PKP2*, which changes a tryptophan amino acid codon to a STOP codon (c.G870A:p.W290X) in patient ARVC 2010 0004;

iv) a homozygous transversion from thiamine to guanine at coding position 2194 of *DSC2*, which changes a leucine amino acid codon to a valine amino acid (c.T2194G:p.L732V; Mutation L732V) in patient ARVC 2010 0010;

v) a heterozygous transversion from cytosine to thiamine at coding position 874 of *DSG2*, which changes an arginine amino acid codon to a cysteine amino acid (c.C874T:p.R292C; Mutation R292C) in patient ARVC 2010 0005;

vi) No variations were found in these five genes in the other seven patients, by capture array.

Patient	Gene	Chr.	Exon	Variation	Reads (%)	Novel (Y/N)
ARVC 2010 0006	DSP	6	11	NM_001008844: c.G1323C:p.K441N	4.17	N
ARVC 2010 0006	PKP2	12	N/A	IVS11-1G>C	3.11	N
ARVC 2010 0009	PKP2	12	N/A	IVS12+1G>A	5.19	rs111517471
False positive	PKP2	12	10	NM_001005242: c.T1900G:p.W634G	17.88	N/A
ARVC 2010 0004	PKP2	12	3	NM_001005242: c.G870A:p.W290X	4.11	N
False positive	PKP2	12	3	NM_001005242: c.A742C:p.T248P	7.36	N/A
ARVC 2010 0010	DSC2	18	14	NM_024422: c.T2194G:p.L732V	3.69	Mutation L732V
ARVC 2010 0005	DSG2	18	8	NM_001943: c.C874T:p.R292C	3.29	Mutation R292C
False positive	DSG2	18	15	NM_001943: c.A2568C:p.K856N	23.87	N/A

Table 3.1. NGS results following a targeted-capture array on ARVC patients. Data analysis has revealed 9 likely disease causing mutations in 12 patients, out of which 3 were false positive calls. Table 3.1 above contains details of the possible affected genes and variations as well as details of patients affected and confirmed by Sanger sequencing.

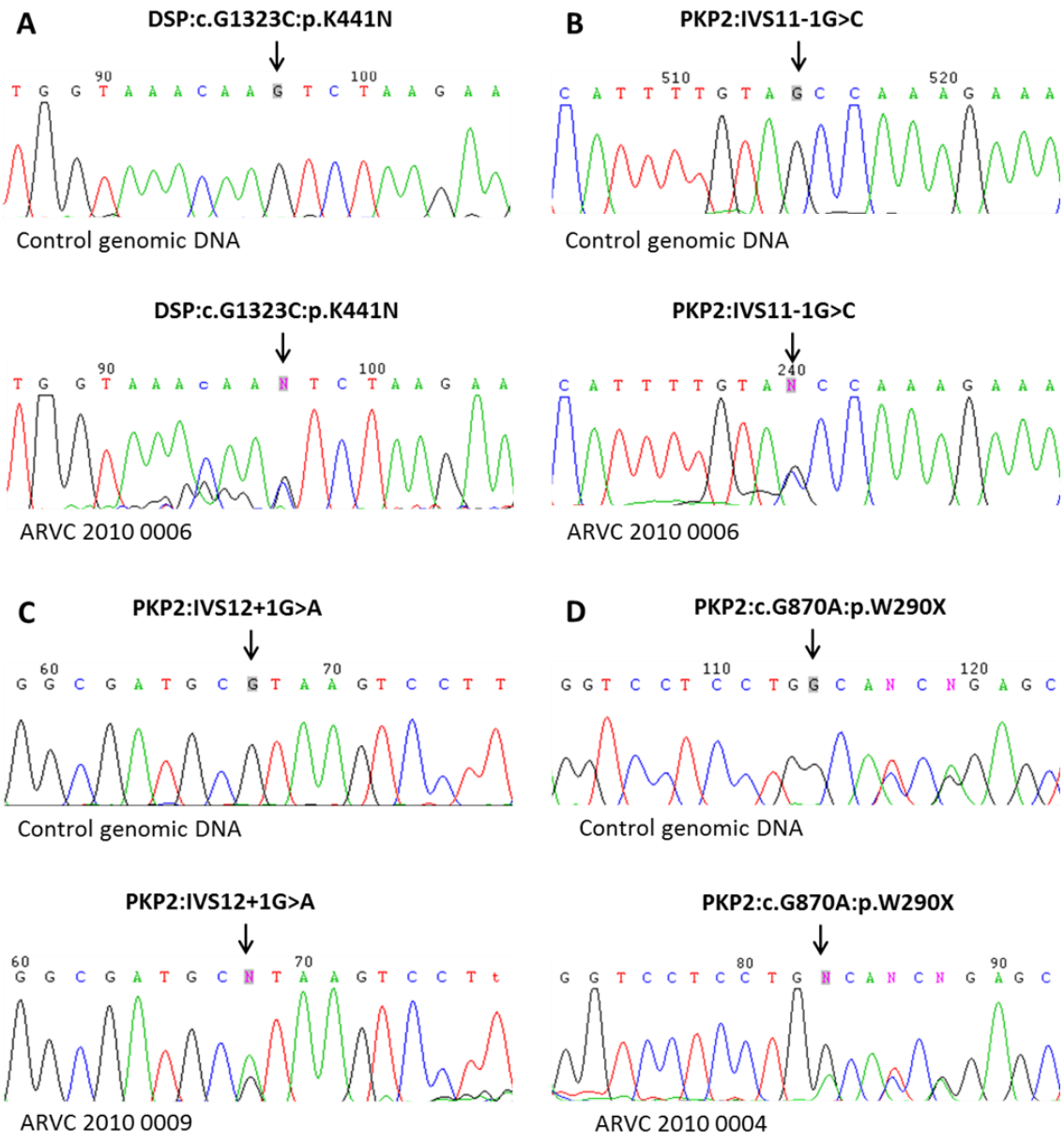

Figure 3.3. Confirmation of mutations in the *DSP*, *PKP2*, *DSG2* and *DSC2* genes of five affected individuals. Electropherograms of control and patient genomic DNA sequences. **(A)** Sequencing of patient DNA revealed a heterozygous transversion from guanine to cytosine at coding position 1323 of *DSP*, which changes a lysine amino acid codon to an asparagine amino acid (c.G1323C:p.K441N). **(B)** and **(C)** Sequencing of patient DNA revealed two heterozygous transversions, from a guanine to cytosine and guanine to adenine, respectively, believed to affect the splice sites of exons 11 (IVS11-1G>C) and 12 (IVS12+1G>A) of *PKP2*. **(D)** Sequencing of patient DNA revealed a heterozygous transversion from guanine to adenine at coding position 870 of *PKP2*, which changes a tryptophan amino acid codon to a STOP codon (c.G870A:p.W290X).

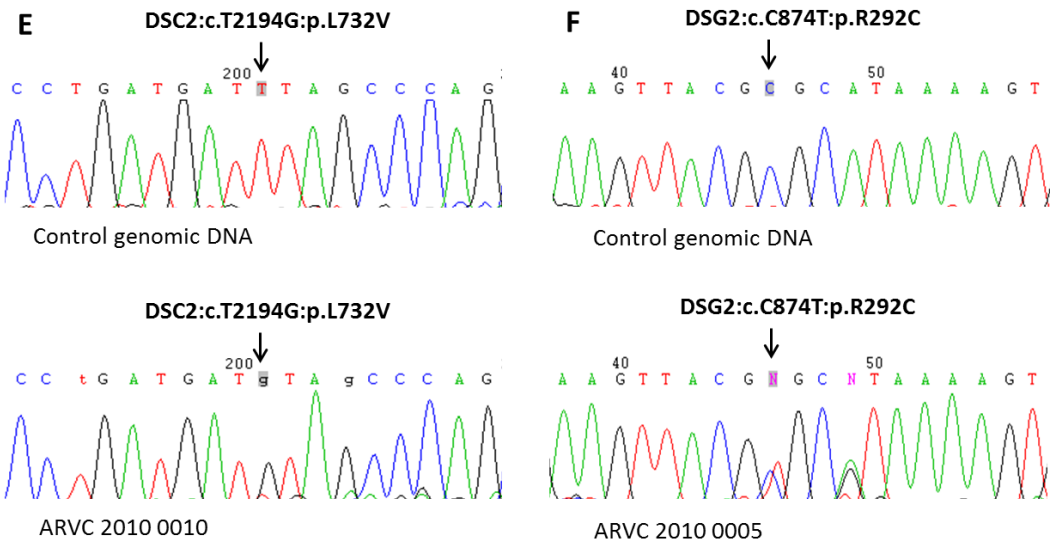

Figure 3.3. Confirmation of mutations in the *DSP, PKP2, DSG2* and *DSC2* genes of five affected individuals (continued). Electropherograms of control and patient genomic DNA sequences. **(E)** Sequencing of patient DNA revealed a homozygous transversion from thiamine to guanine at coding position 2194 of *DSC2*, which changes a leucine amino acid codon to a valine amino acid (c.T2194G:p.L732V). **(F)** Sequencing of patient DNA revealed a heterozygous transversion from cytosine to thiamine at coding position 874 of *DSG2*, which changes an arginine amino acid codon to a cysteine amino acid (c.C874T:p.R292C). Genomic DNA from an unaffected individual was used as control.

3.2.1.3. HaloPlex targeted enrichment system

Given that the molecular analysis of a higher number of ARVC diagnosed patients had to be performed and due to the large volume of Sanger sequencing required for variant confirmation with the previous targeted capture method, a HaloPlex targeted enrichment system was used for targeted NGS. This technique offered the possibility to screen up to 96 patients using unique barcodes which would speed up the confirmation process.

Forty eight genomic DNA samples were analysed on the HaloPlex target enrichment system. This system was specifically designed to cover 120 target regions, where each region was separated by another region by at least one base, with a total target region size of 36978 bp, covered by an average 98.5%. Custom designed probes covered eight genes associated with ARVC: *DSP*, *JUP*, *PKP2*, *DSG2*, *DSC2*, *DES*, *ADAM17* and *TMEM43*. The patient samples screened using this system were as follows: thirty-seven new patients from the UK and NZ, seven patients screened on the capture array and in which no mutations were found, two patients with an unknown, possibly desmosome-related disorder and two control patients screened on the capture array and in which novel mutations were identified by custom capture array (ARVC 2010 0006 and ARVC 2010 0010).

Following enrichment PCR, samples were run on the Illumina Genome Analyser IIx (GAIIx) at the QMUL Genome Centre. Raw 100 bp paired-end FASTQ reads were aligned against the reference genome sequence (Hg19). Unique homozygous changes were identified by filtering the resultant data set against variations reported on dbSNP (*www.ncbi.nlm.nih.gov/snp/*) and the 1000 genome project database (*www.1000genomes.org/*). Initial sequence analysis, including the soft clipping, adapter trimming, and quality calibration options was performed by Dr Michael Barnes at the William Harvey Research Institute. Following initial analysis the remaining calls were filtered by read depth, gene specificity and coverage as described above (Figure 3.4.). Seventeen possible disease-associated variations were identified with the majority in the *PKP2* gene, with one call in *ADAM17* and two in *DSP*. All these variations appeared to be novel (Table 3.2.). The two variations in patients ARVC 2010 0006 and ARVC 2010 0010 were also confirmed.

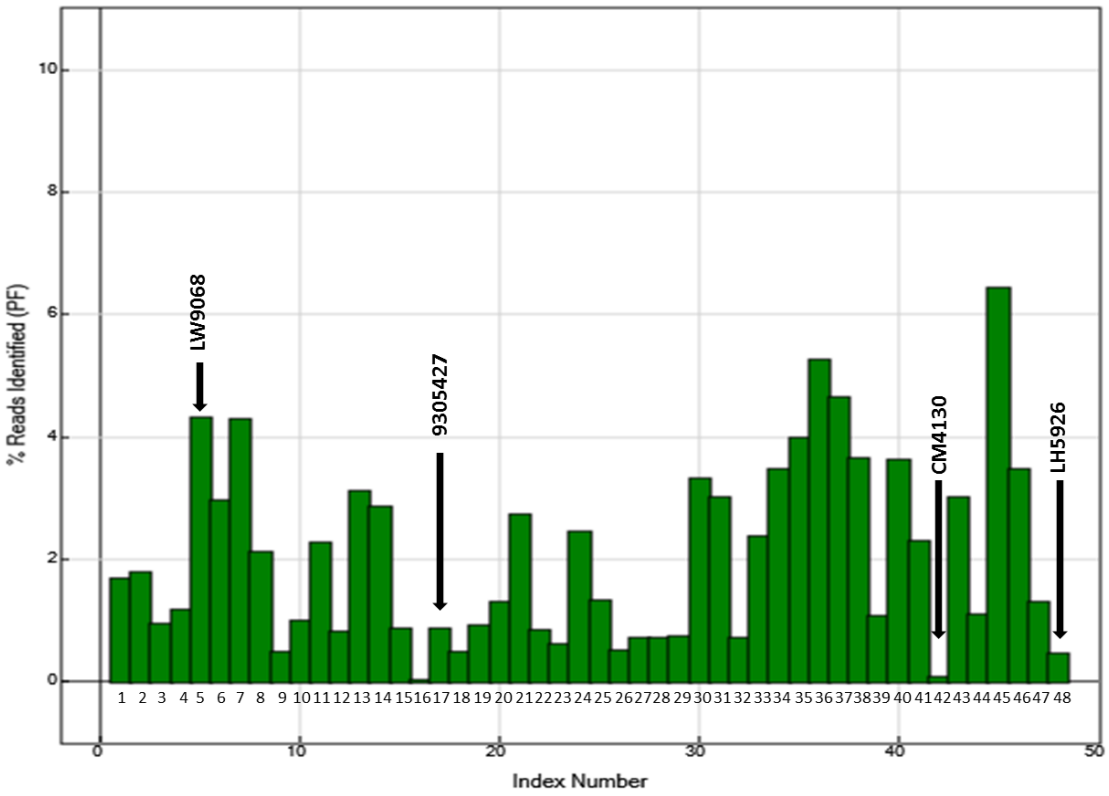

Figure 3.4. Diagram of percentage variation reads for ARVC patients analysed on the HaloPlex targeted resequencing system. NGS data was aligned and analysed against the Human Reference Genome version 19 (Hg19). Index numbers 1 to 48 represent the number for each patient analysed. The four real sequence variants confirmed by Sanger sequencing correspond to index numbers 5 (c.T1926A:p.Y642X), 17 (c.C5299T:p.R1767C), 42 (c.G1939A:p.A647T) and 48 (c.A148C:p.T50A).

Patient	Gene	Exon	Variation	Reads (<2% poor, >2% good)	Real (Y/N)
9305427	DSP	24	NM_001008844:c.C5299T: p.R1767C	Good	Y
RY8012	PKP2	4	NM_001005242:c.C1162T: p.R388W	Good	N
OG0660	PKP2	11	NM_001005242:c.T2193C: p.V731V	Poor	N
FP9310	PKP2	2	NM_004572:c.413delC: p.G99Q	Good	N
ARVC 2011 0020A	PKP2	2	NM_001005242:c.T332C: p.L111P	Poor	N
LW9068	PKP2	9	NM_001005242:c.T1926A: p.Y642X	Good	Y
CM4130	PKP2	9	NM_001005242:c.G1939A: p.A647T	Poor	Y
LU4246	PKP2	12	NM_004572:c.2469delT: p.Y786L	Poor	N
ARVC 2011 0022	PKP2	14	NM_001005242:c.C2479A: p.R827R	Poor	N
LV7711	PKP2	5	NM_001005242:exon5:c.1170 +1G>A	Poor	N
OG0660	PKP2	10	NM_001005242:c.C2120A: p.S707X	Poor	N
WN2786	PKP2	6	NM_001005242:c.C1539T: p.N513N	Good	N
LI8308	ADAM17	8	NM_003183:c.1139delA: p.E319G	Poor	N
LH5926	PKP2	1	NM_001005242:c.A148C: p.T50A	Poor	Y

LH5926	PKP2	12	NM_001005242:c.C2407G: p.L803V	Poor	N
LH5930	DSP	23	NM_004415:c.G5078T: p.S1693I	Poor	N
WN2786	PKP2	12	NM_001005242:c.A2176G: p.T726A	Good	N

Table 3.2. NGS results following a HaloPlex targeted resequencing system on ARVC patients. Data analysis has revealed 17 likely ARVC-causing mutations in 44 ARVC patients, out of which 4 were real calls. Table above contains details of the possible affected genes and variations as well as details of patients affected and confirmed by Sanger sequencing.

3.2.1.4. Genetic screening of DSP, PKP2, JUP, DSC2, DSG2, DES, TMEM43 and ADAM17 genes in patients clinically diagnosed with ARVC following HaloPlex targeted resequencing

Confirmation analysis by PCR and Sanger sequencing of the variations described in Table 3.2. dismissed thirteen calls as false positive and confirmed four novel variants in four unrelated patients (Figure 3.5.). Sequencing of patient DNA revealed a heterozygous transversion from guanine to adenine at coding position 1939 of *PKP2*, which changes an alanine amino acid codon to a threonine amino acid (c.G1939A:p.A647T) in patient CM4130 (Figure 3.5.); a homozygous transversion from adenine to cytosine at coding position 148 of *PKP2*, which changes a threonine amino acid codon to an alanine amino acid (c.A148C:p.T50A) in patient LH5926 (Figure 3.5.); a heterozygous transversion from a thymine to adenine at coding position 1926 of *PKP2*, which changes a tyrosine amino acid codon to a STOP codon (c.T1926A:p.Y642X) in patient LW9068 (Figure 3.5.) and a heterozygous transversion from cytosine to thymine at coding position 5299 of *DSP*, which changes an arginine amino acid to a cysteine amino acid (c.C5299T:p.R1767C; rs28931610) in patient 9305427. Patient 9305427 has a cutaneous syndrome - and this heterozygous variant has previously been associated with a Skin Fragility – Woolly Hair Syndrome (Dimas *et al*., 2008).

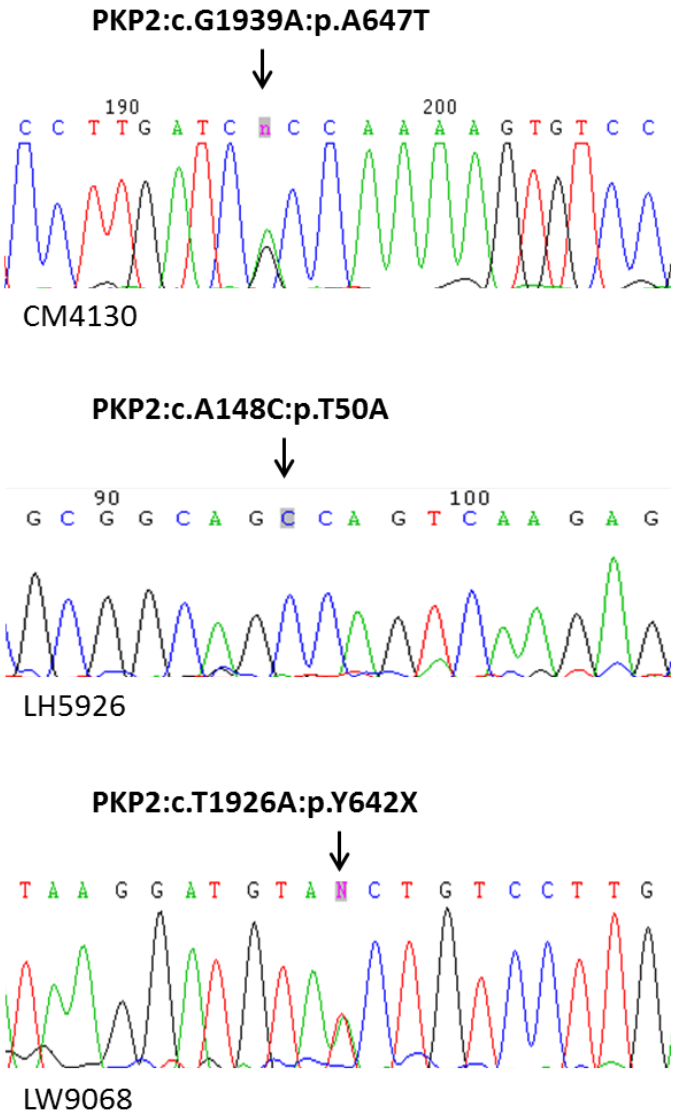

Figure 3.5. Confirmation of mutations in the *PKP2* gene in three affected individuals. Electropherograms of patient genomic DNA sequences. Sequencing of patient DNA reveals a heterozygous transversion from guanine to adenine at coding position 1939 of *PKP2*, which changes an alanine amino acid codon to a threonine amino acid (c.G1939A:p.A647T) in patient CM4130; a homozygous transversion from adenine to cytosine at coding position 148 of *PKP2*, which changes a threonine amino acid codon to an alanine amino acid (c.A148C:p.T50A) in patient LH5926 and a heterozygous transversion from thymine to adenine at coding position 1926 of *PKP2*, which changes a tyrosine amino acid codon to a STOP codon (c.T1926A:p.Y642X) in patient LW9068.

3.2.2. SNP array and exome analysis reveal *DSP* mutation in patients with hypotrichosis and PPK

Three siblings from a consanguineous Pakistani family (Figure 3.6. A) were clinically examined at Birmingham Children's Hospital. The patients, aged between seven months and ten years at the time of examination, had comparable hair and skin phenotypes, which consisted of hypotrichosis of the head, eyebrows and eyelashes, and diffuse, erythematous non-transgradiens palmoplantar keratoderma, (Figure 3.6. B). After ritual shaving, their hair regrew sparse, short and woolly with perifollicular erythema. The middle boy was also atopic and had more marked PPK and hypotrichosis. No other observations were noted and otherwise they appeared healthy. Cardiac assessment, echocardiograph and electrocardiography were performed and did not reveal any cardiac abnormalities. The parents and older sister were unaffected.

Due to the similarity of this phenotype to the cutaneous observations made in patients with desmosomal mutations, a mutation affecting a desmosome-associated protein was expected. The genetic analysis of patients 656 and 657, together with their unaffected parents is described in this subchapter.

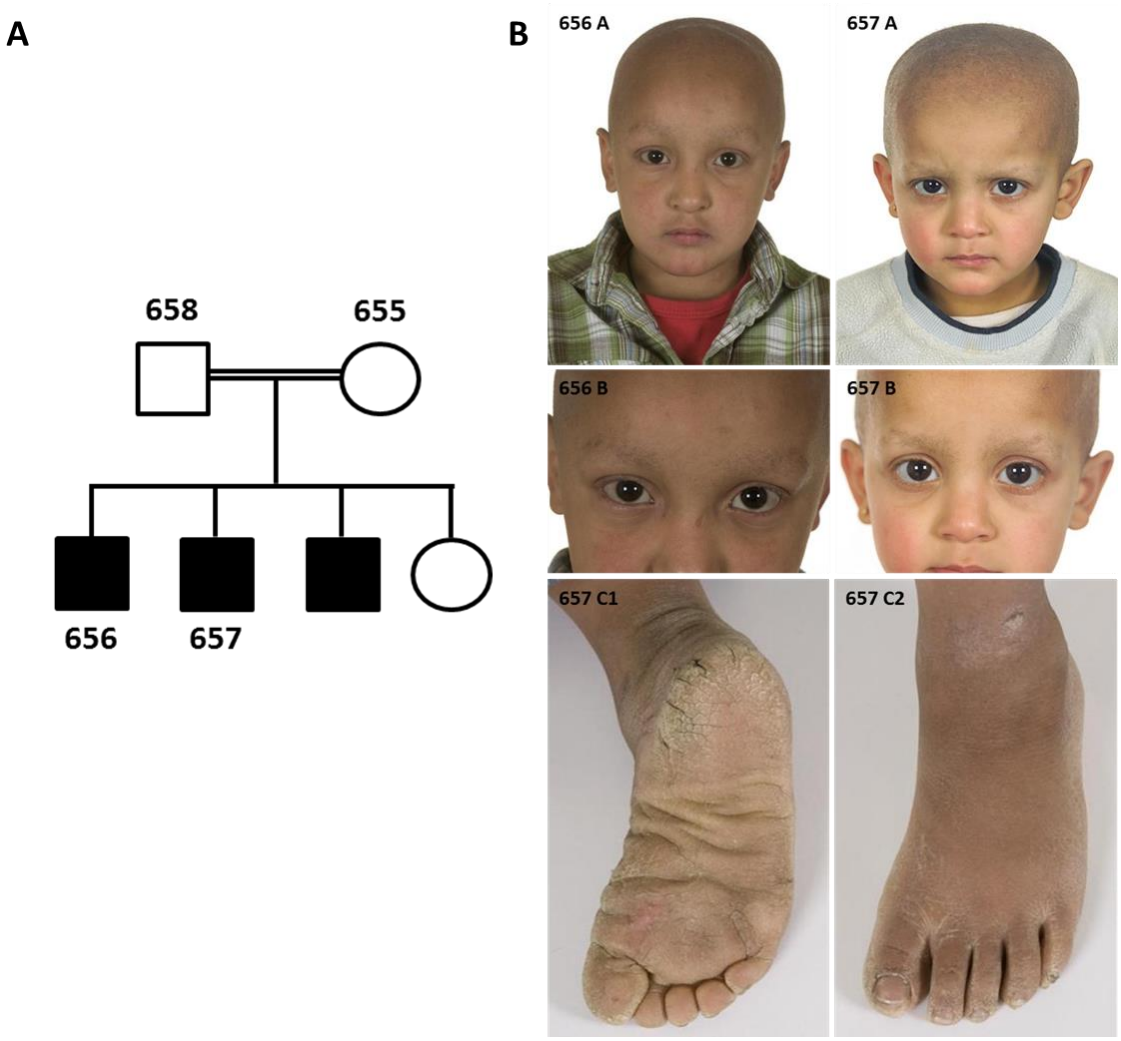

Figure 3.6. Pedigree structure of Pakistani family investigated in this study and clinical phenotype of affected patients showing the hypotrichosis and PPK. (A) Filled symbols represent affected family members (656, 657 and a younger clinically examined sibling) and unaffected family members tested as controls (parents 658 and 655 and an older clinically examined sibling). Squares represent male and circles represent female individuals. **(B)** Clinical phenotype of two older affected siblings. Hypotrichosis of the scalp (656A and 657A), eyebrows and eyelashes (656B and 657B) in older and middle siblings and diffuse, non-transgrediens plantar keratoderma with fissuring in middle aged patient (657 C1 and C2).

3.2.2.1.SNP genomic mapping

Given the apparent recessive mode of inheritance and consanguinity, a genome wide search for regions of common ancestry (homozygosity) was carried out previously by our group in collaboration with Dr Charles Mein from the QMUL Genome Centre. Common regions of genomic homozygosity were identified using the Illumina HumanHap550v3_A Genotyping BeadChip SNP mapping array and size range of clocks of homozygosity common to both patients were identified on chromosomes 1, 4, 5, 6, 11 and 14 (Table 3.3.). Because these regions of homozygosity were too large to explore, exome sequencing was performed on genomic DNA from one of the affected siblings.

Chromosome	Start		End		Size
	CSID	Position	CSID	Position	
1	10801043	189672990	1049472 3	193472504	3,691,286
4	cnvi0012052	45038666	2680758	56992092	11,953,426
5	12521501	31966942	37353	58647773	26,680,831
6	887509	6827116	669036	10620308	3,793,192
11	1852755	13953262	2702703	19357949	5,404,687
14	11543947	22573861	1049831 3	29468627	6,894,766

Table 3.3. SNP Genomic Mapping analysis on siblings with hypotrichosis and PPK. Data analysis has revealed large homozygous SNP regions on chromosomes 1, 4, 5, 6, 11 and 14. Table 3.3 shows the start and end positions and Chromosomal-SNP ID (CSID) together with the size of the homozygous SNP regions.

3.2.2.2. Exome capture

Genomic DNA from one of the siblings clinically diagnosed with hypotrichosis and PPK was analysed on the SeqCap EZ Human Exome Library v2.0. This assay covered approximately 20,000 genes in the human genome, with gene information taken from the following sources: NCBI Reference Sequence RefGene from UCSC - January 2010, CCDS from NCBI - September 2009, miRNAs from miRBase - version 14, September 2009 and customer inputs. A total of 44.1 Mb regions were covered in this assay (*www.nimblegen.com*).

Following enrichment PCR, samples were run on the Illumina Genome Analyser IIx at the QMUL Genome Centre. Raw 72 bp paired-end FASTQ reads were aligned against the reference genome sequence (Hg19). Unique homozygous changes were identified by filtering the resultant data set against variations reported on dbSNP (*www.ncbi.nlm.nih.gov/snp/*) and the 1000 genomes project (*www.1000genomes.org/*). Sequence analysis, including the soft clipping, adapter trimming, and quality calibration options was performed by Dr Vincent Plagnol at University College London.

Table 3.4. presents details of the possible disease-associated genes together with the associated homozygous variation call and percentage depth for each variation.

The novel identified *DSP* variant, c.C1493T:p.P498L, presented the highest percentage read depth (also covered in one of the regions of homozygosity identified in the SNP array data) and appeared to be the most likely disease-associated mutation. Confirmation Sanger sequencing was performed on patient and control genomic DNA.

Gene	Chromosome	Variation	Depth (%)
MAP3K11	11	NM_002419:c.C1876A:p.P626T	7
RAD9A	11	NM_004584:c.A1028T:p.E343V	33
C14orf21	14	NM_174913:c.A1417G:p.M473V	17
DCAF16	4	NM_017741:c.A124G:p.M42V	66
ACSL6	5	NM_015256:c.A1913G:p.Q638R	130
DSP	6	NM_001008844:c.C1493T:p.P498L	214

Table 3.4. NGS results following a genome wide exome analysis on one patient with hypotrichosis and PPK. Taken together, the SNP array and exome data analyses have revealed six likely homozygous disease-causing mutations. Table 3.4 above contains details of the possible affected genes and variations as well as details of variation read depth.

Further analysis by PCR (Figure 3.7. A) followed by Sanger sequencing confirmed this autosomal recessive mutation from a cytosine to a thymine at coding position 1493 of *DSP*, which changes a proline amino acid codon to a leucine amino acid (c.C1493T:p.P498L) in both affected siblings (Figure 3.7. B). Parents were heterozygous carriers for this mutation and genomic DNA from an unrelated individual, used as control, was wild type for this change (Figure 3.7. C). The remaining affected and unaffected siblings have not been screened.

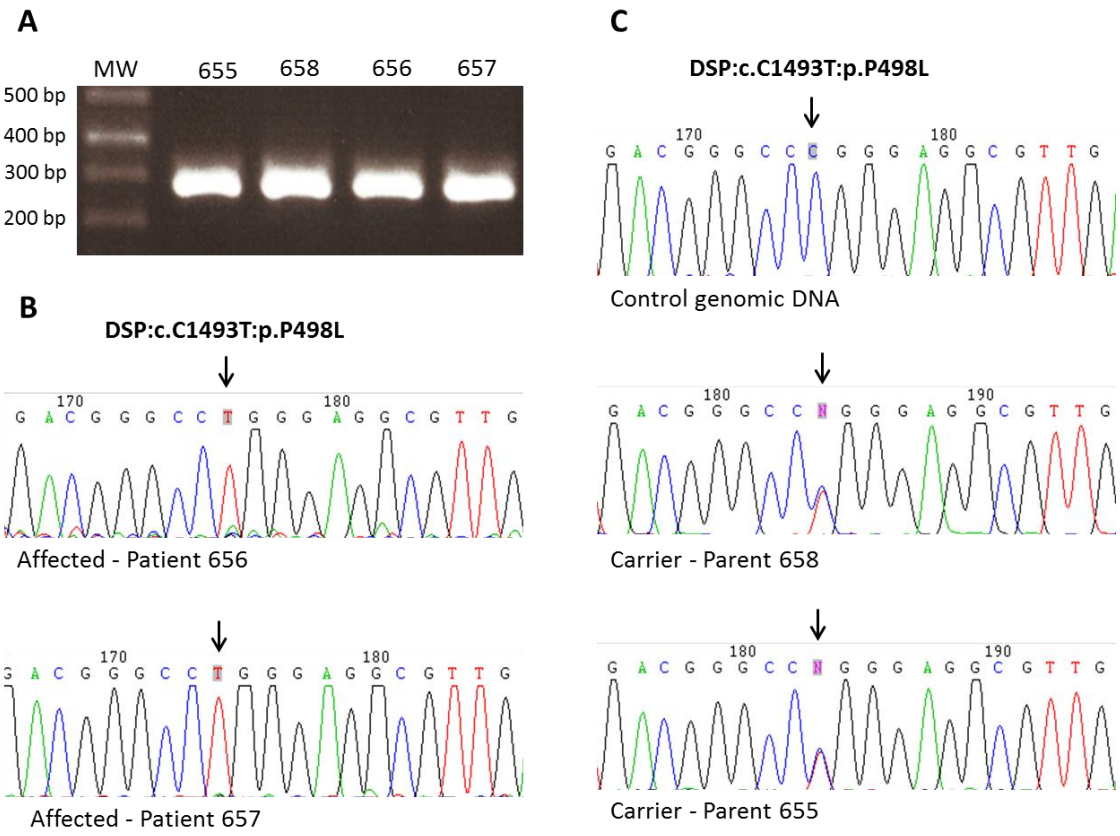

Figure 3.7. Confirmation of mutations in the *DSP* gene of two affected siblings. Electropherograms of control, unaffected parents and patients genomic DNA sequences. **(A)** PCR of control, unaffected parents and patients genomic DNA covering the *DSP* variation as seen on agarose DNA gel electrophoresis. **(B)** Sequencing of patient DNA reveals homozygous transversion from cytosine to thymine at coding position 1493 of *DSP*, which changes a proline amino acid codon to a leucine amino acid (c.C1493T:p.P498L) in both siblings (657 and 656). **(C)** Parents (655 and 658) of affected individuals are heterozygous for this variation. Genomic DNA from an unaffected individual was used as control.

3.2.3. Candidate gene analysis in patients with Acral Peeling Skin Syndrome

Two sisters aged 4 and 6 years, born from non-consanguineous parents, presented with a history of skin peeling on the hands and feet since 6 months of age (Figure 3.8. A). The peeling was notably worse following sweating, friction and immersion in water with development of maceration. Clinical examination revealed superficial peeling on the palms and soles, which extended onto the dorsal surfaces (Figure 3.8. B). Wrinkling and maceration of the palmoplantar skin after contact with water was noted. One sister also had atopic eczema and sinusitis due to confirmed house dust mite allergy. The other sister had ichthyosis vulgaris. Both had asthma and high hypermetropia.

The observed cutaneous phenotype resembles acral peeling skin syndrome (APSS), which is a rare autosomal recessive condition characterised by asymptomatic peeling of the skin of the hands and feet. APSS has been described in association with mutations in *TGM5* gene, which encodes for Transglutaminase 5. Initial screening for mutations in *Keratin 5* (*KRT5*) and *14* (*KRT14*), underlying Epidermolysis Bullosa Simplex (EBS), and in *TGM5*, underlying APSS, was negative.

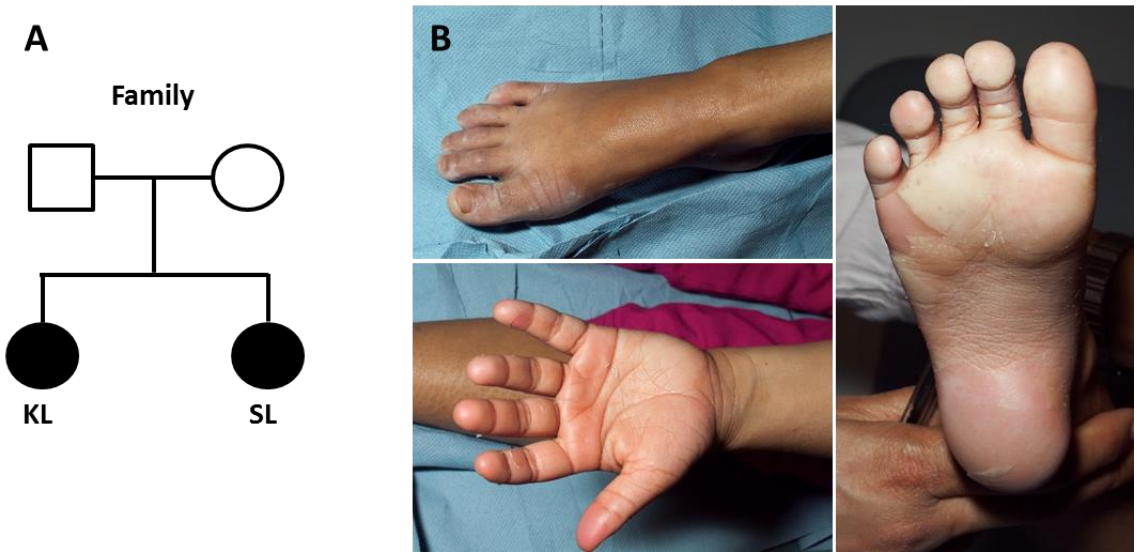

Figure 3.8. Pedigree structure of the family investigated in this study and clinical features showing distinct phenotype of skin fragility and exfoliation. (A) Filled symbols represent affected family members (KL and SL). Squares represent male and circles represent female individuals. **(B)** Clinical phenotype of the two affected patients. Peeling skin on hands and feet.

3.2.3.1. Screening of CSTA by Sanger sequencing

As no mutations were identified in these patients following genetic testing of the *KRT5, KRT14* and *TGM5* genes, it was decided that the *CSTA* gene encoding cystatin A should be screened, as *CSTA* mutations had recently been identified with APSS (Krunic *et al*., 2013). PCR analysis of genomic DNA from these patients, followed by DNA electrophoresis for visualisation under UV light (Figure 3.9 A) were performed. Due to repeated absence of DNA amplification across exon 1 of *CSTA* in the two tested patients, two new primer pairs flanking this exon were designed in order to avoid any polymorphisms that would interfere with the annealing process. DNA electrophoresis with the new primer pairs, designed to amplify exon 1 in two sequences, showed the absence of amplicons in both patients (Figure 3.9 B) which suggested the existence of a large deletion covering all 66 bp of exon 1 and possibly fragments of the flanking introns. This large deletion of 66 bp at the cDNA level, which includes the START codon, leads to a deletion of 22 amino acids at the protein level, this most likely resulting in loss of CSTA expression.

DNA amplification of exon 2 of *CSTA,* followed by Sanger sequencing revealed the existence of a polymorphism, a heterozygous transversion from cytosine to thymine at coding position 154 of *CSTA*, which does not alter the tyrosine amino acid (c.C154T:p.Y34Y; *rs17589*). This polymorphism was also detected in the control genomic DNA (Figure 3.9. C). Exon 3 of *CSTA* was wild type in both affected siblings (Table 3.5.).

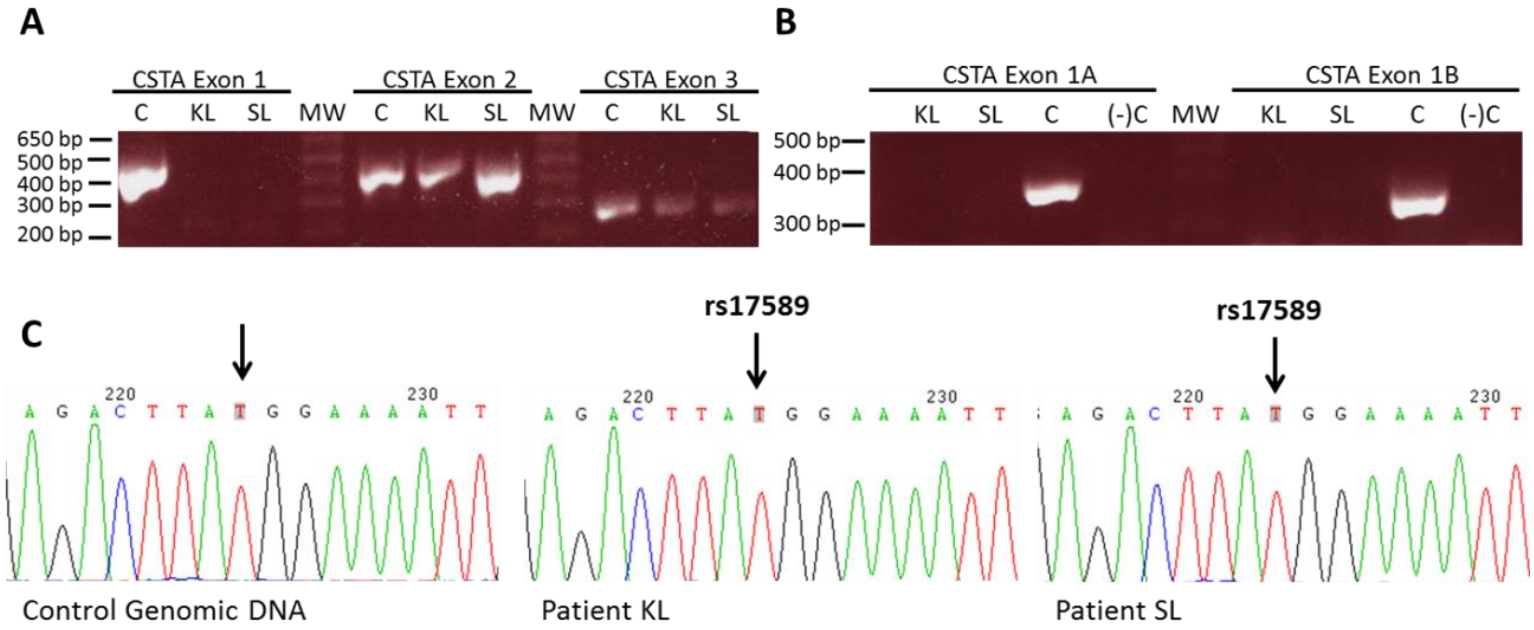

Figure 3.9. Confirmation of mutations in the *CSTA* gene of two affected individuals. (A) PCR with control and patients genomic DNA targeting all exons of the *CSTA* gene as seen on agarose DNA gel electrophoresis. **(B)** PCR on control and patients genomic DNA with two primer sets covering exon 1 in two halves as seen on agarose DNA gel electrophoresis. **(C)** Sequencing of exon 2 of patient genomic DNA reveals a heterozygous transversion from cytosine to thymine at coding position 154 of *CSTA*, which does not alter the tyrosine amino acid (c.C154T:p.Y34Y). This variation is a polymorphism previously identified in the healthy control population (rs17589 – MAF: 0.3928). Genomic DNA from an unaffected individual was used as control and presents the same variation in exon 2 as patient genomic DNA.

Exon	Variation	SNP reference number	Genotype
1	c.1_66del:p.1_22del	Novel	Homozygous
2	c.C154T:p.Y34Y	*rs17589*	Homozygous
3	Wild type	N/A	Wild Type

Table 3.5. Sanger sequencing analysis on two patients with Acral Peeling Syndrome due to *CSTA* mutation. Table above contains details of the affected exons of the *CSTA* gene with variation description.

3.2.4. Candidate gene analysis in a patient with hypotrichosis

3.2.4.1. Screening of DSG4 by Sanger sequencing

Initial screening of this patient, which included PCR amplification of several exons of *DSG4* previously deleted in patients with hypotrichosis (Kljuic *et al*., 2003a), revealed no homozygous deletions in these exons.

Analysis of all fifteen exons of *DSG4* subsequently revealed 3 homozygous changes in exons 4, 5 and 12 as follows: a homozygous transversion from guanine to adenine at coding position 258 in exon 4, which does not alter the arginine amino acid (c.G258A:p.R86R; rs16959856), a homozygous transversion from cytosine to thymine at coding position 495 in exon 5, which does not alter the serine amino acid (c.C495T:p.S165S; rs9956865) and a homozygous transversion from adenine to cytosine at coding position 1930 in exon 12, which changes an isoleucine amino acid into a leucine amino acid (c.A1930C:p.I644L; rs4799570) (Figure 3.10.).

It is believed that these homozygous variations are non-disease causing polymorphisms, as they have also been observed in control genomic DNA from an unaffected individual and were found in the genome database (Table 3.6.).

Exon	Variation	SNP reference number	MAF	Genotype
4	c.G258A:p.R86R	rs16959856	0.2794	Homozygous
5	c.C495T:p.S165S	rs9956865	0.1951	Homozygous
12	c.A1930C:p.I644L	rs4799570	0.0341	Homozygous

Table 3.6. Sanger sequencing analysis of a patient with hypotrichosis. Table above contains details of the affected exons of the *DSG4* gene with variation description. Variation details were extracted using the NCBI reference genome NM_001134453.

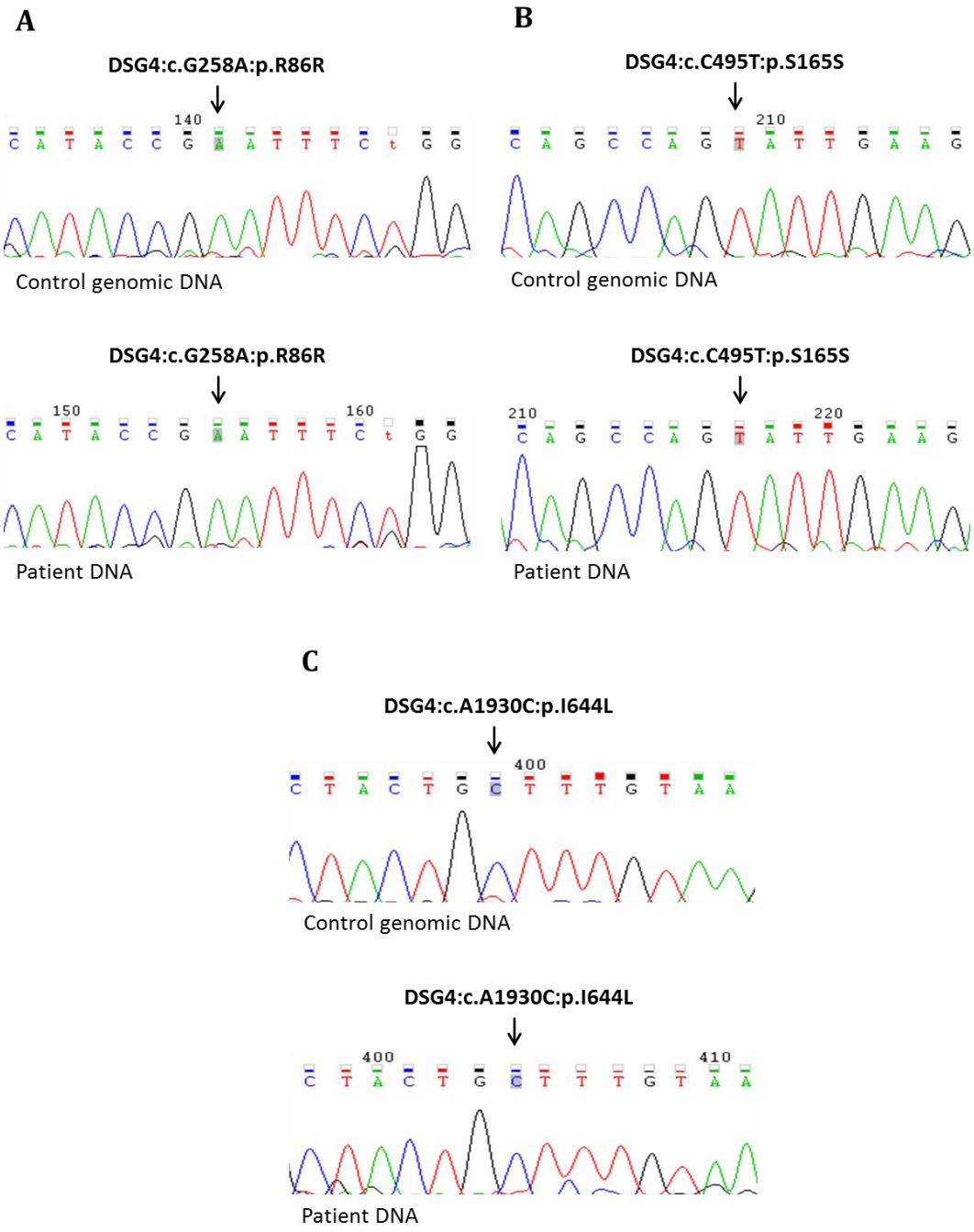

Figure 3.10. *DSG4* mutation analysis by Sanger sequencing of affected individual. Sequencing of *DSG4* in patient genomic DNA revealed **(A)** a homozygous transversion from guanine to adenine at coding position 258 in exon 4, which does not alter the arginine amino acid (c.G258A:p.R86R; rs16959856), **(B)** a homozygous transversion from cytosine to thymine at coding position 495 in exon 5, which does not alter the serine amino acid (c.C495T:p.S165S; rs9956865) and **(C)** a homozygous transversion from adenine to cytosine at coding position 1930 in exon 12, which changes an isoleucine amino acid into a leucine amino acid (c.A1930C:p.I644L; rs4799570).

3.3. Discussion

The principal goal of the work described in this chapter was the identification of novel and previously disease-associated genetic mutations in patients clinically diagnosed with ARVC from the UK and New Zealand.

During the course of this study, three additional families with members diagnosed with hypotrichosis, hypotrichosis and PPK or APSS, all characterised by hair and/or cutaneous abnormalities, were screened for mutations in the disease associated genes *DSG4* and *CSTA* for hypotrichosis and APSS patients, respectively, with a novel disease causing mutation in *DSP* identified in patients with hypotrichosis and PPK.

3.3.1. Candidate gene approach in patients with ARVC reveals novel and known disease-associated mutations

A total of forty-nine patients clinically diagnosed with ARVC were screened for mutations in the known and possibly disease associated genes *DSP*, *DSC2*, *DSG2*, *PKP2*, *JUP*, *DES*, *TMEM43* and *ADAM17*. Following Sanger sequencing, nine variations in eight patients have been confirmed as real calls, in the *DSP*, *PKP2*, *DSC2* and *DSG2* genes.

As disease-causing mutations were identified in only 16% of the patients screened, we suggest that the lack of candidate identification in the remaining 84% may be related to phenotypic errors, incomplete sensitivity of the mutation screening techniques, presence of mutations in non-analysed sequences in some cases due to poor gene coverage and very likely the yet undefined genes. Distribution of the full disease associated genes out of the 49 patients was as follows: *DSP*, 11%; *DSC2*, 11%; *DSG2*, 11% and *PKP2*, 67%.

These results differ from previous reports in which 50-70% of ARVC-related mutations identified were in genes encoding for desmosomal components (Brooke *et al*., 2012), compared to only 16% in our reports. Regardless of the low percentage diagnosis rate, our results support previous statistic data revealing mutations in *PKP2* as responsible for approximately 70% of desmosome related ARVC cases. This difference could be attributed to slightly different methods of patient recruitment

with 66% of mutations identified in twenty-four UK patients and only 33% identified in twenty-five New Zealand patients.

Out of six variations identified in *PKP2*, five mutations were heterozygous and one was homozygous as follows: two heterozygous transversions believed to affect the splice sites of exons 11 (IVS11-1G>C) and 12 (IVS12+1G>A; rs111517471), a heterozygous transversion which changes a tryptophan amino acid codon to a STOP codon (c.G870A:p.W290X), a heterozygous transversion which changes an alanine amino acid codon to a threonine amino acid (c.G1939A:p.A647T), a heterozygous transversion which changes a tyrosine amino acid codon to a STOP codon (c.T1926A:p.Y642X) and a homozygous transversion which changes a threonine amino acid codon to an alanine amino acid (c.A148C:p.T50A).

The IVS11-1G>C mutation at the splice site of exon 11 of *PKP2* was identified together with a heterozygous transversion in *DSP*, which changes a lysine amino acid codon to an asparagine amino acid (c.G1323C:p.K441N) leading to what is called a double heterozygote. Based on a study by Bauce *et al.*, exon 11 skipping in RNA transcripts and the possible generation of a premature STOP codon following the *PKP2* mutation could prove highly pathogenic (Bauce *et al*., 2010). With regards to the *DSP* variant, whether this has any subsequent effect on protein structure and/or its function is unknown.

Two additional variations, previously reported, were identified as follows: a homozygous transversion in *DSC2*, which changes a leucine amino acid codon to a valine amino acid (c.T2194G:p.L732V), and a heterozygous transversion in *DSG2*, which changes an arginine amino acid codon to a cysteine amino acid (c.C874T:p.R292C). Mutation L732V identified in *DSC2*, reported in the Exome Sequencing Project (ESP) database and predicted by PolyPhen as benign, was previously described by Bhuiyan *et al*. in conjunction with a *DSG2* mutation V392I, which suggested that perhaps a single mutation is less likely to cause a full-blown ARVC phenotype (Bhuiyan *et al*., 2009). Variant R292C in *DSG2* confirmed as heterozygous within this chapter has previously only been described in the homozygous state (Sato *et al*., 2012), or in association with a synonymous mutation in *DSP*, D782D, dismissed by Cox *et al*. as silent after initially being listed as likely

pathogenic based on Sorting Intolerant From Tolerant (SIFT) and PolyPhen and its absence in the control population (Cox *et al*., 2011). Variant R292C has also previously been described as a double heterozygote associated with variation S194L in *DSG2* and R577DfsX5 in *PKP2* (Nakajima *et al*., 2012). Despite confirmation of these two variations in *DSC2* and *DSG2* by Sanger sequencing, a causatory effect between these mutations and ARVC requires segregation studies and perhaps analysis of these affected patients by exome sequencing which may reveal alternative causative gene variants.

3.3.2. Candidate gene analysis in patients with hypotrichosis with and without PPK

3.3.2.1. Novel DSP variant identified in siblings with hypotrichosis and PPK

The three affected siblings of Pakistani origin, diagnosed with hypotrichosis and PPK, presented with comparable hair and skin phenotypes consisting of hypotrichosis of the head, eyebrows and eyelashes, together with diffuse, erythematous non-transgradiens PPK. Cardiac assessment, echocardiograph and electrocardiography were performed and did not reveal any cardiac abnormalities in our patients.

SNP array homozygoisty mapping of two of the affected siblings followed by exome sequencing of one of the affected patients revealed a homozygous variant in exon 12 of *DSP*, c.C1493T:p.P498L mapping within a large region of homozygosity on chromsome 6. This call was also confirmed in a second affected sibling and in parents who were heterozygous carriers. Due to the age of the third affected sibling, and no DNA sample having been collected from the unaffected sibling, these individuals have not been tested.

Two significant studies linking mutations in *DSP* to skin disorders reported an autosomal dominant nonsense (p.Q331X) and splice site (939+1G>A) mutations leading to haploinsufficiency (Armstrong *et al*., 1999, Whittock *et al*., 1999). These genetic variations suggest that protein dosage could perhaps be critical for skin integrity. Also, the first recessive *DSP* mutation, identified by Norgett *et al*.,

associated with the Carvajal syndrome leads to truncation of the protein and loss of cell adhesion and collapsed IF network (Norgett *et al*., 2000).

We suggest that due to its position in the protein sequence, the recessive *DSP* variation described in this chapter could possibly affect the normal structure and conformation of the amino-terminus of the protein, involved in binding PG and PKPs and, therefore, destabilise the formation of the desmosomal complex and, indirectly, the tethering of IF network to the plasma membrane.

3.3.2.2. Whole gene analysis reveals DSG4 mutation in patient with hypotrichosis

One other genetic diagnosis described in this chapter was performed in a patient clinically diagnosed with hypotrichosis, presenting with typical clinical disease characteristics as described above, but without any cardio-cutaneous implication.

Initial analysis of this patient, which included PCR amplification of several exons of *DSG4* previously found to be deleted in patients with hypotrichosis, leading to loss-of-function of *DSG4* (Kljuic *et al*., 2003a), revealed no obvious changes in these exons. Exon sequencing revealed three known variations in exons 4, 5 and 12 as follows: a homozygous transversion which does not alter the arginine amino acid (c.G258A:p.R86R; rs16959856), a homozygous transversion which does not alter the serine amino acid (c.C495T:p.S165S; rs9956865) and a homozygous transversion which changes an isoleucine amino acid into a leucine amino acid (c.A1930C:p.I644L; rs4799570).

The first two variations identified in exons 4 and 5, rs16959856 and rs9956865 respectively, with a MAF of 0.28 and 0.19 would not alter the protein conformation due to these variations being synonymous, and are unlikely to be disease-causing based on the high (> 1%) MAF. The last variation present in exon 12, rs4799570, with a MAF of 0.03 appears as tolerated in SIFT and as benign in PolyPhen despite the amino acid change and a MAF < 1%.

Based on these findings we believe that further genetic analysis would be required to accurately diagnose this patient. One possible technique would be exome sequencing which would reveal multiple genetic candidates, including any alternative variants in *DSG4* missed in the initial screening analysis, followed by

conventional Sanger sequencing for mutation confirmation and ideally recruitment of family members for segregation study.

3.3.3. APS syndrome due to novel deleterious *CSTA* mutation

We describe here two siblings, from a non-consanguineous family, which present phenotypical characteristics resembling those of APSS and EBS patients. APSS, as previously described by Cassidy *et al*. is characterised by noninflammatory acral peeling skin with peeling accompanied by erythema (Cassidy *et al*., 2005, Shwayder *et al*., 1997, Hashimoto *et al*., 2000). The abnormality is exacerbated by elevated ambient temperature and humidity. Histological observations, showing that the breakage takes place in the superficial layers of the epidermis, make it distinguishable from EBS where peeling begins in the basal layer.

Cassidy *et al*. are also the first to link APSS to a homozygous missense mutation is *TGM5* (Cassidy *et al*., 2005), the gene encoding transglutaminase 5, whereas EBS has been linked to mutations in the *KRT5* and *KRT14* genes encoding for keratin proteins (Chan *et al*., 1993, Chen *et al*., 1993). Initial genetic testing of the affected siblings for mutations in these three candidate genes, revealed wild type *TGM5*, *KRT5* and *KRT14* genes.

Blaydon *et al*. reported two independent families diagnosed with exfoliative ichthyosis linked to loss-of-function mutations in the gene *CSTA* encoding the protease inhibitor cystatin A (Blaydon *et al*., 2011b). The clinical phenotype of these patients, characterised by peeling of skin on palms and soles worsened upon mechanical stress and humidity (Hatsell *et al*., 2003), and resembled that of the patients described in this chapter which led us to consider *CSTA* as a possible candidate for APSS in these patients.

Genetic analysis of *CSTA* in the two affected siblings revealed two variants in exons 1 and 2. One of these variants was a previously reported polymorphism in exon 2, c.C154T:p.Y34Y described under rs17589 – MAF of 0.40, and a deletion covering exon 1 c.1_66del:p.1_22del and possibly part of the intronic flanking regions. This deletion covers the START codon and affects both splice variants of *CSTA*, most likely leading to almost complete loss of expression, and any expressed protein

would lack the N-terminal domain required for the specific inhibition of the target cathepsins. These findings could be addressed further by analysis of patient skin biopsies and *in vitro* analysis using siRNA mediated-knockdown of *CSTA*.

3.4. Summary

In this chapter we describe a number of molecular techniques used to identify possible disease-associated mutations in genes encoding desmosome-associated proteins and in *CSTA,* the gene encoding the protease inhibitor cystatin A, thought to be involved in desmosomal regulation (discussed in Chapter 4). The majority of screened patients were clinically diagnosed with ARVC without cutaneous or hair abnormalities.

In parallel, in two independent studies, siblings diagnosed with hypotrichosis and PPK presented with a novel homozygous mutation in *DSP*, the gene encoding the desmosomal protein desmoplakin, and a patient diagnosed with hypotrichosis without cutaneous abnormalities was found to present three polymorphisms in *DSG4*, the gene previously linked to this disorder. We discuss here the importance of segregation studies for an accurate genetic diagnosis and also consider other broader genome analysis for novel disease-causing mutations in unidentified disease-associated genes.

The possible reasons behind the variety of mutations affecting different genes leading to the same disorder and mutations affecting the same gene leading to different disorders, together with limitations of genetic testing techniques will be addressed in more detail in Chapter 6.

-Chapter 4-

Functional analysis of loss-of-function mutations in the protease inhibitor Cystatin A

4.1. Introduction

The focus of this chapter was to investigate the functional aspects of recessive loss-of-function (LOF) mutations in the gene encoding the protease inhibitor cystatin A (CSTA). Homozygous LOF mutations in *CSTA* are associated with the skin disorder exfoliative ichthyosis. The following introductory section describes the clinical and genetic aspects of this disorder. Part of the findings presented in this chapter have been published by our group (Blaydon *et al*., 2011b).

4.1.1. Loss-of-function mutations in *CSTA* result in exfoliative ichthyosis

Hatsell *et al*. previously described a large, consanguineous Bedouin family with five members presenting with exfoliative ichthyosis characterised by dry, scaly skin over most of their body with nonerythematous peeling of skin on their palms and feet, exacerbated by moisture and minor trauma (Hatsell *et al*., 2003). Recently, our group identified a homozygous LOF mutation in *CSTA* underlying this disorder in the previously described Bedouin family. In addition, we reported another homozygous *CSTA* mutation in a consanguineous Turkish family (Blaydon *et al*., 2011b). The affected family members from this Turkish family presented a similar clinical phenotype as the initially described Bedouin family.

Genetic screening of the *CSTA* gene in affected individuals from the two families revealed a homozygous 3' splice-site variant (c.67-2A>T) in the Bedouin family and a homozygous nonsense mutation (c.256C>T) in the Turkish family (Blaydon *et al*., 2011b). Electron microscopy of patient skin biopsies showed widening of intercellular spaces in the basal/suprabasal layers of the epidermis together with thickening of the keratin intermediate filaments. Analysis of splicing using a *CSTA* minigene construct revealed that the splice-site mutation, segregating with the skin disorder in the Bedouin patient, leads to skipping of the first 12 base pairs of exon 2 in *CSTA*, resulting in an in-frame deletion of four amino acids in the protein sequence of CSTA. *In silico* modelling supports these observations, revealing that the *CSTA* splice-site mutation would bring conformational changes which would affect the protease-binding and inhibitory role of CSTA. Furthermore, *in vitro* analysis revealed very low level expression of the variant protein, possibly due to low

efficiency of the mutant splice site or instability of the variant protein (Blaydon *et al*., 2011b, Gupta *et al*., 2015).

4.1.2. Summary

This chapter is based on the association of LOF mutations in *CSTA* with exfoliative ichthyosis and focuses on the effect of CSTA depletion on keratinocyte cell-cell adhesion and migration to investigate a possible mechanism of action through desmosome-associated proteins. The importance of protease inhibitors and the target proteases in tissue integrity is once more highlighted through this work.

4.2. Results

4.2.1. Functional analysis of loss-of-function mutations in *CSTA*

Throughout this chapter the influence of *CSTA* LOF mutations on the expression and activity of the inhibited proteases and their subsequent targets was investigated. The patient phenotype was modelled in HaCaT cells, a spontaneously immortalised keratinocyte cell line, using the ON-TARGETplus SMART Pool siRNA targeting all isoforms of *CSTA*.

4.2.1.1. Immunofluorescence of CSTA and the target proteases in the skin and immortalised HaCaT keratinocytes

Immunostaining of CSTA in normal interfollicular (Figure 4.1. Ai) and palm skin (Figure 4.1. Bi) showed that CSTA is expressed throughout all layers of the epidermis with a cytoplasmic diffuse localisation and higher expression levels in the granular layer. In palm skin, CSTA appeared as bright granulations throughout the thick stratum corneum (Figure 4.1. Bi). Immunostaining of the target proteases of CSTA, cathepsins B, H and L in normal skin showed expression throughout all layers of the epidermis (Figure 4.2. Ai-Ci). Due to the lack of patient material for an in depth study of this condition, the HaCaT cell line was used to mimic the *CSTA* LOF phenotype. CSTA (Figure 4.1. Ci) and the three target cathepsins (Figure 4.2. Aiii-Ciii) were also investigated in the immortalised HaCaT cell line.

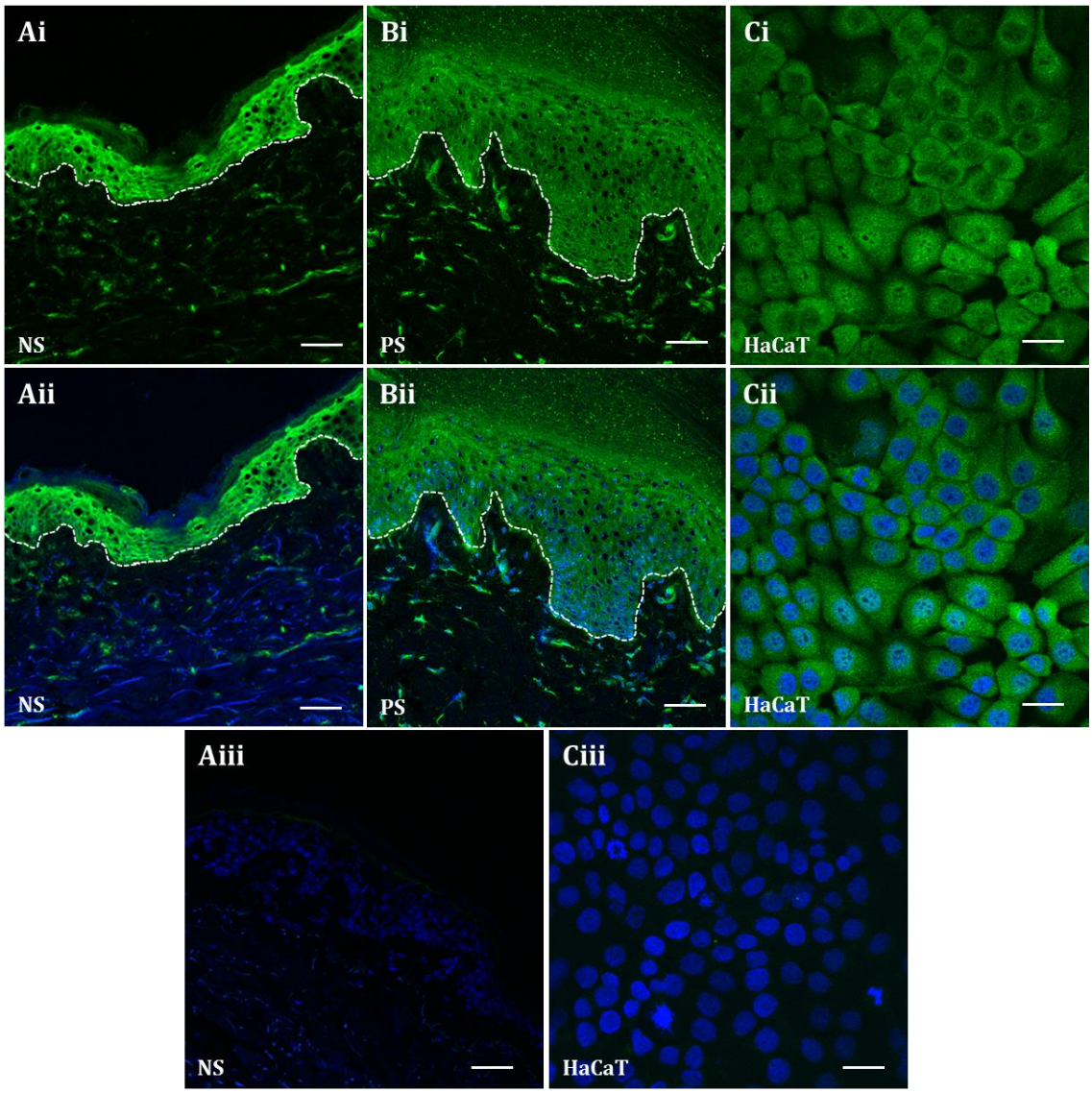

Figure 4.1. Immunofluorescence of CSTA. Immunohistochemistry (IHC) with an anti-CSTA antibody on frozen facelift skin sections **(A)** and frozen palm skin **(B)** from control individuals in the absence **(Ai** and **Bi)** and presence **(Aii** and **Bii)** of DAPI nuclear stain, showed protein expression throughout all layers in both facelift and palm skin with a granular aspect in palm skin. ICC with the same anti-CSTA antibody in HaCaT cells, in the absence **(Ci)** and presence **(Cii)** of DAPI nuclear stain, showed a diffuse cytoplasmic pattern of expression. Negative controls are shown in **(Aiii)** for IHC and **(Ciii)** for ICC. All IHC images were taken at 20 X magnification and Immunocytochemistry (ICC) images at 40 X magnification. IHC imaging was carried out on the Zeiss Meta 710 confocal microscope and ICC imaging was carried out on the LSM 510 confocal microscope. NS – Normal Skin; PS – Palm Skin. CSTA staining is shown in green and DAPI in blue (Scale bar – 50 µm for **A-B** and 20 µm for **C**).

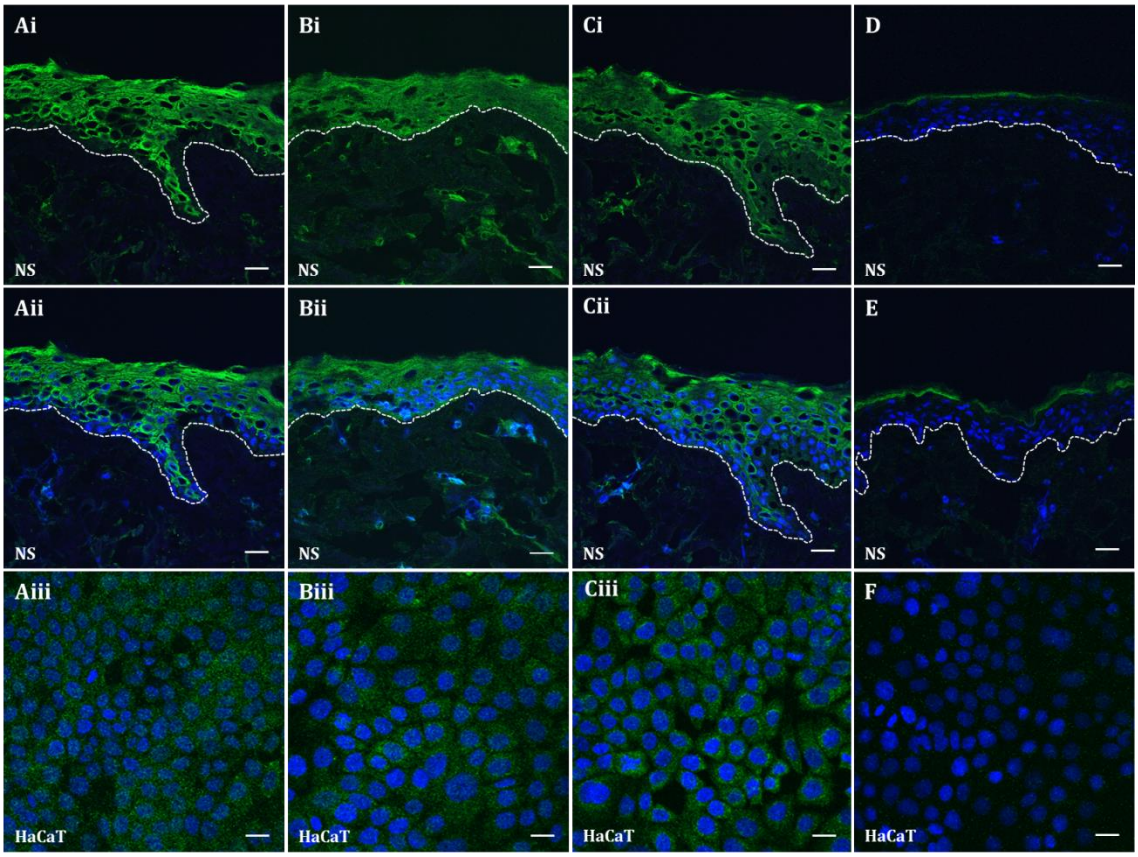

Figure 4.2. Immunofluorescence of the target proteases of CSTA. IHC with anti-cathepsins B **(A)**, H **(B)** and L **(C)** antibodies on frozen facelift skin sections from control individuals in the absence **(Ai**, **Bi** and **Ci)** and presence **(Aii**, **Bii** and **Cii)** of DAPI nuclear stain, showed protein expression throughout all layers of the epidermis. ICC with the same antibodies in immortalised HaCaT cells, in the presence **(Aiii**, **Biii** and **Ciii)** of DAPI nuclear stain, showed good levels of expression with a diffuse localisation pattern similar to observations made in skin sections. Negative controls are shown in **(D** and **E)** for IHC and **(F)** for ICC. All IHC and ICC images were taken at 40 X magnification. Imaging was carried out on the LSM 510 confocal microscope. NS – Normal Skin. Cathepsins B, H and L staining is shown in green and DAPI in blue (Scale bar – 20 μm).

4.2.1.2. Transient siRNA knockdown of CSTA isoforms in HaCaT keratinocytes mimics CSTA LOF mutation

The two identified *CSTA* LOF mutations target both isoforms of *CSTA*. To mimic homozygosity for these LOF mutations, a pool of four siRNAs targeting all mRNAs was purchased from Dharmacon (GE Healthcare). The sequences and targeting sites of this functional siRNA pool are found in Table 2.5. A number of optimisations were performed prior to the siRNA experiments described in this chapter, including optimisation of transfection conditions and time course analysis of *CSTA* knockdown in HaCaT cells. Optimisation of transfection conditions was carried out to find the highest transfection efficiency with reduced cell death. The concentration of the siRNA pool was varied to determine the lowest concentration resulting in significant down-regulation of *CSTA*, in order to reduce off-target effects. A time course analysis was performed to determine the duration of *CSTA* down-regulation. These optimisations are described in Appendix F.1.

The *CSTA* siRNA pool (Figure 4.3. E) reduced *CSTA* expression by 85% in HaCaT cells. Cells transfected with the *CSTA* siRNA pool were designated as *CSTA* siRNA HaCaT cells (Figure 4.3. B). A pool of four non-targeting (NTP) siRNAs was used as a negative control (NTP siRNA cells; Figure 4.3. A).

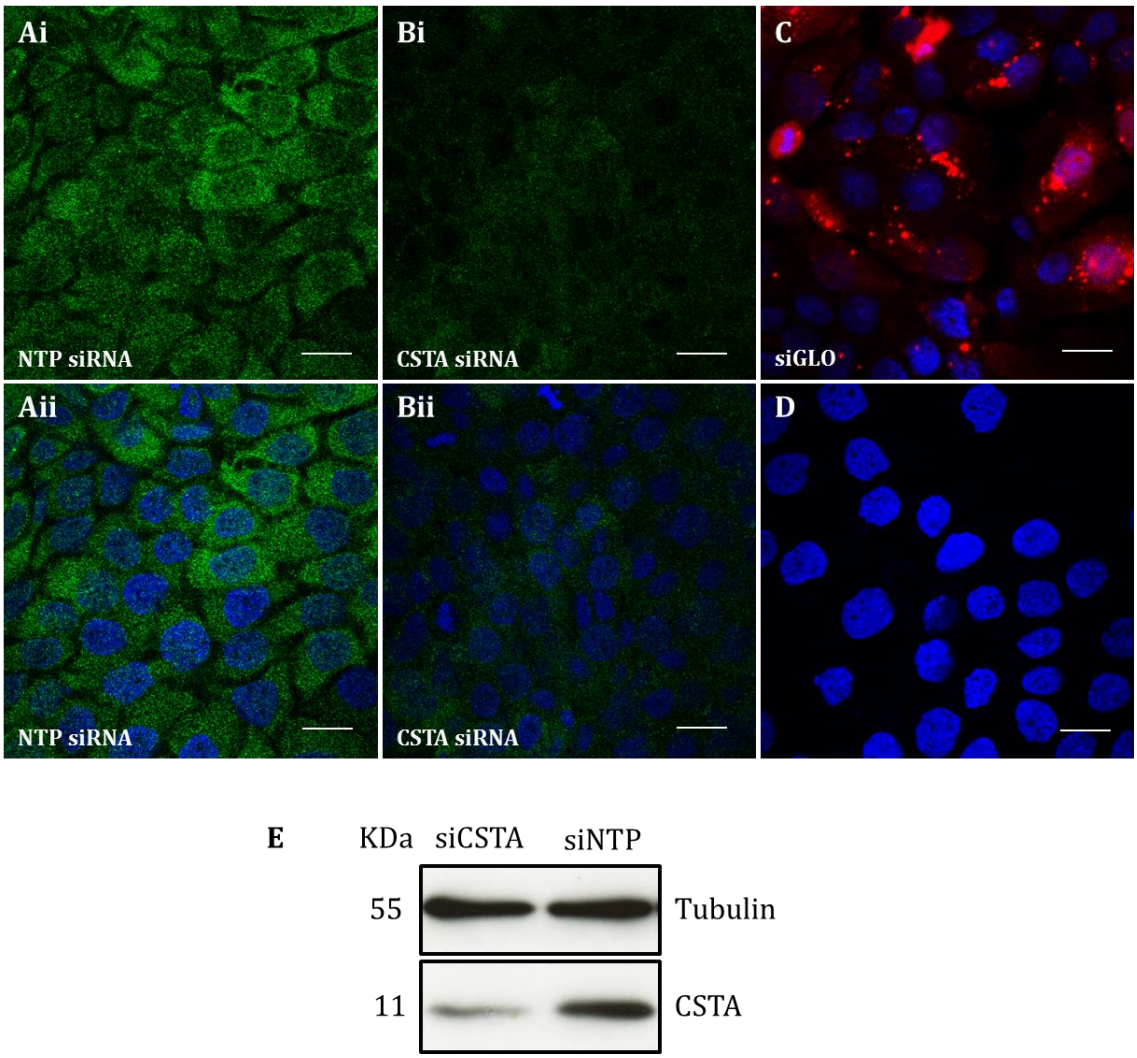

Figure 4.3. Immunocytochemistry and western blot of CSTA in HaCaT cells following siRNA transfection to mimic *CSTA* LOF mutations. ICC with an anti-CSTA antibody in HaCaT cells transfected with a pool of NTP siRNA **(A)** or *CSTA* siRNA **(B)** for 72 h in the absence **(Ai** and **Bi)** and presence **(Aii** and **Bii)** of DAPI as nuclear marker (in blue). A reduction in the CSTA (in green) protein levels can be seen in the *CSTA* siRNA treated cells compared to control cells. siRNA targeting cyclophilin B (**C**; in red) was used as control of transfection. Negative control for ICC is depicted in **(D)**. **(E)** Total protein from HaCaT cell lysates 72 h after transfection with *CSTA* siRNA (lane 1) and NTP siRNA (lane 2) was incubated with an anti-CSTA antibody. Tubulin was used as a loading control. Knockdown of *CSTA* mimics the LOF mutations observed in patients. Imaging was performed with an LSM 510 confocal microscope and images were taken at 63 X magnification (Scale bar – 20 µm).

4.2.1.3. Influence of CSTA LOF mutations on HaCaT intercellular adhesion

To investigate the effects of mechanical stress in *CSTA* siRNA transfected HaCaT cells, the FX-4000™ Cell Stretcher was used. This assay was performed using conditions previously optimised within the group for the same cell line, in order to assess intercellular adhesion (Cabral *et al.*, 2012b). Experimental conditions where NTP control cells showed some degree of mechanical stress but remained attached to the culture dish were used for the assays described in this chapter. Under these conditions and following the electron microscopy observations in patient skin, it was predicted that *CSTA* knockdown cells will have altered cell-cell adhesion properties compared with NTP cells.

CSTA siRNA transfected cells together with NTP siRNA transfected cells as control, were subjected to mechanical stretch at a frequency of 5 Hz (five cycles of stretch and relaxation per second) and an elongation of amplitude ranging from 10% to 14% (increase in diameter across the silicone deformable membrane from 10% to 14%). Cells were stretched for 0 h (non-stretched) and 4 h. Western blots of *CSTA* siRNA HaCaT cell lysates were performed, as previously described, to confirm that *CSTA* knockdown was achieved prior to the stretch assay.

Immunocytochemistry of *CSTA* siRNA-treated cells was performed using an antibody raised against keratin 14 (in green) (Figure 4.4.). After 4 h stretch, under lower magnification, the NTP cell sheet (Figure 4.4. Ai) appeared intact in comparison to the *CSTA* siRNA-transfected cells where the cell monolayer was significantly disrupted (Figure 4.4. Bi). Under higher magnification, in NTP cells, the keratin intermediate filaments appeared normal, however, despite minor intercellular widening of intercellular spaces these cells still appeared connected to each other through intercellular junctions (Figure 4.4. Aii). By comparison, in the *CSTA* siRNA cells, widening of intercellular spaces (arrows) was observed together with thickening of the keratin filaments and in some cases these filaments were retracted towards the nucleus (stars) (Figure 4.4. Bii).

These results suggest that in contrast to NTP cells, which showed a minor increase in intercellular spaces proportional to the exposure to mechanical stretch and no

obvious changes to the keratin filaments, *CSTA* siRNA cells exhibited thicker and retracted filaments and wider intercellular spaces.

To independently assess and quantify the effects of the *CSTA* LOF mutation on cell adhesion, a dispase-based adhesion assay was performed (three independent siRNA experiments with each tested condition in triplicate) (Figure 4.4. C). The cells simulating the *CSTA* LOF mutation showed a much larger, statistically significant, decrease in cell-cell adhesion (indicated by a large number of monolayer fragments produced upon agitation). Additionally, weakened intercellular adhesion could be visualised upon detachment of the cell monolayer from the tissue culture dish by the degree of elastic condensation of the cell sheet. The *CSTA* siRNA monolayer acted identically to the *DSP I/II* siRNA treated cells, used as control for impaired cell-cell adhesion, as previously described by Cabral *et al*., 2012. In contrast, the NTP cell sheet broke into only a small number of fragments. These results are consistent with observations made in the stretch-immunofluorescence assay (Figure 4.4. A), suggesting a role for CSTA in regulation of intercellular adhesion.

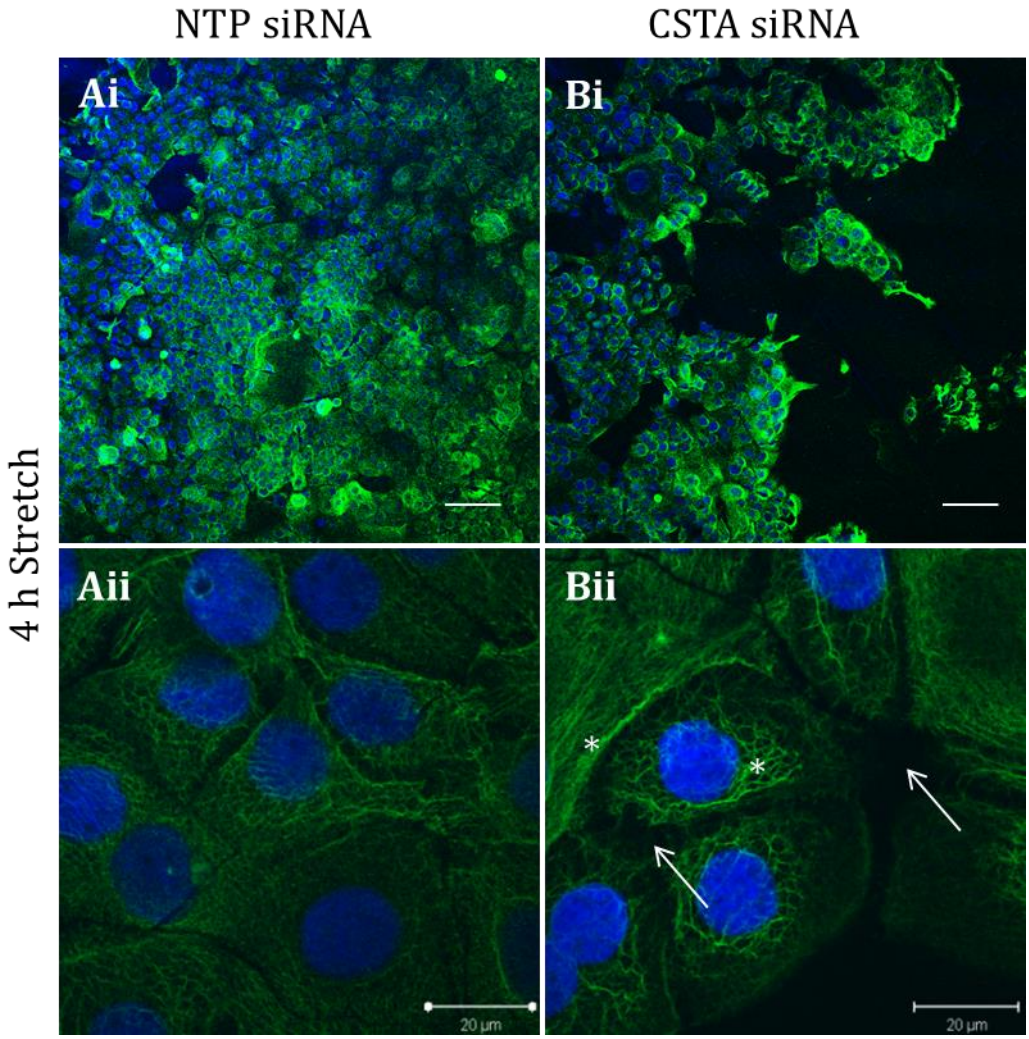

Figure 4.4. Mechanical stress causes reduced cell-cell adhesion and increased IF instability in *CSTA* siRNA treated HaCaT cells. NTP control HaCaT cells **(Ai** and **Aii)** and *CSTA* siRNA cells **(Bi** and **Bii)** mimicking the LOF mutation were subjected to cyclic mechanical stress at a frequency of 5 Hz and amplitude of 10-14% using the Flexcell FX-4000 Tension System for 0 h (non-stretched; Appendix F.2.) and 4 h. ICC with an anti-Keratin 14 antibody revealed that after 4 h stretch, the *CSTA* siRNA cells display thicker and more compact keratin IFs (**Bii**; stars) retracted towards the nuclei. Large intercellular gaps (**Bii**; arrows) were observed predominantly in *CSTA* siRNA, particularly after 4 h stretch, suggesting an adhesion defect. Keratin 14 – in green; DAPI – in blue. Imaging was performed on the LSM 510 confocal microscope and images taken at 10 X **(Ai** and **Bi)** and 63 X magnification **(Aii** and **Bii)** (Scale bar – 100 µm for **Ai** and **Bi**; 20 µm for **Aii** and **Bii**).

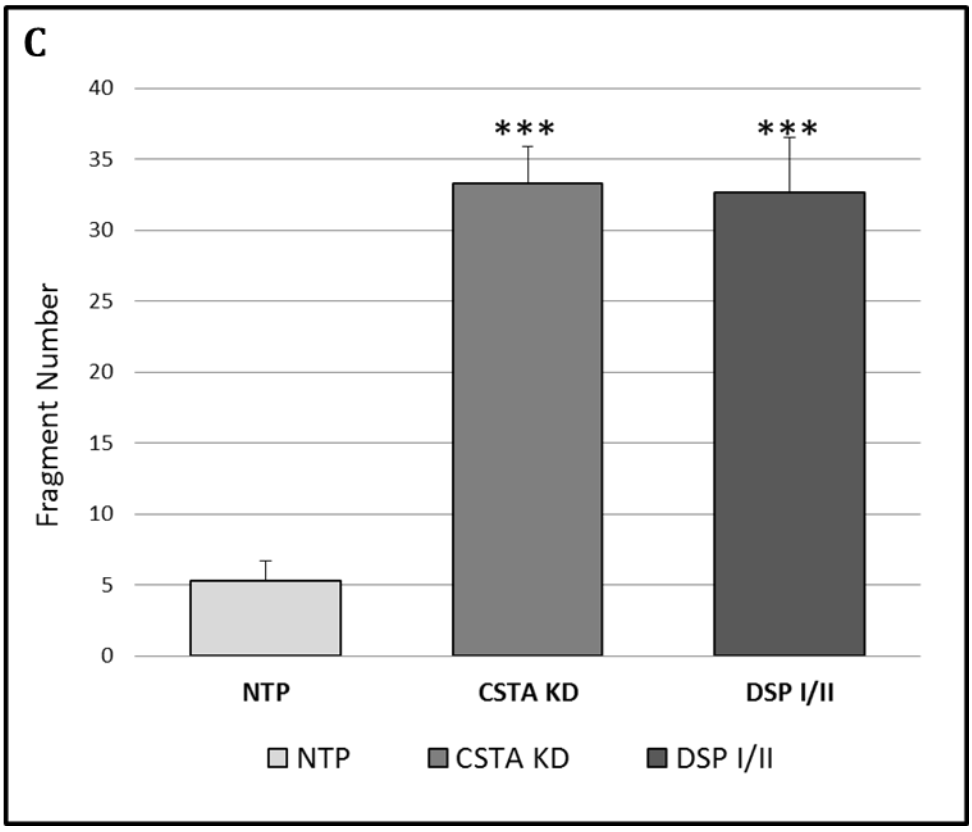

Figure 4.4. Mechanical stress causes reduced cell-cell adhesion and increased IF instability in *CSTA* siRNA treated HaCaT cells (continued). (C) A dispase-based dissociation assay was performed to assess intercellular adhesion by the degree of cell monolayer integrity upon mechanical stress. *CSTA* siRNA cells showed a significant increase in the number of monolayer fragments produced upon agitation, suggesting a statistically significant decrease in cell-cell adhesion, similar to the one observed for *DSPI/II* siRNA treated cells (*** - $p \leq 0.05$) (n=9).

4.2.1.4. Migration is not impaired in CSTA knockdown keratinocytes

A scratch assay was performed to investigate the effects of *CSTA* LOF mutations on cell migration. Three independent knockdown experiments were performed with three repeats per experiment for each siRNA condition. After applying a scratch throughout the *CSTA* siRNA and NTP siRNA cell monolayers, both vertically and horizontally in a cross shape, pictures were taken at set time intervals, 0 h, 24 h and 48 h (Figure 4.5. A), in order to assess and compare the time and speed of scratch closure in *CSTA* siRNA cells compared to control cells. Light microscopy showed normal cell migration in *CSTA* siRNA cells after 48 h comparable to control, and in order to quantify this, the size of the scratch wound was measured for all time intervals. No statistically significant difference was observed, indicative of a normal scratch closure pattern and normal migration process (Figure 4.5. B). Scratch measurements were made using Image J software and resulting scratch measurements are given as arbitrary numbers from a maximum set number.

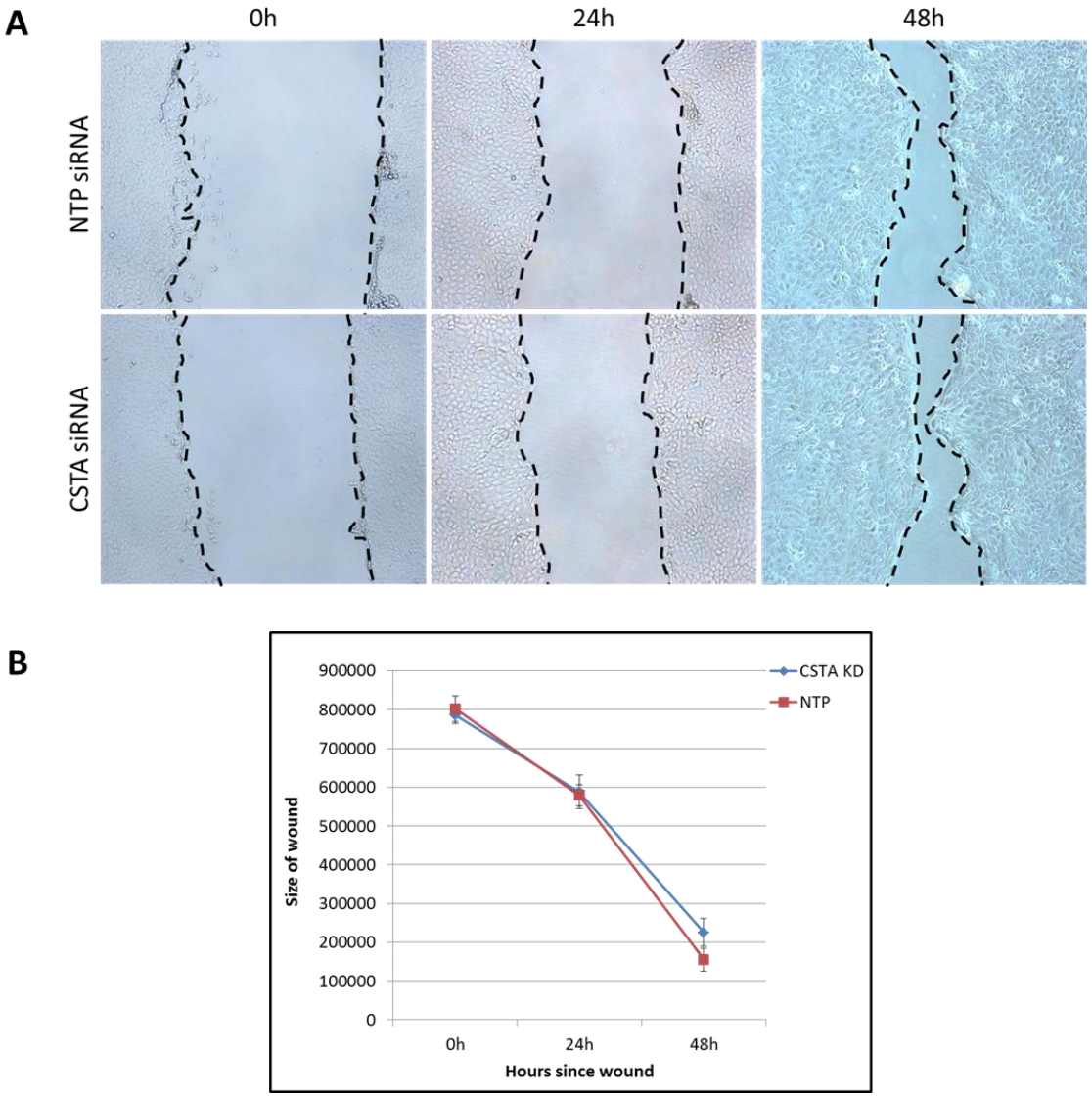

Figure 4.5. "Wound-healing" assay shows normal wound closure after 48 h. (A) Scratch assay to assess migration by the degree of scratch closure after 24 h and 48 h. **(B)** No significant difference was observed between NTP siRNA and *CSTA* siRNA treated cells suggesting that there is no significant reduction in cell migration and scratch closure (n=9).

4.2.1.5. Observations on the expression of CSTA target proteases

Following observations on the intercellular adhesion levels in cells mimicking the *CSTA* LOF phenotype, we decided to assess the expression of the CSTA regulated proteases, cathepsins B and L, in *CSTA* siRNA-treated cells. Cathepsin H was not analysed further due to the low expression observed in the immortalised HaCaT cell line. The levels of secreted and intracellular protein were analysed in cell culture supernatants by ELISA and total protein lysates by western blotting. A number of optimisations for the analysis of cell culture supernatants were performed in order to identify the optimal sample dilutions that would give a clear reading on the luminescence plate reader. Due to the difference in observations following the mechanical stretch and wound-healing assays it was decided that expression of the target cathepsins should be analysed in *CSTA* siRNA-treated cells following both of these assays.

The expression levels of both cathepsins increased upon scratch-wound in both control and *CSTA* siRNA-treated cells with no significant difference between the two conditions. In mechanically stretched cell monolayers the expression of cathepsins B and L presented a slight decrease after 1 h stretch but did not alter significantly after 4 h stretch in comparison to non-stretched cells (Figure 4.6. A). A significant difference was observed between the two proteases in their secreted levels with cathepsin B being secreted at significantly higher levels compared to cathepsin L, following both wound-healing and mechanically-induced stress. This observation was confirmed by western blotting of total protein lysates of *CSTA* siRNA and NTP siRNA cells. Cathepsin B appeared to be expressed in higher levels in comparison to cathepsin L, the observed difference in secretion levels could be interpreted as being due to a difference in baseline expression levels in HaCaT cells (Figure 4.6. B). Cathepsin expression in stretched cells was assessed in triplicate and in scratched cells in duplicate; optical density analysis for the remaining two and respectively one repeat(s) is included in Appendix F.3.

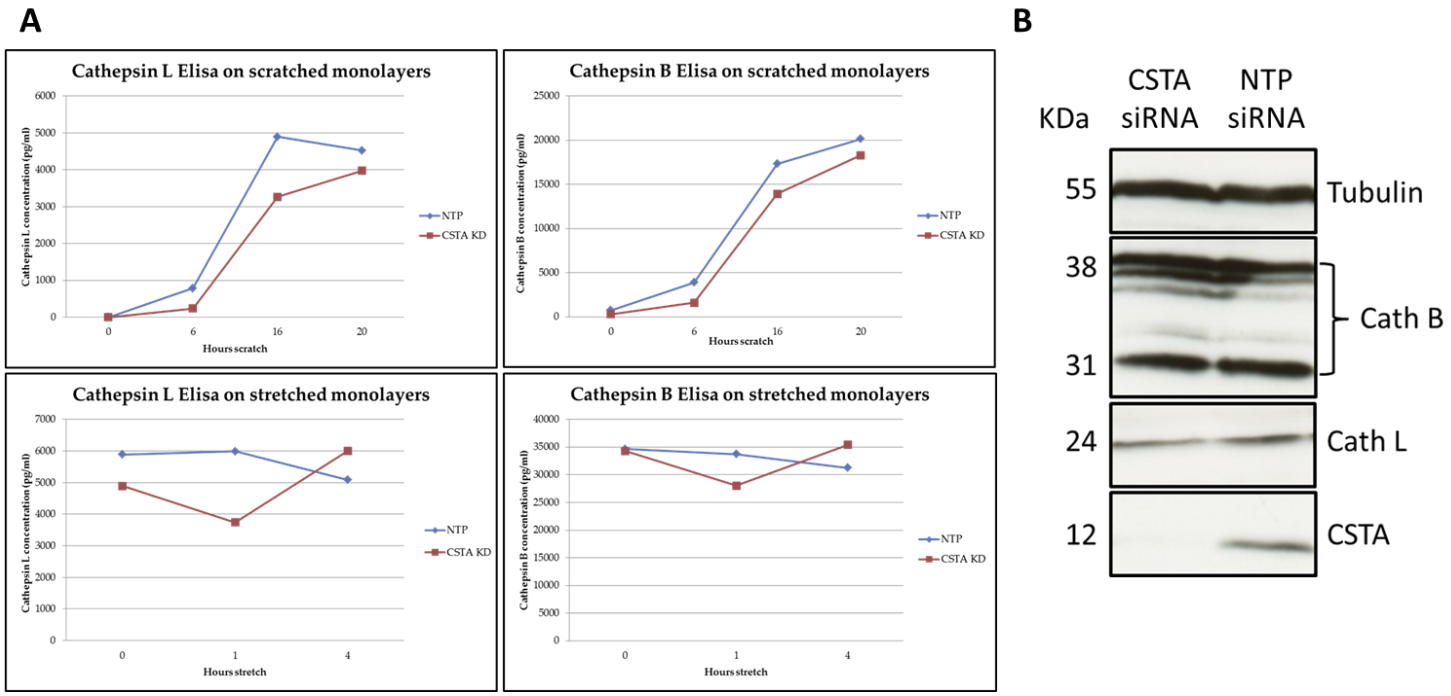

Figure 4.6. ELISA and total protein analysis show unchanged cathepsin B and L levels in culture supernatants and total protein cell lysates. (A) ELISA assay to assess the levels of secreted cathepsins B and L in culture supernatants post scratch-wound (0 h, 6 h, 16 h and 20 h post wound) or mechanical stretch (for 0 h, 1 h and 4 h) in *CSTA* siRNA compared to NTP siRNA. No significant difference was observed between *CSTA* siRNA and control cells (n = 1). **(B)** Total protein cell lysates from HaCaT cells incubated for 72 h with *CSTA* siRNA and NTP siRNA were blotted and incubated with anti-cathepsin L, cathepsin B and CSTA antibodies to check the levels of expression of these proteins. No difference in expression between the two cathepsins was seen between control and *CSTA* siRNA cells.

4.2.1.6. Influence of CSTA LOF mutations on the expression levels of desmosome-associated proteins

The aim of this section was to analyse the expression and localisation of desmosome-associated proteins before and after mechanical stretch in *CSTA* siRNA cells compared to NTP control. This analysis was performed in order to get details about a possible mechanism of action of the target proteases inhibited by CSTA, cathepsins B and L, which possibly could impact on desmosome function.

Total protein cell lysates from HaCaT cells mimicking the LOF *CSTA* mutations and from control cells were obtained and analysed by western blotting. Antibodies targeting DSP, DSC2, DSC3, DSG2, DSG3, PG and PKP2 were used together with anti-vinculin and anti-GAPDH antibodies as loading controls. Three independent siRNA knockdown experiments were conducted and replicate western blots were carried out for each protein in each experiment. Densitometry measurements of western blots were calculated using an image analysis program (Image J, v1.47v) and are graphically depicted in Figure 4.7. B for DSG3, which was consistent between repeats, and Appendix F.4. for all of the other proteins analysed.

A key observation was that DSG3 protein levels showed an increase in expression levels following *CSTA* siRNA knockdown (Figure 4.7. B). Protein levels were normalised against the loading control band, GAPDH, and are presented as a fold change from NTP control for the western blot for DSG3 in Figure 4.6. A. Variable results were observed for DSG2 and DSP expression levels between the three independent experiments, and further repeats would be necessary to draw a conclusion. No detectable differences were observed in the expression levels of the other desmosome-associated proteins, DSC2, DSC3, PG and PKP2, between *CSTA* siRNA cells and NTP control cells, in any of the independent knockdown experiments. All three independent knockdown experiments showed consistent results for the expression level of DSG3, which was increased in *CSTA* siRNA cells compared to NTP cells. Figure 4.7. B shows densitometry analysis results of protein levels of DSG3 calculated from the western blot shown in Figure 4.7. A. The remaining two independent knockdown experiments have been included in Appendix F.4. together with their densitometric analysis.

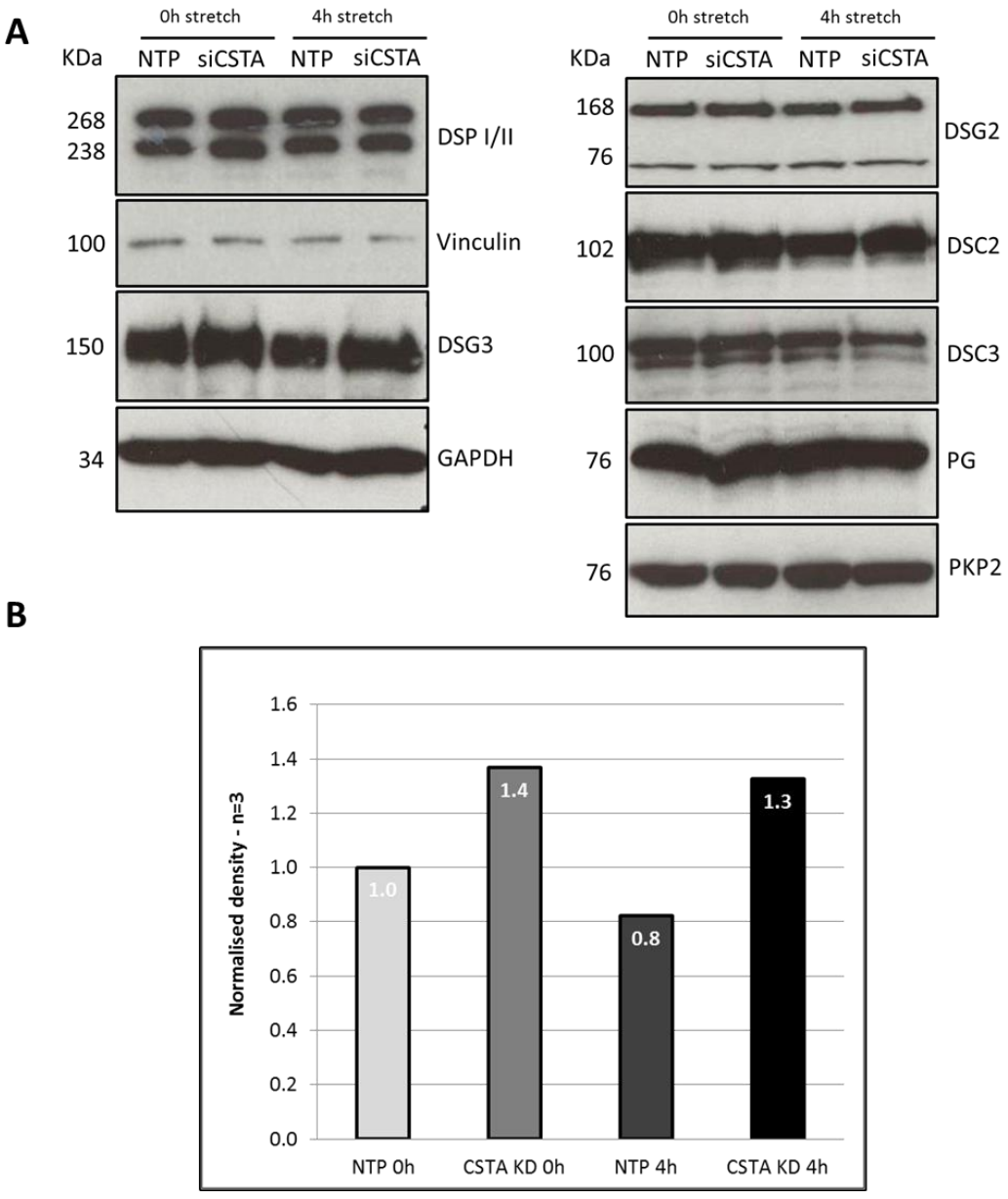

Figure 4.7. Protein levels of desmosomal proteins following *CSTA* knockdown show that DSG3 expression levels are increased in *CSTA* siRNA treated cells. (A) Total protein cell lysates from *CSTA* siRNA and NTP HaCaT cells, non-stretched and stretched for 4 h, were blotted and incubated with anti-DSP, DSC2, DSC3, DSG2, DSG3, PG or PKP2 to check the levels of expression of these proteins. **(B)** Protein levels of DSG3 calculated from densitometry measurements of the western blot image and normalised to loading control (GAPDH). Total DSG3 expression levels are presented as a fraction of the total DSG3 levels of NTP cells; standard error bars are shown on the protein analysis graph included in Appendix F.4. No change was observed for DSC2, DSC3, DSG2, PKP2 and PG. DSP gave variable results and will need to be analysed further (n = 3 blots; densitometry analysis in Appendix F.4.).

Following these observations on western blotting, immunocytochemistry of *CSTA* siRNA-treated cells in comparison to NTP control was performed for DSG3, DSP and DSG1/2. Unfortunately, the anti-DSG3 antibody did not work well by this method (data not shown).

Immunocytochemistry using an anti-DSP antibody on NTP siRNA (Figure 4.8. A and C) and *CSTA* siRNA (Figure 4.8. B and D) treated cells, both in non-stretched and after 4 h stretch conditions, showed similar expression levels in non-stretched *CSTA* siRNA and in NTP control cells. However, following 4 h stretch there appears to be an up-regulation of DSP expression together with an evident increase in DSP levels in the cytoplasmic compartment of cells treated with *CSTA* siRNA (Figure 4.8. D).

Staining using an antibody targeting both DSG1 and 2 on siRNA-treated cells showed up-regulation in protein expression together with an aberrant expression of these cadherins in the cytoplasmic compartment of *CSTA* siRNA-treated cells (Figure 4.9. A), following 4 h mechanical stretch, compared to NTP control treated under the same conditions (Figure 4.9. B).

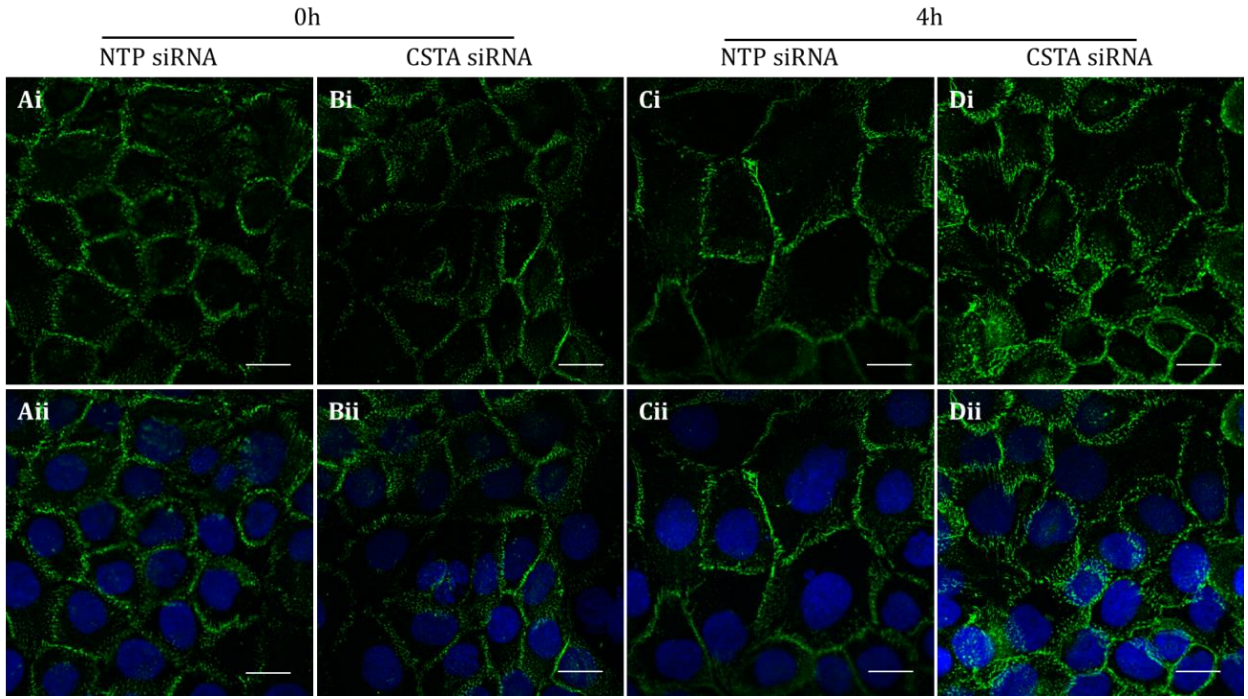

Figure 4.8. Immunocytochemistry of DSP in HaCaT cells following siRNA transfection and mechanical stretch. ICC with an anti-DSP (in green) antibody in HaCaT cells transfected with a pool of NTP siRNA **(A** and **C)** or *CSTA* siRNA **(B** and **D)** both in non-stretched **(A** and **B)** and post 4 h stretch **(C** and **D)** in the absence **(Ai-Di)** and presence **(Aii-Dii)** of DAPI as nuclear marker (in blue). Similar protein levels can be observed for non-stretched NTP and *CSTA* siRNA treated cells **(A** and **B)**. *CSTA* siRNA treated cells post 4 h stretch present with an increased DSP expression and a more significant cytoplasmic appearance **(D)** than NTP control **(C)**. Imaging was performed with the Zeiss Meta 710 confocal microscope and images were taken at 100 X magnification (Scale bar – 20 μm).

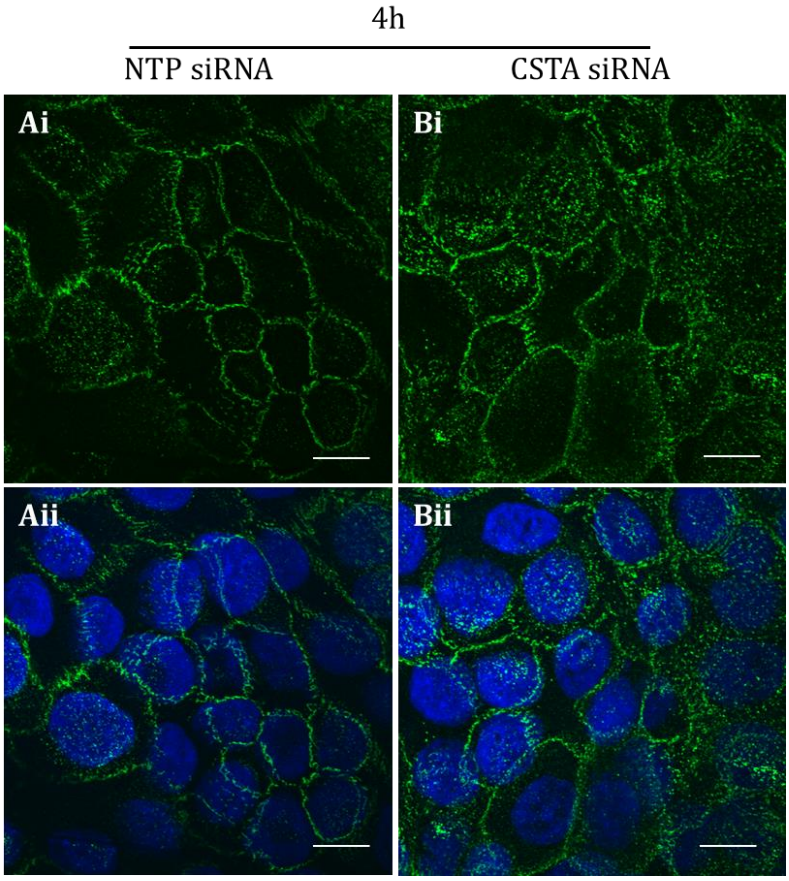

Figure 4.9. Immunocytochemistry of DSG1/2 in HaCaT cells following siRNA transfection and mechanical stretch. ICC with an anti-DSG1/2 (in green) antibody in HaCaT cells transfected with a pool of NTP siRNA **(A)** or *CSTA* siRNA **(B)** post 4 h stretch in the absence **(Ai** and **Bi)** and presence **(Aii** and **Bii)** of DAPI as nuclear marker (in blue). *CSTA* siRNA treated cells post 4 h stretch present with an increased DSG1/2 expression and a slightly increased cytoplasmic appearance **(B)** than NTP control **(A)**. Imaging was performed with the LSM 510 confocal microscope and images were taken at 100 X magnification (Scale bar – 20 μm).

4.3. Discussion

The main focus of the work described in this chapter was the *in vitro* analysis of the mechanism of action by which *CSTA* LOF mutations lead to exfoliative ichthyosis, possibly via regulation of desmosome assembly and migration towards the upper layers of the epidermis. We describe for the first time the importance of CSTA in the basal-suprabasal layers of the epidermis, with a previously unknown role and possibly a novel mechanism of action. Part of the results presented here have been published by Blaydon *et al*. (Blaydon *et al*., 2011b).

4.3.1. Expression of cystatin A in normal skin and *in vitro* cell model

CSTA was previously described as an intracellular protease inhibitor, despite being identified in sweat and in medium from cultured keratinocytes, with functions limited to its involvement in the upper layers of the epidermis, including its role in protection against dust mite allergens Der p 1 and Der f 1 and also associated with psoriasis and atopic dermatitis linked to a defective skin barrier (Kato *et al*., 2005, Vasilopoulos *et al*., 2007, Vasilopoulos *et al*., 2008). No studies have looked at the role played by CSTA in the lower layers of the epidermis, prior to our research findings linking *CSTA* LOF mutations to the skin disorder exfoliative ichthyosis (Blaydon *et al*., 2011b).

Staining of CSTA in normal facelift and palm skin revealed a diffuse cytoplasmic localisation and expression throughout all layers of the epidermis, with increased expression in the granular layer and distinct granulation-like formations mostly in the stratum corneum of palm skin which could perhaps be explained as CSTA-transporting vesicles, possibly due to its function in anti-allergenic protection.

To study further the effect of *CSTA* LOF mutations and due to the lack of patient skin biopsy material, we have manipulated CSTA expression in HaCaT keratinocytes. ICC confirmed observations made on staining of normal epidermis, showing a diffuse cytoplasmic expression of CSTA in the above mentioned cell line.

4.3.2. *CSTA* transient down-regulation leads to impaired intercellular adhesion but normal cell migration

To model the phenotype observed in patients with exfoliative ichthyosis *in vitro*, we used the HaCaT cell line coupled with siRNA mediated knockdown of *CSTA*. This experiment was performed together with the use of an NTP knockdown control and siRNA targeting the cyclophilin B gene (siGlo) as transfection control. A robust *CSTA* knockdown with a significant protein reduction was obtained which remained low between 48 h and 136 h, which was as long as we needed for any of the analyses executed. No obvious effect on cell viability was observed.

One specific phenotypical characteristic of exfoliative ichthyosis is epidermal peeling on areas exposed to mechanical stress and increased humidity such as the palmoplantar regions and the neck area. By electron microscopy, as reported by Blaydon *et al*., widening of the intercellular spaces and thickening of the keratin filaments in the lower layers of the epidermis in patient skin was observed (Blaydon *et al*., 2011b). These observations were replicated *in vitro* in *CSTA* knockdown monolayers by subjecting them to cycling mechanical stretch. Similarly to EM observations, clear widening of the intercellular spaces was noted in *CSTA* knockdown cells post-stretching together with breakage of the cell sheet into a larger number of fragments compared to NTP control and thickening of the keratin intermediate filaments together with retraction from the plasma membrane towards the nucleus. A dispase-based dissociation assay performed on *CSTA* knockdown monolayers versus NTP control strenghtened the observations made by mechanical stretch assay highlighting yet again a significant dysregulation in intercellular adhesion.

Our hypothesis is that this dysregulation of intercellular adhesion, mostly as its seen together with thickening of keratin filaments and their retraction towards the nucleus, could possibly be due to an indirect mechanism targeting some of the adhesive intercellular structures, most likely the desmosomes responsible for binding keratin filaments to the plasma membrane. This mechanism will be discussed further.

The target proteases of CSTA, cathepsins B, H and L, are observed to be frequently upregulated in cancer, and appear to facilitate tumour invasion and metastasis through cleavage of cell-cell adhesion junctions (Strojan *et al*., 2000). This observation, in conjunction with the observations of the dysregulated intercellular connections in stretched *CSTA* knockdown monolayers, cell migration in *CSTA* siRNA treated cell monolayers by the scratch assay was assessed. However, no change in the rate of cell migration was noted following *CSTA* knockdown in comparison to NTP control.

4.3.3. Cathepsin B expression appears significantly upregulated following scratch assay, compared to cathepsin L expression

A study by Strojan *et al*., looking at patients with squamous cell carcinoma (SCC) of the head and neck has observed that decreased expression of CSTA correlates with increased activity of the target proteases, cathepsins B, H and L (Strojan *et al*., 2000). In addition, reduced expression of CSTA was observed in SCC of the head and neck (Anicin *et al*., 2013). Another analysis by Li *et al*., looking at laryngeal cancer patients has reported that in *in vitro* conditions down-regulation of cathepsin B together with up-regulation of CSTA expression significantly inhibited the migration, invasion and proliferation of laryngeal cancer cells (Li *et al*., 2011).

Two *in vitro* studies looking at cathepsin B secretion following scratch assays in HaCaT monolayers have revealed that following wounding these cells secreted increased levels of cysteine protease cathepsin B, which was present in vesicles within cellular protrusions forming cell-cell contact sites (Buth *et al*., 2004, Buth *et al*., 2007). It is, therefore, believed that cysteine proteases contribute to the remodeling of the extracellular matrix and thus the loss or decreased expression of cysteine protease inhibitors could lead to uncontrolled breakage of intercellular connections, as observed in the stretch and dispase-based analyses performed in this thesis.

The expression of cathepsins B and L in *CSTA* siRNA treated cell monolayers in comparison to NTP control cells revealed overall higher endogenous levels of cathepsin B expression compared to cathepsin L, independent of treatment

conditions, with a significant increase in expression of both cathepsins following the application of a scratch wound. No significant change was observed for mechanically stretched monolayers for either of the cathepsins.

These findings confirm the studies reported by Buth *et al*., which have also used HaCaT cells in their experiments. This analysis could be replicated in other keratinocyte cell lines which may present with different baseline cathepsin expression levels.

4.3.4. Dysregulation of desmosome-associated proteins in *CSTA* knockdown cells following mechanical induced stress

A number of studies have reported an overexpression of cathepsin B mRNA, increased cathepsin B staining and elevated cathepsin B activity in different human cancers; these leading to degradation of components of the basement membrane and extracellular matrix, both intracellularly and extracellularly in a cell type-dependent manner (Yan *et al*., 1998, Kos *et al*., 2014). However, there are no reports associating directly cathepsin activity to desmosome regulation.

However, insights into protease regulation are emerging from the studies of genetic skin diseases. For example, Netherton syndrome is associated with mutations in *SPINK5* encoding LEKTI-1 which targets the proteases KLK5, KLK7 and KLK14 (Deraison *et al*., 2007) ultimately leading to DSG1 degradation and desmosome cleavage with detachment of the stratum corneum (D'Alessio *et al*., 2013, Hovnanian, 2013). Inhibition of these proteases by SPINK6 and SPINK9, is reportedly leading to desquamation through their action on DSG1, DSC1 and corneodesmosin (Meyer-Hoffert *et al*., 2009, Meyer-Hoffert *et al*., 2010, Brattsand *et al*., 2009).

Another study reporting a syndrome of severe skin and bowel inflammation, increased susceptibility to infection and cardiomyopathy, associated with *ADAM17* LOF mutations, revealed an increase in DSG2 protein expression, implying a reduction in DSG2 shedding by ADAM17 (Blaydon *et al*., 2011a). By contrast, patients with tylosis with oesophageal cancer (TOC), characterized by PPK, follicular papules and oral keratosis (Ellis *et al*., 1994, Hennies *et al*., 1995, Stevens

et al., 1996), linked to mutations in the *RHBDF2* gene, encoding for iRHOM2 (Blaydon *et al*., 2012, Saarinen *et al*., 2012), present with immature desmosomes lacking the electron dense midlines (Brooke *et al*., 2014). Furthermore, *in vitro* studies in TOC patient derived keratinocyte cell lines revealed a dramatic increase in the iRHOM2-mediated processing and activity of ADAM17, together with an increase in processing of DSG2 (Brooke *et al*., 2014).

In Pemphigus vulgaris (PV), an acquired skin disorder affecting the basal layers of the epidermis, DSG3 autoantibodies lead to internalization of this protein, impairment of correct desmosome assembly, with deficient Ca^{2+}-independent desmosome formation ultimately leading to severe blistering (Cirillo and Al-Jandan, 2013). A more recent study has revealed that enhanced expression of PKP1 protects keratinocytes from PV IgG-induced intercellular loss of adhesion, by clustering DSG3 to DSP through the PG binding tail of DSP and enabling the formation of Ca^{2+}-independent desmosomes in a hyperadhesive state (Tucker *et al*., 2014). The significant difference between PV and Pemphigus foliaceus (PF), characterized by superficial blisters due to autoantibodies targeted against DSG1 (Ishii *et al*., 1997), highlights the important role played by DSG3 in the more basal layers of the epidermis, where DSG1 is not present and cannot therefore compensate for the anti-DSG3 autoantibodies in PV, through the so-called DSG compensation theory (Shirakata *et al*., 1998).

The complex interaction between DSG3 and PG has also been studied in SCC of the head and neck (HNC) by Chen *et al*., showing that DSG3 is overexpressed in HNC and the degree of overexpression is associated with clinico-pathologic features. Silencing of *DSG3* significantly suppressed carcinogenic potential in cellular and *in vivo* animal studies by reducing cell growth, cell migration and invasion abilities through PG translocation to the nucleus and reduction in tumoral target gene expression (Chen *et al*., 2007, Chen *et al*., 2013).

Following the observations of dysregulation of adhesion in *CSTA* LOF cells following mechanical stretch, the expression and localisation of most of the desmosomal proteins expressed in the basal/suprabasal layers of the epidermis, where widening of the intercellular spaces was noted in patient skin, was investigated.

Total protein analysis from stretched *CSTA* siRNA treated cells revealed an up-regulation in DSG3 expression in siRNA treated cells independent of mechanical stress. DSP and DSG1/2 expression appeared increased in siRNA treated cells but as the expression levels varied between experiments we believe that these results should be replicated further. No changes in expression levels were noted for the other desmosomal proteins analysed.

However, immunocytochemical staining of DSP and DSG1/2 in cell monolayers, under the above mentioned conditions, revealed an apparent up-regulation of expression with a clear change in localisation to the cytoplasmic compartment compared to a membranous localisation in NTP cells. This suggests that CSTA could possibly regulate cell-cell adhesion via desmosomes through its target proteases. Staining of the other desmosomal components could also be investigated.

4.4. Summary

This chapter investigated a role for the protease inhibitor CSTA in the basal/suprabasal layers of the epidermis. CSTA and its target cathepsins, B, H and L appear to be expressed throughout all layers of the epidermis and in a keratinocyte cell line. A robust *CSTA* knockdown mimicking the LOF mutations, coupled with mechanical stretch and a dispase-based dissociation assay has revealed a significant reduction in intercellular adhesion levels, but no change in cell migration by scratch assay. We believe that a possible mechanism of action of this protease inhibitor could indirectly target desmosome assembly and remodelling through the target proteases of CSTA. This hypothesis is supported by observations showing that DSG3 appears overexpressed in *CSTA* siRNA treated monolayers independent of mechanical stress, and that DSG1/2 and DSP appear to re-localise to the cytoplasm following mechanical stretch suggesting that breakage of the keratin filaments could also result from dysregulation of the desmosomal complex.

-Chapter 5-

PLACK syndrome due to loss-of-function mutations in the protease inhibitor Calpastatin

5.1. Introduction

In this chapter, the functional aspects of loss-of-function mutations in the *CAST* gene, encoding the protease inhibitor calpastatin, are explored. Our group identified LOF *CAST* mutations associated with a novel clinical entity which we have named PLACK (PSS with Leukonychia, Acral punctate keratoses, Cheilitis and Knuckle pads) syndrome. The following introductory section describes the clinical and genetic aspects of this condition.

5.1.1. *CAST* LOF mutations linked to PLACK syndrome

We identified LOF mutations in CAST, the gene encoding for the protease inhibitor calpastatin, as the genetic cause of the autosomal recessive skin disease PLACK syndrome. Three unrelated families were included in this study. One affected individual (PK1) from a Chinese consanguineous family presented as an adult with generalised skin peeling and a history of superficial acral blistering in childhood, as well as the features above. A second affected individual (PK2) from a Nepalese family developed acral punctate keratoses and cheilitis at the age of 1, acral and limb superficial peeling at the age of 3, as well as leukonychia (Figure 5.1. B). Punctate lesions on the dorsum of the hands coalesced into knuckle callosities with milia. Two affected siblings (PK3 and PK4) were previously described as having a recessive form of pachyonychia congenital. Further clinical investigation revealed a history of blistering and peeling of skin from the age of about 3 months on the hands, feet, knuckles, elbows and knees, leukonychia, leukokeratosis, angular cheilitis, papules on the extensor surface of the fingers and toes, and punctate palmar keratosis and a plantar keratoderma (Haber and Rose, 1986). Exome sequencing of the four affected individuals revealed homozygous LOF mutations in *CAST,* which segregated with the disorder in all families:

PK1: frameshift mutation (c.607_608insAfs, p.I203Nfs*8),

PK2: nonsense mutation (c.A232T, p.K78X),

PK3 and PK4: frameshift mutation (c.1750delG, p.Val584Trpfs*37).

All three mutations were predicted to lead to complete loss of expression of *CAST*. Calpastatin is a specific protease inhibitor of calpains, intracellular cysteine proteases that require calcium or epidermal growth factor for their catalytic activity. The calpains have been related to a variety of processes such as the growth, migration and death of keratinocytes (Carragher and Frame, 2004).

In this chapter we focus on the genetic and functional analysis of the LOF mutations by using siRNA to knockdown *CAST* expression in the immortalised keratinocyte cell line HaCaT. Some of the results presented in this chapter are included in Lin *et al*. (Lin *et al*., 2015).

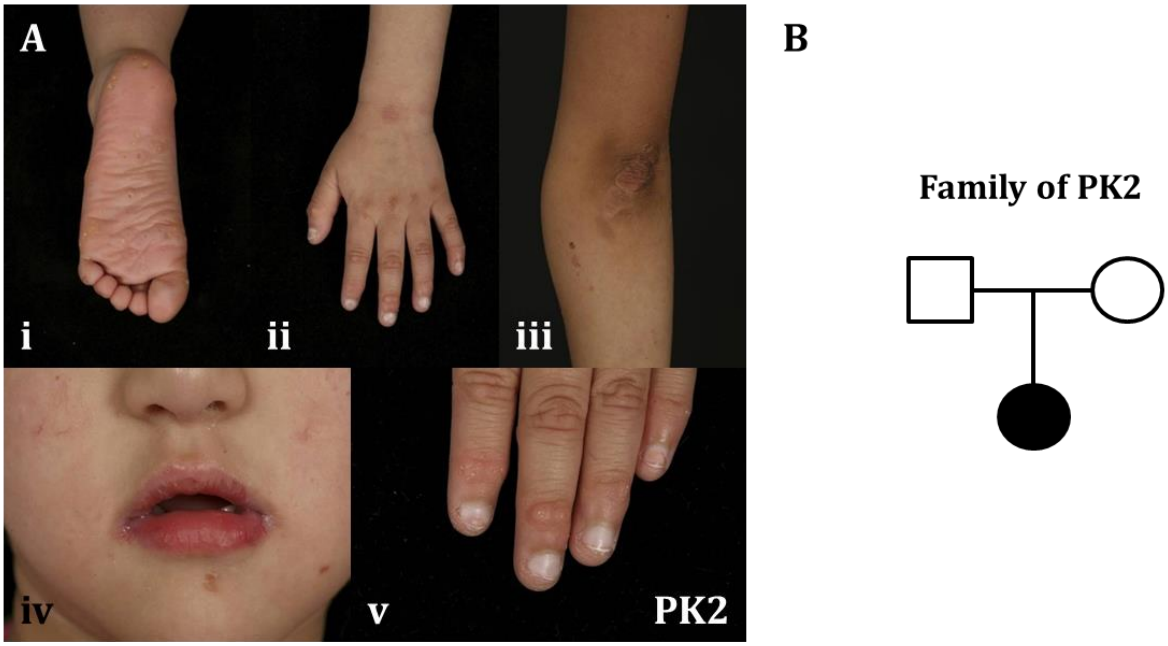

Figure 5.1. PLACK syndrome in PK2 homozygous for p.K78X. (A) Clinical features of PK2 are shown, including skin peeling (iii), cheilitis (iv), punctate keratosis of the soles (i), blistering (ii), leukonychia (v), and knuckle pads with hyperkeratotic micropapules (v). **(B)** Family pedigree of PK2 (Square – Male; Circle – Female; Filled symbol – PK2 homozygous for p.K78X in *CAST*).

5.1.1. Summary

Briefly, the identification of three *CAST* LOF mutations leading to a new clinical entity, which we suggest to be named PLACK syndrome, is described in this thesis. The histological and ultrastructural characteristics of affected skin biopsies are presented together with the *in vitro* analyses of adhesion, cell viability and migration, and desmosome regulation following siRNA-mediated knockdown of *CAST* in HaCaT cells.

5.2. Results

5.2.1. Functional analysis of LOF mutations in *CAST*

This chapter describes the genetic analysis of patient PK2 who harbours the homozygous p.K78X *CAST* mutation, and investigates the effects of the *CAST* LOF mutation on epithelial integrity. The affected phenotypical characteristics were mimicked in an immortalised keratinocyte cell line using the ON-TARGETplus SMART Pool siRNA targeting all isoforms of *CAST*.

5.2.1.1. CAST LOF mutation identified in PK2

Given that the clinical phenotype was complex and no disease-associated genes were known for this condition, an exome capture was performed on affected genomic DNA. Exome sequencing revealed a homozygous nonsense mutation (c.A232T, p.K78X) in *CAST* as the likely underlying genetic cause of the syndrome. Sanger sequencing of affected DNA, performed by Dr Claire Scott, confirmed the existence of a change from adenine to thymine at the genomic DNA level, which changes a lysine amino acid into a STOP codon at the protein level. Control genomic DNA was wild type and parent DNA was heterozygous for this mutation (Figure 5.2.).

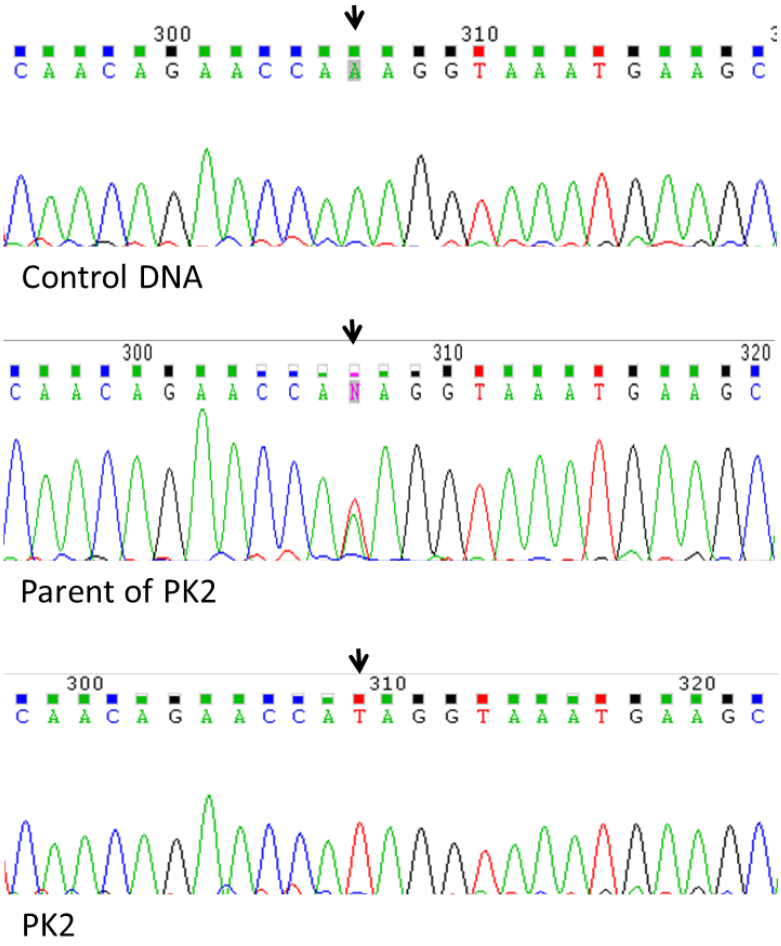

Figure 5.2. Confirmation of p.K78X mutation in the *CAST* gene of PK2. Electropherograms of wild type control, heterozygous parent of PK2, and PK2 genomic DNA sequences. Sanger sequencing revealed a homozygous transversion from adenine to thymine at coding position 232 of *CAST,* which changes a lysine amino acid to a STOP codon at the protein level (c.A232T:p.K78X). Genomic DNA from a non-affected individual was used as wild type control. Sanger sequencing was performed by Dr Claire Scott.

5.2.1.2. Histological and immunohistochemical observations of PK2 skin

Histological examination of a non-lesional skin biopsy from PK2, homozygous for p.K78X in *CAST*, showed minor thickening of the basal layer and widening of intercellular spaces in the basal and suprabasal layers of the epidermis (Figure 5.3. B), in comparison to control skin (NS) (Figure 5.3. A).

Immunohistochemistry of paraffin embedded skin from PK2 with an antibody raised against calpastatin showed a significant reduction in protein expression in skin from PK2 (Figure 5.3. D), compared to bright cytoplasmic staining throughout all layers of the epidermis in normal control skin (Figure 5.3. C).

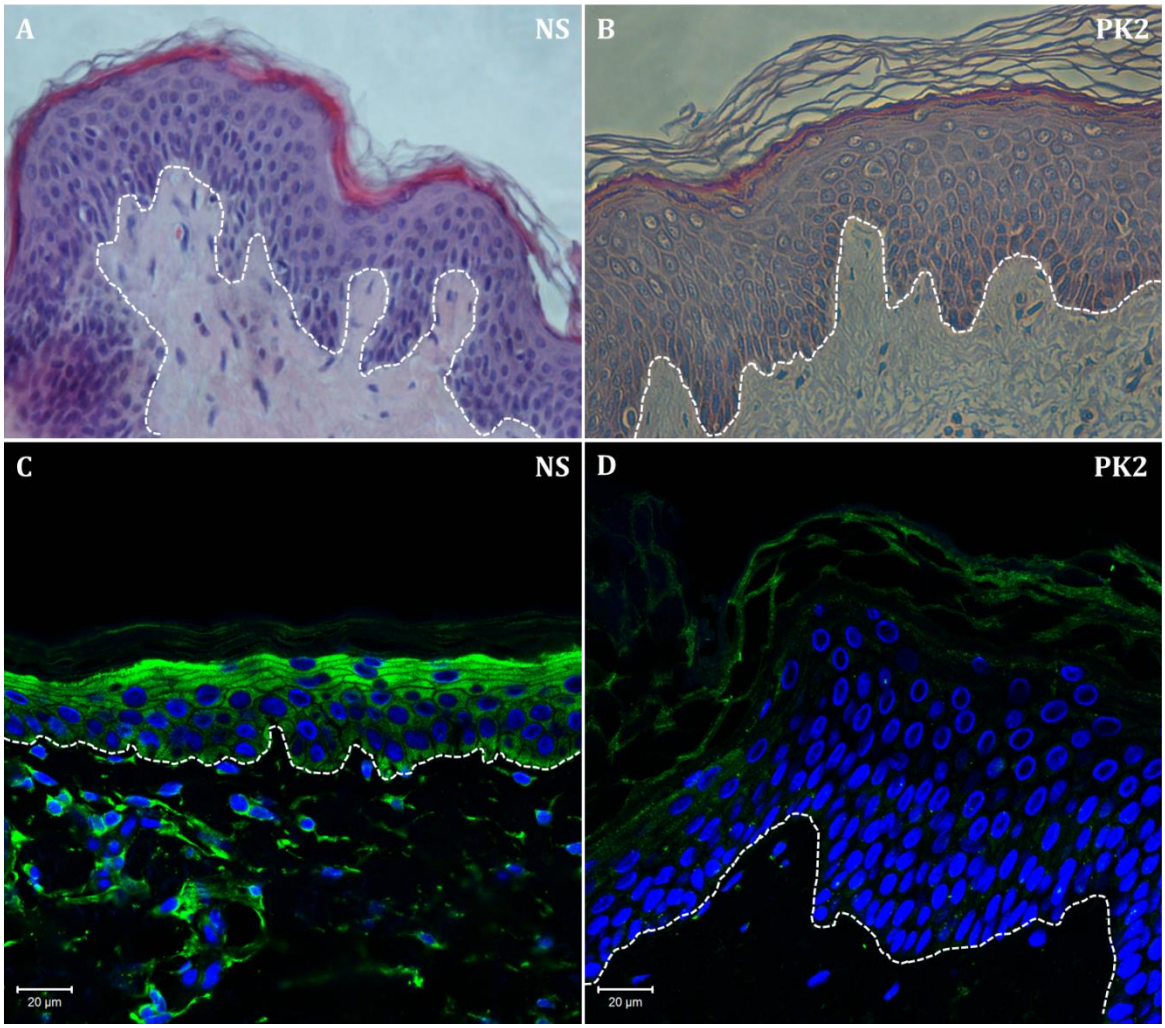

Figure 5.3. Haematoxilin and Eosin (H&E) and immunohistochemistry staining of PK2 skin biopsy. H&E stain of normal skin (NS; **A**) and skin from PK2 **(B)** revealed widened intercellular spaces in the basal - suprabasal layers in affected skin in contrast to NS. H&E was performed by Mr Benjamin Fell. IHC with an anti-calpastatin antibody (in green) showed normal expression of calpastatin throughout all layers of normal skin (NS, **C**) and protein absent from all layers in affected skin (p.K78X; **D**), in the presence of DAPI as nuclear marker (in blue). IHC was performed by Dr Claire Scott. Imaging of H&E staining was carried out on the Nikon Eclipse TE 2000-S and Nikon Digital Sight at 10 X magnification. IHC imaging was carried out on the Zeiss Meta 710 confocal microscope and images were taken at 40 X magnification. NS – Normal skin; PK2 – Affected skin (Scale bar –20 µm for **C** and **D**).

5.2.1.3. Transient siRNA down-regulation of CAST isoforms in HaCaT keratinocytes

To determine the functional consequences of *CAST* LOF mutations *in vitro*, siRNA-mediated knockdown of *CAST* was performed in HaCaT cells, using a specific pool of four siRNAs (ON-TARGETplus Human *CAST* siRNA SMARTpool, GE Healthcare Dharmacon). The sequences and targeting sites of this functional siRNA pool are found in Table 2.5. NTP siRNA (ON-TARGETplus Non-Targeting Pool, GE Healthcare Dharmacon) was used as a control.

A number of optimisations were performed prior to the siRNA-based experiments described in this chapter, including optimisation of transfection conditions and time course analysis of *CAST* down-regulation. Optimisation of transfection conditions was carried out to find the highest transfection efficiency while maintaining cell viability (as described in section 5.2.1.5.). The concentration of the siRNA pool was varied to determine the lowest concentration resulting in down-regulation of *CAST* with minimised risk of off-target effects. The time course analysis was performed to determine the duration of the *CAST* down-regulation. These optimisations are described in Appendix G.1.

Immunocytochemistry performed with an anti-calpastatin antibody on *CAST* siRNA-treated cells and NTP control cells (Figure 5.3.), revealed down-regulation of calpastatin in *CAST* siRNA monolayers compared to a cytoplasmic expression in NTP cells (Figure 5.3. B). Western blots of *CAST* siRNA-treated HaCaT cell lysates were performed, as previously described, to confirm that *CAST* knockdown was achieved prior to any other analysis (Figure 5.4. C). A *CAST* knockdown was obtained which down-regulated all *CAST* isoforms by 50-65% in HaCaT cells.

To investigate *in vitro* the effects of mechanical stress in *CAST* siRNA transfected HaCaT cells, the FX-4000™ cell stretcher was used as previously described for the *CSTA* siRNA studies in HaCaT cells (Chapter 5.2.1.3.). *CAST* siRNA transfected cells together with NTP siRNA transfected cells as control, were subjected to mechanical stretch at a frequency of 5 Hz (five cycles of stretch and relaxation per second) and an elongation of amplitude ranging from 10% to 14% (increase in diameter across the silicone deformable membrane from 10% to 14%). Cells were stretched for 4 h.

Staining of non-stretched and 4 h-stretched *CAST* siRNA-treated cell monolayers and control cells, using an anti-keratin 14 antibody, revealed widening of the intercellular spaces in *CAST* siRNA cells independent of mechanical stress, together with breakage of intercellular junctions (Figure 5.4. Ei and Eii) compared to NTP treated cells where after 4 h stretch these connections appeared disrupted but not broken (Figure 5.4. Dii).

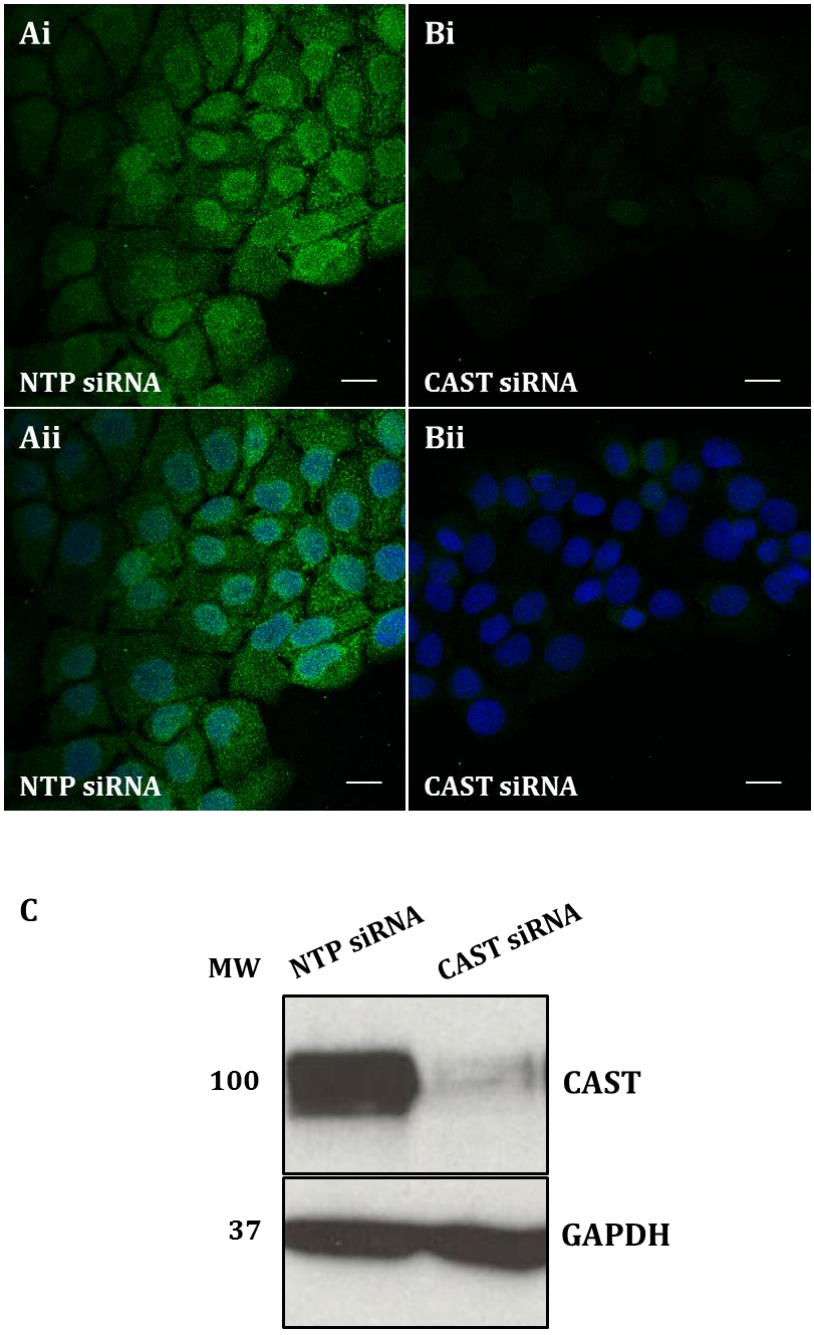

Figure 5.4. *CAST* siRNA transfection and mechanically induced stress on knockdown cell monolayers. HaCaT cells transfected with a pool of *CAST* siRNA **(B)** and NTP siRNA **(A)** for 72 h were stained with an anti-calpastatin antibody (in green) in the absence **(Ai** and **Bi)** and presence **(Aii** and **Bii)** of DAPI (in blue) as nuclear marker. A reduction in the calpastatin protein levels can be seen in *CAST* siRNA treated cells compared to NTP siRNA cells; this was confirmed by western blotting of total cell lysates **(C)**. A reduction in CAST levels can be observed for the *CAST* siRNA treated cells (lane 2). GAPDH was used as a loading control. Imaging was performed on the Zeiss Meta 710 confocal microscope and images taken at 40 X magnification **(A** and **B)** (Scale bar – 20 μm).

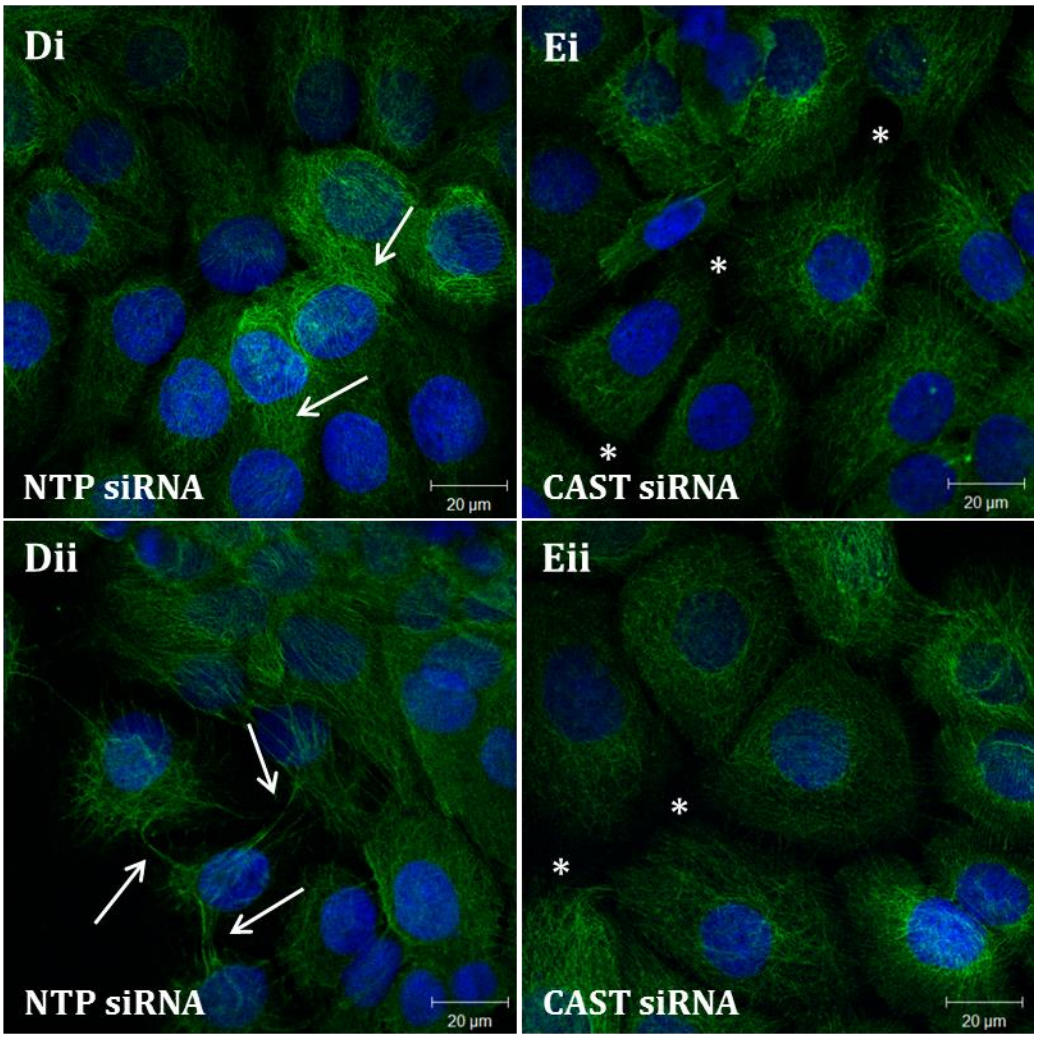

Figure 5.4. *CAST* LOF by siRNA transfection and mechanically induced stress on knockdown cell monolayers (continued). NTP control HaCaT cells **(Di** and **Dii)** and *CAST* siRNA cells **(Ei** and **Eii)** mimicking the LOF mutation were subjected to cyclic mechanical stress at a frequency of 5 Hz and amplitude of 10-14% using the Flexcell FX-4000 Tension System for 0 h (non-stretched, **Di** and **Ei**) and 4 h stretch **(Dii** and **Eii)**. ICC with an anti-keratin 14 antibody revealed that *CAST* siRNA cells display large intercellular gaps (*) both before and after 4 h stretch, suggesting an adhesion defect independent of mechanical stress **(Ei** and **Eii)**. Keratin 14 filaments appeared stretched, but not broken, in NTP treated cells following 4 h stretch (arrows). Keratin 14 – in green; DAPI – in blue. Imaging was performed on the Zeiss Meta 710 confocal microscope and images taken at 63 X magnification **(D** and **E)** (Scale bar – 20 µm).

5.2.1.4. Cell migration appears normal in CAST knockdown keratinocytes

To investigate the effects of the *CAST* LOF mutations on cell migration and "wound-healing", a scratch assay was performed as previously described for the *CSTA* siRNA treated cells. After applying a scratch throughout the *CAST* siRNA and NTP cell monolayers pictures were taken at set time intervals, up to 24 h post-scratch in order to assess and compare the time and speed of scratch-wound closure in *CAST* siRNA cells compared to control cells. Pictures taken at the 0 h, 12 h and 24 h time points showed no significant differences in cell migration in *CAST* siRNA cells after 24 h compared to control (Figure 5.5. A). In order to quantify this, the size of the scratch was measured for these three time intervals. Analysis of measurements of areas migrated between the 0 h, 12 h and 24 h time points showed no significant difference, indicative of a normal cell migration pattern and normal scratch-wound healing process (Figure 5.5. B). The graphical representation below illustrates the analysis of three independent siRNA knockdown experiments (n = 8). Scratch measurements were made with Image J software and resulting scratch measurements are given as arbitrary numbers from a maximum set number.

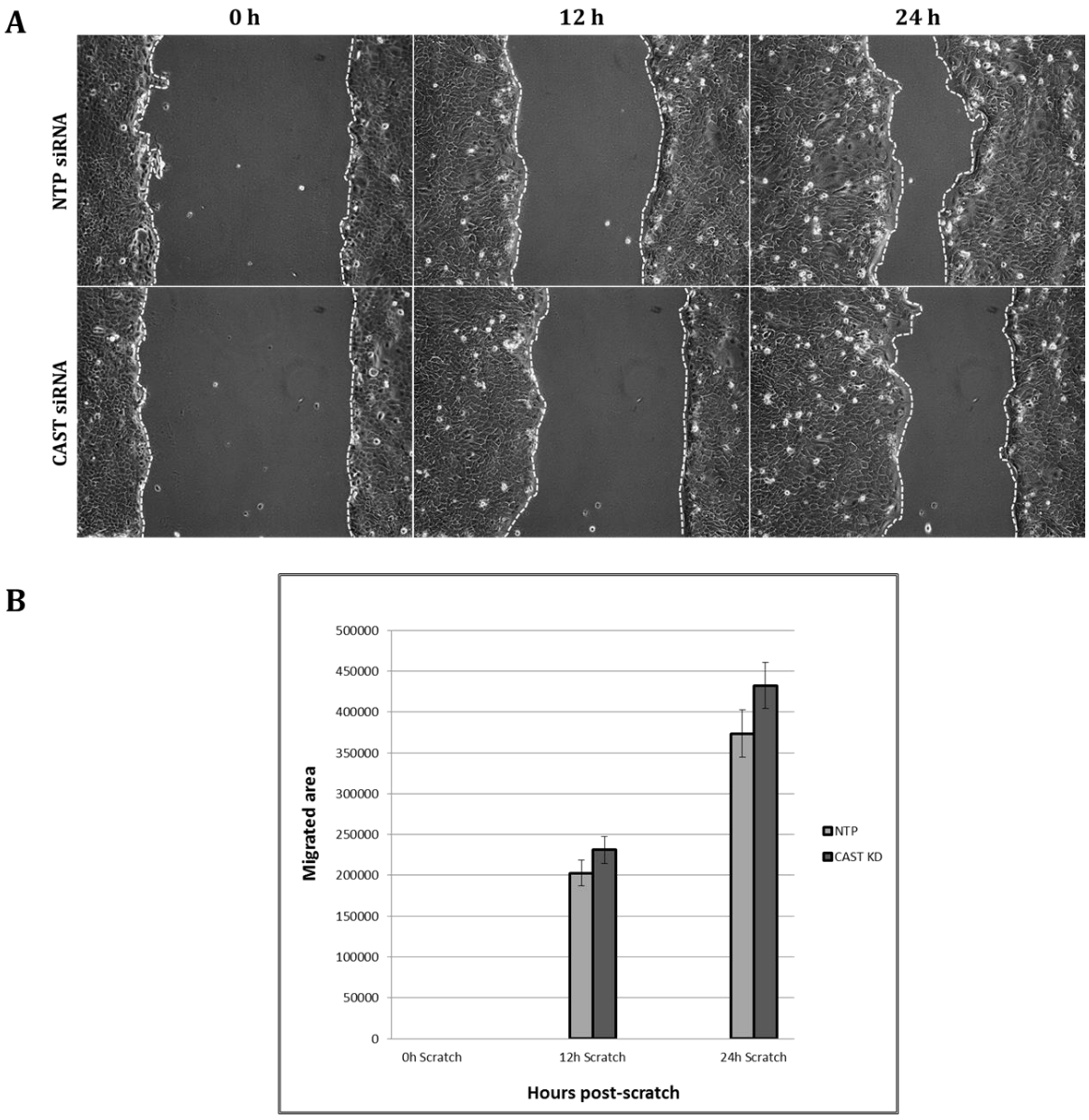

Figure 5.5. "Wound-healing" assay showed normal cell migration after 24 h. (A) Scratch-wound assay to assess migration by the degree of scratch closure after 24 h. **(B)** No significant difference was observed between NTP siRNA and *CAST* siRNA treated cells suggesting that there is no obvious difference in cell migration and scratch closure (n = 8).

5.2.1.5. Analysis of cell viability in CAST siRNA treated cells

Previous studies have reported calpastatin and the target proteases as being implicated in growth, migration and apoptotic cell death (Carragher and Frame, 2004). We have analysed the percentage of early and late apoptosis in *CAST* siRNA cells in comparison to NTP control. *CAST* LOF cells were stained with annexin V – FITC. One siRNA knockdown assay was performed, with three samples for each condition analysed by FACS. Two representative images for the NTP and *CAST* siRNA samples are shown in Figure 5.6. A, together with the graphical representation of the statistical analysis of the three samples from the one siRNA knockdown (Figure 5.6. B). No statistically significant difference was observed between *CAST* siRNA and the control cells. This is indicative of normal apoptotic cell death in *CAST* knockdown cells.

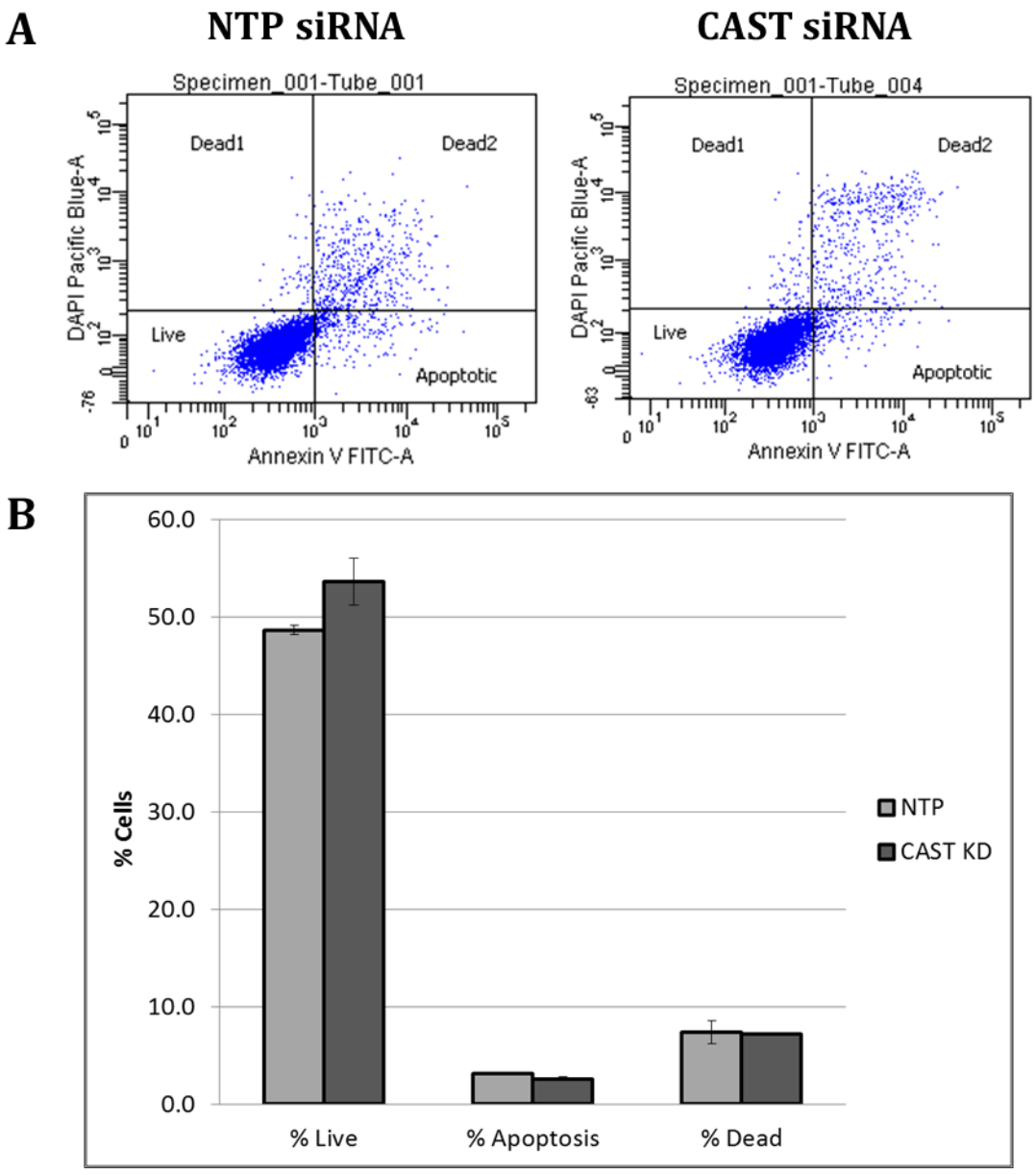

Figure 5.6. Apoptosis analysis by FACS in *CAST* siRNA treated cells. (A) Dot plot of readings for NTP and *CAST* siRNA treated cells. A number of 30,000 events were allowed for each repeat. Gates were used initially to exclude debris and then to separate between living, apoptotic and dead cells. **(B)** Representation of cell death analysis in NTP and *CAST* siRNA treated cells. The columns represent the percentage of live, apoptotic and dead cells. A normal level of apoptotic cell death was observed for *CAST* siRNA treated cells, similar to control.

5.2.1.6. Expression of desmosome-associated proteins in skin from PK2 homozygous for a CAST LOF mutation

Due to the cell adhesion defect in *CAST* LOF skin, the expression and localisation of some of the desmosome-associated proteins was analysed. Immunofluorescence was performed with anti-DSG2 (Figure 5.7.), DSG3 (Figure 5.8.) and DSP I/II (Figure 5.9.) specific antibodies in non-lesional skin sections from PK2 and control skin. In normal epidermis DSG2 appeared with a diffuse cytoplasmic and membranous localisation (Figure 5.7. A), while DSG3 and DSP presented with a membranous localisation (Figure 5.8. A and 5.9. A). In affected skin, DSG2 appeared to present with an expression profile similar to control skin, with areas of increased expression in the basal layer (Figure 5.7. B). Staining of DSG3 and DSP showed a significant increase in protein expression, with both a plasma membrane and cytoplasmic localisation pattern (Figure 5.8. B and 5.9. B), in comparison to the specific membranous pattern in control skin. Staining of DSP in affected skin also highlighted intercellular gaps in the basal/suprabasal layers as seen by histological analysis (Figure 5.9. Bi).

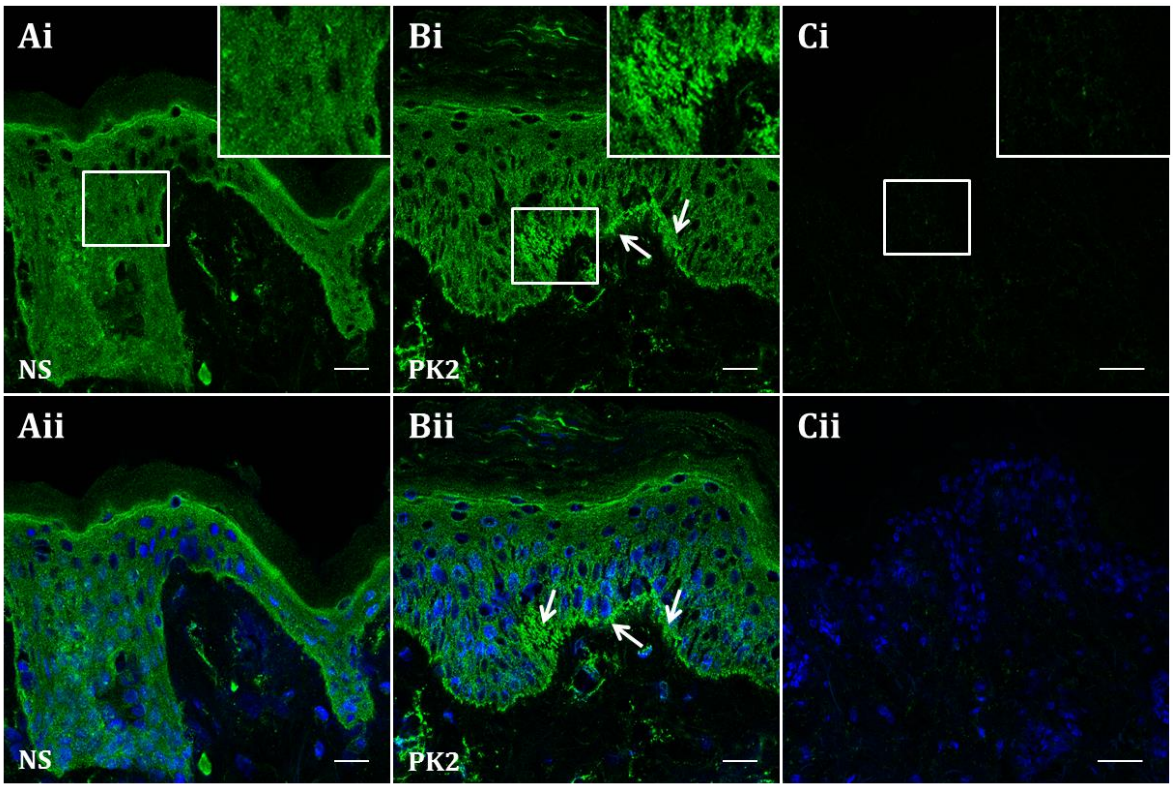

Figure 5.7. Immunofluorescence of DSG2 in skin sections from PK2. IHC with an anti-DSG2 antibody (in green) in control skin **(A)** and skin sections from PK2 **(B)** in the absence **(Ai** and **Bi)** and presence **(Aii** and **Bii)** of DAPI as a nuclear marker (in blue), revealed areas of increased protein expression (arrows) in the basal layer of affected skin compared to control skin. Imaging was performed with the Zeiss Meta 710 confocal microscope and images were taken at 20 X magnification **(A** and **B)** and 10 X magnification for negative control **(C)** (Scale bar – 20 μm for **A** and **B** and 50 μm for **C**).

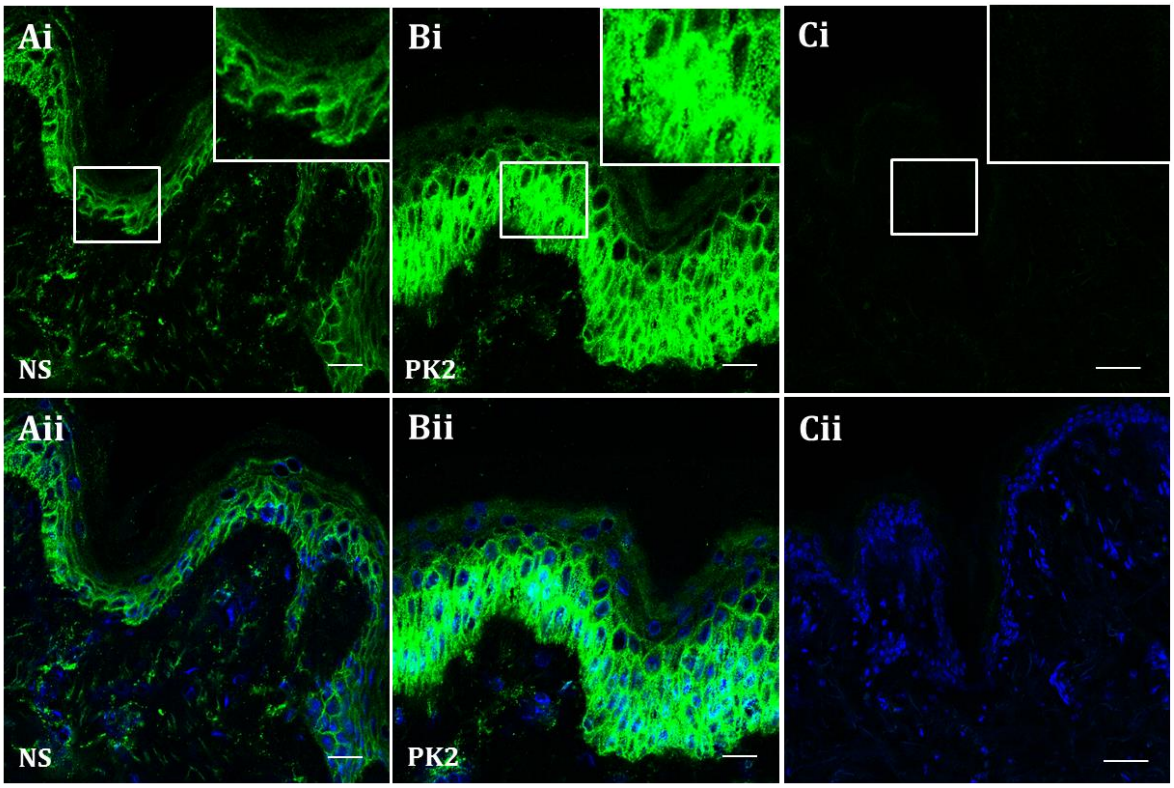

Figure 5.8. Immunofluorescence of DSG3 in skin sections from PK2, homozygous for p.K78X, and control skin. IHC with an anti-DSG3 antibody (in green) in control skin **(A)** and skin sections from PK2 **(B)** in the absence **(Ai** and **Bi)** and presence **(Aii** and **Bii)** of DAPI as a nuclear marker (in blue), revealed a significant increase in protein expression in the basal/suprabasal layers of the epidermis in affected skin compared to control skin. A change from a typical membranous localisation to a both membranous and cytoplasmic localisation of this protein was also noted (lower exposure of DSG3 in Appendix G.2.). Imaging was performed with the Zeiss Meta 710 confocal microscope and images were taken at 20 X magnification **(A** and **B)** and 10 X magnification for negative control **(C)** (Scale bar – 20 μm for **A** and **B** and 50 μm for **C**).

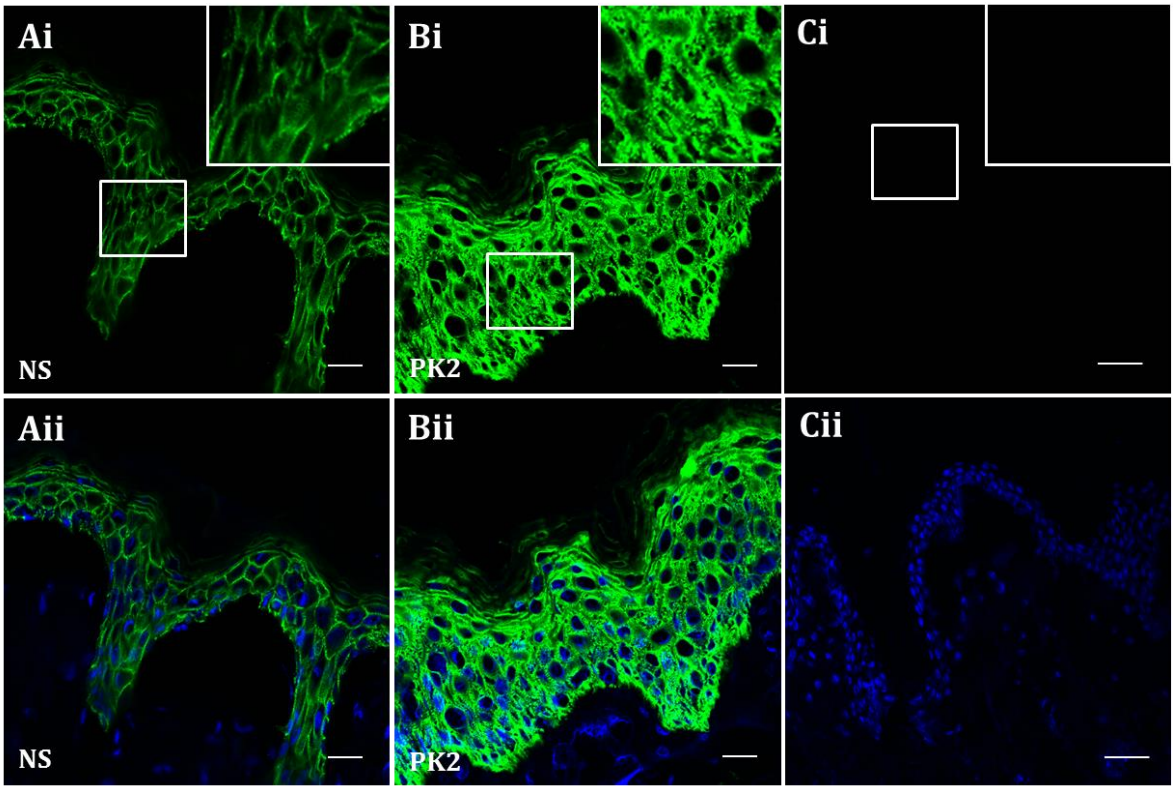

Figure 5.9. Immunofluorescence of DSP in skin sections from PK2, homozygous for p.K78X and control skin. IHC with an anti-DSP antibody (in green) in control skin **(A)** and skin sections from PK2 **(B)** in the absence **(Ai** and **Bi)** and presence **(Aii** and **Bii)** of DAPI as nuclear marker (in blue), revealed a significant increase in protein expression in all layers of the epidermis in affected skin compared to control skin. A change from a typical membranous localisation to a both membranous and cytoplasmic localisation of this protein was also noted, together with more apparent intercellular spaces in the basal/suprabasal layers. Imaging was performed with the Zeiss Meta 710 confocal microscope and images were taken at 20 X magnification **(A** and **B)** and 10 X magnification for negative control **(C)** (Scale bar – 20 µm for **A** and **B** and 50 µm for **C**).

5.2.1.7. Desmosome-associated proteins appear affected by CAST LOF mutations

Following observations on the altered expression and localisation of the desmosome-associated proteins DSG2, DSG3, and DSP I/II in affected skin, these proteins were investigated in *CAST* siRNA-treated cells before and after 4 h mechanically-induced stress.

Total protein cell lysates from NTP and *CAST* siRNA-treated HaCaT cells were obtained and analysed by western blotting. Antibodies targeting DSG2, DSG3, PG and DSP I/II were used together with anti-vinculin and anti-GAPDH antibodies as loading controls (Figure 5.10. A). Independent siRNA knockdown experiments were conducted and replicate western blots were carried out for each protein. Densitometry measurements of western blots were calculated using an image analysis program (Image J, v1.47v) and are graphically depicted in Figure 5.10. B and C for DSG2 and DSG3, which were consistent between repeats, and in Figure 5.10. D for DSP II and Appendix G.3. for PG which appeared with more variability between repeats but with similar expression levels between *CAST* siRNA and NTP treated cells.

DSG2, DSG3 and DSP II protein expression levels appeared increased following *CAST* siRNA knockdown, while PG expression appeared consistent and similar to expression in NTP control cells independent of mechanical stress. Protein levels were normalised against the loading control band, GAPDH for DSG2 and DSG3 and vinculin for DSP I/II, and are presented as a fold change from NTP control for the western blots for DSG2, DSG3 and DSP II in Figure 5.10. A. No change in expression levels was observed for DSP I and PG (Appendix G.3.). Due to the variability in expression levels, despite an overall trend towards up-regulation, further repeats would be necessary together with protein quantification prior to western blotting, in order to draw a conclusion.

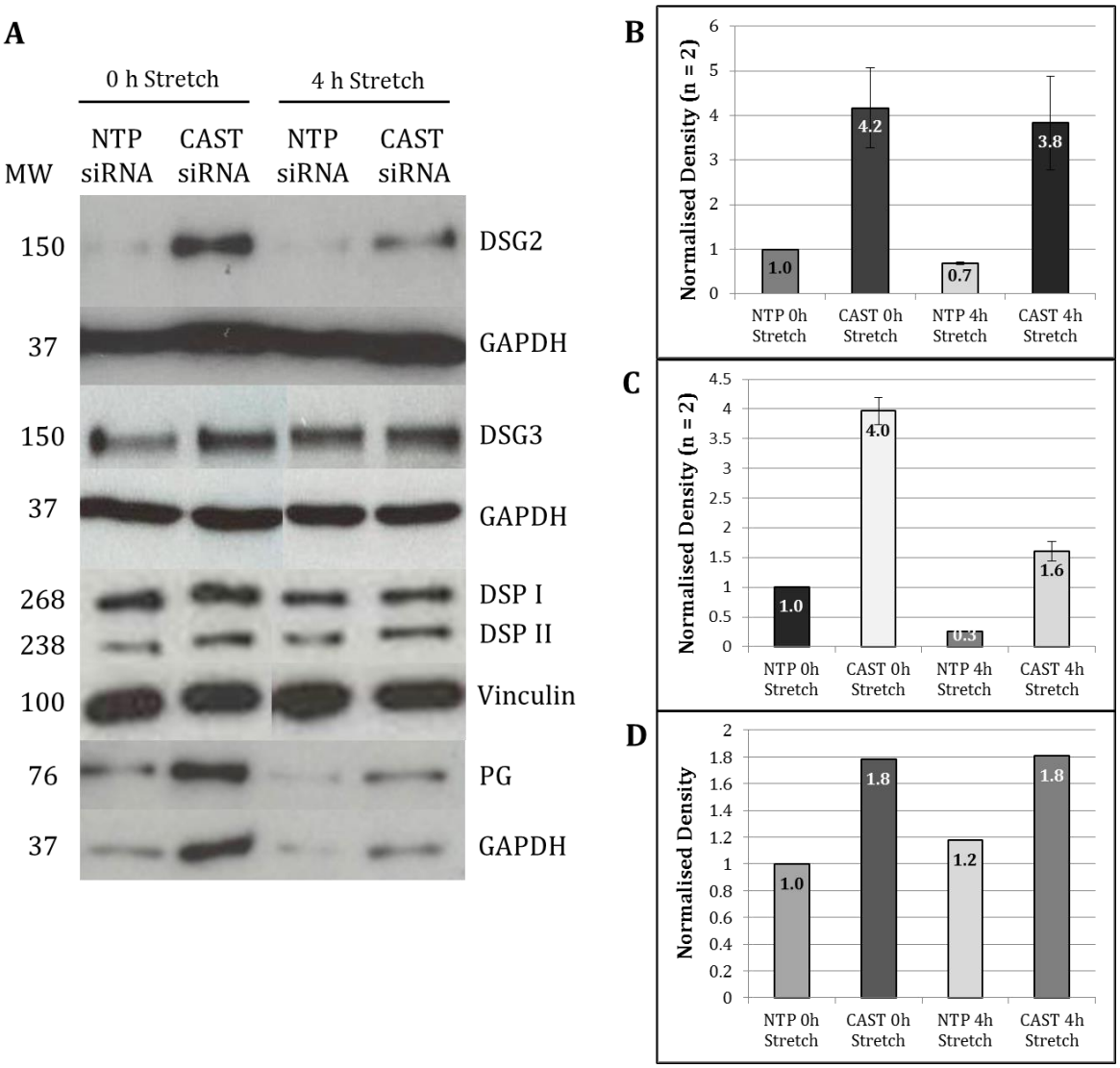

Figure 5.10. Up-regulation of DSG2, DSG3 and possibly DSP II in *CAST* siRNA treated cells. (A) Total protein cell lysates from *CAST* siRNA and NTP siRNA HaCaT cells, non-stretched and stretched for 4 h, were blotted and incubated with anti-DSG2, DSG3, PG or DSP I/II to check the levels of expression of these proteins. **(B-D)** Protein levels of DSG2, DSG3 and DSP II calculated from densitometric measurements of the western blot images and normalised to loading controls (GAPDH for DSG2 and DSG3; Vinculin for DSP II). Total DSG2, DSG3 and DSP II expression levels are presented as a fraction of the total protein level in NTP siRNA cells; more repeats would be necessary for DSP II in order to include standard error bars. Densitometric analysis for PG and DSP I can be found in Appendix G.3. and are showing similar expression levels between *CAST* siRNA and NTP siRNA.

5.3. Discussion

In this chapter, a new clinical entity named PLACK syndrome, and the research on three independent families presenting with mutations in the *CAST* gene, which encodes for the protease inhibitor calpastatin, are described as being linked to this disorder. The main focus of the work described was the characterisation of a skin biopsy from PK2, homozygous for *CAST* p.K78X and *in vitro* studies on desmosomal cell adhesion. Calpastatin and the target calpains appear to regulate cell adhesion in the basal/suprabasal layers of the epidermis.

5.3.1. *CAST* LOF mutations linked to PLACK syndrome, a new clinical entity

We identified three families with a complex type of peeling skin syndrome (PSS), which we have named PLACK syndrome due to the observed clinical phenotype characterised by PSS with leukonychia, acral punctate keratoses, cheilitis and knuckle pads (Lin *et al*., 2015).

Two types of PSS have previously been described, acral PSS (APSS), involving the palmar, plantar and dorsal surfaces of the hands and feet (Shwayder *et al*., 1997, Hashimoto *et al*., 2000), associated with mutations in the *TGM5* gene (Cassidy *et al*., 2005), and generalized PSS (GPSS), which together with the characteristics described for APSS also presents with severe pruritus, food allergies and repeated episodes of angioedema, urticaria, and asthma (Oji *et al*., 2010, Mallet *et al*., 2013), and was associated with mutations in the *CDSN* gene (Oji *et al*., 2010). Recently Blaydon *et al*. (Blaydon *et al*., 2011b) and Krunic *et al*. (Krunic *et al*., 2013) described homozygous nonsense mutations in the *CSTA* gene associated with exfoliative ichthyosis and APSS respectively, while Cabral *et al*. (Cabral *et al*., 2012a) identified *CHST8* as a novel gene linked to PSS.

Through independent exome capture analyses, three distinct homozygous LOF mutations were identified in affected individuals from three PLACK families. All these mutations, c.607dup:p.Ile203Asnfs*8 in PK1, c.A424T:p.Lys142* in PK2 (analysed in this chapter) and c.1750delG:p.Val584Trpfs*37 in PK3 and PK4, were

identified in the *CAST* gene and are predicted to encode for a truncated non-functional protein.

Calpastatin is a specific endogenous inhibitor of the classical calpains 1 and 2, also known as calpains μ (micro) and m (mili) (Corrado *et al*., 2006), on the basis of the calcium concentration required for their activation: a low concentration is needed for μ-calpain and a higher concentration needed for m-calpain (Ono and Sorimachi, 2012).

To investigate the consequences of the *CAST* LOF mutation p.K78X, immunostaining was performed with an anti-calpastatin antibody on non-lesional skin sections from PK2. This has revealed an almost complete absence of protein expression in all layers of the epidermis, in comparison to normal control skin where calpastatin was expressed throughout all layers of the epidermis and had a cytoplasmic appearance. Histologically, intercellular gaps in the basal/suprabasal layers of the epidermis were observed, together with what appears to be a thicker basal layer with specific apical oriented cells.

5.3.2. Transient *CAST* down-regulation leads to disrupted intercellular adhesion *in vitro*

To analyse further the consequences of the *CAST* LOF mutations *in vitro*, siRNA-mediated knockdown of *CAST* using a specific siRNA pool was performed in the immortalised keratinocyte cell line HaCaT, with NTP siRNA used as control. Knockdown of *CAST* was obtained, which reduced calpastatin expression by approximately 50-65%. The level of knockdown was assessed by immunocytochemistry and/or total protein lysates by western blotting prior to any other analysis.

Due to the observed cell adhesion defect in the basal/suprabasal layers in the epidermis from the affected individual, an *in vitro* mechanically-induced stress assay was used to investigate the role of calpastatin in keratinocyte adhesion in *CAST* siRNA and NTP siRNA-treated cells as control. Immunocytochemistry with a specific anti-keratin 14 antibody in non-stretched and 4 h-stretched cell monolayers revealed widened intercellular spaces both in the non-stretched and stretched *CAST*

knockdown cells, which suggests that this disruption happens independently of mechanical stress. In contrast, NTP cells presented with extended keratin 14 filaments post-stretching but no disruption in intercellular adhesion prior to mechanical stress. The direct implication of calpastatin in intercellular adhesion has not, to our knowledge, been reported previously and a possible mechanism of action is discussed below.

Independent studies looking at a variety of cancers have associated calpains, the specific targets of calpastatin, with adhesion, motility, invasion, cell-cycle regulation, cell spreading, apoptosis and myogenesis (Leloup *et al*., 2006). A recent study by Nassar *et al*., using a calpastatin overexpression mouse model observed changes in the wound-healing process in comparison to wild type mice. A significant delay in wound-healing was noted, associated with reduced proliferation and re-epithelialisation, most prominently in the early stages of the wound-healing process (Nassar *et al*., 2012).

To address the possible effects of the *CAST* LOF mutations on keratinocyte migration *in vitro*, a scratch assay was performed in *CAST* knockdown keratinocyte monolayers following inhibition of proliferation. NTP cells were used as a control and were treated in the same manner. Results showed a normal scratch-wound closure pattern, similar to the one observed for NTP control cells, which signifies a normal cell migration process. A *CAST* LOF 3D organotypic cell model or analysis of *Cast* KO mouse may give a more accurate view of any wound-healing and cell migration processes regulated by calpastatin.

Tan *et al*. observed that in embryonic fibroblasts derived from C*apn4* genetically disrupted mice, the calpain deficiency correlated with resistance to ER stress-induced apoptosis, directly related to calpain requirement for activation of both caspase-12 and the ASK1-JNK cascade (Tan *et al*., 2006). Another *in vitro* study demonstrated that increased activity of m-calpain results in apoptosis of HaCaT cells, and that the activation of m-calpain is directly proportional to EGF concentration (Inoue *et al*., 2004).

Analysis of lesional patient skin sections by TUNEL assay and TEM (performed by Dr Zhimiao Lin, Peking University First Hospital, Beijing, China) revealed a

significant increase in the number of apoptotic cells and apoptotic bodies formed, compared to normal control skin. To look at the consequences of *CAST* knockdown *in vitro*, FACS analysis of the cell cycle was performed in *CAST* siRNA treated cells against control NTP cells. The results from one knockdown experiment with each condition in triplicate were analysed and revealed similar percentages of cells in all stages of the cell cycle between *CAST* siRNA and NTP siRNA treated cells.

TUNEL and TEM results suggest that analysis of apoptosis in skin sections from other PLACK patients and the use of a *CAST* LOF 3D cell model may reveal different results to the ones seen in cell monolayers, as the increase in apoptotic cell number in PK1 was in the suprabasal layers of the epidermis.

5.3.3. Dysregulation in expression and appearance of desmosome-associated proteins

Observations in *CAST* LOF affected skin and *in vitro* studies, coupling *CAST* siRNA-mediated knockdown with mechanically-induced stress, indicate a key role for calpastatin in intercellular adhesion.

In order to address the possibility of a direct correlation between *CAST* LOF mutations and an increased calpain activity leading to excessive proteolysis of epidermal desmosomal components, the expression and localisation of some of these proteins in affected skin sections and in *CAST* siRNA keratinocytes was analysed.

Staining of skin sections from PK2, homozygous for p.K78X, with anti-DSG2, DSG3 and DSP I/II specific antibodies, revealed an apparent up-regulation of DSG2 expression in areas of the basal layer of the epidermis and a significant up-regulation of DSG3 and DSP I/II in all layers of the epidermis. Aberrant localisation of these proteins to the cytoplasmic compartment was observed, when compared to normal control skin where DSG3 and DSP I/II appeared mainly expressed at the plasma membrane. Furthermore, western blotting of total protein lysates from *CAST* knockdown cells revealed a general trend towards up-regulation of DSG2, DSG3 and DSP II independent of mechanical stress when compared to NTP cells. Any variation in the levels of up-regulation of DSG2, DSG3 and DSP II between *CAST* knockdown

repeat experiments, may be due to variations in *CAST* knockdown levels and could be addressed by quantification of total protein levels prior to western blotting.

These observations could suggest that the reduction in expression of calpastatin due to *CAST* LOF mutations directly correlates with an increase in the concentration of active calpains. This in turn could lead to proteolysis of DSG2, DSG3 and DSP II in the affected individuals, resulting in acantholysis and impaired resistance of the epidermis to mechanical stretch, seen in affected individuals as blistering and skin peeling.

As calpain-mediated proteolysis of talin and focal adhesion kinase (FAK) reportedly leads to regulation of adhesion dynamics (Franco *et al*., 2004, Chan *et al*., 2010), these proteins could be analysed in PK patient skin and *CAST* siRNA transfected keratinocytes.

5.4. Summary

To summarise, this chapter described the features of a new clinical entity named PLACK syndrome, characterised by PSS, leukonychia, acral punctate keratosis, cheilitis and knuckle pads. Through three independent exome capture analyses of the three families, our group identified autosomal recessive mutations in *CAST*, leading to LOF of calpastatin, the only known inhibitor of calpains.

CAST knockdown mimicking the LOF mutations, coupled with mechanical stretching revealed reduction in intercellular adhesion levels independent of mechanical stress. No change in cell migration or cell cycle was seen by scratch assay or FACS analysis. A possible mechanism of action following *CAST* LOF mutations could be through increased calpain activity leading to the proteolysis of desmosome-associated proteins, as indicated by the *in vivo* and *in vitro* observations showing up-regulation and aberrant localisation of DSG2, DSG3 and DSP II.

-Chapter 6-

Final Discussion and Future Work

6.1. Background

Desmosomes are complex macromolecular structures, playing both structural and signalling roles in bordering cells. Although the precise role of desmosomes as adhesion structures and signalling centres is not yet fully understood, it is widely accepted that their correct assembly and function is crucial in desmosome-presenting tissues such as the skin and myocardium. It has been well acknowledged in a number of studies that dysregulation of desmosome assembly and function, due to genetic variations in desmosomal genes, leads to an array of conditions featuring cardio-cutaneous phenotypes including some with hair abnormalities including woolly hair or alopecia.

The two main focuses of this thesis were, firstly, the genetic analysis of patients clinically diagnosed with ARVC or genodermatoses, resulting in the discovery of novel and previously disease-linked mutations in genes encoding for desmosome-associated proteins, and secondly, the *in vitro* analysis of loss-of-function (Loffek *et al*.) mutations in two genes encoding for the protease inhibitors, cystatin A and calpastatin, leading to the skin disorders exfoliative ichthyosis and PLACK syndrome respectively. The molecular mechanisms behind mutations affecting the desmosomal complex, either directly through changes in desmosomal proteins or indirectly affecting proteins involved in desmosome regulation, are continuously being uncovered and highlight the importance of these structures in desmosome-bearing organs.

6.2. Genetic heterogeneity in ARVC and genodermatoses

6.2.1. PKP2 is the major affected desmosome-associated protein in ARVC

A number of dominant and recessive mutations identified to date in genes encoding for the desmosome-associated proteins DSP, DSC2, DSG2, PKP2 and PG lead to non-syndromic ARVC.

PKP2 mutations account for a significant number of ARVC cases (Sen-Chowdhry *et al*., 2010), and were initially identified following a large study by Gerull *et al*. who

uncovered 25 different novel *PKP2* mutations in 32 probands out of a total of 120 patients, ranging from missense and nonsense to insertion, deletion and splice-site mutations, most of which affected the C-terminus end of the protein, while the others were scattered throughout the gene (Gerull *et al*., 2004). Both founder and recurrent mutations were identified up to date (van der Zwaag *et al*., 2010). The recurrent mutations suggest the presence of "hot spot" mutagenic regions in *PKP2* (Gerull *et al*., 2004, Dalal *et al*., 2006), the frequency in C>T mutations pointing at the CpG hot spots as targets of spontaneous mutations (Awad *et al*., 2008a).

Here, six dominant and recessive variations in *PKP2*, ranging from splice-site of exons 11 (IVS11-1G>C) and 12 (IVS12+1G>A; rs111517471) to nonsense (c.G870A:p.W290X and c.T1926A:p.Y642X) and missense (c.G1939A:p.A647T and c.A148C:p.T50A) mutations were identified. Bauce *et al.* have shown that skipping of exon 11 in RNA transcripts and the possible generation of a premature STOP codon following the *PKP2* mutation could prove highly pathogenic (Bauce *et al*., 2010). The rs111517471 variation, with a minor allele frequency of less than 0.01, has also previously been associated with ARVC and is believed to be highly pathogenic (Scherer *et al*., 2006). We suggest that the two missense mutations identified by our studies would lead to conformational changes through single amino acid modifications while the two nonsense mutations would lead to more severe truncations of the PKP2 protein structure, which in turn would most likely affect desmosome assembly and function. Truncating mutations are thought to lead to haploinsuficiency because of their instability (Joshi-Mukherjee *et al*., 2008).

Co-immunoprecipitation and yeast two hybrid system studies have reported direct interactions between PKP2 and other desmosome-associated proteins such as DSP, PG, DSC1a and 2a, DSG1 and 2, some of which are of high importance in cardiac desmosomes (Bonne *et al*., 1999, Chen *et al*., 2002). Additional interactions have been reported with the intermediate filaments (Hofmann *et al*., 2000) and β-catenin regulating its signalling activity (Chen *et al*., 2002). Thus mutant or reduced (due to haploinsufficiency mutation) PKP2 is likely to impair its association with other desmosomal proteins and their assembly in the heart, thus leading to cardiomyocyte adhesion problems. PKP2 is the only isoform in the heart, while in the epidermis is found to be expressed together with PKP1 and 3, which could perhaps compensate

for the PKP2-deficiency; this could possibly explain the non-syndromic phenotype in ARVC patients. This hypothesis is also supported by a *Pkp2* knockout mouse model which resulted in lethal cardiac damage at mid-gestation, characterised by defective intercellular adhesion at the intercalated disks and blood loss into the pericardial cavity, associated with a reduction in expression of DSP and PG (Grossmann *et al*., 2004).

Another hypothesis, supported by a number of *in vitro* siRNA studies on rat and human cardiomyocytes, associates ARVC-linked *PKP2* mutations with a redistribution of connexins (Oxford *et al*., 2007, Pieperhoff *et al*., 2008), in particular with abnormalities in total connexin 43 (Cx43) expression which appears to be a consistent feature in patients with advanced ARVC (Antoniades *et al*., 2006, Fidler *et al*., 2009, Kannankeril *et al*., 2006, Lahtinen *et al*., 2008, Asimaki *et al*., 2009). In an independent study using neonatal rat ventricular myocytes, Joshi-Mukherjee *et al*. have shown that the p.Arg79X nonsense mutation in *Pkp2* led to a reduction in Cx43 expression and the failure of the two proteins to interact (Joshi-Mukherjee *et al*., 2008).

In desmosome-containing epithelial cells, PKP2 appears to be associated with DSP and together migrate from the cytoplasmic compartment to the plasma membrane during desmosome assembly (Godsel *et al*., 2005). These observations together with an *in vitro* study on PKP2-deficient cells, showing that DSP-PKCα complexes dissociate while DSP remains anchored to the intermediate filaments failing to reach the plasma membrane (Bass-Zubek *et al*., 2008).

6.2.2. Disease heterogeneity associated with *DSP* mutations

The most frequent genes mutated in ARVC except for *PKP2* are *DSP* (10-15% of diagnosed cases) and *DSG2* (10-15% of diagnosed cases) (Pilichou *et al*., 2006) and represent the "big 3" target genes (Sen-Chowdhry *et al*., 2010), with compound and double heterozygotes having been reported in up to 33% of genetically diagnosed cases.

Here, a double heterozygote presenting one of the *PKP2* mutations (IVS11-1G>C) presented above, together with a heterozygous transversion in exon 11 of *DSP*,

c.G1323C:p.K441N, is presented. Also, during the course of the ARVC study, genetic screening of two siblings with hypotrichosis and PPK revealed a homozygous mutation in exon 12 of *DSP*, c.C1493T:p.P498L. This phenotypical exclusivity resulting from mutations in the same gene is a matter of intense controversy and high interest, mostly as ARVC diagnosis is proving to be extremely difficult and variable despite the existing guidelines.

A number of cardio-cutaneous syndromes with varying degrees of severity have been reported since the first linkage of *DSP* mutations with an exclusively cutaneous disorder, autosomal dominant SPPK (Armstrong *et al*., 1999, Whittock *et al*., 2002), and with the autosomal recessive Carvajal syndrome, a cardio-cutaneous phenotype coupled with hair abnormalities (Norgett *et al*., 2000). In SPPK, the dominantly inherited mutations were LOF suggesting that the mechanism of action was haploinsufficiency and that protein dosage was key in the stressed areas of the skin such as the palm and sole, a hypothesis confirmed by histology findings (Armstrong *et al*., 1999). In comparison, the homozygous *DSP* mutation linked to the Carvajal syndrome would lead to the loss of the IF-binding site and impaired cell adhesion with the collapse of the IF network (Huen *et al*., 2002, Getsios *et al*., 2004). The first case of non-syndromic ARVC linked to mutations in *DSP* was reported by Rampazzo *et al*. who noted that the missense *DSP* mutation was affecting the PG-binding domain of DSP (Rampazzo *et al*., 2002). It is well accepted now that the DSP isoforms have different functions and are differentially expressed in desmosome-presenting tissues, with DSP II expressed at very low levels in the heart (Uzumcu *et al*., 2006), while having a more significant role than DSP I in maintaining keratinocyte adhesion in the epidermis (Cabral *et al*., 2012b).

Similarly to the mutation identified by Rampazzo *et al*., it is believed that the ARVC-linked *DSP* mutation identified in this study (p.K441N) would affect the N-terminal end of all DSP isoforms and thus destabilise the binding of DSP to PG and PKPs, and at the same time the tethering of the intermediate filaments to the plasma membrane. It is yet unclear why no cutaneous phenotype was described in this patient, unless any existing skin modifications are very subtle compared to the cardiac manifestations aggravated by the *PKP2* mutation. Skipping of *PKP2* exon 11 in mRNA transcripts and the possible generation of a STOP codon could prove highly

pathogenic (Bauce *et al*., 2010), but at the same time Xu *et al*. have shown that in 42% of their affected individuals a second mutation in another desmosomal gene was needed to cause overt clinical disease (Xu *et al*., 2010), therefore the question of whether the *DSP* missense mutation contributes to the severity of the phenotype can only be clarified by *in vitro* studies. As mentioned before, a compensatory mechanism would be possible in the epidermis where PKP2 is expressed together with PKP1 which can promote desmosome formation by recruiting desmosomal proteins at the plasma membrane and within desmosomes (Wahl, 2005, Bornslaeger *et al*., 2001), and is able to bind to DSP, DSG1, DSC1, actin and keratin intermediate filaments (Hatzfeld *et al*., 2000, Hofmann *et al*., 2000, Kapprell *et al*., 1988, Smith and Fuchs, 1998), thus explaining why no cutaneous phenotype is seen in this patient.

In comparison, the second recessive missense *DSP* mutation (p.P498L) identified in siblings with hypotrichosis and PPK appears exclusive to the hair and palmoplantar areas exposed to mechanical stress. Due to the oldest sibling being only 11 years old at the time they were seen in clinic, we cannot completely exclude the possibility of any cardiac abnormalities appearing in the future. Clinically, it is important to regard PPK in combination with woolly hair or alopecia as a "warning signal" for the development of cardiomyopathy, as suggested by Norgett *et al.* (Norgett *et al*., 2006). Whittock *et al*. have described a similar but more severe form of palmoplantar keratoderma and woolly hair associated with skin fragility due to compound heterozygous mutations in *DSP*. Each of the two patients described in their study was heterozygous for nonsense and missense mutations, transcript analysis demonstrating that the nonsense allele was probably degraded via the nonsense-mediated mRNA decay, and that each affected individual was in essence homozygous for the missense mutation in the N- or C-terminal domains (Whittock *et al*., 2002). It is possible that homozygosity for p.P498L could affect the formation of the protein secondary structure in the absence of wild-type DSP. These changes may affect binding of DSP to the intermediate filaments and/or other desmosomal proteins, such as PG and PKP1 (Kurzen *et al*., 1998), which represent the main armadillo members present in the hair follicle, explaining why in most recessive desmosomal diseases hair is absent or woolly. Mice expressing a truncated PG,

lacking its armadillo repeats, showed stunted hair growth indicating that PG supresses epithelial proliferation and hair growth *in vivo* (Charpentier *et al*., 2000). It is therefore likely that the functionally impaired DSP may lead to a reduction in PG and/or PKP1 levels, leading to the woolly hair phenotype seen in our patients.

6.2.3. The importance of segregation studies is highlighted through mutations in cadherin genes linked to non-syndromic ARVC and hypotrichosis

Dominant (Pilichou *et al*., 2006) and recessive (Syrris *et al*., 2007) *DSG2* mutations are described in up to 15% of non-syndromic ARVC genetically diagnosed cases. The role of DSC2 is unclear, although a recessive 1-base pair deletion mutation in *DSC2* has been linked to ARVC with mild PPK and woolly hair (Simpson *et al*., 2009b). Mutation L732V identified in *DSC2*, and predicted by PolyPhen as benign, was previously described by Bhuiyan *et al*. in conjunction with a *DSG2* mutation V392I (Bhuiyan *et al*., 2009).

Following the genetic analysis on patients with ARVC, two previously reported variations, a heterozygous mutation in *DSG2*, c.C874T:p.R292C (R292C), and a homozygous mutation in *DSC2*, c.T2194G:p.L732V (L732V) were identified. Variant R292C in *DSG2*, heterozygous in our ARVC case has previously been described as homozygous (Sato *et al*., 2012), or in association with a synonymous probably non-pathogenic mutation in *DSP*, D782D, (Cox *et al*., 2011). R292C has also been described in heterozygosity with S194L in *DSG2* and R577DfsX5 in *PKP2* (Nakajima *et al*., 2012).

In a parallel study the genetic anaysis of a patient clinically diagnosed with hypotrichosis with no cardio-cutaneous phenotype was performed. A variety of mutations in *DSG4*, including frameshift, splice-site, missense and nonsense have been linked to the autosomal recessive hair conditions Monilethrix and hypotrichosis (Schaffer *et al*., 2006, Zlotogorski *et al*., 2006, Shimomura *et al*., 2006). In our patient, three known substitutions were identified in exons 4 (c.G258A:p.R86R; rs16959856), 5 (c.C495T:p.S165S; rs9956865) and 12 (c.A1930C:p.I644L; rs4799570) of *DSG4*. It is believed that the first two synonymous

changes in exons 4 and 5 would not alter the secondary protein conformation of DSG4 and therefore they are unlikely to be disease-associated. With regards to the third mutation in exon 12, despite the amino acid change, this change appears as tolerated in SIFT. Thus, the genetic basis of hypotrichosis in this patient is still to be identified.

Even though previous studies have linked mutations in the desmosomal cadherin genes *DSC2*, *DSG2* and *DSG4* with the above mentioned disorders, the importance of segregation studies, particularly for *DSC2* proposed mutations, and screening for mutations in yet unknown disease-associated genes is highlighted again as a basic requirement before establishing a causatory effect.

6.2.4. Genetic testing limitations in ARVC diagnosis

ARVC is a particularly heterogeneous disorder characterised by myocardial degeneration and fibrofatty replacement, mostly affecting the right ventricle, but in some cases extending to the left ventricle and the interventricular septum, culminating in ventricle failure, frequent arrhythmias and sudden cardiac death. The original International Task Force Criteria (TFC) for ARVC diagnosis was established in 1994 (McKenna *et al*., 1994) in the absence of a gold standard criteria, and was updated in 2010 to include quantitative parameters for improving diagnostic sensitivity while maintaining specificity (Marcus *et al*., 2010).

The estimated prevalence of ARVC in the general population is 1:2000 to 1:5000 (Corrado *et al*., 2006a), with men more frequently affected than women, at a ratio of up to 1:3 (Azaouagh *et al*., 2011), and most likely to manifest in the young, competing athletes and individuals previously resuscitated from sudden cardiac death. These numbers appear to be study- and population-specific, with Mediterranean countries, such as Spain and France reaching 1:1000 disease prevalence (Sen-Chowdhry *et al*., 2010), while in Italy ARVC is responsible of up to 26% of sudden cardiac deaths (Corrado *et al*., 1990). These statistics support one of our hypotheses by which the low percentage of disease-causing mutations, identified in only 16% of the total number of screened patients, with 66% identified in patients seen in the UK and 33% in patients seen in New Zealand, could be

attributed to slightly different methods of patient recruitment and perhaps stricter phenotypic parameters applied in differentiating between ARVC and other heart disorders in the UK.

Another variable in disease diagnosis is age of onset, as shown by independent studies looking at patients with *PKP2* mutations which have presented conflicting data. A Japanese study reported a significantly earlier age of onset in their patients (Andreasen *et al*., 2013), compared to a later age of onset reported by Alcalde *et al*. in their Spanish patient cohort (Alcalde *et al*., 2014). Alcalde *et al*. have also shown that in their patient cohort with familial ARVC, patients presenting missense mutations in *PKP2* had an earlier age of disease onset (Alcalde *et al*., 2014).

Genetic variability and the yet incomplete genotype-phenotype associations, with only up to 50% of ARVC cases linked to mutations in the cardiac desmosomal genes *DSP* (10-15%), *JUP*, *PKP2* (40% and up to 70% in familial ARVC), *DSG2* (10-15%) and *DSC2* (approximately 1%), add to the variability resulted from the clinical diagnosis of ARVC in the general population. Following our genetic analyses, the percentages of possibly disease-associated desmosomal genes were *DSP*, 11%; *DSC2*, 11%; *DSG2*, 11% and *PKP2*, 67%, support previous statistics regardless of the low percentage diagnosis rate.

Other non-desmosomal genes where mutations have been linked to ARVC are the transforming growth factor (*TGF-β3*), which encodes for a cytokine-stimulating fibrosis and is believed to modulate cell adhesion (Beffagna *et al*., 2005), and the transmembrane protein *TMEM43*, which functions as a response element for the adipogenic transcription factor PPAR gamma, which may explain the fibrofatty replacement of the myocardium (Merner *et al*., 2008). Another gene initially associated with ARVC was the human ryanodine receptor 2 (*RYR2*), which induces the release of calcium from the myocardial sarcoplasmic reticulum (Bauce *et al*., 2000), but since publication it is more likely to be a phenocopy rather than true ARVC (Basso *et al*., 2012). We have included *TMEM43* in one of our genetic analyses on 39 of our patients, but no mutations were found in this gene.

A number of gene candidates with increasing interest are several desmosomal components and related proteins, such as plectin (*PLEC*) and pinin (*PNN*) (Sen-

Chowdhry *et al*., 2010), which have already been under investigation for their link to human dermatoses, desmin (*DES*), striatin (*STRN*), titin (*TTN*), lamins A (*LMNA*) and C (*LMNC*), more commonly associated with DCM (Taylor *et al*., 2011, van Tintelen *et al*., 2009, Merner *et al*., 2008, Klauke *et al*., 2010, Meurs *et al*., 2010, Quarta *et al*., 2011), and NFκB interacting protein 1 (*PPP1R13L* or *iASPP*) which has been identified in cattle/mice with ARVC and woolly haircoat syndrome (Simpson *et al*., 2009a, Herron *et al*., 2005). Nevertheless, the multitude of genetic studies have shown that from individuals with a desmosomal mutation, only 30-50% fulfil clinical diagnostic criteria (Towbin, 2008), and that modifier genes could play a great role in the variation between individuals, even within the same family.

Another complexity of genetic testing in families is the presence of compound or digenic mutations, a characteristic of diseases with low penetrance (Xu *et al*., 2010). We have identified in our genetic studies one such case of a digenic ARVC patient, presenting a mutation in *PKP2* and a second mutation in *DSP*, making it difficult to decide whether a "second" variant is sufficient to cause disease and making genotype-phenotype correlation difficult if only one allele is analysed.

In addition to the likelihood of, as yet, unidentified genes for ARVC, the incomplete sensitivity of the mutation screening techniques used such as the presence of mutations in non-analysed sequences in some cases may contribute to the absence of unidentified mutations.

With regard to highly heterogeneous disorders, like ARVC, mutation screening has improved considerably from the laborious, time consuming and ultimately expensive conventional PCR and Sanger sequencing techniques, while whole genome analysis is becoming an option when faced with the possibility of zooming on a region of interest as a more attractive and cost saving technique, mostly as a greater number of samples can be screened together. Array-based sequence capture using a 385K Roche NimbleGen and the HaloPlex target enrichment system were performed on 49 ARVC diagnosed patients to screen for mutations in eight disease-associated genes, *DSP*, *JUP*, *PKP2*, *DSC2*, *DSG2*, *DES*, *TMEM43,* and the possibly disease-associated gene *ADAM17*.

While array-based sequence capture systems have been used successfully in the discovery of novel variants linked to a number of disorders, ultimately Sanger sequencing was required for the confirmation and allocation of mutations to specific samples thus making the process time consuming and laborious when the genetic diagnosis of a larger set of samples is needed. Less than a dozen studies have been published in the last two years, using the HaloPlex target enrichment system, on disorders such as cystic fibrosis (Nakano and Tluczek, 2014), chronic lymphocytic, acute lymphoblastic and acute myeloid leukaemias (Sutton *et al*., 2014, Berglund *et al*., 2013, Bolli *et al*., 2014), primary immunodeficiencies (PIDs) (Stoddard *et al*., 2014), the Usher syndrome (Aparisi *et al*., 2014), neurodegenerative disorders (Pihlstrom *et al*., 2014, Liu *et al*., 2014), breast, ovarian and colon cancers (Arvai *et al*., 2014, Mathot *et al*., 2013) and ARVC (Green *et al*., 2014). This system allowed the use of smaller DNA samples, while sample indexing facilitated posterior identification of the sample where a variant occurred, resulting in a more accurate estimation of allele frequencies. However some studies have reported that the presence of an index tag complicated experimental procedures and decreased capture specificity in inappropriately indexed samples (Nijman *et al*., 2010, Ramos *et al*., 2012). Bolli *et al*. have used HaloPlex to screen a set of AML patients, and showed that the two most important parameters affecting coverage of target regions are amplicon tiling and read length relative to amplicon length, which could give variable coverage to adjacent genomic regions (Bolli *et al*., 2014). These taken into consideration in ARVC genetic diagnosis, the mutational hotspots, such as the CpG regions in *PKP2* and the N-terminus of *DSP*, should be checked by Sanger sequencing to ensure adequate coverage.

In this study, all but two samples had a higher than 70% base coverage above a read depth of 15 X, a cut off which would reduce the probability of missing variants caused by sampling error. As two previously confirmed mutations were also found by HaloPlex, we speculate that the difference between the expected average percentage coverage of 98.5% and achieved percentage coverage could be due to a number of reasons such as:

(i) variations in sample concentrations which would give a lower sample coverage,

(ii) the enzymatic fragmentation step which creates blocks of reads with the same start and end positions, thus if the distance between two restriction sites is longer than the read length, then coverage gaps will occur (Coonrod *et al*., 2014),

(iii) a poorly performed adapter trimming step,

(iv) the lowest anticipated and observed coverage was for *PKP2* and despite the high number of mutations expected only three mutations were real calls in 37 ARVC samples, which could possibly be due to low coverage of mutational "hot spots" in this gene.

Although no INDELS were identified in our study, it has previously been shown that this system is proving efficient at detecting this particularly difficult to distinguish variation (Aparisi *et al*., 2014, Bolli *et al*., 2014).

In our case the identification of disease-causing mutations in genes already known to be implicated in ARVC has proven challenging, with a high potential for false negatives due to variable coverage, perhaps associated to high GC-content, highly homologous sequences or repeat regions. Moreover these techniques would only cover exonic regions included in the sequencing panel, while any intronic, promoter and regulatory regions would not be detected (Stoddard *et al*., 2014). Any novel variants should be considered in the context of a region-by-region coverage report and would still require validation by Sanger sequencing and functional assays to prove genotype-phenotype correlations, mostly as ARVC presents such a high genetic and phenotypical variability.

If to these observations we add some important environmental factors, including sex, exercise, hormones, emotional stress, inflammation and the use of medicines, all of which play a role in disease expression (Sen-Chowdhry *et al*., 2010), it is understandable why genetic, epigenetic and environmental factors should be considered a package in ARVC diagnosis.

6.3. *In vitro* studies reveal a new role for cystatin A in basal epidermal adhesion

The *in vitro* analyses presented in Chapter 4 are based on the first reported LOF *CSTA* mutations linked to autosomal-recessive exfoliative ichthyosis (Blaydon *et al*., 2011b), and they reveal a previously unknown role for the protease inhibitor cystatin A in keratinocyte adhesion in the basal layers of the skin epidermis.

Initially described as an intracellular cysteine protease inhibitor of several cathepsins, and later on reported in sweat and secreted in medium from cultured keratinocytes, CSTA was functionally limited to the upper layers of the epidermis, mostly associated with atopic dermatitis and psoriasis (Kato *et al*., 2005, Vasilopoulos *et al*., 2007, Vasilopoulos *et al*., 2008). Furthermore, immunohistochemistry on facelift and palm skin samples confirmed that CSTA was expressed throughout the epidermis (Blaydon *et al*., 2011b), supporting previous studies (Basel-Vanagaite *et al*., 2007).

Using *in silico* splice-site predictor programs Blaydon *et al*. have described that the splice-site *CSTA* mutation identified in homozygosity in one of the exfoliative ichthyosis families, would lead to the loss of the 3' splice-acceptor site and a much lower maximum entropy score for the mutant splice-site when compared to wild type. This would lead to a substantial reduction in protein expression and due to changes in protein conformation any expressed protein would most likely be dysfunctional (Blaydon *et al*., 2011b). Due to the lack of patient material for the study of these mutations, the immortalised keratinocyte cell line HaCaT together with siRNA based knockdown of *CSTA*, were used for all *in vitro* analyses described.

Electron microscopy of the basal and suprabasal layers of patient epidermis and *in vitro CSTA* LOF 3D models have revealed widening of intercellular spaces and thickening of keratin filaments in these layers of patient skin, believed to be due to impaired intercellular adhesion and increased mechanical stress in the palmoplantar regions (Blaydon *et al*., 2011b). The *CSTA* knockdown 3D skin model described by Blaydon *et al*., demonstrated hyperkeratosis, parakeratosis and moderate epidermal hyperplasia together with a disturbance of the basal epidermal

architecture and without changes in epidermal barrier (Blaydon *et al*., 2011b). Further analyses described in Chapter 4, performed using the *in vitro* cell model HaCaT, as also revealed breakage of intercellular connections upon stretching of *CSTA* knockdown monolayers together with thickening and retraction of the keratin 14 filaments toward the nucleus. Also, a significant reduction in keratinocyte adhesion was observed following treatment with either dispase, or in mechanically stressed *CSTA* knockdown monolayers, in contrast to control keratinocytes. The histological and cell biology studies indicate that CSTA plays an important role in adhesion in the basal layers of the epidermis. If the change in keratin 14 filaments, observed in stretched *CSTA* knockdown monolayers, is considered together with the information that these intermediate filaments connect to the plasma membrane through desmosomes then it can be speculated that indirectly the *CSTA* LOF mutations contribute to the dysregulation of desmosome assembly or function, most probably through some of the target proteases, cathepsins B, H, L, S or V.

A number of desmosome-associated proteins have been reported as targets of proteases, for example, in Netherton syndrome associated with mutations in *SPINK5* encoding LEKTI-1 which targets the proteases KLK5, KLK7 and KLK14 (Deraison *et al*., 2007), ultimately leading to DSG1 degradation and desmosome cleavage with detachment of the stratum corneum (D'Alessio *et al*., 2013, Hovnanian, 2013). Inhibition of these proteases by SPINK6 and SPINK9, is reportedly leading to desquamation through their action on DSG1, DSC1 and corneodesmosin (Meyer-Hoffert, 2009, Meyer-Hoffert *et al*., 2010, Brattsand *et al*., 2009).

In a syndrome of severe skin and bowel inflammation, associated with *ADAM17* LOF mutations, Blaydon *et al*. revealed an increase in DSG2 protein expression, implying a reduction in DSG2 shedding by ADAM17 (Blaydon *et al*., 2011a). In contrast, patients with TOC (Ellis *et al*., 1994, Hennies *et al*., 1995, Stevens *et al*., 1996), linked to mutations affecting iRHOM2 (Blaydon *et al*., 2012, Saarinen *et al*., 2012), present with immature desmosomes lacking the electron dense midlines (Brooke *et al*., 2014). Furthermore, *in vitro* studies in TOC patient derived keratinocyte cell lines revealed a dramatic increase in the iRHOM2-mediated processing and activity of ADAM17, together with an increase in processing of DSG2 (Brooke *et al*., 2014).

One possible mechanism of action, explaining the phenotypical limitation to the basal layers of the epidermis, would be that the cathepsins target specific desmosomal components which are differentially expressed throughout the skin. A particular difference between desmosomes of the basal layers and corneodesmosomes of the stratum corneum is the expression of DSG1 and DSC1 in the stratum corneum compared to the expression of DSG2 and 3 and DSC2 and 3 decreasing towards the upper layers. This hypothesis can be discussed through differences between the autoimmune disorders PV and PF, where DSG3 and/or 1 are differentially targeted by autoantibodies leading to severe blistering in PV (Cirillo and Al-Jandan, 2013) and superficial blisters in PF (Ishii *et al*., 1997). The important role played by DSG3 in the more basal layers of the epidermis, where DSG1 is not present and cannot therefore compensate for the anti-DSG3 autoantibodies in PV, through the so called DSG compensation theory, is very well highlighted in these disorders (Shirakata *et al*., 1998). This hypothesis was partially tested by analysis of DSP and DSG1/2 in *CSTA* knockdown monolayers which have shown an up-regulation and aberrant localisation of these components in the cytoplasmic compartment of *CSTA* knockdown stretched cells, while an up-regulation in DSG3 expression in siRNA treated cells was seen independent of mechanical stretch.

Another difference between the various layers of the epidermis is the differentiation-specific expression of diverse keratins as keratinocytes migrate towards the upper layers, with keratins 5 and 14 expressed exclusively in the basal layers. Additional immunomicroscopy analysis of keratin 5 and keratins 1 and 10 expressed in the upper layers of the epidermis, on *CSTA* LOF 3D models could perhaps clarify the extent of breakage of these filaments and possibly give an indication on whether breakage is taking place on the cytoplasmic side of the plasma membrane or intercellularly.

The expression and activity of the target proteases inhibited by CSTA, cathepsins B, H and L, have mainly been analysed in the context of tumour progression, invasion and metastasis, where dysregulation of their expression and activity was reported to play a role (Strojan *et al*., 2000, Leinonen *et al*., 2007, Li *et al*., 2011, Anicin *et al*., 2013). The analysis of cathepsin expression, before and after mechanical stretch or

"scratch-wound" of *CSTA* KD monolayers, has revealed normal expression levels for both cathepsins B and L in all conditions. The analysis of the activity of these proteases under the conditions described above should be performed to decipher the role played by these proteins in the mechanism of epidermal disruption.

A study looking at neonatal and adult murine skin has shown exceptionally strong expression of Csta in neonatal skin during periods of keratinocyte proliferation and differentiation suggesting a critical role for this protein either in the promotion or regulation of these processes (Scott *et al*., 2007). Interestingly, in double *Csta* and *Stfa2l1* knockout mice, no obvious phenotype such as epidermal peeling was observed, including no spontaneous tumours being formed in mice observed for up to 12 months (Bilodeau *et al*., 2009). These observations probably reflect differences in human and mouse skin.

6.4. New clinical entity linked to LOF mutations in *CAST*

In Chapter 5 of this thesis we described the clinical aspects and genetic analysis of three unrelated families, presenting loss-of-function mutations in *CAST*, the gene encoding for the protease inhibitor calpastatin, linked to a novel clinical entity which we have assigned the acronym PLACK (Lin *et al*., 2015). This syndrome is a complex form of generalised PSS, previously linked to mutations in the *CDSN* gene (Oji *et al*., 2010), and in our patients is accompanied by leukonychia, acral punctate keratoses, cheilitis and knuckle pads. The genetic and *in vitro* analyses, presented in the above mentioned chapter of this thesis are included in a study published by Lin *et al*., expanding the spectrum of cutaneous disorders linked to mutations in protease inhibitors (Lin *et al*., 2015).

As demonstrated by previous studies, mutations in genes encoding for protease inhibitors can cause a number of genetic cutaneous disorders, such as *SPINK5* in Netherton syndrome (Chavanas *et al*., 2000), *SERPINB7* in Nagashima-type palmoplantar keratosis (Kubo *et al*., 2013), *CSTA* in exfoliative ichthyosis (Blaydon *et al*., 2011b), by mechanisms involving disruption of the skin barrier, impairment of keratinocyte adhesion and/or dysregulation of cell signalling.

It is predicted that the identified *CAST* mutations lead to changes in the conformational structure of CAST and as confirmed by immunomicroscopy and hematological analysis, on non-lesional patient skin, they also lead to a significant down-regulation in protein expression. In comparison, normal control skin showed expression of CAST throughout all layers of the epidermis.

One additional aspect observed in *CAST* LOF skin was abnormally thicker basal/suprabasal layers with typically apical-oriented cells, indicative of a possible dysregulation in keratinocyte differentiation, perhaps explaining the hyperkeratosis seen in patient skin. A number of *in vitro* and *in vivo* mouse model studies have looked at the role of CAST and the target proteases, calpains 1 and 2, in skin disorders and the mechanisms associated. These studies have shown that: calpain 1 and CAST are involved in the processing of profilaggrin to filaggrin monomers and the processing of keratin filaments in cell differentiation (Yamazaki *et al*., 1997), calpain 2 is involved in the catabolism of filaggrin and filaggrin 2 during terminal differentiation (Hsu *et al*., 2011, Kamata *et al*., 2009), and an increase in calpain 2 activity leads to apoptosis (Inoue *et al*., 2004), in turn this leading to skin hyperkeratosis (Lin *et al*., 2012, Wang *et al*., 2015). Lin *et al*. have observed a significant increase in apoptotic cells in lesional skin from another *CAST* LOF patient included in the study (Lin *et al*., 2015). We suggest that an increase in the activity of calpains 1 and 2 in *CAST* LOF patients may trigger apoptosis by cleavage of pro- or anti-apoptotic proteins, as previously shown (Tan *et al*., 2006). This process has also been demonstrated in HaCaT cells where an increase in activity of calpain 2 resulted in increased programmed cell death (Inoue *et al*., 2004). However, the analysis of apoptotic cell death, in an *in vitro* model using HaCaT cells and siRNA mediated knockdown of *CAST*, has revealed a normal cell cycle when compared to control NTP cells.

In the same *CAST* siRNA cell model, the analysis of the strength of keratinocyte adhesion was addressed, as some intercellular gaps were observed in non-lesional patient skin. This analysis has confirmed that, *in vitro*, breakage of intercellular connections happens independently of mechanical stress in *CAST* siRNA monolayers. This could perhaps explain why the PLACK phenotype seen in affected individuals is not limited to the palmoplantar regions. As the *CSTA* knockdown

model presented breakage of intercellular connections, the analysis of desmosomal proteins was performed. Staining of non-lesional skin revealed an apparent up-regulation of DSG2 expression in areas of the basal layers of the epidermis and a significant up-regulation in the expression of DSG3 and DSP I/II in all layers of the epidermis, together with an aberrant localisation to the cytoplasmic compartment. *In vitro* analysis of *CAST* knockdown monolayers presented variable results and more repeat experiments would be required to draw a clear conclusion. The variability of the *in vitro* observations could be due to a relatively low level of knockdown, of 50-65%, in comparison to the expected level of 85%, which can be attributed to a high protein stability or extended half-life of calpastatin. An increased level of *CAST* knockdown could be achieved by double siRNA-mediated *CAST* knockdown or alternatively by permanent knockout using shRNA or the CRISPR-Cas9 system. Based on the observations gathered, it is suggested that the reduction in expression of calpastatin due to *CAST* LOF mutations directly correlates with an increase in the concentration of calpains, which in turn could lead to proteolysis of DSG2, DSG3 and DSP II in the affected individuals, resulting in acantholysis and impaired resistance of the epidermis to mechanical stretch, seen as blistering and skin peeling. As calpain-mediated proteolysis of talin and focal adhesion kinase (FAK) is reportedly leading to regulation of adhesion dynamics (Franco *et al*., 2004, Chan *et al*., 2010), these proteins could be analysed in patient skin and *CAST* siRNA keratinocytes. In order to better address these probabilities, activation of calpains by Ca^{2+} mobilisation, with ionomycin, or GF stimulation, with EGF, should be performed following siRNA mediated *CAST* knockdown and prior to analysis of expression and localisation of any possible target proteins of calpains. Calpain activity could be monitored by zymography following Ca^{2+} activation.

Independent studies looking at a variety of cancers have associated calpains with adhesion, motility, invasion, cell-cycle regulation, cell spreading, apoptosis and myogenesis (Leloup *et al*., 2006). Interestingly, in *in vivo* mouse models, the up-regulation in expression of both calpains 1 and 2 in skin wound healing was reported (Zhao *et al*., 2009), while more recently, Nassar *et al*. using *Cast* overexpression mice have shown a delay in wound healing, re-epithelialisation and angiogenesis (Nassar *et al*., 2012). In contrast, a *Cast* knockout mouse model, which

showed increased activity of the target calpains 1 and 2, revealed no defect under normal conditions (Takano *et al*., 2005), although only slight behavioural changes have been seen in a stressful environment (Nakajima *et al*., 2008). The *in vitro* analysis described here showed a normal scratch-wound closure pattern, suggesting a normal cell migration process. An analysis on *Cast* knockout mouse epidermis or CRISPR-Cas9 *CAST* knockout 3D models may give a more accurate view of any wound-healing and cell migration processes regulated by CAST. These phenotypical differences seen between humans and mice indicate once again the difference in physiological functions, and that observations made on mouse models should be considered carefully.

6.5. Conclusion

Although it is possible that common pathways lead to a variety of desmosome-associated genetic disorders, the understanding of the consequences of those initial mutations or different molecular mechanisms leading to a common phenotype are crucial in unveiling the array of functions each desmosome-associated protein is playing and how these functions are altered in disease. The importance of the differential expression of desmosomal proteins in different tissues, such as the skin and heart, is becoming another factor of great importance in understanding different molecular mechanisms, mostly as some desmosomal proteins appear to be part of more complex signaling cascades. Therefore, the same protein might be subject to different regulation, perform different functions and genetic variations might lead to different outcomes, despite possibly overlapping mechanisms of disease. Moreover, regulation of desmosome assembly and/or function appears to be an indirect target of mutations in protease inhibitors, linked to a number of cutaneous disorders characterized by impaired intercellular adhesion.

In summary, this thesis explored the increasing significance of genetic analyses in disease diagnosis using high-throughput sequencing platforms, coupled with the importance of the careful consideration of any novel variants in the disease context. Well-designed functional assays are essential to confirm disease causality and to investigate genotype-phenotype correlations.

Bibliography

ABRAHAMSON, M., ALVAREZ-FERNANDEZ, M. & NATHANSON, C. M. 2003. Cystatins. *Biochem Soc Symp*, 179-99.

ACEHAN, D., PETZOLD, C., GUMPER, I., SABATINI, D. D., MULLER, E. J., COWIN, P. & STOKES, D. L. 2008. Plakoglobin is required for effective intermediate filament anchorage to desmosomes. *J Invest Dermatol,* 128, 2665-75.

AL-JASSAR, C., BIKKER, H., OVERDUIN, M. & CHIDGEY, M. 2013. Mechanistic basis of desmosome-targeted diseases. *J Mol Biol,* 425, 4006-22.

ALCALAI, R., METZGER, S., ROSENHECK, S., MEINER, V. & CHAJEK-SHAUL, T. 2003. A recessive mutation in desmoplakin causes arrhythmogenic right ventricular dysplasia, skin disorder, and woolly hair. *Journal of the American College of Cardiology,* 42, 319-327.

ALCALDE, M., CAMPUZANO, O., BERNE, P., GARCIA-PAVIA, P., DOLTRA, A., ARBELO, E., SARQUELLA-BRUGADA, G., IGLESIAS, A., ALONSO-PULPON, L., BRUGADA, J. & BRUGADA, R. 2014. Stop-gain mutations in PKP2 are associated with a later age of onset of arrhythmogenic right ventricular cardiomyopathy. *PLoS One,* 9, e100560.

AMAGAI, M. 2010. Autoimmune and infectious skin diseases that target desmogleins. *Proceedings of the Japan Academy, Series B,* 86, 524-537.

AMAGAI, M., AHMED, A. R., KITAJIMA, Y., BYSTRYN, J. C., MILNER, Y., GNIADECKI, R., HERTL, M., PINCELLI, C., KURZEN, H., FRIDKIS-HARELI, M., AOYAMA, Y., FRUSIC-ZLOTKIN, M., MULLER, E., DAVID, M., MIMOUNI, D., VIND-KEZUNOVIC, D., MICHEL, B., MAHONEY, M. & GRANDO, S. 2006. Are desmoglein autoantibodies essential for the immunopathogenesis of pemphigus vulgaris, or just "witnesses of disease"? *Exp Dermatol,* 15, 815-31.

AMAGAI, M., KLAUS-KOVTUN, V. & STANLEY, J. R. 1991. Autoantibodies against a novel epithelial cadherin in pemphigus vulgaris, a disease of cell adhesion. *Cell,* 67**,** 869-77.

AMAGAI, M., MATSUYOSHI, N., WANG, Z. H., ANDL, C. & STANLEY, J. R. 2000. Toxin in bullous impetigo and staphylococcal scalded-skin syndrome targets desmoglein 1. *Nat Med,* 6**,** 1275-7.

AMAGAI, M. & STANLEY, J. R. 2012. Desmoglein as a target in skin disease and beyond. *J Invest Dermatol,* 132**,** 776-84.

AMAGAI, M., YAMAGUCHI, T., HANAKAWA, Y., NISHIFUJI, K., SUGAI, M. & STANLEY, J. R. 2002. Staphylococcal exfoliative toxin B specifically cleaves desmoglein 1. *J Invest Dermatol,* 118**,** 845-50.

ANDO, Y., IMAMURA, S., MURACHI, T. & KANNAGI, R. 1988. Calpain activates two transglutaminases from porcine skin. *Arch Dermatol Res,* 280**,** 380-4.

ANDREASEN, C., NIELSEN, J. B., REFSGAARD, L., HOLST, A. G., CHRISTENSEN, A. H., ANDREASEN, L., SAJADIEH, A., HAUNSO, S., SVENDSEN, J. H. & OLESEN, M. S. 2013. New population-based exome data are questioning the pathogenicity of previously cardiomyopathy-associated genetic variants. *Eur J Hum Genet,* 21**,** 918-28.

ANGST, B. D., MARCOZZI, C. & MAGEE, A. I. 2001. The cadherin superfamily. *J Cell Sci,* 114**,** 625-6.

ANGST, B. D., NILLES, L. A. & GREEN, K. J. 1990. Desmoplakin II expression is not restricted to stratified epithelia. *J Cell Sci,* 97 (Pt 2)**,** 247-57.

ANICIN, A., GALE, N., SMID, L., KOS, J. & STROJAN, P. 2013. Expression of stefin A is of prognostic significance in squamous cell carcinoma of the head and neck. *Eur Arch Otorhinolaryngol,* 270**,** 3143-51.

ANTONIADES, L., TSATSOPOULOU, A., ANASTASAKIS, A., SYRRIS, P., ASIMAKI, A., PANAGIOTAKOS, D., ZAMBARTAS, C., STEFANADIS, C., MCKENNA, W. J. & PROTONOTARIOS, N. 2006. Arrhythmogenic right ventricular cardiomyopathy caused by deletions in plakophilin-2 and plakoglobin (Naxos disease) in families from Greece and Cyprus: genotype-phenotype relations, diagnostic features and prognosis. *Eur Heart J,* 27**,** 2208-16.

AOYAMA, Y., NAGAI, M. & KITAJIMA, Y. 2010. Binding of pemphigus vulgaris IgG to antigens in desmosome core domains excludes immune complexes rather than directly splitting desmosomes. *Br J Dermatol,* 162**,** 1049-55.

APARISI, M. J., ALLER, E., FUSTER-GARCIA, C., GARCIA-GARCIA, G., RODRIGO, R., VAZQUEZ-MANRIQUE, R. P., BLANCO-KELLY, F., AYUSO, C., ROUX, A. F., JAIJO, T. & MILLAN, J. M. 2014. Targeted next generation sequencing for molecular diagnosis of Usher syndrome. *Orphanet J Rare Dis,* 9**,** 168.

ARMSTRONG, D. K., MCKENNA, K. E., PURKIS, P. E., GREEN, K. J., EADY, R. A., LEIGH, I. M. & HUGHES, A. E. 1999. Haploinsufficiency of desmoplakin causes a striate subtype of palmoplantar keratoderma. *Hum Mol Genet,* 8**,** 143-8.

ARVAI, K., HORVATH, P., BALLA, B., TOKES, A. M., TOBIAS, B., TAKACS, I., NAGY, Z., LAKATOS, P. & KOSA, J. P. 2014. Rapid and cost effective screening of breast and ovarian cancer genes using novel sequence capture method in clinical samples. *Fam Cancer,* 13**,** 583-9.

ASIMAKI, A., SYRRIS, P., WICHTER, T., MATTHIAS, P., SAFFITZ, J. E. & MCKENNA, W. J. 2007. A novel dominant mutation in plakoglobin causes arrhythmogenic right ventricular cardiomyopathy. *Am J Hum Genet,* 81**,** 964-73.

ASIMAKI, A., TANDRI, H., HUANG, H., HALUSHKA, M. K., GAUTAM, S., BASSO, C., THIENE, G., TSATSOPOULOU, A., PROTONOTARIOS, N., MCKENNA, W. J., CALKINS, H. & SAFFITZ, J. E. 2009. A new diagnostic test for arrhythmogenic right ventricular cardiomyopathy. *N Engl J Med,* 360**,** 1075-84.

ATTARDI, L. D., RECZEK, E. E., COSMAS, C., DEMICCO, E. G., MCCURRACH, M. E., LOWE, S. W. & JACKS, T. 2000. PERP, an apoptosis-associated target of p53, is a novel member of the PMP-22/gas3 family. *Genes Dev,* 14**,** 704-18.

AWAD, M. M., CALKINS, H. & JUDGE, D. P. 2008a. Mechanisms of disease: molecular genetics of arrhythmogenic right ventricular dysplasia/cardiomyopathy. *Nat Clin Pract Cardiovasc Med,* 5**,** 258-67.

AWAD, M. M., DALAL, D., TICHNELL, C., JAMES, C., TUCKER, A., ABRAHAM, T., SPEVAK, P. J., CALKINS, H. & JUDGE, D. P. 2006. Recessive arrhythmogenic right ventricular dysplasia due to novel cryptic splice mutation in PKP2. *Hum Mutat,* 27**,** 1157.

AWAD, T. S., HELGASON, T., KRISTBERGSSON, K., WEISS, J., DECKER, E. A. & MCCLEMENTS, D. J. 2008b. Temperature scanning ultrasonic velocity study of complex thermal transformations in solid lipid nanoparticles. *Langmuir,* 24**,** 12779-84.

AYUB, M., BASIT, S., JELANI, M., UR REHMAN, F., IQBAL, M., YASINZAI, M. & AHMAD, W. 2009. A homozygous nonsense mutation in the human desmocollin-3 (DSC3) gene underlies hereditary hypotrichosis and recurrent skin vesicles. *Am J Hum Genet,* 85**,** 515-20.

AZAOUAGH, A., CHURZIDSE, S., KONORZA, T. & ERBEL, R. 2011. Arrhythmogenic right ventricular cardiomyopathy/dysplasia: a review and update. *Clin Res Cardiol,* 100**,** 383-94.

BANNON, L. J., CABRERA, B. L., STACK, M. S. & GREEN, K. J. 2001. Isoform-specific differences in the size of desmosomal cadherin/catenin complexes. *J Invest Dermatol,* 117**,** 1302-6.

BARNOY, S., GLASNER, T. & KOSOWER, N. S. 1996. The role of calpastatin (the specific calpain inhibitor) in myoblast differentiation and fusion. *Biochem Biophys Res Commun,* 220**,** 933-8.

BARNOY, S., MAKI, M. & KOSOWER, N. S. 2005. Overexpression of calpastatin inhibits L8 myoblast fusion. *Biochem Biophys Res Commun,* 332**,** 697-701.

BASEL-VANAGAITE, L., ATTIA, R., ISHIDA-YAMAMOTO, A., RAINSHTEIN, L., BEN AMITAI, D., LURIE, R., PASMANIK-CHOR, M., INDELMAN, M., ZVULUNOV, A., SABAN, S., MAGAL, N., SPRECHER, E. & SHOHAT, M. 2007. Autosomal recessive ichthyosis with hypotrichosis caused by a mutation in ST14, encoding type II transmembrane serine protease matriptase. *Am J Hum Genet,* 80**,** 467-77.

BASS-ZUBEK, A. E., HOBBS, R. P., AMARGO, E. V., GARCIA, N. J., HSIEH, S. N., CHEN, X., WAHL, J. K., 3RD, DENNING, M. F. & GREEN, K. J. 2008. Plakophilin 2: a critical scaffold for PKC alpha that regulates intercellular junction assembly. *J Cell Biol,* 181**,** 605-13.

BASSO, C., BAUCE, B., CORRADO, D. & THIENE, G. 2012. Pathophysiology of arrhythmogenic cardiomyopathy. *Nat Rev Cardiol,* 9**,** 223-33.

BAUCE, B., NAVA, A., BEFFAGNA, G., BASSO, C., LORENZON, A., SMANIOTTO, G., DE BORTOLI, M., RIGATO, I., MAZZOTTI, E., STERIOTIS, A., MARRA, M. P., TOWBIN, J. A., THIENE, G., DANIELI, G. A. & RAMPAZZO, A. 2010. Multiple mutations in desmosomal proteins encoding genes in arrhythmogenic right ventricular cardiomyopathy/dysplasia. *Heart Rhythm,* 7**,** 22-9.

BAUCE, B., NAVA, A., RAMPAZZO, A., DALIENTO, L., MURIAGO, M., BASSO, C., THIENE, G. & DANIELI, G. A. 2000. Familial effort polymorphic ventricular arrhythmias in arrhythmogenic right ventricular cardiomyopathy map to chromosome 1q42-43. *Am J Cardiol,* 85**,** 573-9.

BAZZI, H., MARTINEZ-MIR, A., KLJUIC, A. & CHRISTIANO, A. M. 2005. Desmoglein 4 mutations underlie localized autosomal recessive hypotrichosis in humans, mice, and rats. *J Investig Dermatol Symp Proc,* 10**,** 222-4.

BEAUDRY, V. G., IHRIE, R. A., JACOBS, S. B., NGUYEN, B., PATHAK, N., PARK, E. & ATTARDI, L. D. 2010a. Loss of the desmosomal component perp impairs wound healing *in vivo*. *Dermatol Res Pract,* 2010**,** 759731.

BEAUDRY, V. G., JIANG, D., DUSEK, R. L., PARK, E. J., KNEZEVICH, S., RIDD, K., VOGEL, H., BASTIAN, B. C. & ATTARDI, L. D. 2010b. Loss of the p53/p63 regulated desmosomal protein Perp promotes tumorigenesis. *PLoS Genet,* 6**,** e1001168.

BEFFAGNA, G., OCCHI, G., NAVA, A., VITIELLO, L., DITADI, A., BASSO, C., BAUCE, B., CARRARO, G., THIENE, G., TOWBIN, J. A., DANIELI, G. A. & RAMPAZZO, A. 2005. Regulatory mutations in transforming growth factor-beta3 gene cause arrhythmogenic right ventricular cardiomyopathy type 1. *Cardiovasc Res,* 65**,** 366-73.

BERGLUND, E. C., LINDQVIST, C. M., HAYAT, S., OVERNAS, E., HENRIKSSON, N., NORDLUND, J., WAHLBERG, P., FORESTIER, E., LONNERHOLM, G. & SYVANEN, A. C. 2013. Accurate detection of subclonal single nucleotide variants in whole genome amplified and pooled cancer samples using HaloPlex target enrichment. *BMC Genomics,* 14**,** 856.

BHUIYAN, Z. A., JONGBLOED, J. D., VAN DER SMAGT, J., LOMBARDI, P. M., WIESFELD, A. C., NELEN, M., SCHOUTEN, M., JONGBLOED, R., COX, M. G., VAN WOLFEREN, M., RODRIGUEZ, L. M., VAN GELDER, I. C., BIKKER, H., SUURMEIJER, A. J., VAN DEN BERG, M. P., MANNENS, M. M., HAUER, R. N., WILDE, A. A. & VAN TINTELEN, J. P. 2009. Desmoglein-2 and desmocollin-2 mutations in dutch arrhythmogenic right ventricular dysplasia/cardiomypathy patients: results from a multicenter study. *Circ Cardiovasc Genet,* 2**,** 418-27.

BIERKAMP, C., MCLAUGHLIN, K. J., SCHWARZ, H., HUBER, O. & KEMLER, R. 1996. Embryonic heart and skin defects in mice lacking plakoglobin. *Dev Biol,* 180**,** 780-5.

BILODEAU, M., MACRAE, T., GABOURY, L., LAVERDURE, J. P., HARDY, M. P., MAYOTTE, N., PARADIS, V., HARTON, S., PERREAULT, C. & SAUVAGEAU, G. 2009. Analysis of blood stem cell activity and cystatin gene expression in a mouse model presenting a chromosomal deletion encompassing Csta and Stfa2l1. *PLoS One,* 4**,** e7500.

BLAYDON, D. C., BIANCHERI, P., DI, W. L., PLAGNOL, V., CABRAL, R. M., BROOKE, M. A., VAN HEEL, D. A., RUSCHENDORF, F., TOYNBEE, M., WALNE, A., O'TOOLE, E. A., MARTIN, J. E., LINDLEY, K., VULLIAMY, T., ABRAMS, D. J., MACDONALD, T. T., HARPER, J. I. & KELSELL, D. P. 2011a. Inflammatory skin and bowel disease linked to ADAM17 deletion. *N Engl J Med,* 365**,** 1502-8.

BLAYDON, D. C., ETHERIDGE, S. L., RISK, J. M., HENNIES, H. C., GAY, L. J., CARROLL, R., PLAGNOL, V., MCRONALD, F. E., STEVENS, H. P., SPURR, N. K., BISHOP, D. T., ELLIS, A., JANKOWSKI, J., FIELD, J. K., LEIGH, I. M., SOUTH, A. P. & KELSELL, D. P. 2012. RHBDF2 mutations are associated with tylosis, a familial esophageal cancer syndrome. *Am J Hum Genet,* 90**,** 340-6.

BLAYDON, D. C., NITOIU, D., ECKL, K. M., CABRAL, R. M., BLAND, P., HAUSSER, I., VAN HEEL, D. A., RAJPOPAT, S., FISCHER, J., OJI, V., ZVULUNOV, A., TRAUPE, H., HENNIES, H. C. & KELSELL, D. P. 2011b. Mutations in CSTA, encoding Cystatin A, underlie exfoliative ichthyosis and reveal a role for this protease inhibitor in cell-cell adhesion. *Am J Hum Genet,* 89**,** 564-71.

BODE, W., ENGH, R., MUSIL, D., THIELE, U., HUBER, R., KARSHIKOV, A., BRZIN, J., KOS, J. & TURK, V. 1988. The 2.0 A X-ray crystal structure of chicken egg white cystatin and its possible mode of interaction with cysteine proteinases. *EMBO J,* 7**,** 2593-9.

BOLLI, N., MANES, N., MCKERREL, T., CHI, J., PARK, N., GUNDEM, G., QUAIL, M. A., SATHIASEELAN, V., HERMAN, B., CRAWLEY, C., CRAIG, J. I., CONTE, N., GROVE, C., PAPAEMMANUIL, E., CAMPBELL, P. J., VARELA, I., COSTEAS, P. & VASSILIOU, G. S. 2014. Characterization of gene mutations and copy number changes in acute myeloid leukemia using a rapid target enrichment protocol. *Haematologica*.

BOLLING, M. C. & JONKMAN, M. F. 2009. Skin and heart: une liaison dangereuse. *Exp Dermatol,* 18**,** 658-68.

BONAZZI, M. & COSSART, P. 2011. Impenetrable barriers or entry portals? The role of cell-cell adhesion during infection. *J Cell Biol,* 195**,** 349-58.

BONNE, S., VAN HENGEL, J., NOLLET, F., KOOLS, P. & VAN ROY, F. 1999. Plakophilin-3, a novel armadillo-like protein present in nuclei and desmosomes of epithelial cells. *J Cell Sci,* 112 (Pt 14)**,** 2265-76.

BORNSLAEGER, E. A., GODSEL, L. M., CORCORAN, C. M., PARK, J. K., HATZFELD, M., KOWALCZYK, A. P. & GREEN, K. J. 2001. Plakophilin 1 interferes with plakoglobin binding to desmoplakin, yet together with plakoglobin promotes clustering of desmosomal plaque complexes at cell-cell borders. *J Cell Sci,* 114**,** 727-38.

BOULE, S., FRESSART, V., LAUX, D., MALLET, A., SIMON, F., DE GROOTE, P., BONNET, D., KLUG, D. & CHARRON, P. 2012. Expanding the phenotype associated with a desmoplakin dominant mutation: Carvajal/Naxos syndrome associated with leukonychia and oligodontia. *Int J Cardiol,* 161**,** 50-2.

BOYCE, A. E., MCGRATH, J. A., TECHANUKUL, T., MURRELL, D. F., CHOW, C. W., MCGREGOR, L. & WARREN, L. J. 2012. Ectodermal dysplasia-skin fragility syndrome due to a new homozygous internal deletion mutation in the PKP1 gene. *Australas J Dermatol,* 53**,** 61-5.

BRANCOLINI, C., BENEDETTI, M. & SCHNEIDER, C. 1995. Microfilament reorganization during apoptosis: the role of Gas2, a possible substrate for ICE-like proteases. *EMBO J,* 14**,** 5179-90.

BRANCOLINI, C., SGORBISSA, A. & SCHNEIDER, C. 1998. Proteolytic processing of the adherens junctions components beta-catenin and gamma-catenin/plakoglobin during apoptosis. *Cell Death Differ,* 5**,** 1042-50.

BRATTSAND, M., STEFANSSON, K., HUBICHE, T., NILSSON, S. K. & EGELRUD, T. 2009. SPINK9: a selective, skin-specific Kazal-type serine protease inhibitor. *J Invest Dermatol,* 129**,** 1656-65.

BRENNAN, D. & MAHONEY, M. G. 2009. Increased expression of Dsg2 in malignant skin carcinomas: A tissue-microarray based study. *Cell Adh Migr,* 3**,** 148-54.

BRENNAN, D., PELTONEN, S., DOWLING, A., MEDHAT, W., GREEN, K. J., WAHL, J. K., 3RD, DEL GALDO, F. & MAHONEY, M. G. 2012. A role for caveolin-1 in desmoglein binding and desmosome dynamics. *Oncogene,* 31**,** 1636-48.

BREUNINGER, S., REIDENBACH, S., SAUER, C. G., STROBEL, P., PFITZENMAIER, J., TROJAN, L. & HOFMANN, I. 2010. Desmosomal plakophilins in the prostate and prostatic adenocarcinomas: implications for diagnosis and tumor progression. *Am J Pathol,* 176**,** 2509-19.

BROOKE, M. A., ETHERIDGE, S. L., KAPLAN, N., SIMPSON, C., O'TOOLE, E. A., ISHIDA-YAMAMOTO, A., MARCHES, O., GETSIOS, S. & KELSELL, D. P. 2014. iRHOM2-dependent regulation of ADAM17 in cutaneous disease and epidermal barrier function. *Hum Mol Genet,* 23**,** 4064-76.

BROOKE, M. A., NITOIU, D. & KELSELL, D. P. 2012. Cell-cell connectivity: desmosomes and disease. *J Pathol,* 226**,** 158-71.

BROWN, W. M. & DZIEGIELEWSKA, K. M. 1997. Friends and relations of the cystatin superfamily--new members and their evolution. *Protein Sci,* 6**,** 5-12.

BURGESON, R. E. & NIMNI, M. E. 1992. Collagen types. Molecular structure and tissue distribution. *Clin Orthop Relat Res***,** 250-72.

BUTH, H., LUIGI BUTTIGIEG, P., OSTAFE, R., REHDERS, M., DANNENMANN, S. R., SCHASCHKE, N., STARK, H. J., BOUKAMP, P. & BRIX, K. 2007. Cathepsin B is essential for regeneration of scratch-wounded normal human epidermal keratinocytes. *Eur J Cell Biol,* 86**,** 747-61.

BUTH, H., WOLTERS, B., HARTWIG, B., MEIER-BORNHEIM, R., VEITH, H., HANSEN, M., SOMMERHOFF, C. P., SCHASCHKE, N., MACHLEIDT, W., FUSENIG, N. E., BOUKAMP, P. & BRIX, K. 2004. HaCaT keratinocytes secrete lysosomal cysteine proteinases during migration. *Eur J Cell Biol,* 83**,** 781-95.

BUTLER, M. W., FUKUI, T., SALIT, J., SHAYKHIEV, R., MEZEY, J. G., HACKETT, N. R. & CRYSTAL, R. G. 2011. Modulation of cystatin A expression in human airway epithelium related to genotype, smoking, COPD, and lung cancer. *Cancer Res,* 71**,** 2572-81.

CABRAL, R. M., KURBAN, M., WAJID, M., SHIMOMURA, Y., PETUKHOVA, L. & CHRISTIANO, A. M. 2012a. Whole-exome sequencing in a single proband reveals a mutation in the CHST8 gene in autosomal recessive peeling skin syndrome. *Genomics,* 99**,** 202-8.

CABRAL, R. M., LIU, L., HOGAN, C., DOPPING-HEPENSTAL, P. J., WINIK, B. C., ASIAL, R. A., DOBSON, R., MEIN, C. A., BASELAGA, P. A., MELLERIO, J. E., NANDA, A., BOENTE MDEL, C., KELSELL, D. P., MCGRATH, J. A. & SOUTH, A. P. 2010a. Homozygous mutations in the 5' region of the JUP gene result in cutaneous disease but normal heart development in children. *J Invest Dermatol,* 130**,** 1543-50.

CABRAL, R. M., TATTERSALL, D., PATEL, V., MCPHAIL, G. D., HATZIMASOURA, E., ABRAMS, D. J., SOUTH, A. P. & KELSELL, D. P. 2012b. The DSPII splice variant is crucial for desmosome-mediated adhesion in HaCaT keratinocytes. *J Cell Sci,* 125**,** 2853-61.

CABRAL, R. M., WAN, H., COLE, C. L., ABRAMS, D. J., KELSELL, D. P. & SOUTH, A. P. 2010b. Identification and characterization of DSPIa, a novel isoform of human desmoplakin. *Cell Tissue Res,* 341**,** 121-9.

CALKINS, C. C., SETZER, S. V., JENNINGS, J. M., SUMMERS, S., TSUNODA, K., AMAGAI, M. & KOWALCZYK, A. P. 2006. Desmoglein endocytosis and desmosome disassembly are coordinated responses to pemphigus autoantibodies. *J Biol Chem,* 281**,** 7623-34.

CARRAGHER, N. O. & FRAME, M. C. 2004. Focal adhesion and actin dynamics: a place where kinases and proteases meet to promote invasion. *Trends Cell Biol,* 14**,** 241-9.

CASPAR, D. L., GOODENOUGH, D. A., MAKOWSKI, L. & PHILLIPS, W. C. 1977. Gap junction structures. I. Correlated electron microscopy and x-ray diffraction. *J Cell Biol,* 74**,** 605-28.

CASSIDY, A. J., VAN STEENSEL, M. A., STEIJLEN, P. M., VAN GEEL, M., VAN DER VELDEN, J., MORLEY, S. M., TERRINONI, A., MELINO, G., CANDI, E. & MCLEAN, W. H. 2005. A homozygous missense mutation in TGM5 abolishes epidermal transglutaminase 5 activity and causes acral peeling skin syndrome. *Am J Hum Genet,* 77**,** 909-17.

CHALABREYSSE, L., SENNI, F., BRUYERE, P., AIME, B., OLLAGNIER, C., BOZIO, A. & BOUVAGNET, P. 2011. A new hypo/oligodontia syndrome: Carvajal/Naxos syndrome secondary to desmoplakin-dominant mutations. *J Dent Res,* 90**,** 58-64.

CHAN, K. T., BENNIN, D. A. & HUTTENLOCHER, A. 2010. Regulation of adhesion dynamics by calpain-mediated proteolysis of focal adhesion kinase (FAK). *J Biol Chem,* 285**,** 11418-26.

CHAN, Y. M., YU, Q. C., FINE, J. D. & FUCHS, E. 1993. The genetic basis of Weber-Cockayne epidermolysis bullosa simplex. *Proc Natl Acad Sci U S A,* 90**,** 7414-8.

CHARPENTIER, E., LAVKER, R. M., ACQUISTA, E. & COWIN, P. 2000. Plakoglobin suppresses epithelial proliferation and hair growth *in vivo*. *J Cell Biol,* 149**,** 503-20.

CHAVANAS, S., BODEMER, C., ROCHAT, A., HAMEL-TEILLAC, D., ALI, M., IRVINE, A. D., BONAFE, J. L., WILKINSON, J., TAIEB, A., BARRANDON, Y., HARPER, J. I., DE PROST, Y. & HOVNANIAN, A. 2000. Mutations in SPINK5, encoding a serine protease inhibitor, cause Netherton syndrome. *Nat Genet,* 25**,** 141-2.

CHEN, M. A., BONIFAS, J. M., MATSUMURA, K., BLUMENFELD, A. & EPSTEIN, E. H., JR. 1993. A novel three-nucleotide deletion in the helix 2B region of keratin 14 in epidermolysis bullosa simplex: delta E375. *Hum Mol Genet,* 2**,** 1971-2.

CHEN, X., BONNE, S., HATZFELD, M., VAN ROY, F. & GREEN, K. J. 2002. Protein binding and functional characterization of plakophilin 2. Evidence for its diverse roles in desmosomes and beta -catenin signaling. *J Biol Chem,* 277**,** 10512-22.

CHEN, Y. J., CHANG, J. T., LEE, L., WANG, H. M., LIAO, C. T., CHIU, C. C., CHEN, P. J. & CHENG, A. J. 2007. DSG3 is overexpressed in head neck cancer and is a potential molecular target for inhibition of oncogenesis. *Oncogene,* 26**,** 467-76.

CHEN, Y. J., LEE, L. Y., CHAO, Y. K., CHANG, J. T., LU, Y. C., LI, H. F., CHIU, C. C., LI, Y. C., LI, Y. L., CHIOU, J. F. & CHENG, A. J. 2013. DSG3 facilitates cancer cell growth and invasion through the DSG3-plakoglobin-TCF/LEF-Myc/cyclin D1/MMP signaling pathway. *PLoS One,* 8**,** e64088.

CHERNYAVSKY, A. I., ARREDONDO, J., KITAJIMA, Y., SATO-NAGAI, M. & GRANDO, S. A. 2007. Desmoglein versus non-desmoglein signaling in pemphigus acantholysis: characterization of novel signaling pathways downstream of pemphigus vulgaris antigens. *J Biol Chem,* 282**,** 13804-12.

CHIDGEY, M., BRAKEBUSCH, C., GUSTAFSSON, E., CRUCHLEY, A., HAIL, C., KIRK, S., MERRITT, A., NORTH, A., TSELEPIS, C., HEWITT, J., BYRNE, C., FASSLER, R. & GARROD, D. 2001. Mice lacking desmocollin 1 show epidermal fragility accompanied by barrier defects and abnormal differentiation. *J Cell Biol,* 155**,** 821-32.

CHOI, H. J., GROSS, J. C., POKUTTA, S. & WEIS, W. I. 2009. Interactions of plakoglobin and beta-catenin with desmosomal cadherins: basis of selective exclusion of alpha- and beta-catenin from desmosomes. *J Biol Chem,* 284**,** 31776-88.

CHOI, H. J., PARK-SNYDER, S., PASCOE, L. T., GREEN, K. J. & WEIS, W. I. 2002. Structures of two intermediate filament-binding fragments of desmoplakin reveal a unique repeat motif structure. *Nat Struct Biol,* 9**,** 612-20.

CHOI, H. J. & WEIS, W. I. 2005. Structure of the armadillo repeat domain of plakophilin 1. *J Mol Biol,* 346**,** 367-76.

CHRISTIANO, A. M. & UITTO, J. 1994. Molecular pathology of the elastic fibers. *J Invest Dermatol,* 103**,** 53S-57S.

CIRILLO, N. & AL-JANDAN, B. A. 2013. Desmosomal adhesion and pemphigus vulgaris: the first half of the story. *Cell Commun Adhes,* 20**,** 1-10.

CIRILLO, N., LANZA, A. & PRIME, S. S. 2010. Induction of hyper-adhesion attenuates autoimmune-induced keratinocyte cell-cell detachment and processing of adhesion molecules via mechanisms that involve PKC. *Exp Cell Res,* 316**,** 580-92.

CITI, S. & CORDENONSI, M. 1998. Tight junction proteins. *Biochim Biophys Acta,* 1448**,** 1-11.

COLLINS, J. E., LEGAN, P. K., KENNY, T. P., MACGARVIE, J., HOLTON, J. L. & GARROD, D. R. 1991. Cloning and sequence analysis of desmosomal glycoproteins 2 and 3 (desmocollins): cadherin-like desmosomal adhesion molecules with heterogeneous cytoplasmic domains. *J Cell Biol,* 113**,** 381-91.

CONACCI-SORRELL, M., ZHURINSKY, J. & BEN-ZE'EV, A. 2002. The cadherin-catenin adhesion system in signaling and cancer. *J Clin Invest,* 109**,** 987-91.

COONROD, E. M., DURTSCHI, J. D., VANSANT WEBB, C., VOELKERDING, K. V. & KUMANOVICS, A. 2014. Next-generation sequencing of custom amplicons to improve coverage of HaloPlex multigene panels. *Biotechniques,* 57**,** 204-7.

CORRADO, D., MIGLIORE, F., BASSO, C. & THIENE, G. 2006a. Exercise and the risk of sudden cardiac death. *Herz,* 31**,** 553-8.

CORRADO, D., THIENE, G., NAVA, A., ROSSI, L. & PENNELLI, N. 1990. Sudden death in young competitive athletes: clinicopathologic correlations in 22 cases. *Am J Med,* 89**,** 588-96.

CORRADO, E., MILIO, G. & NOVO, S. 2006b. Response to letter by Drs. Mohammed Abbas, Maria Sessa, and Francesco Corea. *Arch Med Res,* 37**,** 810-1.

COTTIN, P., BRUSTIS, J. J., POUSSARD, S., ELAMRANI, N., BRONCARD, S. & DUCASTAING, A. 1994. Ca(2+)-dependent proteinases (calpains) and muscle cell differentiation. *Biochim Biophys Acta,* 1223**,** 170-8.

COX, M. G., VAN DER ZWAAG, P. A., VAN DER WERF, C., VAN DER SMAGT, J. J., NOORMAN, M., BHUIYAN, Z. A., WIESFELD, A. C., VOLDERS, P. G., VAN LANGEN, I. M., ATSMA, D. E., DOOIJES, D., VAN DEN WIJNGAARD, A., HOUWELING, A. C., JONGBLOED, J. D., JORDAENS, L., CRAMER, M. J., DOEVENDANS, P. A., DE BAKKER, J. M., WILDE, A. A., VAN TINTELEN, J. P. & HAUER, R. N. 2011. Arrhythmogenic right ventricular dysplasia/cardiomyopathy: pathogenic desmosome mutations in index-patients predict outcome of family screening: Dutch arrhythmogenic right ventricular dysplasia/cardiomyopathy genotype-phenotype follow-up study. *Circulation,* 123**,** 2690-700.

CROUCH, D. H., FINCHAM, V. J. & FRAME, M. C. 1996. Targeted proteolysis of the focal adhesion kinase pp125 FAK during c-MYC-induced apoptosis is suppressed by integrin signalling. *Oncogene,* 12**,** 2689-96.

D'ALESSIO, M., FORTUGNO, P., ZAMBRUNO, G. & HOVNANIAN, A. 2013. Netherton syndrome and its multifaceted defective protein LEKTI. *G Ital Dermatol Venereol,* 148**,** 37-51.

DALAL, D., JAMES, C., DEVANAGONDI, R., TICHNELL, C., TUCKER, A., PRAKASA, K., SPEVAK, P. J., BLUEMKE, D. A., ABRAHAM, T., RUSSELL, S. D., CALKINS, H. & JUDGE, D. P. 2006. Penetrance of mutations in plakophilin-2 among families with arrhythmogenic right ventricular dysplasia/cardiomyopathy. *J Am Coll Cardiol,* 48**,** 1416-24.

DAVIES, M. E. & BARRETT, A. J. 1984. Immunolocalization of human cystatins in neutrophils and lymphocytes. *Histochemistry,* 80**,** 373-7.

DEDIEU, S., POUSSARD, S., MAZERES, G., GRISE, F., DARGELOS, E., COTTIN, P. & BRUSTIS, J. J. 2004. Myoblast migration is regulated by calpain through its involvement in cell attachment and cytoskeletal organization. *Exp Cell Res,* 292**,** 187-200.

DELA CADENA, R. A. & COLMAN, R. W. 1991. Structure and functions of human kininogens. *Trends Pharmacol Sci,* 12**,** 272-5.

DELMAR, M. & MCKENNA, W. J. 2010. The cardiac desmosome and arrhythmogenic cardiomyopathies: from gene to disease. *Circ Res,* 107**,** 700-14.

DELVA, E., JENNINGS, J. M., CALKINS, C. C., KOTTKE, M. D., FAUNDEZ, V. & KOWALCZYK, A. P. 2008. Pemphigus vulgaris IgG-induced desmoglein-3 endocytosis and desmosomal disassembly are mediated by a clathrin- and dynamin-independent mechanism. *J Biol Chem,* 283**,** 18303-13.

DELVA, E., TUCKER, D. K. & KOWALCZYK, A. P. 2009. The desmosome. *Cold Spring Harb Perspect Biol,* 1**,** a002543.

DERAISON, C., BONNART, C., LOPEZ, F., BESSON, C., ROBINSON, R., JAYAKUMAR, A., WAGBERG, F., BRATTSAND, M., HACHEM, J. P., LEONARDSSON, G. & HOVNANIAN, A. 2007. LEKTI fragments specifically inhibit KLK5, KLK7, and KLK14 and control desquamation through a pH-dependent interaction. *Mol Biol Cell,* 18**,** 3607-19.

DESAI, B. V., HARMON, R. M. & GREEN, K. J. 2009. Desmosomes at a glance. *J Cell Sci,* 122**,** 4401-7.

DIMAS, A. S., STRANGER, B. E., BEAZLEY, C., FINN, R. D., INGLE, C. E., FORREST, M. S., RITCHIE, M. E., DELOUKAS, P., TAVARE, S. & DERMITZAKIS, E. T. 2008. Modifier effects between regulatory and protein-coding variation. *PLoS Genet,* 4**,** e1000244.

DING, X., AOKI, V., MASCARO, J. M., JR., LOPEZ-SWIDERSKI, A., DIAZ, L. A. & FAIRLEY, J. A. 1997. Mucosal and mucocutaneous (generalized) pemphigus vulgaris show distinct autoantibody profiles. *J Invest Dermatol,* 109**,** 592-6.

DUSEK, R. L. & ATTARDI, L. D. 2011. Desmosomes: new perpetrators in tumour suppression. *Nat Rev Cancer,* 11**,** 317-23.

EGBERTS, F., HEINRICH, M., JENSEN, J. M., WINOTO-MORBACH, S., PFEIFFER, S., WICKEL, M., SCHUNCK, M., STEUDE, J., SAFTIG, P., PROKSCH, E. & SCHUTZE, S. 2004. Cathepsin D is involved in the regulation of transglutaminase 1 and epidermal differentiation. *J Cell Sci,* 117**,** 2295-307.

ELLIS, A., FIELD, J. K., FIELD, E. A., FRIEDMANN, P. S., FRYER, A., HOWARD, P., LEIGH, I. M., RISK, J., SHAW, J. M. & WHITTAKER, J. 1994. Tylosis associated with carcinoma of the oesophagus and oral leukoplakia in a large Liverpool family--a review of six generations. *Eur J Cancer B Oral Oncol,* 30B**,** 102-12.

ERKEN, H., YARIZ, K. O., DUMAN, D., KAYA, C. T., SAYIN, T., HEPER, A. O. & TEKIN, M. 2011. Cardiomyopathy with alopecia and palmoplantar keratoderma (CAPK) is caused by a JUP mutation. *Br J Dermatol,* 165**,** 917-21.

ERSOY-EVANS, S., ERKIN, G., FASSIHI, H., CHAN, I., PALLER, A. S., SURUCU, S. & MCGRATH, J. A. 2006. Ectodermal dysplasia-skin fragility syndrome resulting from a new homozygous mutation, 888delC, in the desmosomal protein plakophilin 1. *J Am Acad Dermatol,* 55**,** 157-61.

FARQUHAR, M. G. & PALADE, G. E. 1963. Junctional complexes in various epithelia. *J Cell Biol,* 17**,** 375-412.

FIDLER, L. M., WILSON, G. J., LIU, F., CUI, X., SCHERER, S. W., TAYLOR, G. P. & HAMILTON, R. M. 2009. Abnormal connexin43 in arrhythmogenic right ventricular cardiomyopathy caused by plakophilin-2 mutations. *J Cell Mol Med,* 13**,** 4219-28.

FRANCO, S. J., RODGERS, M. A., PERRIN, B. J., HAN, J., BENNIN, D. A., CRITCHLEY, D. R. & HUTTENLOCHER, A. 2004. Calpain-mediated proteolysis of talin regulates adhesion dynamics. *Nat Cell Biol,* 6**,** 977-83.

FRANKE, W. W., BORRMANN, C. M., GRUND, C. & PIEPERHOFF, S. 2006. The area composita of adhering junctions connecting heart muscle cells of vertebrates. I. Molecular definition in intercalated disks of cardiomyocytes by immunoelectron microscopy of desmosomal proteins. *Eur J Cell Biol,* 85**,** 69-82.

FRANKE, W. W., SCHUMACHER, H., BORRMANN, C. M., GRUND, C., WINTER-SIMANOWSKI, S., SCHLECHTER, T., PIEPERHOFF, S. & HOFMANN, I. 2007. The area composita of adhering junctions connecting heart muscle cells of vertebrates - III: assembly and disintegration of intercalated disks in rat cardiomyocytes growing in culture. *Eur J Cell Biol,* 86**,** 127-42.

FUCHS, E. 1990. Epidermal differentiation: the bare essentials. *J Cell Biol,* 111**,** 2807-14.

FUCHS, E. 2007. Scratching the surface of skin development. *Nature,* 445**,** 834-42.

FURUKAWA, C., DAIGO, Y., ISHIKAWA, N., KATO, T., ITO, T., TSUCHIYA, E., SONE, S. & NAKAMURA, Y. 2005. Plakophilin 3 oncogene as prognostic marker and therapeutic target for lung cancer. *Cancer Res,* 65**,** 7102-10.

FUTEI, Y., AMAGAI, M., HASHIMOTO, T. & NISHIKAWA, T. 2003. Conformational epitope mapping and IgG subclass distribution of desmoglein 3 in paraneoplastic pemphigus. *J Am Acad Dermatol,* 49**,** 1023-8.

GABRIJELCIC, D., SVETIC, B., SPAIC, D., SKRK, J., BUDIHNA, M., DOLENC, I., POPOVIC, T., COTIC, V. & TURK, V. 1992. Cathepsins B, H and L in human breast carcinoma. *Eur J Clin Chem Clin Biochem,* 30**,** 69-74.

GALLICANO, G. I., BAUER, C. & FUCHS, E. 2001. Rescuing desmoplakin function in extra-embryonic ectoderm reveals the importance of this protein in embryonic heart, neuroepithelium, skin and vasculature. *Development,* 128**,** 929-41.

GALLICANO, G. I., KOUKLIS, P., BAUER, C., YIN, M., VASIOUKHIN, V., DEGENSTEIN, L. & FUCHS, E. 1998. Desmoplakin is required early in development for assembly of desmosomes and cytoskeletal linkage. *J Cell Biol,* 143**,** 2009-22.

GARROD, D. R., BERIKA, M. Y., BARDSLEY, W. F., HOLMES, D. & TABERNERO, L. 2005. Hyper-adhesion in desmosomes: its regulation in wound healing and possible relationship to cadherin crystal structure. *J Cell Sci,* 118**,** 5743-54.

GARROD, D. R., MERRITT, A. J. & NIE, Z. 2002. Desmosomal cadherins. *Curr Opin Cell Biol,* 14**,** 537-45.

GERULL, B., HEUSER, A., WICHTER, T., PAUL, M., BASSON, C. T., MCDERMOTT, D. A., LERMAN, B. B., MARKOWITZ, S. M., ELLINOR, P. T., MACRAE, C. A., PETERS, S., GROSSMANN, K. S., DRENCKHAHN, J., MICHELY, B., SASSE-KLAASSEN, S., BIRCHMEIER, W., DIETZ, R., BREITHARDT, G., SCHULZE-BAHR, E. & THIERFELDER, L. 2004. Mutations in the desmosomal protein plakophilin-2 are common in arrhythmogenic right ventricular cardiomyopathy. *Nat Genet,* 36**,** 1162-4.

GETSIOS, S., HUEN, A. C. & GREEN, K. J. 2004. Working out the strength and flexibility of desmosomes. *Nat Rev Mol Cell Biol,* 5**,** 271-81.

GODSEL, L. M., DUBASH, A. D., BASS-ZUBEK, A. E., AMARGO, E. V., KLESSNER, J. L., HOBBS, R. P., CHEN, X. & GREEN, K. J. 2010. Plakophilin 2 couples actomyosin remodeling to desmosomal plaque assembly via RhoA. *Mol Biol Cell,* 21**,** 2844-59.

GODSEL, L. M., HSIEH, S. N., AMARGO, E. V., BASS, A. E., PASCOE-MCGILLICUDDY, L. T., HUEN, A. C., THORNE, M. E., GAUDRY, C. A., PARK, J. K., MYUNG, K., GOLDMAN, R. D., CHEW, T. L. & GREEN, K. J. 2005. Desmoplakin assembly dynamics in four dimensions: multiple phases differentially regulated by intermediate filaments and actin. *J Cell Biol,* 171**,** 1045-59.

GOLDBACH-MANSKY, R., LEE, J., MCCOY, A., HOXWORTH, J., YARBORO, C., SMOLEN, J. S., STEINER, G., ROSEN, A., ZHANG, C., MENARD, H. A., ZHOU, Z. J., PALOSUO, T., VAN VENROOIJ, W. J., WILDER, R. L., KLIPPEL, J. H., SCHUMACHER, H. R., JR. & EL-GABALAWY, H. S. 2000. Rheumatoid arthritis associated autoantibodies in patients with synovitis of recent onset. *Arthritis Res,* 2**,** 236-43.

GOLDBERG, G. S., VALIUNAS, V. & BRINK, P. R. 2004. Selective permeability of gap junction channels. *Biochim Biophys Acta,* 1662**,** 96-101.

GOLL, D. E., THOMPSON, V. F., LI, H., WEI, W. & CONG, J. 2003. The calpain system. *Physiol Rev,* 83**,** 731-801.

GREEN, A., GREEN, H., REHNBERG, M., SVENSSON, A., GUNNARSSON, C. & JONASSON, J. 2014. Assessment of HaloPlex Amplification for Sequence Capture and Massively Parallel Sequencing of Arrhythmogenic Right Ventricular Cardiomyopathy-Associated Genes. *J Mol Diagn*.

GREEN, K. J. & GAUDRY, C. A. 2000. Are desmosomes more than tethers for intermediate filaments? *Nat Rev Mol Cell Biol,* 1**,** 208-16.

GREEN, K. J., GETSIOS, S., TROYANOVSKY, S. & GODSEL, L. M. 2010. Intercellular junction assembly, dynamics, and homeostasis. *Cold Spring Harb Perspect Biol,* 2**,** a000125.

GROSSMANN, K. S., GRUND, C., HUELSKEN, J., BEHREND, M., ERDMANN, B., FRANKE, W. W. & BIRCHMEIER, W. 2004. Requirement of plakophilin 2 for heart morphogenesis and cardiac junction formation. *J Cell Biol,* 167**,** 149-60.

GUPTA, A., NITOIU, D., BRENNAN-CRISPI, D., ADDYA, S., RIOBO, N.A., KELSELL, D.P. & MAHONEY, M.G. 2015. Cell cycle- and cancer-associated gene networks activated by dsg2: evidence of cystatin a deregulation and a potential role in cell-cell adhesion. *PLoS One*, 10, e0120091.

HABER, R. M. & ROSE, T. H. 1986. Autosomal recessive pachyonychia congenita. *Arch Dermatol,* 122**,** 919-23.

HAKIMELAHI, S., PARKER, H. R., GILCHRIST, A. J., BARRY, M., LI, Z., BLEACKLEY, R. C. & PASDAR, M. 2000. Plakoglobin regulates the expression of the anti-apoptotic protein BCL-2. *J Biol Chem,* 275**,** 10905-11.

HALPER, J. & KJAER, M. 2014. Basic components of connective tissues and extracellular matrix: elastin, fibrillin, fibulins, fibrinogen, fibronectin, laminin, tenascins and thrombospondins. *Adv Exp Med Biol,* 802**,** 31-47.

HANAKAWA, Y., SELWOOD, T., WOO, D., LIN, C., SCHECHTER, N. M. & STANLEY, J. R. 2003. Calcium-dependent conformation of desmoglein 1 is required for its cleavage by exfoliative toxin. *J Invest Dermatol,* 121**,** 383-9.

HANNA, R. A., CAMPBELL, R. L. & DAVIES, P. L. 2008. Calcium-bound structure of calpain and its mechanism of inhibition by calpastatin. *Nature,* 456**,** 409-12.

HASHIMOTO, K., HAMZAVI, I., TANAKA, K. & SHWAYDER, T. 2000. Acral peeling skin syndrome. *J Am Acad Dermatol,* 43**,** 1112-9.

HATSELL, S. J., STEVENS, H., JACKSON, A. P., KELSELL, D. P. & ZVULUNOV, A. 2003. An autosomal recessive exfoliative ichthyosis with linkage to chromosome 12q13. *Br J Dermatol,* 149**,** 174-80.

HATZFELD, M. 2005. The p120 family of cell adhesion molecules. *Eur J Cell Biol,* 84**,** 205-14.

HATZFELD, M. 2007. Plakophilins: Multifunctional proteins or just regulators of desmosomal adhesion? *Biochim Biophys Acta,* 1773**,** 69-77.

HATZFELD, M., HAFFNER, C., SCHULZE, K. & VINZENS, U. 2000. The function of plakophilin 1 in desmosome assembly and actin filament organization. *J Cell Biol,* 149**,** 209-22.

HEID, H. W., SCHMIDT, A., ZIMBELMANN, R., SCHAFER, S., WINTER-SIMANOWSKI, S., STUMPP, S., KEITH, M., FIGGE, U., SCHNOLZER, M. & FRANKE, W. W. 1994. Cell type-specific desmosomal plaque proteins of the plakoglobin family: plakophilin 1 (band 6 protein). *Differentiation,* 58**,** 113-31.

HENNIES, H. C., HAGEDORN, M. & REIS, A. 1995. Palmoplantar keratoderma in association with carcinoma of the esophagus maps to chromosome 17q distal to the keratin gene cluster. *Genomics,* 29**,** 537-40.

HERNANDEZ-MARTIN, A., TORRELO, A., CIRIA, S., COLMENERO, I., AGUILAR, A., GRIMALT, R. & GONZALEZ-SARMIENTO, R. 2013. Ectodermal dysplasia-skin fragility syndrome: a novel mutation in the PKP1 gene. *Clin Exp Dermatol,* 38**,** 787-90.

HERRON, B. J., RAO, C., LIU, S., LAPRADE, L., RICHARDSON, J. A., OLIVIERI, E., SEMSARIAN, C., MILLAR, S. E., STUBBS, L. & BEIER, D. R. 2005. A mutation in NFkB interacting protein 1 results in cardiomyopathy and abnormal skin development in wa3 mice. *Hum Mol Genet,* 14**,** 667-77.

HEUSER, A., PLOVIE, E. R., ELLINOR, P. T., GROSSMANN, K. S., SHIN, J. T., WICHTER, T., BASSON, C. T., LERMAN, B. B., SASSE-KLAASSEN, S., THIERFELDER, L., MACRAE, C. A. & GERULL, B. 2006. Mutant desmocollin-2 causes arrhythmogenic right ventricular cardiomyopathy. *Am J Hum Genet,* 79**,** 1081-8.

HOFMANN, I., MERTENS, C., BRETTEL, M., NIMMRICH, V., SCHNOLZER, M. & HERRMANN, H. 2000. Interaction of plakophilins with desmoplakin and intermediate filament proteins: an *in vitro* analysis. *J Cell Sci,* 113 (Pt 13)**,** 2471-83.

HOFMANN, I., SCHLECHTER, T., KUHN, C., HERGT, M. & FRANKE, W. W. 2009. Protein p0071 - an armadillo plaque protein that characterizes a specific subtype of adherens junctions. *J Cell Sci,* 122**,** 21-4.

HOLTHOFER, B., WINDOFFER, R., TROYANOVSKY, S. & LEUBE, R. E. 2007. Structure and function of desmosomes. *Int Rev Cytol,* 264**,** 65-163.

HOUBEN, C. H., CHU, W., CHEUNG, G., LEE, K. & YEUNG, C. 2008. Antenatal ovarian torsion: a "free-floating" cyst. *Ultraschall Med,* 29**,** 311-3.

HOUBEN, E., DE PAEPE, K. & ROGIERS, V. 2007. A keratinocyte's course of life. *Skin Pharmacol Physiol,* 20**,** 122-32.

HOVNANIAN, A. 2013. Netherton syndrome: skin inflammation and allergy by loss of protease inhibition. *Cell Tissue Res,* 351**,** 289-300.

HSU, C. Y., HENRY, J., RAYMOND, A. A., MECHIN, M. C., PENDARIES, V., NASSAR, D., HANSMANN, B., BALICA, S., BURLET-SCHILTZ, O., SCHMITT, A. M., TAKAHARA, H., PAUL, C., SERRE, G. & SIMON, M. 2011. Deimination of human filaggrin-2 promotes its proteolysis by calpain 1. *J Biol Chem,* 286**,** 23222-33.

HU, P., BERKOWITZ, P., MADDEN, V. J. & RUBENSTEIN, D. S. 2006. Stabilization of plakoglobin and enhanced keratinocyte cell-cell adhesion by intracellular O-glycosylation. *J Biol Chem,* 281**,** 12786-91.

HUEN, A. C., PARK, J. K., GODSEL, L. M., CHEN, X., BANNON, L. J., AMARGO, E. V., HUDSON, T. Y., MONGIU, A. K., LEIGH, I. M., KELSELL, D. P., GUMBINER, B. M. & GREEN, K. J. 2002. Intermediate filament-membrane attachments function synergistically with actin-dependent contacts to regulate intercellular adhesive strength. *J Cell Biol,* 159**,** 1005-17.

IHRIE, R. A., MARQUES, M. R., NGUYEN, B. T., HORNER, J. S., PAPAZOGLU, C., BRONSON, R. T., MILLS, A. A. & ATTARDI, L. D. 2005. Perp is a p63-regulated gene essential for epithelial integrity. *Cell,* 120**,** 843-56.

INOUE, A., YAMAZAKI, M., ISHIDOH, K. & OGAWA, H. 2004. Epidermal growth factor activates m-calpain, resulting in apoptosis of HaCaT keratinocytes. *J Dermatol Sci,* 36**,** 60-2.

ISHIDA-YAMAMOTO, A., IGAWA, S. & KISHIBE, M. 2011. Order and disorder in corneocyte adhesion. *J Dermatol,* 38**,** 645-54.

ISHII, K., AMAGAI, M., HALL, R. P., HASHIMOTO, T., TAKAYANAGI, A., GAMOU, S., SHIMIZU, N. & NISHIKAWA, T. 1997. Characterization of autoantibodies in pemphigus using antigen-specific enzyme-linked immunosorbent assays with baculovirus-expressed recombinant desmogleins. *J Immunol,* 159**,** 2010-7.

IWATSUKI, K., TAKIGAWA, M., IMAIZUMI, S. & YAMADA, M. 1989. *In vivo* binding site of pemphigus vulgaris antibodies and their fate during acantholysis. *J Am Acad Dermatol,* 20**,** 578-82.

JAHODA, C. A., KLJUIC, A., O'SHAUGHNESSY, R., CROSSLEY, N., WHITEHOUSE, C. J., ROBINSON, M., REYNOLDS, A. J., DEMARCHEZ, M., PORTER, R. M., SHAPIRO, L. & CHRISTIANO, A. M. 2004. The lanceolate hair rat phenotype results from a missense mutation in a calcium coordinating site of the desmoglein 4 gene. *Genomics,* 83**,** 747-56.

JANICKE, R. U., NG, P., SPRENGART, M. L. & PORTER, A. G. 1998. Caspase-3 is required for alpha-fodrin cleavage but dispensable for cleavage of other death substrates in apoptosis. *J Biol Chem,* 273**,** 15540-5.

JARVINEN, M. & HOPSU-HAVU, V. K. 1975. Alpha-N-benzoylarginine-2-naphthylamide hydrolase (cathepsin B1?) from rat skin. I. Preliminary experiments with skin extract. *Acta Chem Scand B,* 29**,** 671-6.

JENKO, S., DOLENC, I., GUNCAR, G., DOBERSEK, A., PODOBNIK, M. & TURK, D. 2003. Crystal structure of Stefin A in complex with cathepsin H: N-terminal residues of inhibitors can adapt to the active sites of endo- and exopeptidases. *J Mol Biol,* 326**,** 875-85.

JONKMAN, M. F., PASMOOIJ, A. M., PASMANS, S. G., VAN DEN BERG, M. P., TER HORST, H. J., TIMMER, A. & PAS, H. H. 2005. Loss of desmoplakin tail causes lethal acantholytic epidermolysis bullosa. *Am J Hum Genet,* 77**,** 653-60.

JOSHI-MUKHERJEE, R., COOMBS, W., MUSA, H., OXFORD, E., TAFFET, S. & DELMAR, M. 2008. Characterization of the molecular phenotype of two arrhythmogenic right ventricular cardiomyopathy (ARVC)-related plakophilin-2 (PKP2) mutations. *Heart Rhythm,* 5**,** 1715-23.

KAMATA, Y., TANIGUCHI, A., YAMAMOTO, M., NOMURA, J., ISHIHARA, K., TAKAHARA, H., HIBINO, T. & TAKEDA, A. 2009. Neutral cysteine protease bleomycin hydrolase is essential for the breakdown of deiminated filaggrin into amino acids. *J Biol Chem,* 284**,** 12829-36.

KANNANKERIL, P. J., BHUIYAN, Z. A., DARBAR, D., MANNENS, M. M., WILDE, A. A. & RODEN, D. M. 2006. Arrhythmogenic right ventricular cardiomyopathy due to a novel plakophilin 2 mutation: wide spectrum of disease in mutation carriers within a family. *Heart Rhythm,* 3**,** 939-44.

KAPPRELL, H. P., OWARIBE, K. & FRANKE, W. W. 1988. Identification of a basic protein of Mr 75,000 as an accessory desmosomal plaque protein in stratified and complex epithelia. *J Cell Biol,* 106**,** 1679-91.

KATO, T., TAKAI, T., MITSUISHI, K., OKUMURA, K. & OGAWA, H. 2005. Cystatin A inhibits IL-8 production by keratinocytes stimulated with Der p 1 and Der f 1: biochemical skin barrier against mite cysteine proteases. *J Allergy Clin Immunol,* 116**,** 169-76.

KAWASAKI, H., EMORI, Y. & SUZUKI, K. 1993. Calpastatin has two distinct sites for interaction with calpain--effect of calpastatin fragments on the binding of calpain to membranes. *Arch Biochem Biophys,* 305**,** 467-72.

KELLY, D. E. 1966. Fine structure of desmosomes. , hemidesmosomes, and an adepidermal globular layer in developing newt epidermis. *J Cell Biol,* 28**,** 51-72.

KEPPLER, D. & SIERRA, F. 2005. Role of cystatins in tumor neovascularization. *Future Oncol,* 1**,** 661-72.

KIELTY, C. M. & SHUTTLEWORTH, C. A. 1997. Microfibrillar elements of the dermal matrix. *Microsc Res Tech,* 38**,** 413-27.

KIMURA, T. E., MERRITT, A. J. & GARROD, D. R. 2007. Calcium-independent desmosomes of keratinocytes are hyper-adhesive. *J Invest Dermatol,* 127**,** 775-81.

KING, I. A., SULLIVAN, K. H., BENNETT, R., JR. & BUXTON, R. S. 1995. The desmocollins of human foreskin epidermis: identification and chromosomal assignment of a third gene and expression patterns of the three isoforms. *J Invest Dermatol,* 105**,** 314-21.

KITAJIMA, Y. 2013. New insights into desmosome regulation and pemphigus blistering as a desmosome-remodeling disease. *Kaohsiung J Med Sci,* 29**,** 1-13.

KLAUKE, B., KOSSMANN, S., GAERTNER, A., BRAND, K., STORK, I., BRODEHL, A., DIEDING, M., WALHORN, V., ANSELMETTI, D., GERDES, D., BOHMS, B., SCHULZ, U., ZU KNYPHAUSEN, E., VORGERD, M., GUMMERT, J. & MILTING, H. 2010. De novo desmin-mutation N116S is associated with arrhythmogenic right ventricular cardiomyopathy. *Hum Mol Genet,* 19**,** 4595-607.

KLJUIC, A., BAUER, R. C. & CHRISTIANO, A. M. 2004. Genomic organization of mouse desmocollin genes reveals evolutionary conservation. *DNA Seq,* 15**,** 148-52.

KLJUIC, A., BAZZI, H., SUNDBERG, J. P., MARTINEZ-MIR, A., O'SHAUGHNESSY, R., MAHONEY, M. G., LEVY, M., MONTAGUTELLI, X., AHMAD, W., AITA, V. M., GORDON, D., UITTO, J., WHITING, D., OTT, J., FISCHER, S., GILLIAM, T. C., JAHODA, C. A., MORRIS, R. J., PANTELEYEV, A. A., NGUYEN, V. T. & CHRISTIANO, A. M. 2003a. Desmoglein 4 in hair follicle differentiation and epidermal adhesion: evidence from inherited hypotrichosis and acquired pemphigus vulgaris. *Cell,* 113**,** 249-60.

KLJUIC, A., GILEAD, L., MARTINEZ-MIR, A., FRANK, J., CHRISTIANO, A. M. & ZLOTOGORSKI, A. 2003b. A nonsense mutation in the desmoglein 1 gene underlies striate keratoderma. *Exp Dermatol,* 12**,** 523-7.

KO, M. S. & MARINKOVICH, M. P. 2010. Role of dermal-epidermal basement membrane zone in skin, cancer, and developmental disorders. *Dermatol Clin,* 28**,** 1-16.

KOCH, P. J., MAHONEY, M. G., ISHIKAWA, H., PULKKINEN, L., UITTO, J., SHULTZ, L., MURPHY, G. F., WHITAKER-MENEZES, D. & STANLEY, J. R. 1997. Targeted disruption of the pemphigus vulgaris antigen (desmoglein 3) gene in mice causes loss of keratinocyte cell adhesion with a phenotype similar to pemphigus vulgaris. *J Cell Biol,* 137**,** 1091-102.

KOS, J., MITROVIC, A. & MIRKOVIC, B. 2014. The current stage of cathepsin B inhibitors as potential anticancer agents. *Future Med Chem,* 6**,** 1355-71.

KOS, J., SMID, A., KRASOVEC, M., SVETIC, B., LENARCIC, B., VRHOVEC, I., SKRK, J. & TURK, V. 1995. Lysosomal proteases cathepsins D, B, H, L and their inhibitors stefins A and B in head and neck cancer. *Biol Chem Hoppe Seyler,* 376**,** 401-5.

KOTTKE, M. D., DELVA, E. & KOWALCZYK, A. P. 2006. The desmosome: cell science lessons from human diseases. *J Cell Sci,* 119**,** 797-806.

KOWALCZYK, A. P., HATZFELD, M., BORNSLAEGER, E. A., KOPP, D. S., BORGWARDT, J. E., CORCORAN, C. M., SETTLER, A. & GREEN, K. J. 1999. The head domain of plakophilin-1 binds to desmoplakin and enhances its recruitment to desmosomes. Implications for cutaneous disease. *J Biol Chem,* 274**,** 18145-8.

KOWALCZYK, A. P., STAPPENBECK, T. S., PARRY, D. A., PALKA, H. L., VIRATA, M. L., BORNSLAEGER, E. A., NILLES, L. A. & GREEN, K. J. 1994. Structure and function of desmosomal transmembrane core and plaque molecules. *Biophys Chem,* 50**,** 97-112.

KROGER, C., LOSCHKE, F., SCHWARZ, N., WINDOFFER, R., LEUBE, R. E. & MAGIN, T. M. 2013. Keratins control intercellular adhesion involving PKC-alpha-mediated desmoplakin phosphorylation. *J Cell Biol,* 201**,** 681-92.

KRUNIC, A. L., STONE, K. L., SIMPSON, M. A. & MCGRATH, J. A. 2013. Acral peeling skin syndrome resulting from a homozygous nonsense mutation in the CSTA gene encoding cystatin A. *Pediatr Dermatol,* 30**,** e87-8.

KUBO, A., SHIOHAMA, A., SASAKI, T., NAKABAYASHI, K., KAWASAKI, H., ATSUGI, T., SATO, S., SHIMIZU, A., MIKAMI, S., TANIZAKI, H., UCHIYAMA, M., MAEDA, T., ITO, T., SAKABE, J., HEIKE, T., OKUYAMA, T., KOSAKI, R., KOSAKI, K., KUDOH, J., HATA, K., UMEZAWA, A., TOKURA, Y., ISHIKO, A., NIIZEKI, H., KABASHIMA, K., MITSUHASHI, Y. & AMAGAI, M. 2013. Mutations in SERPINB7, encoding a member of the serine protease inhibitor superfamily, cause Nagashima-type palmoplantar keratosis. *Am J Hum Genet,* 93**,** 945-56.

KUOPIO, T., KANKAANRANTA, A., JALAVA, P., KRONQVIST, P., KOTKANSALO, T., WEBER, E. & COLLAN, Y. 1998. Cysteine proteinase inhibitor cystatin A in breast cancer. *Cancer Res,* 58**,** 432-6.

KURZEN, H., MOLL, I., MOLL, R., SCHAFER, S., SIMICS, E., AMAGAI, M., WHEELOCK, M. J. & FRANKE, W. W. 1998. Compositionally different desmosomes in the various compartments of the human hair follicle. *Differentiation,* 63**,** 295-304.

KURZEN, H., MUNZING, I. & HARTSCHUH, W. 2003. Expression of desmosomal proteins in squamous cell carcinomas of the skin. *J Cutan Pathol,* 30**,** 621-30.

LAH, T. T., KOKALJ-KUNOVAR, M., STRUKELJ, B., PUNGERCAR, J., BARLIC-MAGANJA, D., DROBNIC-KOSOROK, M., KASTELIC, L., BABNIK, J., GOLOUH, R. & TURK, V. 1992. Stefins and lysosomal cathepsins B, L and D in human breast carcinoma. *Int J Cancer,* 50**,** 36-44.

LAHTINEN, A. M., LEHTONEN, A., KAARTINEN, M., TOIVONEN, L., SWAN, H., WIDEN, E., LEHTONEN, E., LEHTO, V. P. & KONTULA, K. 2008. Plakophilin-2 missense mutations in arrhythmogenic right ventricular cardiomyopathy. *Int J Cardiol,* 126**,** 92-100.

LAI CHEONG, J. E., WESSAGOWIT, V. & MCGRATH, J. A. 2005. Molecular abnormalities of the desmosomal protein desmoplakin in human disease. *Clin Exp Dermatol,* 30**,** 261-6.

LEGAN, P. K., YUE, K. K., CHIDGEY, M. A., HOLTON, J. L., WILKINSON, R. W. & GARROD, D. R. 1994. The bovine desmocollin family: a new gene and expression patterns reflecting epithelial cell proliferation and differentiation. *J Cell Biol,* 126**,** 507-18.

LEINONEN, T., PIRINEN, R., BOHM, J., JOHANSSON, R., RINNE, A., WEBER, E. & KOSMA, V. M. 2007. Biological and prognostic role of acid cysteine proteinase inhibitor (ACPI, cystatin A) in non-small-cell lung cancer. *J Clin Pathol,* 60**,** 515-9.

LELOUP, L., MAZERES, G., DAURY, L., COTTIN, P. & BRUSTIS, J. J. 2006. Involvement of calpains in growth factor-mediated migration. *Int J Biochem Cell Biol,* 38**,** 2049-63.

LENARCIC, B., KRIZAJ, I., ZUNEC, P. & TURK, V. 1996. Differences in specificity for the interactions of stefins A, B and D with cysteine proteinases. *FEBS Lett,* 395**,** 113-8.

LETAVERNIER, E., DANSOU, B., LOCHNER, M., PEREZ, J., BELLOCQ, A., LINDENMEYER, M. T., COHEN, C. D., HAYMANN, J. P., EBERL, G. & BAUD, L. 2011. Critical role of the calpain/calpastatin balance in acute allograft rejection. *Eur J Immunol,* 41**,** 473-84.

LI, C., CHEN, L., WANG, J., ZHANG, L., TANG, P., ZHAI, S., GUO, W., YU, N., ZHAO, L., LIU, M. & YANG, S. 2011. Expression and clinical significance of cathepsin B and stefin A in laryngeal cancer. *Oncol Rep,* 26**,** 869-75.

LI, D., ZHANG, W., LIU, Y., HANELINE, L. S. & SHOU, W. 2012. Lack of plakoglobin in epidermis leads to keratoderma. *J Biol Chem,* 287**,** 10435-43.

LI, J. & RADICE, G. L. 2010. A new perspective on intercalated disc organization: implications for heart disease. *Dermatol Res Pract,* 2010**,** 207835.

LI, W., DING, F., ZHANG, L., LIU, Z., WU, Y., LUO, A., WU, M., WANG, M., ZHAN, Q. & LIU, Z. 2005. Overexpression of stefin A in human esophageal squamous cell carcinoma cells inhibits tumor cell growth, angiogenesis, invasion, and metastasis. *Clin Cancer Res,* 11**,** 8753-62.

LIN, T. K., CRUMRINE, D., ACKERMAN, L. D., SANTIAGO, J. L., ROELANDT, T., UCHIDA, Y., HUPE, M., FABRIAS, G., ABAD, J. L., RICE, R. H. & ELIAS, P. M. 2012. Cellular changes that accompany shedding of human corneocytes. *J Invest Dermatol,* 132**,** 2430-9.

LIN, Z., ZHAO, J., NITOIU, D., SCOTT, C. A., PLAGNOL, V., WILSON, N., COLE, C., SCHWARTZ, M., MCLEAN, I., SMITH, F., WANG, H., FENG, C., DUO, L., ZHOU, E. Y., REN, Y., DAI, L., CHEN, Y., ZHANG, J., XU, X., O'TOOLE, E. A., KELSELL, D. P. & YANG, Y. 2015. Loss-of-function mutations in CAST cause peeling skin, leukonychia, acral punctate keratoses, cheilitis and knuckle pads (PLACK) syndrome. *The American Journal of Human Genetics,* 96, 440-7.

LIU, Z. J., LI, H. F., TAN, G. H., TAO, Q. Q., NI, W., CHENG, X. W., XIONG, Z. Q. & WU, Z. Y. 2014. Identify mutation in amyotrophic lateral sclerosis cases using HaloPlex target enrichment system. *Neurobiol Aging,* 35**,** 2881 e11-5.

LOFFEK, S., BRUCKNER-TUDERMAN, L. & MAGIN, T. M. 2012. Involvement of the ubiquitin-proteasome system in the stabilization of cell-cell contacts in human keratinocytes. *Exp Dermatol,* 21**,** 791-3.

MACHLEIDT, W., BORCHART, U., FRITZ, H., BRZIN, J., RITONJA, A. & TURK, V. 1983. Protein inhibitors of cysteine proteinases. II. Primary structure of stefin, a cytosolic protein inhibitor of cysteine proteinases from human polymorphonuclear granulocytes. *Hoppe Seylers Z Physiol Chem,* 364**,** 1481-6.

MAGISTER, S. & KOS, J. 2013. Cystatins in immune system. *J Cancer,* 4**,** 45-56.

MAHONEY, M. G., WANG, Z., ROTHENBERGER, K., KOCH, P. J., AMAGAI, M. & STANLEY, J. R. 1999. Explanations for the clinical and microscopic localization of lesions in pemphigus foliaceus and vulgaris. *J Clin Invest,* 103**,** 461-8.

MALLET, A., KYPRIOTOU, M., GEORGE, K., LECLERC, E., RIVERO, D., MAZEREEUW-HAUTIER, J., SERRE, G., HUBER, M., JONCA, N. & HOHL, D. 2013. Identification of the first nonsense CDSN mutation with expression of a truncated protein causing peeling skin syndrome type B. *Br J Dermatol,* 169**,** 1322-5.

MAO, X., CHOI, E. J. & PAYNE, A. S. 2009. Disruption of desmosome assembly by monovalent human pemphigus vulgaris monoclonal antibodies. *J Invest Dermatol,* 129**,** 908-18.

MARCUS, F. I., MCKENNA, W. J., SHERRILL, D., BASSO, C., BAUCE, B., BLUEMKE, D. A., CALKINS, H., CORRADO, D., COX, M. G., DAUBERT, J. P., FONTAINE, G., GEAR, K., HAUER, R., NAVA, A., PICARD, M. H., PROTONOTARIOS, N., SAFFITZ, J. E., SANBORN, D. M., STEINBERG, J. S., TANDRI, H., THIENE, G., TOWBIN, J. A., TSATSOPOULOU, A., WICHTER, T. & ZAREBA, W. 2010. Diagnosis of arrhythmogenic right ventricular cardiomyopathy/dysplasia: proposed modification of the task force criteria. *Circulation,* 121**,** 1533-41.

MATHOT, L., WALLIN, M. & SJOBLOM, T. 2013. Automated serial extraction of DNA and RNA from biobanked tissue specimens. *BMC Biotechnol,* 13**,** 66.

MATSUSHITA, Y., SHIMADA, Y., KAWARA, S., TAKEHARA, K. & SATO, S. 2005. Autoantibodies directed against the protease inhibitor calpastatin in psoriasis. *Clin Exp Immunol,* 139**,** 355-62.

MCGRATH, J. A., MCMILLAN, J. R., SHEMANKO, C. S., RUNSWICK, S. K., LEIGH, I. M., LANE, E. B., GARROD, D. R. & EADY, R. A. 1997. Mutations in the plakophilin 1 gene result in ectodermal dysplasia/skin fragility syndrome. *Nat Genet,* 17**,** 240-4.

MCKENNA, W. J., THIENE, G., NAVA, A., FONTALIRAN, F., BLOMSTROM-LUNDQVIST, C., FONTAINE, G. & CAMERINI, F. 1994. Diagnosis of arrhythmogenic right ventricular dysplasia/cardiomyopathy. Task Force of the Working Group Myocardial and Pericardial Disease of the European Society of Cardiology and of the Scientific Council on Cardiomyopathies of the International Society and Federation of Cardiology. *Br Heart J,* 71**,** 215-8.

MCKOY, G., PROTONOTARIOS, N., CROSBY, A., TSATSOPOULOU, A., ANASTASAKIS, A., COONAR, A., NORMAN, M., BABOONIAN, C., JEFFERY, S. & MCKENNA, W. J. 2000. Identification of a deletion in plakoglobin in arrhythmogenic right ventricular cardiomyopathy with palmoplantar keratoderma and woolly hair (Naxos disease). *Lancet,* 355**,** 2119-24.

MENG, W. & TAKEICHI, M. 2009. Adherens junction: molecular architecture and regulation. *Cold Spring Harb Perspect Biol,* 1**,** a002899.

MENZIES, F. M., GARCIA-ARENCIBIA, M., IMARISIO, S., O'SULLIVAN, N. C., RICKETTS, T., KENT, B. A., RAO, M. V., LAM, W., GREEN-THOMPSON, Z. W., NIXON, R. A., SAKSIDA, L. M., BUSSEY, T. J., O'KANE, C. J. & RUBINSZTEIN, D. C. 2014. Calpain inhibition mediates autophagy-dependent protection against polyglutamine toxicity. *Cell Death Differ*.

MERNER, N. D., HODGKINSON, K. A., HAYWOOD, A. F., CONNORS, S., FRENCH, V. M., DRENCKHAHN, J. D., KUPPRION, C., RAMADANOVA, K., THIERFELDER, L., MCKENNA, W., GALLAGHER, B., MORRIS-LARKIN, L., BASSETT, A. S., PARFREY, P. S. & YOUNG, T. L. 2008. Arrhythmogenic right ventricular cardiomyopathy type 5 is a fully penetrant, lethal arrhythmic disorder caused by a missense mutation in the TMEM43 gene. *Am J Hum Genet,* 82**,** 809-21.

MERTENS, C., KUHN, C. & FRANKE, W. W. 1996. Plakophilins 2a and 2b: constitutive proteins of dual location in the karyoplasm and the desmosomal plaque. *J Cell Biol,* 135**,** 1009-25.

MERTENS, C., KUHN, C., MOLL, R., SCHWETLICK, I. & FRANKE, W. W. 1999. Desmosomal plakophilin 2 as a differentiation marker in normal and malignant tissues. *Differentiation,* 64**,** 277-90.

MEURS, K. M., MAUCELI, E., LAHMERS, S., ACLAND, G. M., WHITE, S. N. & LINDBLAD-TOH, K. 2010. Genome-wide association identifies a deletion in the 3' untranslated region of striatin in a canine model of arrhythmogenic right ventricular cardiomyopathy. *Hum Genet,* 128**,** 315-24.

MEYER-HOFFERT, U. 2009. Reddish, scaly, and itchy: how proteases and their inhibitors contribute to inflammatory skin diseases. *Arch Immunol Ther Exp (Warsz),* 57**,** 345-54.

MEYER-HOFFERT, U. & SCHRODER, J. M. 2011. Epidermal proteases in the pathogenesis of rosacea. *J Investig Dermatol Symp Proc,* 15**,** 16-23.

MEYER-HOFFERT, U., WU, Z., KANTYKA, T., FISCHER, J., LATENDORF, T., HANSMANN, B., BARTELS, J., HE, Y., GLASER, R. & SCHRODER, J. M. 2010. Isolation of SPINK6 in human skin: selective inhibitor of kallikrein-related peptidases. *J Biol Chem,* 285**,** 32174-81.

MEYER-HOFFERT, U., WU, Z. & SCHRODER, J. M. 2009. Identification of lympho-epithelial Kazal-type inhibitor 2 in human skin as a kallikrein-related peptidase 5-specific protease inhibitor. *PLoS One,* 4**,** e4372.

MINOBE, E., ASMARA, H., SAUD, Z. A. & KAMEYAMA, M. 2011. Calpastatin domain L is a partial agonist of the calmodulin-binding site for channel activation in Cav1.2 Ca2+ channels. *J Biol Chem,* 286**,** 39013-22.

MOLDOVEANU, T., GEHRING, K. & GREEN, D. R. 2008. Concerted multi-pronged attack by calpastatin to occlude the catalytic cleft of heterodimeric calpains. *Nature,* 456**,** 404-8.

MOON, R. T., BOWERMAN, B., BOUTROS, M. & PERRIMON, N. 2002. The promise and perils of Wnt signaling through beta-catenin. *Science,* 296**,** 1644-6.

MOOSBRUGGER-MARTINZ, V., JALILI, A., SCHOSSIG, A. S., JAHN-BASSLER, K., ZSCHOCKE, J., SCHMUTH, M., STINGL, G., ECKL, K. M., HENNIES, H. C. & GRUBER, R. 2014. Epidermal barrier abnormalities in exfoliative ichthyosis with a novel homozygous loss-of-function mutation in CSTA. *Br J Dermatol*.

MORETTI, D., DEL BELLO, B., ALLAVENA, G. & MAELLARO, E. 2014. Calpains and cancer: Friends or enemies? *Arch Biochem Biophys,* 564C**,** 26-36.

NAKAJIMA, R., TAKAO, K., HUANG, S. M., TAKANO, J., IWATA, N., MIYAKAWA, T. & SAIDO, T. C. 2008. Comprehensive behavioral phenotyping of calpastatin-knockout mice. *Mol Brain,* 1**,** 7.

NAKAJIMA, T., KANEKO, Y., IRIE, T., TAKAHASHI, R., KATO, T., IIJIMA, T., ISO, T. & KURABAYASHI, M. 2012. Compound and digenic heterozygosity in desmosome genes as a cause of arrhythmogenic right ventricular cardiomyopathy in Japanese patients. *Circ J,* 76**,** 737-43.

NAKANO, S. J. & TLUCZEK, A. 2014. Genomic breakthroughs in the diagnosis and treatment of cystic fibrosis. *Am J Nurs,* 114**,** 36-43; quiz 44-5.

NASSAR, D., LETAVERNIER, E., BAUD, L., ARACTINGI, S. & KHOSROTEHRANI, K. 2012. Calpain activity is essential in skin wound healing and contributes to scar formation. *PLoS One,* 7**,** e37084.

NAVA, P., LAUKOETTER, M. G., HOPKINS, A. M., LAUR, O., GERNER-SMIDT, K., GREEN, K. J., PARKOS, C. A. & NUSRAT, A. 2007. Desmoglein-2: a novel regulator of apoptosis in the intestinal epithelium. *Mol Biol Cell,* 18**,** 4565-78.

NEKRASOVA, O. & GREEN, K. J. 2013. Desmosome assembly and dynamics. *Trends Cell Biol,* 23**,** 537-46.

NIJMAN, I. J., MOKRY, M., VAN BOXTEL, R., TOONEN, P., DE BRUIJN, E. & CUPPEN, E. 2010. Mutation discovery by targeted genomic enrichment of multiplexed barcoded samples. *Nat Methods,* 7**,** 913-5.

NISHIFUJI, K., SHIMIZU, A., ISHIKO, A., IWASAKI, T. & AMAGAI, M. 2010. Removal of amino-terminal extracellular domains of desmoglein 1 by staphylococcal exfoliative toxin is sufficient to initiate epidermal blister formation. *J Dermatol Sci,* 59**,** 184-91.

NITOIU, D., ETHERIDGE, S. L. & KELSELL, D. P. 2014. Insights into desmosome biology from inherited human skin disease and cardiocutaneous syndromes. *Cell Commun Adhes,* 21**,** 129-40.

NORGETT, E. E., HATSELL, S. J., CARVAJAL-HUERTA, L., CABEZAS, J. C., COMMON, J., PURKIS, P. E., WHITTOCK, N., LEIGH, I. M., STEVENS, H. P. & KELSELL, D. P. 2000. Recessive mutation in desmoplakin disrupts desmoplakin-intermediate filament interactions and causes dilated cardiomyopathy, woolly hair and keratoderma. *Hum Mol Genet,* 9**,** 2761-6.

NORGETT, E. E., LUCKE, T. W., BOWERS, B., MUNRO, C. S., LEIGH, I. M. & KELSELL, D. P. 2006. Early death from cardiomyopathy in a family with autosomal dominant striate palmoplantar keratoderma and woolly hair associated with a novel insertion mutation in desmoplakin. *J Invest Dermatol,* 126**,** 1651-4.

NORMAN, M., SIMPSON, M., MOGENSEN, J., SHAW, A., HUGHES, S., SYRRIS, P., SEN-CHOWDHRY, S., ROWLAND, E., CROSBY, A. & MCKENNA, W. J. 2005. Novel mutation in desmoplakin causes arrhythmogenic left ventricular cardiomyopathy. *Circulation,* 112**,** 636-42.

NORTH, A. J., CHIDGEY, M. A., CLARKE, J. P., BARDSLEY, W. G. & GARROD, D. R. 1996. Distinct desmocollin isoforms occur in the same desmosomes and show reciprocally graded distributions in bovine nasal epidermis. *Proc Natl Acad Sci U S A,* 93**,** 7701-5.

ODA, H. & TAKEICHI, M. 2011. Evolution: structural and functional diversity of cadherin at the adherens junction. *J Cell Biol,* 193**,** 1137-46.

OJI, V., ECKL, K. M., AUFENVENNE, K., NATEBUS, M., TARINSKI, T., ACKERMANN, K., SELLER, N., METZE, D., NURNBERG, G., FOLSTER-HOLST, R., SCHAFER-KORTING, M., HAUSSER, I., TRAUPE, H. & HENNIES, H. C. 2010. Loss of corneodesmosin leads to severe skin barrier defect, pruritus, and atopy: unraveling the peeling skin disease. *Am J Hum Genet,* 87**,** 274-81.

OKTARINA, D. A., VAN DER WIER, G., DIERCKS, G. F., JONKMAN, M. F. & PAS, H. H. 2011. IgG-induced clustering of desmogleins 1 and 3 in skin of patients with pemphigus fits with the desmoglein nonassembly depletion hypothesis. *Br J Dermatol,* 165**,** 552-62.

ONO, Y. & SORIMACHI, H. 2012. Calpains: an elaborate proteolytic system. *Biochim Biophys Acta,* 1824**,** 224-36.

OXFORD, E. M., MUSA, H., MAASS, K., COOMBS, W., TAFFET, S. M. & DELMAR, M. 2007. Connexin43 remodeling caused by inhibition of plakophilin-2 expression in cardiac cells. *Circ Res,* 101**,** 703-11.

PALUNGWACHIRA, P., KAKUTA, M., YAMAZAKI, M., YAGUCHI, H., TSUBOI, R., TAKAMORI, K. & OGAWA, H. 2002. Immunohistochemical localization of cathepsin L and cystatin A in normal skin and skin tumors. *J Dermatol,* 29**,** 573-9.

PARRISH, E. P., STEART, P. V., GARROD, D. R. & WELLER, R. O. 1987. Antidesmosomal monoclonal antibody in the diagnosis of intracranial tumours. *J Pathol,* 153**,** 265-73.

PASDAR, M., LI, Z. & CHAN, H. 1995. Desmosome assembly and disassembly are regulated by reversible protein phosphorylation in cultured epithelial cells. *Cell Motil Cytoskeleton,* 30**,** 108-21.

PIEPERHOFF, S., BARTH, M., RICKELT, S. & FRANKE, W. W. 2010. Desmosomal molecules in and out of adhering junctions: normal and diseased States of epidermal, cardiac and mesenchymally derived cells. *Dermatol Res Pract,* 2010**,** 139167.

PIEPERHOFF, S., SCHUMACHER, H. & FRANKE, W. W. 2008. The area composita of adhering junctions connecting heart muscle cells of vertebrates. V. The importance of plakophilin-2 demonstrated by small interference RNA-mediated knockdown in cultured rat cardiomyocytes. *Eur J Cell Biol,* 87**,** 399-411.

PIGORS, M., KIRITSI, D., KRUMPELMANN, S., WAGNER, N., HE, Y., PODDA, M., KOHLHASE, J., HAUSSER, I., BRUCKNER-TUDERMAN, L. & HAS, C. 2011. Lack of plakoglobin leads to lethal congenital epidermolysis bullosa: a novel clinico-genetic entity. *Hum Mol Genet,* 20**,** 1811-9.

PIHLSTROM, L., RENGMARK, A., BJORNARA, K. A. & TOFT, M. 2014. Effective variant detection by targeted deep sequencing of DNA pools: an example from Parkinson's disease. *Ann Hum Genet,* 78**,** 243-52.

PILICHOU, K., NAVA, A., BASSO, C., BEFFAGNA, G., BAUCE, B., LORENZON, A., FRIGO, G., VETTORI, A., VALENTE, M., TOWBIN, J., THIENE, G., DANIELI, G. A. & RAMPAZZO, A. 2006. Mutations in desmoglein-2 gene are associated with arrhythmogenic right ventricular cardiomyopathy. *Circulation,* 113**,** 1171-9.

POKUTTA, S. & WEIS, W. I. 2007. Structure and mechanism of cadherins and catenins in cell-cell contacts. *Annu Rev Cell Dev Biol,* 23**,** 237-61.

PROTONOTARIOS, N. & TSATSOPOULOU, A. 2004. Naxos disease and Carvajal syndrome: cardiocutaneous disorders that highlight the pathogenesis and broaden the spectrum of arrhythmogenic right ventricular cardiomyopathy. *Cardiovasc Pathol,* 13**,** 185-94.

QUARTA, G., MUIR, A., PANTAZIS, A., SYRRIS, P., GEHMLICH, K., GARCIA-PAVIA, P., WARD, D., SEN-CHOWDHRY, S., ELLIOTT, P. M. & MCKENNA, W. J. 2011. Familial evaluation in arrhythmogenic right ventricular cardiomyopathy: impact of genetics and revised task force criteria. *Circulation,* 123**,** 2701-9.

RAMOS, E., LEVINSON, B. T., CHASNOFF, S., HUGHES, A., YOUNG, A. L., THORNTON, K., LI, A., VALLANIA, F. L., PROVINCE, M. & DRULEY, T. E. 2012. Population-based rare variant detection via pooled exome or custom hybridization capture with or without individual indexing. *BMC Genomics,* 13**,** 683.

RAMPAZZO, A., NAVA, A., MALACRIDA, S., BEFFAGNA, G., BAUCE, B., ROSSI, V., ZIMBELLO, R., SIMIONATI, B., BASSO, C., THIENE, G., TOWBIN, J. A. & DANIELI, G. A. 2002. Mutation in human desmoplakin domain binding to plakoglobin causes a dominant form of arrhythmogenic right ventricular cardiomyopathy. *Am J Hum Genet,* 71**,** 1200-6.

RAO, M. V., MOHAN, P. S., PETERHOFF, C. M., YANG, D. S., SCHMIDT, S. D., STAVRIDES, P. H., CAMPBELL, J., CHEN, Y., JIANG, Y., PASKEVICH, P. A., CATALDO, A. M., HAROUTUNIAN, V. & NIXON, R. A. 2008. Marked calpastatin (CAST) depletion in Alzheimer's disease accelerates cytoskeleton disruption and neurodegeneration: neuroprotection by CAST overexpression. *J Neurosci,* 28**,** 12241-54.

RASANEN, O., JARVINEN, M. & RINNE, A. 1978. Localization of the human SH-protease inhibitor in the epidermis. Immunofluorescent studies. *Acta Histochem,* 63**,** 193-6.

RAWLINGS, N. D. & BARRETT, A. J. 1990. Evolution of proteins of the cystatin superfamily. *J Mol Evol,* 30**,** 60-71.

RENKO, M., POZGAN, U., MAJERA, D. & TURK, D. 2010. Stefin A displaces the occluding loop of cathepsin B only by as much as required to bind to the active site cleft. *FEBS J,* 277**,** 4338-45.

RESNIK, N., SEPCIC, K., PLEMENITAS, A., WINDOFFER, R., LEUBE, R. & VERANIC, P. 2011. Desmosome assembly and cell-cell adhesion are membrane raft-dependent processes. *J Biol Chem,* 286**,** 1499-507.

RICKMAN, L., SIMRAK, D., STEVENS, H. P., HUNT, D. M., KING, I. A., BRYANT, S. P., EADY, R. A., LEIGH, I. M., ARNEMANN, J., MAGEE, A. I., KELSELL, D. P. & BUXTON, R. S. 1999. N-terminal deletion in a desmosomal cadherin causes the autosomal dominant skin disease striate palmoplantar keratoderma. *Hum Mol Genet,* 8**,** 971-6.

RINNE, A. 2010. Epidermal SH-protease inhibitor (ACPI, cystatin A) in cancer. A short historical review. *Pathol Res Pract,* 206**,** 259-62.

RINNE, A., JARVINEN, M. & RASANEN, O. 1978. A protein reminiscent of the epidermal SH-protease inhibitor occurs in squamous epithelia of man and rat. *Acta Histochem,* 63**,** 183-92.

RINNE, A., JARVINEN, M., RASANEN, O. & DORN, A. 1980. [Demonstration of an epidermal SH-protease inhibitor in normal epithelium and in some human neoplasms--an immunological study (author's transl)]. *Acta Histochem Suppl,* 22**,** 325-9.

RIVENBARK, A. G. & COLEMAN, W. B. 2009. Epigenetic regulation of cystatins in cancer. *Front Biosci (Landmark Ed),* 14**,** 453-62.

RUIZ, P., BRINKMANN, V., LEDERMANN, B., BEHREND, M., GRUND, C., THALHAMMER, C., VOGEL, F., BIRCHMEIER, C., GUNTHERT, U., FRANKE, W. W. & BIRCHMEIER, W. 1996. Targeted mutation of plakoglobin in mice reveals essential functions of desmosomes in the embryonic heart. *J Cell Biol,* 135**,** 215-25.

RUNSWICK, S. K., O'HARE, M. J., JONES, L., STREULI, C. H. & GARROD, D. R. 2001. Desmosomal adhesion regulates epithelial morphogenesis and cell positioning. *Nat Cell Biol,* 3**,** 823-30.

SAARINEN, S., VAHTERISTO, P., LEHTONEN, R., AITTOMAKI, K., LAUNONEN, V., KIVILUOTO, T. & AALTONEN, L. A. 2012. Analysis of a Finnish family confirms RHBDF2 mutations as the underlying factor in tylosis with esophageal cancer. *Fam Cancer,* 11**,** 525-8.

SALEHIN, D., FROMBERG, I., HAUGK, C., DOHMEN, B., GEORG, T., BOHLE, R. M., BAUERSCHLAG, D., THILL, M. & FRIEDRICH, M. 2011. Immunhistochemical analysis for expression of calpain 1, calpain 2 and calpastatin in ovarian cancer. *Eur J Gynaecol Oncol,* 32**,** 628-35.

SAMUELOV, L., SARIG, O., HARMON, R. M., RAPAPORT, D., ISHIDA-YAMAMOTO, A., ISAKOV, O., KOETSIER, J. L., GAT, A., GOLDBERG, I., BERGMAN, R., SPIEGEL, R., EYTAN, O., GELLER, S., PELEG, S., SHOMRON, N., GOH, C. S., WILSON, N. J., SMITH, F. J., POHLER, E., SIMPSON, M. A., MCLEAN, W. H., IRVINE, A. D., HOROWITZ, M., MCGRATH, J. A., GREEN, K. J. & SPRECHER, E. 2013. Desmoglein 1 deficiency results in severe dermatitis, multiple allergies and metabolic wasting. *Nat Genet,* 45**,** 1244-8.

SATO, A., SAKAMOTO, N., ANDO, K., KANESHIRO, T., UEKITA, H., SUGIMOTO, K., YAMAKI, T., KUNII, H., NAKAZATO, K., SUZUKI, H., SAITOH, S., SATO, M., TAMAGAWA, K., ARIMURA, T., KIMURA, A. & TAKEISHI, Y. 2012. Dilated phase of hypertrophic cardiomyopathy caused by two different sarcomere mutations, treated with surgical left ventricular reconstruction and cardiac resynchronization therapy with a defibrillator. *Intern Med,* 51**,** 2559-64.

SATO, M., AOYAMA, Y. & KITAJIMA, Y. 2000. Assembly pathway of desmoglein 3 to desmosomes and its perturbation by pemphigus vulgaris-IgG in cultured keratinocytes, as revealed by time-lapsed labeling immunoelectron microscopy. *Lab Invest,* 80**,** 1583-92.

SCHAFER, S., STUMPP, S. & FRANKE, W. W. 1996. Immunological identification and characterization of the desmosomal cadherin Dsg2 in coupled and uncoupled epithelial cells and in human tissues. *Differentiation,* 60**,** 99-108.

SCHAFFER, J. V., BAZZI, H., VITEBSKY, A., WITKIEWICZ, A., KOVICH, O. I., KAMINO, H., SHAPIRO, L. S., AMIN, S. P., ORLOW, S. J. & CHRISTIANO, A. M. 2006. Mutations in the desmoglein 4 gene underlie localized autosomal recessive hypotrichosis with monilethrix hairs and congenital scalp erosions. *J Invest Dermatol,* 126**,** 1286-91.

SCHERER, S. E., MUZNY, D. M., BUHAY, C. J., CHEN, R., CREE, A., DING, Y., DUGAN-ROCHA, S., GILL, R., GUNARATNE, P., HARRIS, R. A., HAWES, A. C., HERNANDEZ, J., HODGSON, A. V., HUME, J., JACKSON, A., KHAN, Z. M., KOVAR-SMITH, C., LEWIS, L. R., LOZADO, R. J., METZKER, M. L., MILOSAVLJEVIC, A., MINER, G. R., MONTGOMERY, K. T., MORGAN, M. B., NAZARETH, L. V., SCOTT, G., SODERGREN, E., SONG, X. Z., STEFFEN, D., LOVERING, R. C., WHEELER, D. A., WORLEY, K. C., YUAN, Y., ZHANG, Z., ADAMS, C. Q., ANSARI-LARI, M. A., AYELE, M., BROWN, M. J., CHEN, G., CHEN, Z., CLERC-BLANKENBURG, K. P., DAVIS, C., DELGADO, O., DINH, H. H., DRAPER, H., GONZALEZ-GARAY, M. L., HAVLAK, P., JACKSON, L. R., JACOB, L. S., KELLY, S. H., LI, L., LI, Z., LIU, J., LIU, W., LU, J., MAHESHWARI, M., NGUYEN, B. V., OKWUONU, G. O., PASTERNAK, S., PEREZ, L. M., PLOPPER, F. J., SANTIBANEZ, J., SHEN, H., TABOR, P. E., VERDUZCO, D., WALDRON, L., WANG, Q., WILLIAMS, G. A., ZHANG, J., ZHOU, J., ALLEN, C. C., AMIN, A. G., ANYALEBECHI, V., BAILEY, M., BARBARIA, J. A., BIMAGE, K. E., BRYANT, N. P., BURCH, P. E., BURKETT, C. E., BURRELL, K. L., CALDERON, E., CARDENAS, V., CARTER, K., CASIAS, K., CAVAZOS, I., CAVAZOS, S. R., CEASAR, H., CHACKO, J., CHAN, S. N., CHAVEZ, D., CHRISTOPOULOS, C., CHU, J., COCKRELL, R., COX, C. D., DANG, M., DATHORNE, S. R., DAVID, R.,

DAVIS, C. M., DAVY-CARROLL, L., DESHAZO, D. R., *et al*. 2006. The finished DNA sequence of human chromosome 12. *Nature,* 440**,** 346-51.

SCHMEISER, K. & GRAND, R. J. 1999. The fate of E- and P-cadherin during the early stages of apoptosis. *Cell Death Differ,* 6**,** 377-86.

SCHMIDT, A., LANGBEIN, L., RODE, M., PRATZEL, S., ZIMBELMANN, R. & FRANKE, W. W. 1997. Plakophilins 1a and 1b: widespread nuclear proteins recruited in specific epithelial cells as desmosomal plaque components. *Cell Tissue Res,* 290**,** 481-99.

SCOTT, C. A. & KELSELL, D. P. 2011. Key functions for gap junctions in skin and hearing. *Biochem J,* 438**,** 245-54.

SCOTT, D. K., LORD, R., MULLER, H. K., MALLEY, R. C. & WOODS, G. M. 2007. Proteomics identifies enhanced expression of stefin A in neonatal murine skin compared with adults: functional implications. *Br J Dermatol,* 156**,** 1156-62.

SEKIGUCHI, M., FUTEI, Y., FUJII, Y., IWASAKI, T., NISHIKAWA, T. & AMAGAI, M. 2001. Dominant autoimmune epitopes recognized by pemphigus antibodies map to the N-terminal adhesive region of desmogleins. *J Immunol,* 167**,** 5439-48.

SEN-CHOWDHRY, S., MORGAN, R. D., CHAMBERS, J. C. & MCKENNA, W. J. 2010. Arrhythmogenic cardiomyopathy: etiology, diagnosis, and treatment. *Annu Rev Med,* 61**,** 233-53.

SHIMIZU, A., ISHIKO, A., OTA, T., TSUNODA, K., AMAGAI, M. & NISHIKAWA, T. 2004. IgG binds to desmoglein 3 in desmosomes and causes a desmosomal split without keratin retraction in a pemphigus mouse model. *J Invest Dermatol,* 122**,** 1145-53.

SHIMIZU, H., MASUNAGA, T., ISHIKO, A., KIKUCHI, A., HASHIMOTO, T. & NISHIKAWA, T. 1995. Pemphigus vulgaris and pemphigus foliaceus sera show an inversely graded binding pattern to extracellular regions of desmosomes in different layers of human epidermis. *J Invest Dermatol,* 105**,** 153-9.

SHIMOMURA, Y., SAKAMOTO, F., KARIYA, N., MATSUNAGA, K. & ITO, M. 2006. Mutations in the desmoglein 4 gene are associated with monilethrix-like congenital hypotrichosis. *J Invest Dermatol,* 126**,** 1281-5.

SHIRAKATA, Y., AMAGAI, M., HANAKAWA, Y., NISHIKAWA, T. & HASHIMOTO, K. 1998. Lack of mucosal involvement in pemphigus foliaceus may be due to low expression of desmoglein 1. *J Invest Dermatol,* 110**,** 76-8.

SHWAYDER, T., CONN, S. & LOWE, L. 1997. Acral peeling skin syndrome. *Arch Dermatol,* 133**,** 535-6.

SIMPSON, M. A., COOK, R. W., SOLANKI, P., PATTON, M. A., DENNIS, J. A. & CROSBY, A. H. 2009a. A mutation in NFkappaB interacting protein 1 causes cardiomyopathy and woolly haircoat syndrome of Poll Hereford cattle. *Anim Genet,* 40**,** 42-6.

SIMPSON, M. A., MANSOUR, S., AHNOOD, D., KALIDAS, K., PATTON, M. A., MCKENNA, W. J., BEHR, E. R. & CROSBY, A. H. 2009b. Homozygous mutation of desmocollin-2 in arrhythmogenic right ventricular cardiomyopathy with mild palmoplantar keratoderma and woolly hair. *Cardiology,* 113**,** 28-34.

SINHA, A. A., QUAST, B. J., KORKOWSKI, J. C., WILSON, M. J., REDDY, P. K., EWING, S. L., SLOANE, B. F. & GLEASON, D. F. 1999. The relationship of cathepsin B and stefin A mRNA localization identifies a potentially aggressive variant of human prostate cancer within a Gleason histologic score. *Anticancer Res,* 19**,** 2821-9.

SKLYAROVA, T., BONNE, S., D'HOOGE, P., DENECKER, G., GOOSSENS, S., DE RYCKE, R., BORGONIE, G., BOSL, M., VAN ROY, F. & VAN HENGEL, J. 2008. Plakophilin-3-deficient mice develop hair coat abnormalities and are prone to cutaneous inflammation. *J Invest Dermatol,* 128**,** 1375-85.

SMITH, E. A. & FUCHS, E. 1998. Defining the interactions between intermediate filaments and desmosomes. *J Cell Biol,* 141**,** 1229-41.

SOBOLIK-DELMAIRE, T., REDDY, R., PASHAJ, A., ROBERTS, B. J. & WAHL, J. K., 3RD 2010. Plakophilin-1 localizes to the nucleus and interacts with single-stranded DNA. *J Invest Dermatol,* 130**,** 2638-46.

SODERSTROM, K. O., LAATO, M., WU, P., HOPSU-HAVU, V. K., NURMI, M. & RINNE, A. 1995. Expression of acid cysteine proteinase inhibitor (ACPI) in the normal human prostate, benign prostatic hyperplasia and adenocarcinoma. *Int J Cancer,* 62**,** 1-4.

SODERSTROM, K. O., RINNE, R., HOPSU-HAVU, V. K., JARVINEN, M. & RINNE, A. 1994. Identification of acid cysteine proteinase inhibitor (cystatin A) in the human thymus. *Anat Rec,* 240**,** 115-9.

STAEHELIN, L. A. 1974. Structure and function of intercellular junctions. *Int Rev Cytol,* 39**,** 191-283.

STAHLEY, S. N., SAITO, M., FAUNDEZ, V., KOVAL, M., MATTHEYSES, A. L. & KOWALCZYK, A. P. 2014. Desmosome assembly and disassembly are membrane raft-dependent. *PLoS One,* 9**,** e87809.

STANLEY, J. R. & AMAGAI, M. 2006. Pemphigus, bullous impetigo, and the staphylococcal scalded-skin syndrome. *N Engl J Med,* 355**,** 1800-10.

STEVENS, H. P., KELSELL, D. P., BRYANT, S. P., BISHOP, D. T., SPURR, N. K., WEISSENBACH, J., MARGER, D., MARGER, R. S. & LEIGH, I. M. 1996. Linkage of an American pedigree with palmoplantar keratoderma and malignancy (palmoplantar ectodermal dysplasia type III) to 17q24. Literature survey and proposed updated classification of the keratodermas. *Arch Dermatol,* 132**,** 640-51.

STODDARD, J. L., NIEMELA, J. E., FLEISHER, T. A. & ROSENZWEIG, S. D. 2014. Targeted NGS: A Cost-Effective Approach to Molecular Diagnosis of PIDs. *Front Immunol,* 5**,** 531.

STORME, M. L., SINNAEVE, B. A. & VAN BOCXLAER, J. F. 2005. The use of tryptic marker-peptides for the quantitative analysis of cystatin C. *J Sep Sci,* 28**,** 1759-63.

STROJAN, P., ANICIN, A., SVETIC, B., SMID, L. & KOS, J. 2011. Proteolytic profile of cysteine proteases and inhibitors determines tumor cell phenotype in squamous cell carcinoma of the head and neck. *Int J Biol Markers,* 26**,** 247-54.

STROJAN, P., BUDIHNA, M., SMID, L., SVETIC, B., VRHOVEC, I., KOS, J. & SKRK, J. 2000. Prognostic significance of cysteine proteinases cathepsins B and L and their endogenous inhibitors stefins A and B in patients with squamous cell carcinoma of the head and neck. *Clin Cancer Res,* 6**,** 1052-62.

SUTTON, L. A., LJUNGSTROM, V., MANSOURI, L., YOUNG, E., CORTESE, D., NAVRKALOVA, V., MALCIKOVA, J., MUGGEN, A. F., TRBUSEK, M., PANAGIOTIDIS, P., DAVI, F., BELESSI, C., LANGERAK, A. W., GHIA, P., POSPISILOVA, S., STAMATOPOULOS, K. & ROSENQUIST, R. 2014. Targeted next-generation sequencing in chronic lymphocytic leukemia: a high-throughput yet tailored approach will facilitate implementation within a clinical setting. *Haematologica*.

SYRRIS, P., WARD, D., ASIMAKI, A., EVANS, A., SEN-CHOWDHRY, S., HUGHES, S. E. & MCKENNA, W. J. 2007. Desmoglein-2 mutations in arrhythmogenic right ventricular cardiomyopathy: a genotype-phenotype characterization of familial disease. *Eur Heart J,* 28**,** 581-8.

SYRRIS, P., WARD, D., EVANS, A., ASIMAKI, A., GANDJBAKHCH, E., SEN-CHOWDHRY, S. & MCKENNA, W. J. 2006. Arrhythmogenic right ventricular dysplasia/cardiomyopathy associated with mutations in the desmosomal gene desmocollin-2. *Am J Hum Genet,* 79**,** 978-84.

SZEGEDI, A., PAYER, E., CZIFRA, G., TOTH, B. I., SCHMIDT, E., KOVACS, L., BLUMBERG, P. M. & BIRO, T. 2009. Protein kinase C isoenzymes differentially regulate the differentiation-dependent expression of adhesion molecules in human epidermal keratinocytes. *Exp Dermatol,* 18**,** 122-9.

TAKANO, E., NOSAKA, T., LEE, W. J., NAKAMURA, K., TAKAHASHI, T., FUNAKI, M., OKADA, H., HATANAKA, M. & MAKI, M. 1993. Molecular diversity of calpastatin in human erythroid cells. *Arch Biochem Biophys,* 303**,** 349-54.

TAKANO, E., UEDA, M., TSUNEKAWA, S., MURAKAMI, T., MAKI, M., HATANAKA, M. & MURACHI, T. 1991. Molecular diversity of erythrocyte calpastatin. *Biomed Biochim Acta,* 50**,** 517-21.

TAKANO, J., TOMIOKA, M., TSUBUKI, S., HIGUCHI, M., IWATA, N., ITOHARA, S., MAKI, M. & SAIDO, T. C. 2005. Calpain mediates excitotoxic DNA fragmentation via mitochondrial pathways in adult brains: evidence from calpastatin mutant mice. *J Biol Chem,* 280**,** 16175-84.

TAKEICHI, M. 1977. Functional correlation between cell adhesive properties and some cell surface proteins. *J Cell Biol,* 75**,** 464-74.

TAKEICHI, M. 1990. Cadherins: a molecular family important in selective cell-cell adhesion. *Annu Rev Biochem,* 59**,** 237-52.

TAMAI, K., KANEDA, Y. & UITTO, J. 2009. Molecular therapies for heritable blistering diseases. *Trends Mol Med,* 15**,** 285-92.

TAN, Y., DOURDIN, N., WU, C., DE VEYRA, T., ELCE, J. S. & GREER, P. A. 2006. Ubiquitous calpains promote caspase-12 and JNK activation during endoplasmic reticulum stress-induced apoptosis. *J Biol Chem,* 281**,** 16016-24.

TANAKA, A., LAI-CHEONG, J. E., CAFE, M. E., GONTIJO, B., SALOMAO, P. R., PEREIRA, L. & MCGRATH, J. A. 2009. Novel truncating mutations in PKP1 and DSP cause similar skin phenotypes in two Brazilian families. *Br J Dermatol,* 160**,** 692-7.

TAYLOR, M., GRAW, S., SINAGRA, G., BARNES, C., SLAVOV, D., BRUN, F., PINAMONTI, B., SALCEDO, E. E., SAUER, W., PYXARAS, S., ANDERSON, B., SIMON, B., BOGOMOLOVAS, J., LABEIT, S., GRANZIER, H. & MESTRONI, L. 2011. Genetic variation in titin in arrhythmogenic right ventricular cardiomyopathy-overlap syndromes. *Circulation,* 124**,** 876-85.

TEMM-GROVE, C. J., WERT, D., THOMPSON, V. F., ALLEN, R. E. & GOLL, D. E. 1999. Microinjection of calpastatin inhibits fusion in myoblasts. *Exp Cell Res,* 247**,** 293-303.

TOWBIN, J. A. 2008. Arrhythmogenic right ventricular cardiomyopathy: a paradigm of overlapping disorders. *Ann Noninvasive Electrocardiol,* 13**,** 325-6.

TSELEPIS, C., CHIDGEY, M., NORTH, A. & GARROD, D. 1998. Desmosomal adhesion inhibits invasive behavior. *Proc Natl Acad Sci U S A,* 95**,** 8064-9.

TUCKER, D. K., STAHLEY, S. N. & KOWALCZYK, A. P. 2014. Plakophilin-1 protects keratinocytes from pemphigus vulgaris IgG by forming calcium-independent desmosomes. *J Invest Dermatol,* 134**,** 1033-43.

TURK, B., KRIZAJ, I., KRALJ, B., DOLENC, I., POPOVIC, T., BIETH, J. G. & TURK, V. 1993. Bovine stefin C, a new member of the stefin family. *J Biol Chem,* 268**,** 7323-9.

UEYAMA, H., KUMAMOTO, T., FUJIMOTO, S., MURAKAMI, T. & TSUDA, T. 1998. Expression of three calpain isoform genes in human skeletal muscles. *J Neurol Sci,* 155**,** 163-9.

UZUMCU, A., NORGETT, E. E., DINDAR, A., UYGUNER, O., NISLI, K., KAYSERILI, H., SAHIN, S. E., DUPONT, E., SEVERS, N. J., LEIGH, I. M., YUKSEL-APAK, M., KELSELL, D. P. & WOLLNIK, B. 2006. Loss of desmoplakin isoform I causes early onset cardiomyopathy and heart failure in a Naxos-like syndrome. *J Med Genet,* 43**,** e5.

VAN DER ZWAAG, P. A., COX, M. G., VAN DER WERF, C., WIESFELD, A. C., JONGBLOED, J. D., DOOIJES, D., BIKKER, H., JONGBLOED, R., SUURMEIJER, A. J., VAN DEN BERG, M. P., HOFSTRA, R. M., HAUER, R. N., WILDE, A. A. & VAN TINTELEN, J. P. 2010. Recurrent and founder mutations in the Netherlands : Plakophilin-2 p.Arg79X mutation causing arrhythmogenic right ventricular cardiomyopathy/dysplasia. *Neth Heart J,* 18**,** 583-91.

VAN TINTELEN, J. P., VAN GELDER, I. C., ASIMAKI, A., SUURMEIJER, A. J., WIESFELD, A. C., JONGBLOED, J. D., VAN DEN WIJNGAARD, A., KUKS, J. B., VAN SPAENDONCK-ZWARTS, K. Y., NOTERMANS, N., BOVEN, L., VAN DEN HEUVEL, F., VEENSTRA-KNOL, H. E., SAFFITZ, J. E., HOFSTRA, R. M. & VAN DEN BERG, M. P. 2009. Severe cardiac phenotype with right ventricular predominance in a large cohort of patients with a single missense mutation in the DES gene. *Heart Rhythm,* 6**,** 1574-83.

VASILOPOULOS, Y., CORK, M. J., TEARE, D., MARINOU, I., WARD, S. J., DUFF, G. W. & TAZI-AHNINI, R. 2007. A nonsynonymous substitution of cystatin A, a cysteine protease inhibitor of house dust mite protease, leads to decreased mRNA stability and shows a significant association with atopic dermatitis. *Allergy,* 62**,** 514-9.

VASILOPOULOS, Y., WALTERS, K., CORK, M. J., DUFF, G. W., SAGOO, G. S. & TAZI-AHNINI, R. 2008. Association analysis of the skin barrier gene cystatin A at the PSORS5 locus in psoriatic patients: evidence for interaction between PSORS1 and PSORS5. *Eur J Hum Genet,* 16**,** 1002-9.

VASIOUKHIN, V., BOWERS, E., BAUER, C., DEGENSTEIN, L. & FUCHS, E. 2001. Desmoplakin is essential in epidermal sheet formation. *Nat Cell Biol,* 3**,** 1076-85.

WAHL, J. K., 3RD 2005. A role for plakophilin-1 in the initiation of desmosome assembly. *J Cell Biochem,* 96**,** 390-403.

WALLIS, S., LLOYD, S., WISE, I., IRELAND, G., FLEMING, T. P. & GARROD, D. 2000. The alpha isoform of protein kinase C is involved in signaling the response of desmosomes to wounding in cultured epithelial cells. *Mol Biol Cell,* 11**,** 1077-92.

WANG, H., CAO, X., LIN, Z., LEE, M., JIA, X., REN, Y., DAI, L., GUAN, L., ZHANG, J., LIN, X., ZHANG, J., CHEN, Q., FENG, C., ZHOU, E. Y., YIN, J., XU, G. & YANG, Y. 2015. Exome sequencing reveals mutation in GJA1 as a cause of keratoderma-hypotrichosis-leukonychia totalis syndrome. *Hum Mol Genet,* 24**,** 243-50.

WATT, F. M., MATTEY, D. L. & GARROD, D. R. 1984. Calcium-induced reorganization of desmosomal components in cultured human keratinocytes. *J Cell Biol,* 99**,** 2211-5.

WEI, C. J., XU, X. & LO, C. W. 2004. Connexins and cell signaling in development and disease. *Annu Rev Cell Dev Biol,* 20**,** 811-38.

WEISKE, J., SCHONEBERG, T., SCHRODER, W., HATZFELD, M., TAUBER, R. & HUBER, O. 2001. The fate of desmosomal proteins in apoptotic cells. *J Biol Chem,* 276**,** 41175-81.

WENDT, A., THOMPSON, V. F. & GOLL, D. E. 2004. Interaction of calpastatin with calpain: a review. *Biol Chem,* 385**,** 465-72.

WHITTOCK, N. V., ASHTON, G. H., DOPPING-HEPENSTAL, P. J., GRATIAN, M. J., KEANE, F. M., EADY, R. A. & MCGRATH, J. A. 1999. Striate palmoplantar keratoderma resulting from desmoplakin haploinsufficiency. *J Invest Dermatol,* 113**,** 940-6.

WHITTOCK, N. V., WAN, H., MORLEY, S. M., GARZON, M. C., KRISTAL, L., HYDE, P., MCLEAN, W. H., PULKKINEN, L., UITTO, J., CHRISTIANO, A. M., EADY, R. A. & MCGRATH, J. A. 2002. Compound heterozygosity for non-sense and mis-sense mutations in desmoplakin underlies skin fragility/woolly hair syndrome. *J Invest Dermatol,* 118**,** 232-8.

WITHANA, N. P., BLUM, G., SAMENI, M., SLANEY, C., ANBALAGAN, A., OLIVE, M. B., BIDWELL, B. N., EDGINGTON, L., WANG, L., MOIN, K., SLOANE, B. F., ANDERSON, R. L., BOGYO, M. S. & PARKER, B. S. 2012. Cathepsin B inhibition limits bone metastasis in breast cancer. *Cancer Res,* 72**,** 1199-209.

WOLF, A. & HATZFELD, M. 2010. A role of plakophilins in the regulation of translation. *Cell Cycle,* 9**,** 2973-8.

WOLFF, K., GOLDSMITH, L., KATZ, S., GILCHREST, B. A., PALLER, A. & LEFFELL, D. J. 2007. *Fitzpatrick's Dermatology In General Medicine, Seventh Edition*, McGraw-Hill.

XU, T., YANG, Z., VATTA, M., RAMPAZZO, A., BEFFAGNA, G., PILICHOU, K., SCHERER, S. E., SAFFITZ, J., KRAVITZ, J., ZAREBA, W., DANIELI, G. A., LORENZON, A., NAVA, A., BAUCE, B., THIENE, G., BASSO, C., CALKINS, H., GEAR, K., MARCUS, F., TOWBIN, J. A. & MULTIDISCIPLINARY STUDY OF RIGHT VENTRICULAR DYSPLASIA, I. 2010. Compound and digenic heterozygosity contributes to arrhythmogenic right ventricular cardiomyopathy. *J Am Coll Cardiol,* 55**,** 587-97.

YAMADA, S., POKUTTA, S., DREES, F., WEIS, W. I. & NELSON, W. J. 2005. Deconstructing the cadherin-catenin-actin complex. *Cell,* 123**,** 889-901.

YAMAZAKI, M., ISHIDOH, K., SUGA, Y., SAIDO, T. C., KAWASHIMA, S., SUZUKI, K., KOMINAMI, E. & OGAWA, H. 1997. Cytoplasmic processing of human profilaggrin by active mu-calpain. *Biochem Biophys Res Commun,* 235**,** 652-6.

YAN, S., SAMENI, M. & SLOANE, B. F. 1998. Cathepsin B and human tumor progression. *Biol Chem,* 379**,** 113-23.

YIN, T. & GREEN, K. J. 2004. Regulation of desmosome assembly and adhesion. *Semin Cell Dev Biol,* 15**,** 665-77.

YONEMURA, S. 2011. Cadherin-actin interactions at adherens junctions. *Curr Opin Cell Biol,* 23**,** 515-22.

ZHAO, R., GUAN, D. W., ZHANG, W., DU, Y., XIONG, C. Y., ZHU, B. L. & ZHANG, J. J. 2009. Increased expressions and activations of apoptosis-related factors in cell signaling during incised skin wound healing in mice: a preliminary study for forensic wound age estimation. *Leg Med (Tokyo),* 11 Suppl 1**,** S155-60.

ZHENG, R., BU, D. F. & ZHU, X. J. 2005. Compound heterozygosity for new splice site mutations in the plakophilin 1 gene (PKP1) in a Chinese case of ectodermal dysplasia-skin fragility syndrome. *Acta Derm Venereol,* 85**,** 394-9.

ZHURINSKY, J., SHTUTMAN, M. & BEN-ZE'EV, A. 2000. Differential mechanisms of LEF/TCF family-dependent transcriptional activation by beta-catenin and plakoglobin. *Mol Cell Biol,* 20**,** 4238-52.

ZLOTOGORSKI, A., MAREK, D., HOREV, L., ABU, A., BEN-AMITAI, D., GERAD, L., INGBER, A., FRYDMAN, M., REZNIK-WOLF, H., VARDY, D. A. & PRAS, E. 2006. An autosomal recessive form of monilethrix is caused by mutations in DSG4: clinical overlap with localized autosomal recessive hypotrichosis. *J Invest Dermatol,* 126**,** 1292-6.

MULTALIN INTERFACE PAGE

http://bioinfo.genotoul.fr/multalin/multalin.html

NATIONAL CENTER FOR BIOTECHNOLOGY INFORMATION

http://www.ncbi.nlm.nih.gov/

1000 GENOMES
http://www.1000genomes.org/

ENSEMBL
http://www.ensembl.org/

-Appendices-

Appendix A. Patient samples for genetic screening

Patient study ID	Country of origin of sample	Screening technique	Disease
ARVC 2010 0001	UK	385K Sequence Capture Array	ARVC
ARVC 2010 0002	UK	385K Sequence Capture Array	ARVC
ARVC 2010 0003 SA	UK	385K Sequence Capture Array	ARVC
ARVC 2010 0003 AA	UK	385K Sequence Capture Array	ARVC
ARVC 2010 0004	UK	385K Sequence Capture Array	ARVC
ARVC 2010 0005	UK	385K Sequence Capture Array	ARVC
ARVC 2010 0006	UK	385K Sequence Capture Array	ARVC
ARVC 2010 0007	UK	385K Sequence Capture Array	ARVC
ARVC 2010 0008	UK	385K Sequence Capture Array	ARVC
ARVC 2010 0009	UK	385K Sequence Capture Array	ARVC
ARVC 2010 0010	UK	385K Sequence Capture Array	ARVC
ARVC 2010 0011	UK	385K Sequence Capture Array	ARVC
ARVC 2010 0012	UK	HaloPlex Targeted Resequencing	ARVC

Patient study ID	Country of origin of sample	Screening technique	Disease
ARVC 2010 0013	UK	HaloPlex Targeted Resequencing	ARVC
ARVC 2010 0014	UK	HaloPlex Targeted Resequencing	ARVC
ARVC 2010 0015	UK	HaloPlex Targeted Resequencing	ARVC
ARVC 2010 0016	UK	HaloPlex Targeted Resequencing	ARVC
ARVC 2011 0017	UK	HaloPlex Targeted Resequencing	ARVC
ARVC 2011 0018	UK	HaloPlex Targeted Resequencing	ARVC
ARVC 2011 0019	UK	HaloPlex Targeted Resequencing	ARVC
ARVC 2011 0020A	UK	HaloPlex Targeted Resequencing	ARVC
ARVC 2011 0020D	UK	HaloPlex Targeted Resequencing	ARVC
ARVC 2011 0021	UK	HaloPlex Targeted Resequencing	ARVC
ARVC 2011 0022	UK	HaloPlex Targeted Resequencing	ARVC
FP9310	NZ	HaloPlex Targeted Resequencing	ARVC
LU4246	NZ	HaloPlex Targeted Resequencing	ARVC
RN2662	NZ	HaloPlex Targeted Resequencing	ARVC

Patient study ID	Country of origin of sample	Screening technique	Disease
RY8012	NZ	HaloPlex Targeted Resequencing	ARVC
CM4130	NZ	HaloPlex Targeted Resequencing	ARVC
LI8441	NZ	HaloPlex Targeted Resequencing	ARVC
LN2209	NZ	HaloPlex Targeted Resequencing	ARVC
YP8962	NZ	HaloPlex Targeted Resequencing	ARVC
CJ0829	NZ	HaloPlex Targeted Resequencing	ARVC
LK7659	NZ	HaloPlex Targeted Resequencing	ARVC
LH5926	NZ	HaloPlex Targeted Resequencing	ARVC
LI8308	NZ	HaloPlex Targeted Resequencing	ARVC
LH5930	NZ	HaloPlex Targeted Resequencing	ARVC
NE2908	NZ	HaloPlex Targeted Resequencing	ARVC
OG0660	NZ	HaloPlex Targeted Resequencing	ARVC
LW9068	NZ	HaloPlex Targeted Resequencing	ARVC
LJ6113	NZ	HaloPlex Targeted Resequencing	ARVC

Patient study ID	Country of origin of sample	Screening technique	Disease
LI7542	NZ	HaloPlex Targeted Resequencing	ARVC
LI8325	NZ	HaloPlex Targeted Resequencing	ARVC
MC5702	NZ	HaloPlex Targeted Resequencing	ARVC
LH5931	NZ	HaloPlex Targeted Resequencing	ARVC
WN2786	NZ	HaloPlex Targeted Resequencing	ARVC
LV7711	NZ	HaloPlex Targeted Resequencing	ARVC
FT6012	NZ	HaloPlex Targeted Resequencing	ARVC
FT6011	NZ	HaloPlex Targeted Resequencing	ARVC
9395171	UK	HaloPlex Targeted Resequencing	Unknown
9305427	UK	HaloPlex Targeted Resequencing	Unknown
BLGC DNA657	UK	Exome capture	hypotrichosis and PPK
BLGC DNA656	UK	Exome capture	hypotrichosis and PPK
BLGC DNA658	UK	Control parent	Parent of hypotrichosis and PPK patient

Patient study ID	Country of origin of sample	Screening technique	Disease
BLGC DNA655	UK	Control parent	Parent of hypotrichosis and PPK patient
KL	UK	Sanger sequencing	Acral Peeling Syndrome
SL	UK	Sanger sequencing	Acral Peeling Syndrome
DK-2013-UNK-04	UK	Exome capture	PLACK Syndrome
Control Genomic DNA	UK	Sanger sequencing	N/A

Table A. Patient samples with accompanying information. Forty-nine patients, diagnosed with ARVC, were recruited from Barts and The London NHS Trust and from two collaborating centres, Bristol Heart Institute and the Cardiac Inherited Disease Group based in Auckland, New Zealand (Dr Dominic Abrams). Two patients seen by Prof Edel O'Toole at the Royal London Hospital presented with unknown skin disorders. A family of four, were seen by Dr Celia Moss at the Birmingham Children's Hospital and the affected patients were diagnosed with Hypotrochosis and PPK. Two patients seen by Dr Kapila Batta at the Watford General Hospital were diagnosed with Acral Peeling Skin Syndrome. One patient seen by Prof Edel O'Toole at the Royal London Hospital was diagnosed with a novel clinical entity PLACK syndrome.

Appendix B. Primers for mutation analysis

B.1. Primers used for confirmation of capture array variants

Gene (Exon)	Forward primer seq (5'-3')	Reverse primer seq (5'-3')	AT (^{0}C)	Size (bp)
DSG2 (15)	AAGTTTGCCTGGGTCAAAAA	ACTGGGAAGCTACTGCCAGA	56	157
PKP2 (10)	TCCTTTTGTGTGTGGTCAGC	CAGGCCCAATACTCACTGGT	57	209
PKP2 (3)	TGTTAGCGACACCGTTTTTG	GGAAGCCCTGTTCTGAGTGA	57	184
PKP2 (3)	GCAACCTCTTGGAGAAGGAG	CTCTCCTCCCGCTGGAAT	58	192
PKP2 (N/A)	ATGCACGCGACCTTCTAAAC	atcctgtttgctgccatgtt	58	184
PKP2 (N/A)	gagcaagattccgtctcaaaa	CTCGGGACTGTGTCAGGAAT	63	171
DSP (11)	TGCAGGTTGAAAATCTCCTCT	GTCTGGGTTACGAGGCTTCA	56	167

Table B.1. Primers and cycling conditions used for sequencing of variations identified following the ARVC capture array.

B.2. Primers used to check for expression of cathepsins B and L by RT-PCR

Gene (Exon)	Forward primer sequence (5'-3')	Reverse primer sequence (5'-3')	AT (^{0}C)	Size (bp)
CathB - 1,2,3	CTAGGATCCGGCTTCCAAC	CACCCAGGAAGGTACCACAT	62	212
CathB - 8,9	GGCCGAGATCTACAAAAACG	CATTGTCACCCCAGTCAGTG	62	203
CathL – 1	GTCTTTTCAGGAGCCACTCG	CGGTTCGTGGCTTGTTTACT	-----	177
CathL – 2,3	CTGGGAATTGCCTCAGCTAC	TGAAGCTGTGTTTCCCTTCC	55	187

Table B.2. Primers and cycling conditions used for RT-PCR of cathepsins B and L.

B.3. Primers used to confirm DSP variation in hypotrichosis and PPK patients

Exon	Forward primer seq (5'-3')	Reverse primer seq (5'-3')	AT (^{0}C)	Size (bp)
12	TTCATTTGAGGGGAAAAACG	GCAAGGCATCGTGTGTCTAA	57	385

Table B.3. Primers and cycling conditions used for sequencing of exon 15 of DSP to confirm variation in hypotrichosis and PPK patients and parents.

B.4. Primers used for confirmation of variations identified following HaloPlex targeted resequencing

Gene (Exon)	Forward primer seq (5'-3')	Reverse primer seq (5'-3')	AT (^{0}C)
DSP (23)	CACCTGAGGGAAAAGCAGAG	CATCAAGTGCTCCTTGGTCA	65
PKP2 (2)	gcagGAAATCTTCACCGAAC	ttgggaaaagtaaacactcaaaaa	61
PKP2 (14)	gacttgaccctgggaagaaa	GGTGTTTTCCTTTGGGGATT	64
PKP2 (9)	tccttttgtgtgtggtcagC	caggcccaatactcaTGGT	64
PKP2 (1)	CCAGCTGAGTACGGCTACATC	CTGCACCTGCTCCTGGAT	65
PKP2 (12)	gcctcactcattctccctga	ggccattattacctggctctg	64
PKP2 (4)	GCTGCCATCCAGGATTTCT	tttcagtgtgcaaagtcacca	65
PKP2 (11)	caatctttttaatcaagtgttttgttt	TTTTGGATTATGTTGTTCAATGTG	61
PKP2 (4)	TCTGGAGCGAGCAGTGAGTA	tgaaagtgtgttgcgctttg	58
PKP2 (10)	GTGGCTCAGACAGTTGTCCA	ccgactcacCAATTTCATTCT	65
PKP2 (6)	TGCTTACGCTGACGGAGAAT	cttctatcagggcagggtaca	64
PKP2 (12)	ctgggcaacagagcaagatt	CTCGGGACTGTGTCAGGAAT	65
ADAM17 (8)	CGCATTCTCAAGTCTCCACA	actgcttctgggtgtccatc	65

Table B.4. Primers and cycling conditions used for confirmation of variations following HaloPlex targeted resequencing on patient genomic DNA.

B.5. Primers used for patient diagnosis screening of CSTA

Exon	Forward primer seq (5'-3')	Reverse primer seq (5'-3')	AT (^{0}C)	Size (bp)
1	cttgcccatttgttcatcct	cctgaacaaagccacaaaca	61	431
1A	ttttccccatgcctctttgc	CTCCTGGATTTCTGGAGTGGCG	65	200
1B	GTTCACTTTGGTTCCAGCATCCTG	caaccacagcctttccacag	65	193
2	tgaattcagcctaaagcaacaa	tccaccacttggaaggaatc	63	454
3	tttgtagacctgtggctctctc	TGATGGTTATATTTATCAGCAAGGA	63	289

Table B.5. Primers and cycling conditions used for patient diagnosis by PCR and Sanger sequencing of CSTA.

B.6. Desmoplakin cDNA primers used for confirmation of site-directed mutagenesis

Exon	Forward primer seq (5'-3')	Reverse primer seq (5'-3')	Size (bp)
1	CAACACCAACACCCAGCTC	ATCAAGCAGTCGGAGCAGTT	522
2	ACTCGGACGGCTACTGTCAA	CAGGTCGGCTTTGATTTTGT	572
3	TGGAGCAGCACATTAACAGC	GCAGGGGTACTTCTTCCTGA	575
4	TCTGAAAGAAAATGCTGCCTA	TCATGGCCCTGATCTTCTCT	578
5	GCAGTACTACGAAGCCATCTTG	TGGTGAGAAGATCCCTGGTC	522
6	CAGAAGATTCGCAGGCAGAT	GCCAACAACGACTTCTTCAA	461
7	CAGGCTCACTGAGGAGGAAA	GGTATGTTCAGCAGAGTTTCCAG	570
8	TTGCGCCAATTCAATTAAGG	CCTTGCTTTCTGCAGTTGGT	580
9	TGAGAAGATCACCCGACTGAC	CTGCATGACCTGCTTCAGTT	577
10	GAAGGCGAGCTGAAGAAAAC	TCTCCTCTGTTCGCATCTGA	585
11	CCACTGGCTCTGAGGTGTCT	TTAACAATGGATGCCTGCTC	574
12	CTCCTGCAAGAGGAAGAAGC	CCTGTCTCAAATTTTCCCTCTC	587
13	AGCTGCAGATCAGCAACAAC	GGGCGCTGTCTGAGTTTATC	574
14	AAGAGAGGTGCAGGCGTAAG	TCTTGCCTGAAAATGGATCA	582
15	TAGCTCGGGACCTCATTGAC	TATGCCTGCTATGCAGCTTG	572

Exon	Forward primer seq (5'-3')	Reverse primer seq (5'-3')	Size (bp)
16	TGAGACCGTCCACTGTCAAT	TCTTCAGTGTTGGGGTCAAA	583
17	GGGGCTATTTCAATGAGGAA	CGGGAGCTGCTAAAAACATC	577
18	CAGCCTCACTCAATTTGCTG	TTATCCTCCCATGCACTTCC	581
19	AGCAGCAGAGGCAGTGAAAG	AAGCACCGGGATTTTCTTTT	581
20	GTCAGTTGGGAGTGGTTGCT	TCCACACTCTGAAACTAAAGGAGA	513
21	GGAGATAAAAATTAAATGGATCACTG	TTTTTAATGGTATTTCTTCACAGGT	468

Table B.6. Primers and cycling conditions for DSP I cDNA primers, used for verification of DSP I clones following site-directed mutagenesis.

B.7. pCR II-TOPO specific primers used for amplification of inserted DSP fragment

Exon	Forward primer seq (5'-3')	Reverse primer seq (5'-3')
M13	GTAAAACGACGGCCAG	CAGGAAACAGCTATGAC

Table B.7. Primers used to verify the correct insertion of DSP cDNA in pCR II-TOPO and to check plasmid post site-directed mutagenesis.

Appendix C. Primary antibodies used for immunomicroscopy and western blotting

Primary Antibody	Clone	Host	WB dilution	ICC dilution	Source
Mab anti-CSTA	---------	Ms	1:500	1:100	Abcam (Cambridge, UK)
Pab anti-CSTA	---------	Rb	1:500	1:50	Abcam
Pab anti-CAST	H-300	Rb	1:1000	1:100	Santa Cruz Biotechnology
Mab anti-β-actin	AC-15	Ms	1:5000	---------	Sigma
Pab anti-E-cadherin	HECD-1	Rb	1:1000	---------	Abcam
Mab anti-Tubulin	DM1A	Ms	1:10000	---------	Abcam
Pab anti-GAPDH	---------	Rb	1:1000	---------	Abcam
Pab anti-Vinculin	---------	Rb	1:1000	---------	Abcam
Pab anti-Lamin A	---------	Rb	1:1000	---------	Abcam
Mab anti-LAMP1	---------	Ms	1:1000	---------	Abcam
Mab anti-K14	LL001	Ms	---------	1:100	CRUK
Mab anti-Pan-cytokeratin	AE1/AE3	Ms	---------	1:100	Dako (Glostrup, Denmark)
Mab anti-Cath L	33/2	Ms	1:200	1:50	Abcam

Primary Antibody	Clone	Host	WB dilution	ICC dilution	Source
Pab anti-Cath B	CA10	Rb	1:200	1:25	Abcam
Mab anti-Cath H	---------	Ms	---------	1:25	Abcam
Mab anti-DSG1	MCA2271	Ms	1:500	---------	AbD Serotec, Bio-Rad
Mab anti-DSG1/2	DG3.10	Ms	1:500	1:250	Progen (Heidelberg, Germany)
Pab anti-DSG2	Ab10	Rb	1:10000	1:500	Kind gift from Dr Mỹ Mahoney
Pab anti-DSC2	---------	Rb	1:2000	---------	Progen
Mab anti-DSG 3	5G11	Ms	1:200	---------	Abcam
Mab anti-DSG 3	3G133	Ms	1:500	---------	Abcam
Mab anti-DSC3	U114	Ms	1:250	---------	Progen
Pab anti-PKP2	518	Rb	1:100	---------	Progen
Mab anti-PG	5.1	Ms	1:1000	---------	AbD Serotec (Serotec, Kidlington, UK)
Mab anti-DSP I/II	5-11F	Ms	1:250	1:50	Kind gift from Prof. David Garrod (Parrish *et al*., 1987)

Table C. Primary antibodies used for western blotting and immunomicroscopy. Details of antibodies used, together with the source, clone and specific assay-specific dilutions.

Appendix D. Buffers

Buffer	Reagents
RM^+	40µg/ml Hydrocortisone 500µg/ml Insulin 1µg/ml EGF 10-8 (0.84 µg/ml) Cholera toxin 500µg/ml Transferrin 1.3µg/ml Lyothyronine (L4)
Normal media (add to DMEM or DMEM-F12)	10% (v/v) FBS 2 mM L-glutamine 100 U/ml Penicillin 100 µg/ml Streptomycin 1% RM^+
TBE Buffer	9M Tris base 9M Boric acid 0.2M EDTA, pH 8.0
DNA Loading Buffer	50% (v/v) Glycerol 0.2% (w/v) Orange G
Western Blotting Polyacrylamide Running Gel (10%) in 5 ml	1.7 ml of Acrylamide mix [Protogel 30% (w/v) acrylamide : 0.8% (w/v) Bis-acrylamide stock solution (37.5:1)] 1.9 ml of ddH2O 1.3 ml of 1.5 M Tris, pH 8.8 0.05 ml of 10% SDS 0.05 ml of APS 0.002 ml of TEMED

Buffer	Reagents
Western Blotting Polyacrylamide Stacking Gel (5%) in 1 ml	0.17 ml of Acrylamide mix [Protogel 30% (w/v) acrylamide : 0.8% (w/v) Bis-acrylamide stock solution (37.5:1)] 0.68 ml of ddH2O 0.13 ml of 1.0 M Tris, pH 6.8 0.01 ml of 10% SDS 0.01 ml of APS 0.001 ml of TEMED
SDS Protein Loading Buffer	0.100 M Tris-HCl, pH 6.8 4% SDS 20% Glycerol 0.001% Bromophenol Blue 1.44 M Beta-mercaptoethanol (10%)
Western Blotting 10x Running Buffer	0.25M Tris base 1.92M Glycine 1% SDS
Coomassie Stain	40% dH_2O 10% Acetic acid 50% Methanol 0.25% Coomassie Brilliant Blue R-250
Ponceau Stain	20mg/ml Ponceau S 0.3g Trichloroacetic acid
Western Blotting 10 x Transfer Buffer	0.48M Tris base 0.30M Glycine 0.37% (w/v) SDS Add 20% (v/v) Methanol to 1 x Transfer Buffer
Western Blotting 10 x Transfer Buffer for DSP	0.48M Tris base 0.30M Glycine 0.37% (w/v) SDS Add 5% (v/v) Methanol to 1 x Transfer Buffer

Buffer	Reagents
10 x TBS	0.5M Tris-HCl, pH 7.5 1.5M NaCl
1 x T-TBS (Tween 20-TBS)	0.05M Tris-HCl, pH 7.5 0.15M NaCl 0.1% (v/v) Tween-20
Western Blotting Stripping Buffer	62.5 mM Tris-HCl, pH6.8 2% SDS 0.7% β-Mercaptoethanol dH_2O
ELISA Wash Buffer, pH 7.2-7.4	0.05% Tween 20 1 x PBS
ELISA Reagent Diluent, pH 7.2-7.4	1% BSA 1 x PBS
ELISA Stop Solution	2N H_2SO_4

Table D. Buffers used in Chapter 2 and the component reagents.

Appendix E. Generation of mutant *DSP* clones for *in vitro* analysis of ARVC and genodermatoses

E.1. Selection of DSP constructs by restriction digest and sequencing

This section is based on the identification of three novel mutations in the *DSP* gene in three individuals, as follows: one patient with cardiomyopathy, striate PPK and woolly hair; a second patient with cardiomyopathy and a third patient with hypotrichosis and PPK. The first patient, previously described by Norgett *et al*., presented with a heterozygous thirty base pair insertion in exon 14 of *DSP*, which would lead to a 10 amino acid insertion at the protein level (Norgett *et al*., 2006). The second patient, clinically diagnosed with cardiomyopathy and no cutaneous or hair phenotypes, was genetically analysed using a custom capture array, as described in Chapter 3, Table 3.1., and a novel heterozygous variation was identified in exon 11 of *DSP* (c.G1323C:p.K441N). The third patient together with two other siblings, were diagnosed with hypotrichosis and PPK and no obvious cardiac abnormalities at the time of examination. Exome analysis of this patient revealed a homozygous mutation in exon 12 of *DSP* (c.C1493T:p.P498L), which was confirmed in one other sibling and in heterozygous parents.

As the 30 bp insertion mutation was previously cloned and stable mutant keratinocyte cell lines were generated by Dr Rita Cabral in our group, this section will focus on describing the cloning process for the second and third *DSP* mutations described above.

A wild type *DSP I* cDNA clone was previously generated by Dr Rita Cabral, using three overlapping RT-PCR reactions using total RNA from primary normal human keratinocytes (NHK). Briefly, four cDNA fragments were PCR amplified and cloned individually into pCRII-TOPO vector, subsequently each fragment was extracted using restriction enzymes, and joined in a precise order due to common restriction sites. The final product which contained all fragments was then transfected into chemically competent *E. coli* cells, which were amplified and stored as glycerol stocks (Cabral *et al*., 2010b).

For the site-directed mutagenesis several *DSP I* clones which contain various pieces of the *DSP I* construct cloned into pCRII-TOPO were selected. A restriction digest with *KpnI* and *NotI* restriction enzymes which selectively cut at the ends of pCRII-TOPO vector has confirmed the correct size fragments in selected clones. A fragment of approximately 4,000 bp was obtained for all clones and corresponds to the pCRII-TOPO cloning vector. Alongside the fragment matching the size of the cloning vector, other fragments corresponding to the *DSP I* various piece combinations were observed as follows (Figure E.1.):

lane 1 – final *DSP I* construct (pieces 1+2a+2b+3), digest failed;

lane 2 – *DSP I* pieces 1+2a+2b, expected fragment of approximately 6,100 bp;

lane 3 – *DSP I* piece 1, smear observed at approximately 4,000 bp which is the correct size for both the vector and *DSP I* piece 1;

lane 4 – *DSP I* piece 3, expected fragment of approximately 3,600 bp;

lane 5 – *DSP I* piece 2a, expected fragment of approximately 1,000 bp;

lane 6 – *DSP I* pieces 2a+2b, expected fragment of approximately 2,000 bp;

lane 7 – *DSP I* pieces 1+2a, expected fragment of approximately 5,200 bp;

lane 8 – *DSP I* piece 2a, fragment of approximately 1,500 bp observed instead of the corresponding fragment of 1,000 bp;

lane 9 – *DSP I* piece 1, smear observed at approximately 4,000 bp which is the correct size for both the vector and *DSP I* piece 1;

lane 10 – *DSP I* pieces 2a+2b, expected fragment of approximately 2,000 bp;

lanes 11, 12 and 13 – final *DSP I* constructs (pieces 1+2a+2b+3), expected fragment of approximately 9,700 bp was observed in all three lanes; all fragment sizes were determined by comparison to the 1 Kb plus ladder used as a size indicator.

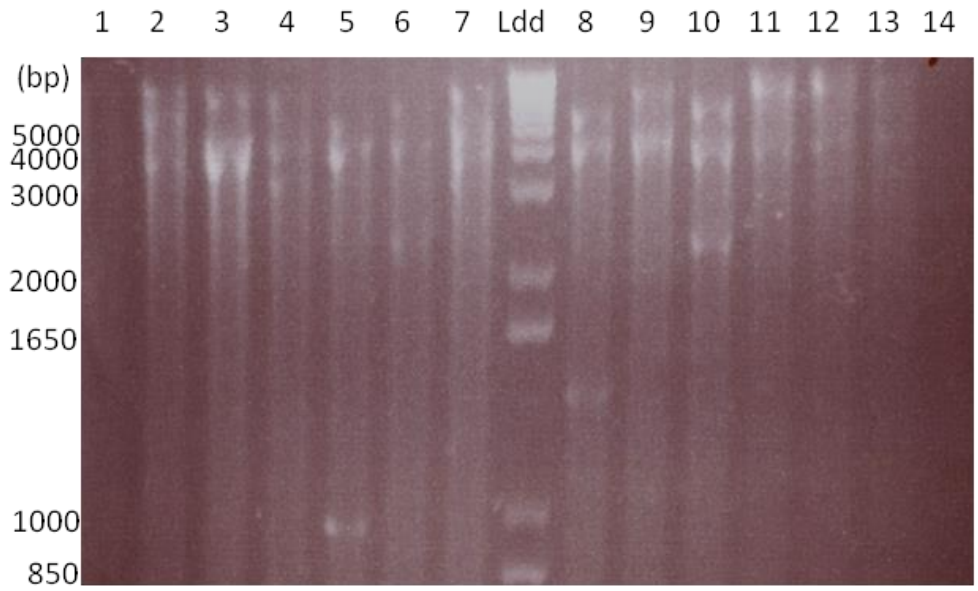

Figure E.1. Restriction digest with *KpnI* and *NotI* restriction enzymes on selected *DSP I* clones.

The restriction digest observations were confirmed by Sanger sequencing of these clones, using the M13 (-20) forward and M13 reverse primers which anneal to the pCRII-TOPO cloning vector and sequence the inserted constructs (data not shown). Three clones which included fragment 1 of *DSP I* in pCRII-TOPO were selected.

E.2. Site-directed mutagenesis and transformation of chemically competent bacterial cells

Site-directed mutagenesis (SDM) is a technique that uses special custom made primers which include the desired change and are used to amplify the entire vector and insert, resulting in an identical vector which incorporates the desired mutation instead of the wild type sequence. SDM can be used to make single point mutations, replace amino acids and delete or insert single or multiple amino acids. The two primers anneal by complementarity to the region to be mutated and sequence the vector in both the forward and reverse directions.

To further characterise the c.G1323C *DSP* mutation identified in the ARVC patient, and the c.C1493T *DSP* mutation identified in the hypotrichosis and PPK patient we have performed SDM on the selected *DSP I* clones which contain the required fragment 1 affected by these mutations (Figure E.2. A and B).

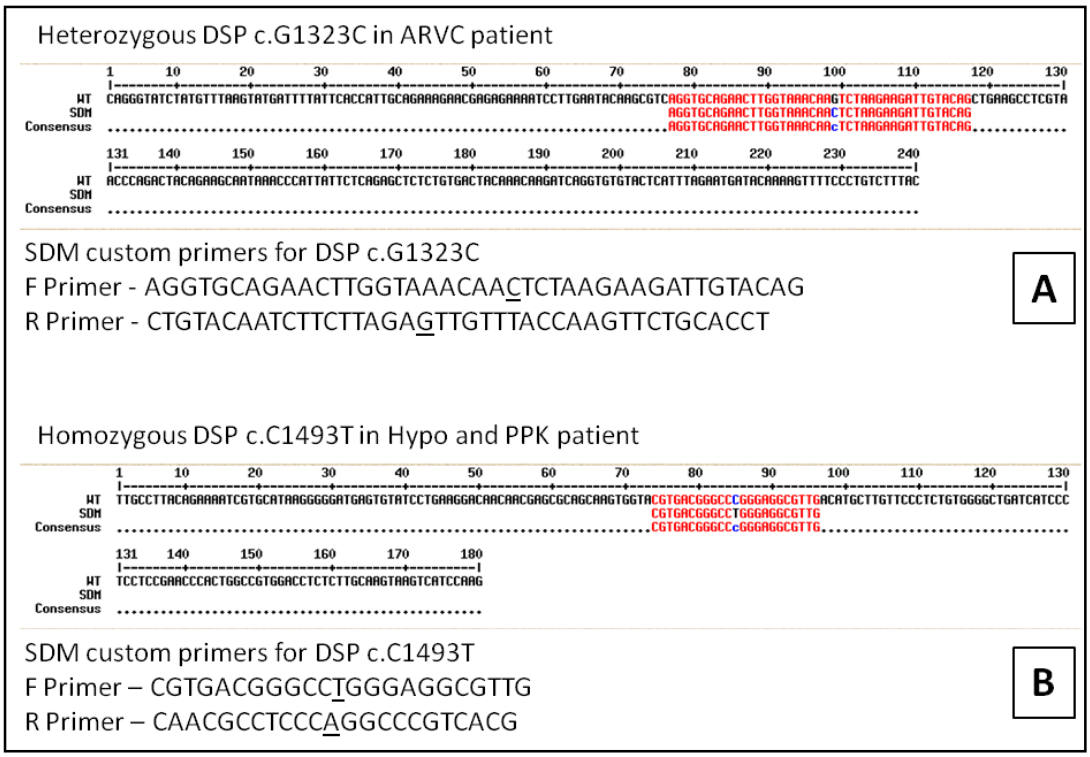

Figure E.2. Representation of annealing position of SDM primers with *DSP* c.G1323C (A) and *DSP* c.C1493T (B) mutations as expected post-SDM.

DpnI restriction enzyme was used post-SDM to digest parental DNA vectors based on this enzyme's specificity for methylated and hemimethylated DNA, thus selecting for mutation-containing newly synthesized vectors. These vectors were then transformed into chemically ultracompetent *E. coli* bacterial cells which were amplified and screened for the correct vector sequence expected following SDM (data not shown). All correctly amplified mutant vectors were sequenced further in order to eliminate any vectors which might have other mutations produced during the SDM process.

Similarly to the 30 bp insertion mutant, the following steps would be to excise the mutated *DSP* clone from the pCRII-TOPO vector and insert it into pBABE-Puro retroviral expression vector which will be transfected into the immortalised keratinocyte cell line HaCaT. The mutant stable cell lines will be used for *in vitro* studies looking at the differences in expression and localisation of mutant DSP but also at the possible mechanisms of action behind the three *DSP* mutations, linked to the above mentioned cardio/cutaneous disorders.

Appendix F.

F.1. Optimisations of CSTA siRNA mediated knockdown

Prior to the *CSTA* siRNA-based analysis presented in Chapter 4, the transfection efficiency of the *CSTA* siRNA pool was assessed with varied cell densities and time points, in order to find the highest transfection and knockdown efficiency with the lowest cell death rate. Lipid-based transfections using the DharmaFECT transfection reagent (Thermo Fisher Scientific) were performed to deliver siRNAs into HaCaT cells.

As shown in Figure F1.Ai., HaCaT cells were seeded at 2 x 10^5 and 4 x 10^5 cell densities and incubated with NTP siRNA and *CSTA* siRNA for 48 and 72 h. Western blotting of total cell lysates with an anti-cystatin A antibody revealed a significant reduction in cystatin A for both time points and cell densities, with a higher knockdown level achieved after 72 h (Figure F1.Aii.). As some of the analyses required extended time points we have used the same technique to check if the knockdown level was maintained up to 134 h. Cells were seeded at a 2 x 10^5 cell density and incubated with NTP and *CSTA* siRNA for 86, 110 and 134 h. Western blotting of total cell lysates revealed that the knockdown level was robust up to the longest analysed time point (Figure F1.Bi and Bii). These transfection conditions were used in all subsequent experiments.

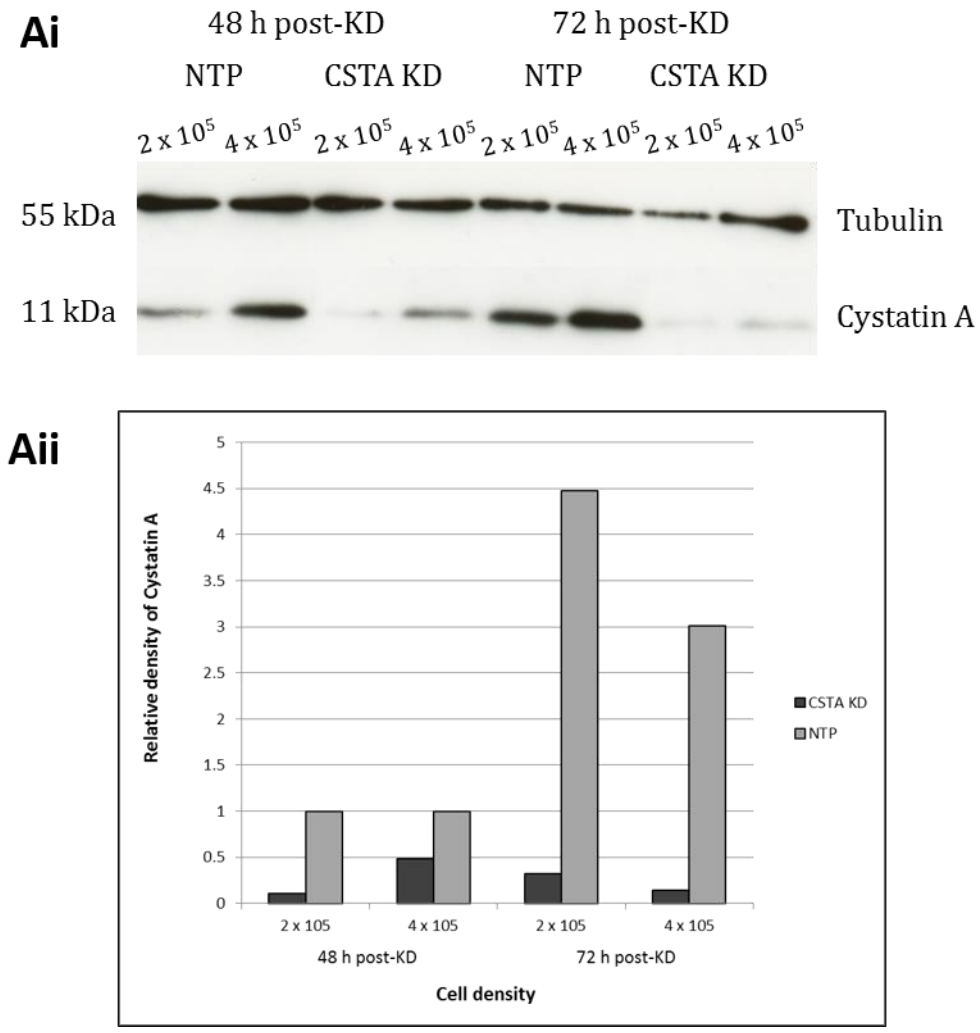

Figure F.1. Optimisation of *CSTA* siRNA transfection in HaCaT cells. (Ai) Total protein from HaCaT cell lysates 48 h and 72 h after transfection with *CSTA* siRNA (lanes 3-4 and 7-8) and NTP siRNA (lanes 1-2 and 5-6) was incubated with an anti-CSTA antibody (11 kDa). **(Aii)** Densitometric analysis of western blotting bands in **(Ai)** is showing a significant decrease in CSTA expression following *CSTA* siRNA-mediated knockdown, more accentuated after 72 h KD. Tubulin was used as a loading control (55 kDa).

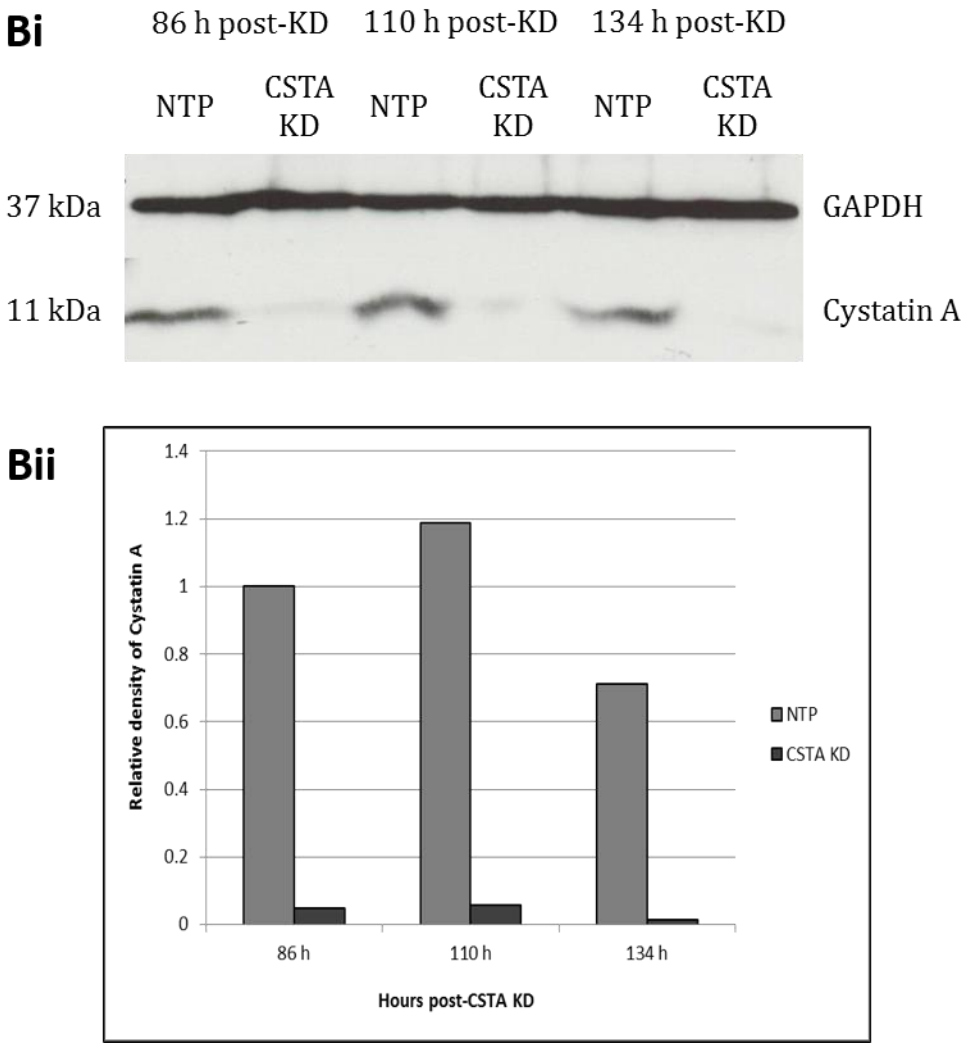

Figure F.1. Optimisation of *CSTA* siRNA transfection in HaCaT cells (continued). (Bi) Total protein cell lysates after 86 h, 110 h and 134 h from CSTA siRNA (lanes 2, 4 and 6) and NTP siRNA cells (lanes 1, 3 and 5) were incubated with an anti-CSTA antibody. **(Bii)** Densitometric analysis of western blotting bands in **(Bi)** is showing a significant decrease in CSTA expression following *CSTA* siRNA-mediated knockdown, for all time points analysed. Tubulin was used as a loading control (55 kDa).

F.2. Keratin 14 in non-stretched CSTA and NTP siRNA cells

Immunocytochemistry of NTP and *CSTA* siRNA cells was performed using an antibody raised against keratin 14 (in green) (Figure F2.A and B). After 0 h stretch, under 100 X magnification, NTP cells (Figure F2.Aii) and *CSTA* siRNA treated cells (Figure F2.Bii) the intercellular connections and keratin filaments appeared intact.

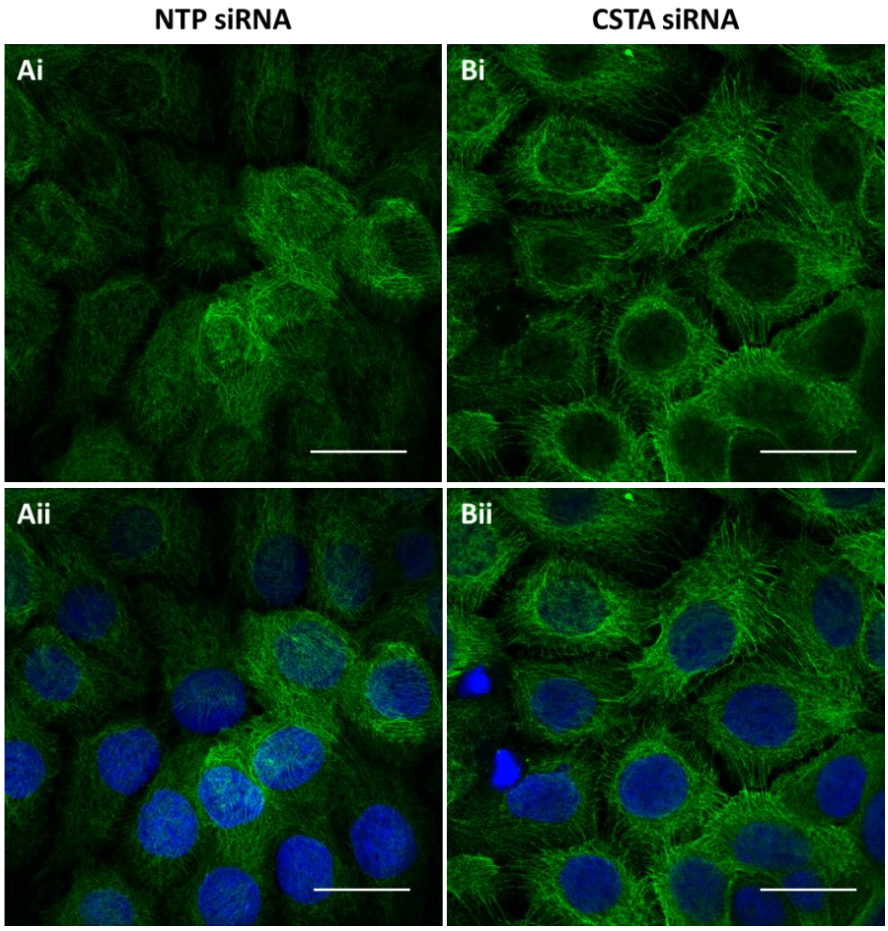

Figure F.2. Keratin 14 in non-stretched *CSTA* KD cell monolayers. ICC with an anti-keratin 14 antibody shows normal intercellular adhesion and keratin filaments in non-stretched *CSTA* siRNA **(A)** cells in comparison to control NTP **(B)**. Keratin 14 – in green; DAPI – in blue. Imaging was performed on the LSM 710 confocal microscope and images taken at 100 X (Scale bar – 20 µm).

F.3. Analysis of expression of cathepsins B and L in siRNA-treated stretched and scratched monolayers

The levels of secreted and intracellular cathepsins B and L were analysed in cell culture supernatants by ELISA following NTP and *CSTA* siRNA-treatment subjected to scratch and mechanical-stretch assays. The expression of the two cathepsins was initially analysed in NTP and *CSTA* siRNA treated cells prior to any stress being applied (Figure F3.A and B). The expression levels of both cathepsins increased upon scratch-wound in both control and *CSTA* siRNA cells with no significant difference between the two conditions (Figure F3.E and F). In mechanically-stretched cell monolayers the expression of cathepsins B and L presented a small

decrease after 1 h stretch but did not alter significantly after 4 h stretch in comparison to non-stretched cells (Figure F3.C and D). A significant difference in secretion levels was observed between the two proteases, with cathepsin B being secreted at significantly higher levels compared to cathepsin L, following both scratch-wound and mechanically-induced stress assays. Cathepsin expression in stretched cells was assessed in triplicate and in scratched cells in duplicate; optical density analysis for the remaining two and respectively one repeat(s) is included below.

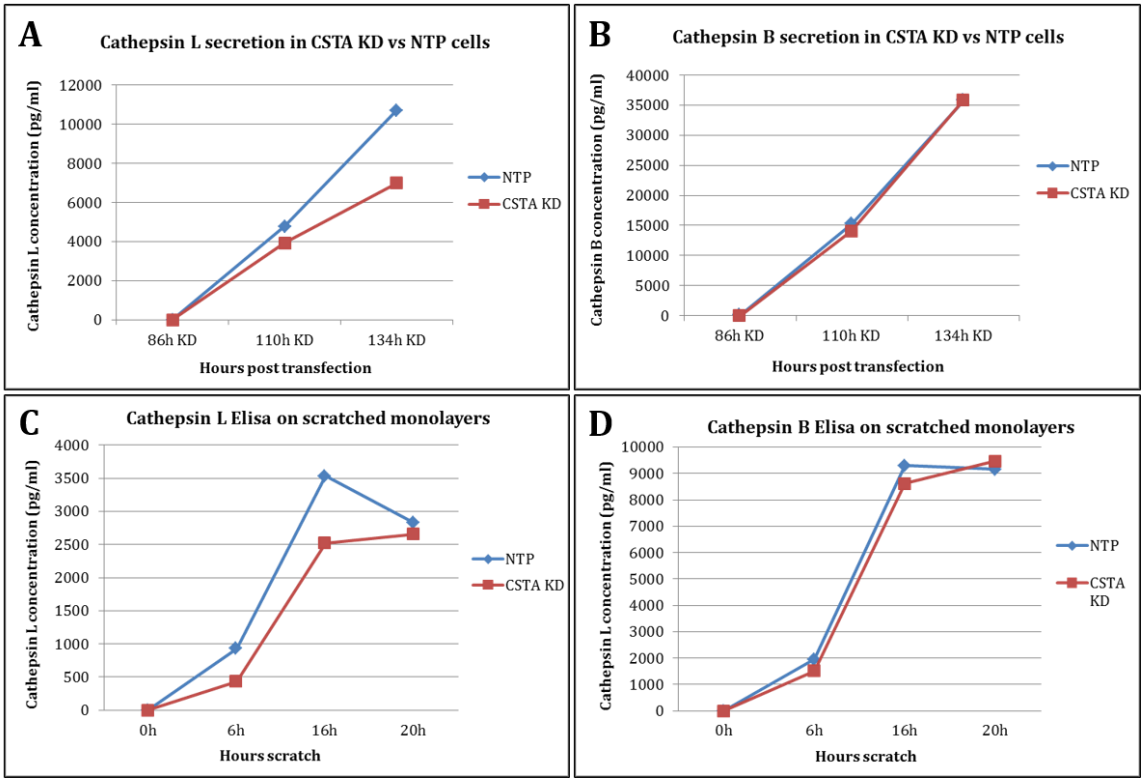

Figure F.3. Expression of cathepsins B and L in *CSTA* KD cells following "scratch-wound" and stretch assays. ELISA assay to assess the levels of secreted cathepsins B and L in culture supernatants post scratch-wound (0 h, 6 h, 16 h and 20 h post wound) or mechanical stretch (for 0 h, 1 h and 4 h) in *CSTA* siRNA compared to NTP siRNA. No significant difference was observed between *CSTA* siRNA and control cells.

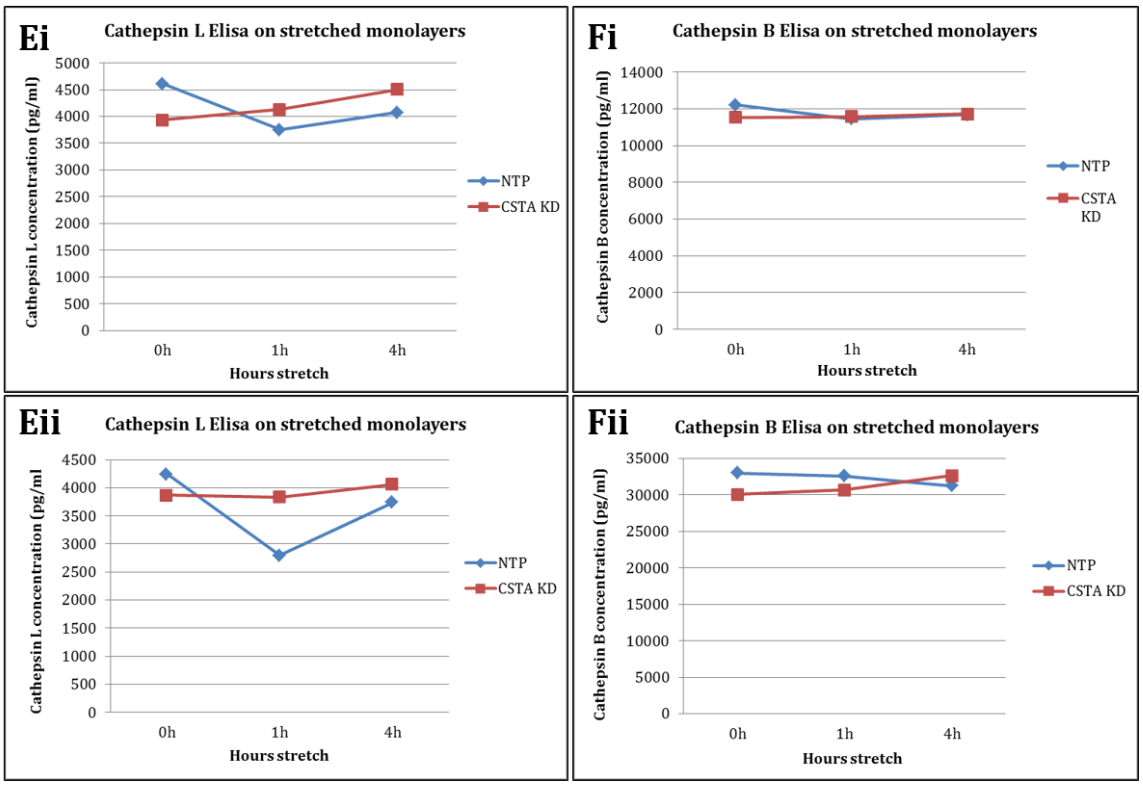

Figure F.3. Expression of cathepsins B and L in *CSTA* KD cells following "scratch-wound" and stretch assays (continued). ELISA assay to assess the levels of secreted cathepsins B and L in culture supernatants post scratch-wound (0 h, 6 h, 16 h and 20 h post wound) or mechanical stretch (for 0 h, 1 h and 4 h) in *CSTA* siRNA compared to NTP siRNA. No significant difference was observed between *CSTA* siRNA and control cells.

F.4. Densitometric analysis of desmosome-associated proteins in CSTA siRNA treated cells

Three independent *CSTA* knockdown experiments were performed and a number of western blots were carried out for each protein of interest. Antibodies targeting DSP, DSC2, DSC3, DSG2, DSG3, PG and PKP2 were used together with anti-vinculin or anti-GAPDH antibodies as loading controls. Densitometric measurements of western blots were calculated using an image analysis program (Image J, v1.47v) and are graphically depicted in Figure F4. No detectable differences were observed in the expression levels of DSG2, DSC2, DSC3, PG and PKP2, between *CSTA* siRNA cells and NTP control cells, in any of the independent knockdown experiments (Figure F4.C-G). Variable differences were seen for DSP (Figure F4.B) between independent knockdown experiments. DSG3 (Figure F4.A) presented a general trend of up-regulation of expression following *CSTA* knockdown in both stretched

and non-stretched cell monolayers with a small variability between independent knockdown experiments. The discrepancy between knockdown experiments could perhaps reflect the variability between western blots and a larger number of western blots for each knockdown repeat would be necessary to confirm the changes in the levels of expression of DSG3 and DSP.

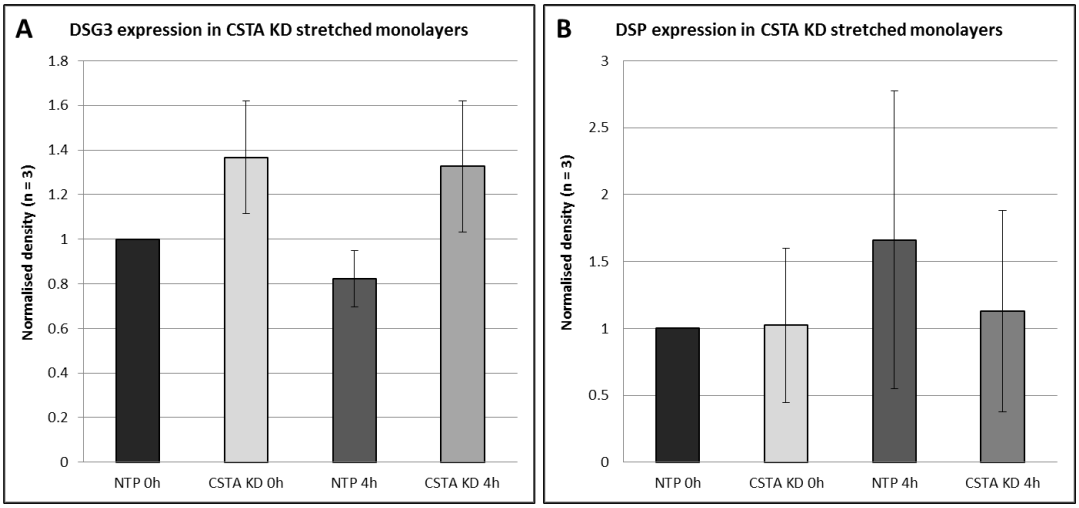

Figure F.4. Densitometric analysis of desmosomal proteins in *CSTA* KD cells. Protein levels of DSP, DSG3, DSC2, DSC3, PG and PKP2 calculated from densitometry measurements of western blot images and normalised to loading controls (Vinculin for DSP or GAPDH for all other proteins). Desmosome-associated protein expression levels are presented as a fraction of the total protein expression levels of non-stretched NTP cells. **(A)** DSG3 (n = 3) presented with a general trend of up-regulation in all knockdown repeats with different expression values, as seen through the standard error bars. (B) DSP (n = 3) gave variable results and will need to be analysed further.

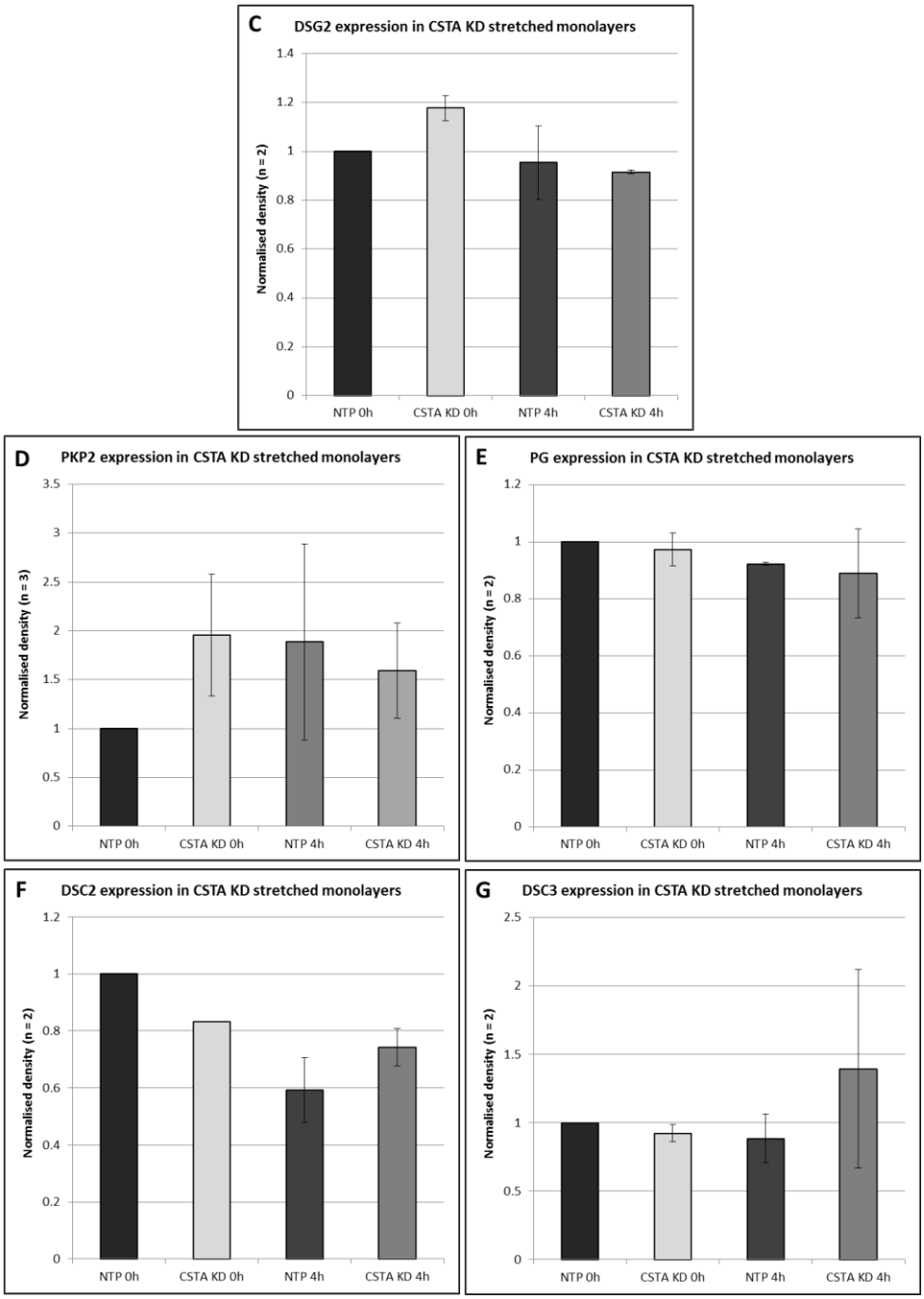

Figure F.4. Densitometric analysis of desmosomal proteins in *CSTA* KD cells (continued). Protein levels of DSP, DSG2, DSG3, DSC2, DSC3, PG and PKP2 calculated from densitometry measurements of western blot images and normalised to loading controls (Vinculin for DSP or GAPDH for all other proteins). Desmosome-associated protein expression levels are presented as a fraction of the total protein expression levels of non-stretched NTP cells. **(C-G)** No differences in expression were observed for DSG2, DSC2, DSC3, PKP2 and PG in *CSTA* KD cells compared to control (n = 3 for PKP2 and n = 2 for all other proteins).

Appendix G.

G.1. Optimisation of CAST siRNA transfection

A series of optimisations of *CAST* siRNA transfection were performed prior to the siRNA-based analyses presented in Chapter 5. The knockdown efficiency of the *CAST* siRNA pool was assessed over a number of time points by western blotting of total protein lysates. Similarly to the *CSTA* siRNA transfections, the DharmaFECT transfection reagent was used to deliver siRNAs into HaCaT cells and *CSTA* siRNA was used as control of knockdown efficiency.

Densitometric analysis of calpastatin following *CAST* knockdown, in comparison to NTP control, revealed a reduction in calpastatin for all of the time points analysed, significantly increasing after 72 h (Figure G1). As some of the *CAST* knockdown-based analyses required extended time points we have checked if the knockdown level was maintained up to 120 h. These transfection conditions were used in all subsequent *in vitro* experiments.

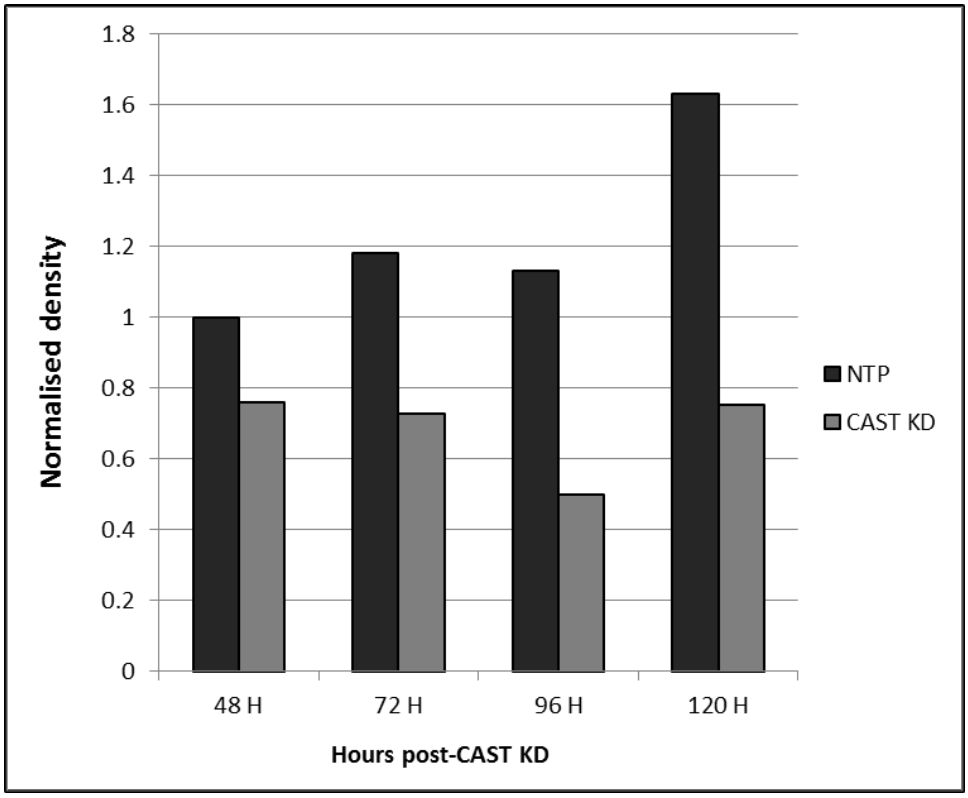

Figure G.1. Densitometric analysis of *CAST* siRNA knockdown. Total protein lysates from *CAST* siRNA and NTP siRNA treated cells were incubated with an anti-calpastatin antibody. Calpastatin expression decreased significantly after 72 h.

G.2. DSG3 expression in PK2 skin biopsies

Due to the cell adhesion defect in *CAST* LOF skin, the analysis of the expression and localisation of the desmosome-associated proteins DSG2, DSP and DSG3 was performed in patient skin. Figure G2. shows the expression and localisation of DSG3 in patient skin (Figure G2.B) in comparison to normal control skin (Figure G2.A.). The immunohistochemistry picture of calpastatin in PK2 skin is taken at a lower exposure than the one presented in figure 5.8. (Chapter 5), and it better shows a change in localisation of DSG3 from a predominantly membranous compartment to both a plasma membrane and cytoplasmic localisation.

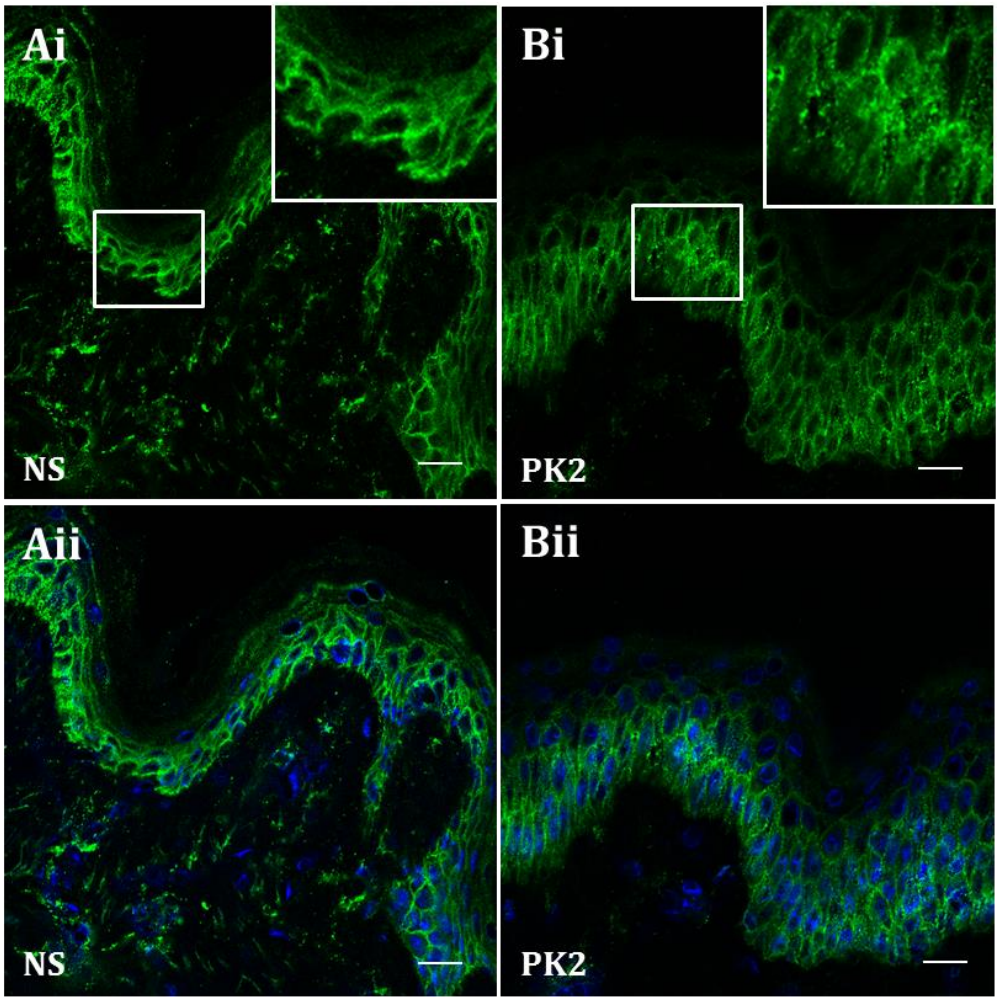

Figure G.2. Immunofluorescence of DSG3 in skin sections from PK2. IHC with an anti-DSG3 antibody (in green) in control skin **(A)** and skin sections from PK2 **(B)** in the absence **(Ai** and **Bi)** and presence **(Aii** and **Bii)** of DAPI as nuclear marker (in blue), revealed a significant increase in protein expression in affected skin compared to control skin. A change from a typical membranous localisation to a both membranous and cytoplasmic localisation of this protein was also noted. Imaging was performed with the Zeiss Meta 710 confocal microscope and images were taken at 20 X magnification **(A** and **B)** (Scale bar – 20 µm for **A** and **B**).

G.3. Desmosome-associated protein expression in CAST siRNA cells

Following observations on the altered expression and localisation of the desmosome-associated proteins DSG2, DSG3, and DSP I/II in affected skin, these proteins were investigated in *CAST* siRNA-treated cells before and after 4 h mechanically-induced stress. Total protein cell lysates from NTP and *CAST* siRNA-treated HaCaT cells were analysed by western blotting with antibodies targeting PG

and DSP I. Densitometric measurements of western blots were calculated as previously described, and are graphically depicted in Figure G3. for DSP I and Figure G4. for PG. Both proteins appeared to have similar expression levels between *CAST* siRNA and NTP treated cells.

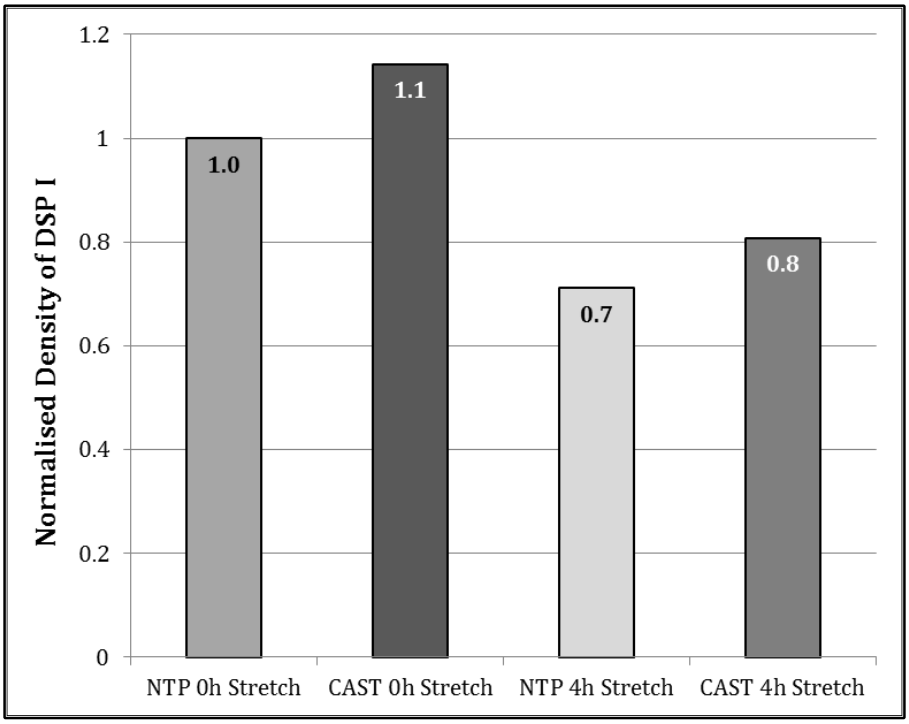

Figure G.3. Expression of DSP I in *CAST* KD cells. Total protein cell lysates from *CAST* siRNA and NTP siRNA HaCaT cells, non-stretched and stretched for 4 h, were blotted and incubated with an anti-DSP I antibody. Protein levels of DSP I were calculated from densitometric measurements of the western blot images, normalised against vinculin as loading control and are presented as a fraction of the total protein levels in NTP siRNA cells (n = 1).

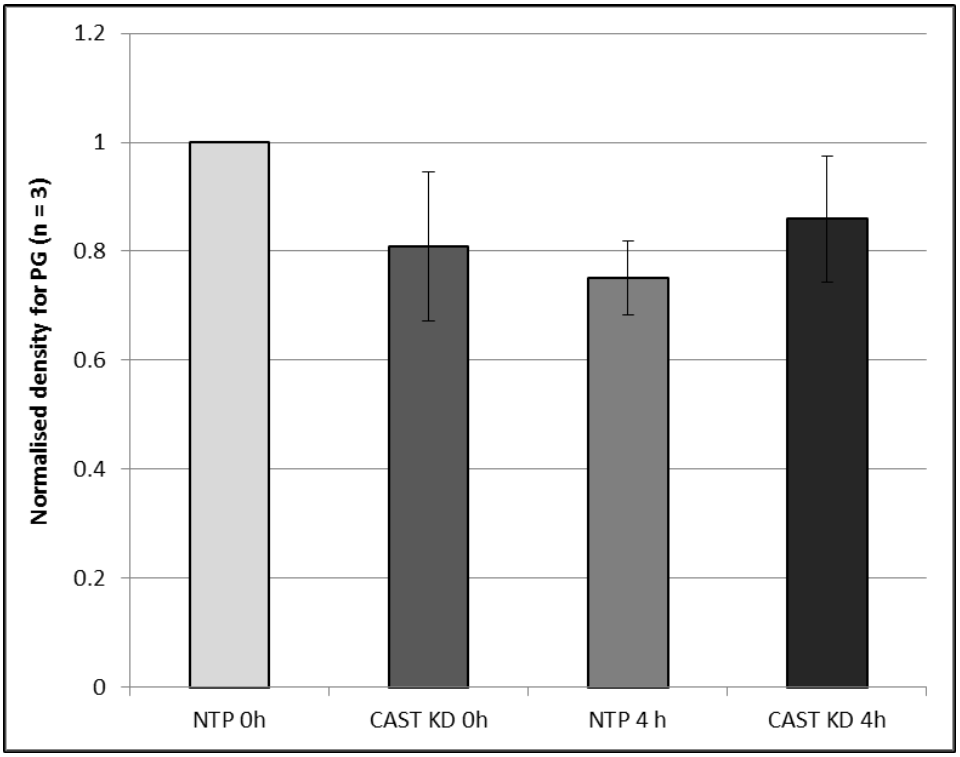

Figure G.3. Expression of PG in *CAST* KD cells (continued). Total protein cell lysates from *CAST* siRNA and NTP siRNA HaCaT cells, non-stretched and stretched for 4 h, were blotted and incubated with an anti-PG antibody. Protein levels of PG were calculated from densitometric measurements of the western blot images, normalised against GAPDH as loading control and are presented as a fraction of the total protein levels in NTP siRNA cells (n = 3).